SYNTHESES AND CHARACTERIZATION OF MACROCYCLIC LIGANDS CONTAINING NITROGEN AND SULPHUR DONOR ATOMS.

by

Becky Chak
B.Sc., University of Victoria, 1988

A Dissertation Submitted in Partial Fulfilment of the
Requirements for the Degree of

DOCTOR OF PHILOSOPHY

in the Department of Chemistry

We accept this thesis as conforming
to the required standard

Dr. A. McAuley, Supervisor (Department of Chemistry)

Dr. D. Harrington, Department Member (Department of Chemistry)

Dr. T. Fyles, Department Member (Department of Chemistry)

Dr. L. Robertson, Outside Member (Department of Physics)

Dr. N. Curtis, External Examiner (Department of Chemistry)

Supervisor: Dr. Alexander McAuley

ABSTRACT

Macrocyclic ligands containing nitrogen and sulphur donor atoms, as well as with pyridine or thiophene pendant arms were synthesized. The Co(II), Ni(II), Cu(II) and Pd(II) complexes have been characterized by crystallography, UV/Vis, NMR or ESR spectroscopy and the redox chemistry have been studied by cyclic voltammetry (CV).

The Pd(II) complex of [14]aneNS$_3$ (1,4,7-trithia-11-azacyclotetradecane), is square-planar whereas the structures of Pd(II) macrocyclic complexes with pyridine or thiophene pendent arms may be described as pseudo five-coordinate. There is considerable interaction between the apical sulphur donor atom and the palladium metal centre.

In solution, the Pd(II) complex of py[14]aneNS$_3$ (N-(2'-pyridylmethyl)-1,4,7-trithia-11-azacyclotetradecane) exhibits fluxional behavior. There is an exchange process involving the metal-coordinated and -uncoordinated thioether atoms. By analyzing the NMR spectra obtained at different temperatures, the mechanism for the fluxional process is proposed.

The cyclic voltammograms of the Pd(II) macrocyclic complexes showed irreversible reduction to Pd(I) and no oxidation to Pd(III) could be detected in the potential range studied. In the case of the Pd(II) complex with thiophene pendent arms, a quasi-reversible reduction to Pd(I) was observed. This unique behavior is rationalized as due to the proximity of a thiophene moiety in the

apical position which inhibits dimerization to the Pd(I) generated, due to steric reasons.

The Ni(II) complex of py[14]aneS_3 is peudo-octahedral whereas the Co(II) complex exists as two linkage isomers. In the nitrate salt, [Co(py[14]aneNS_3)$(NO_3)_2(CH_3CN)$], the cobalt centre is octahedral, being coordinated to only the nitrogen donors from the ligand and the remaining coordination sites are occupied by acetonitrile and oxygen atoms from two nitrate groups. In the perchlorate salt, [Co(py[14]aneNS_3)]$(ClO_4)_2$, solution studies (ESR and CV) suggest that the cobalt(II) ion is being coordinated by the nitrogen and sulphur donor atoms from the ligand.

The Cu(II) complexes of these mixed donor ligands have also been studied and their spectroscopic (UV/Vis and ESR) characteristics and Cu(II)/Cu(I) reduction potential were compared to the type I Blue copper protein.

Dr. A. McAuley

Dr. D. Harrington

Dr. T. Fyles

Dr. L. Robertson

Dr. N. Curtis

TABLE OF CONTENTS

page

LIST OF TABLES

LIST OF FIGURES

LIST OF ABBREVIATIONS

[9]aneN$_3$	1,4,7-triazacyclononane
[9]aneS$_3$	1,4,7-trithiacyclononane
[9]aneN$_2$S	1-thia-4,7-diazacyclononane
py$_3$[9]aneN$_3$	1,4,7-tris(2-pyridylmethyl)-1,4,7-triazacyclononane
[12]aneS$_4$	1,4,7,10-tetrathiacyclododecane
[14]aneS$_4$	1,4,8,11-tetrathiacyclotetradecane
[12]aneN$_2$S$_2$	1,7-dithia-4,10-diazacyclododecane
[18]aneS$_6$	1,4,7,10,13,16-hexathiacyclooctadecane
[14]aneNS$_3$	1,4,7-trithia-11-azacyclotetradecane
py[14]aneNS$_3$	N-(2'-pyridylmethyl)-1,4,7-trithia-11-azacyclotetradecane
en	1,2-diaminoethane
cyclam	1,4,8,11-tetraazacyclotetradecane
bicycloSN$_4$	1-thia-5,8,12,17-tetraazacyclo[10.5.2]-nonadecane
2,3,2-tet	1,4,8,11-tetraazaundecane
daptacn	1,4-di-(3-aminopropyl)-1,4,7-triazacyclononane
Fc	ferrocene

ACKNOWLEDGEMENTS

I would like to thank my supervisor, Dr. A. McAuley, for his encouragement and guidance throughout the course of this work. I would also like to thank members of the group: B. Cameron, K. Coulter, Dr. T. Whitcombe and Dr. C. Xu for their support. The assistance of Kathy Beveridge and Dr. G. Bushnell with X-ray crystallography and Ms Chris Greenwood with various high field NMR experiments is also greatly appreciated. Finally, I would also like to thank NSERC for financial funding through a post-graduate scholarship.

CHAPTER 1

INTRODUCTION

1.1 Historical Development of Coordination Chemistry

Coordination chemistry is the study of the manner in which the reactivity of a metal ion is modified by the ligand environment surrounding it. Traditionally, coordination complexes have been regarded as a separate class of molecular compounds[1]. They consist of a central metal ion surrounded by inorganic or organic moieties called ligands. The ligands may be a set of small independent atoms, e.g., F^-, Cl^- or an elaborate arrangement of atoms connecting those few that are bonded directly to the central atom, e.g., ethylenediaminetetraacetate ($EDTA^{4-}$). However, each donor **must** have at least one pair of electrons that can interact with the central metal ion.

The first recorded observation of a coordination compound was reported by Tassaert in 1798. He observed the formation of $[Co(NH_3)_6]^{2+}$ in solution when he attempted to precipitate cobalt hydroxide by the addition of ammonia to a solution of cobalt salt[2]. The discovery of other metal ammines[3] soon followed, e.g., Zeise's salt, $K[PtCl_3C_2H_4]$ and Magnus salt, $[Pt(NH_3)_4]^{2+}[PtCl_4]^{2-}$. However, it was Jørgensen (1837-1914) who started the extensive studies of coordination compounds formed by cobalt, chromium, rhodium and platinum[4].

The true nature of the bonding in these complexes was first explained by Werner's coordination theory[5] in 1893. He proposed that besides the usual primary valence, atoms might exhibit a secondary combining tendency called coordination. Therefore an atom is surrounded by a constant number of atoms or groups. In the case of $CoCl_3.6NH_3$, neutral ammonia molecules are bound

directly to the metal so that the correct formulation should be $[Co(NH_3)_6]Cl_3$. He further explained the presence of structural isomers observed by assuming that the ligands occupied different positions that describe the corners of an octahedron or a square plane. For instance, two different isomers are found for $[Pt(NH_3)_2Cl_2]$ and $[Pd(NH_3)_2Cl_2]$ and therefore the complexes must be square planar and not tetrahedral.

In 1927, Werner's coordination theory was recast in electronic terms by Lewis and Sidgwick[6]. They proposed that a chemical bond required the sharing of an electron pair. This led to the idea of dative covalent bond in which a molecule with an electron pair (Lewis base) can donate these electrons to a metal ion or other electron acceptor (Lewis acid). This was followed by Pauling's valence bond theory[7] which suggested the hybridization of s, p and d orbitals of the metal ion that led to the formation of octahedral, square pyramidal, trigonal bipyramid or square planar geometry in metal complexes. He also viewed each ligand as a two-electron donor with a sigma bond to the metal ion[7].

In the 1930s, the crystal field theory was proposed by Bethe[8] and Van Vleck[9] to explain the electronic spectra and magnetic properties of simple transition metal compounds in the solid state. This theory treats the ligands around the metal ion in a complex as a set of point negative charges which interact repulsively with electrons on the metal ion, resulting in the loss of degeneracy of the orbitals on the metal ions. Any specific bonding interactions

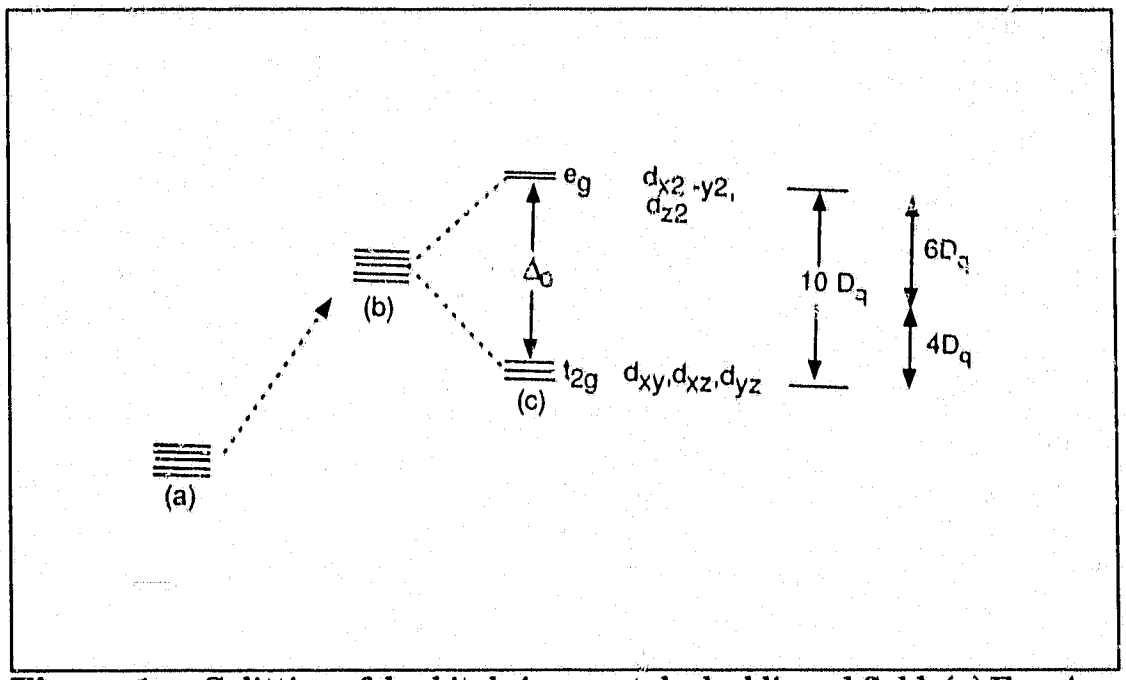

Figure 1 Splitting of d orbitals in an octahedral ligand field. (a) Free ion, (b) Hypothetical ion in a spherically symmetric field, (c) Hypothetical ion in an octahedral field. (Adapted from ref. 10a).

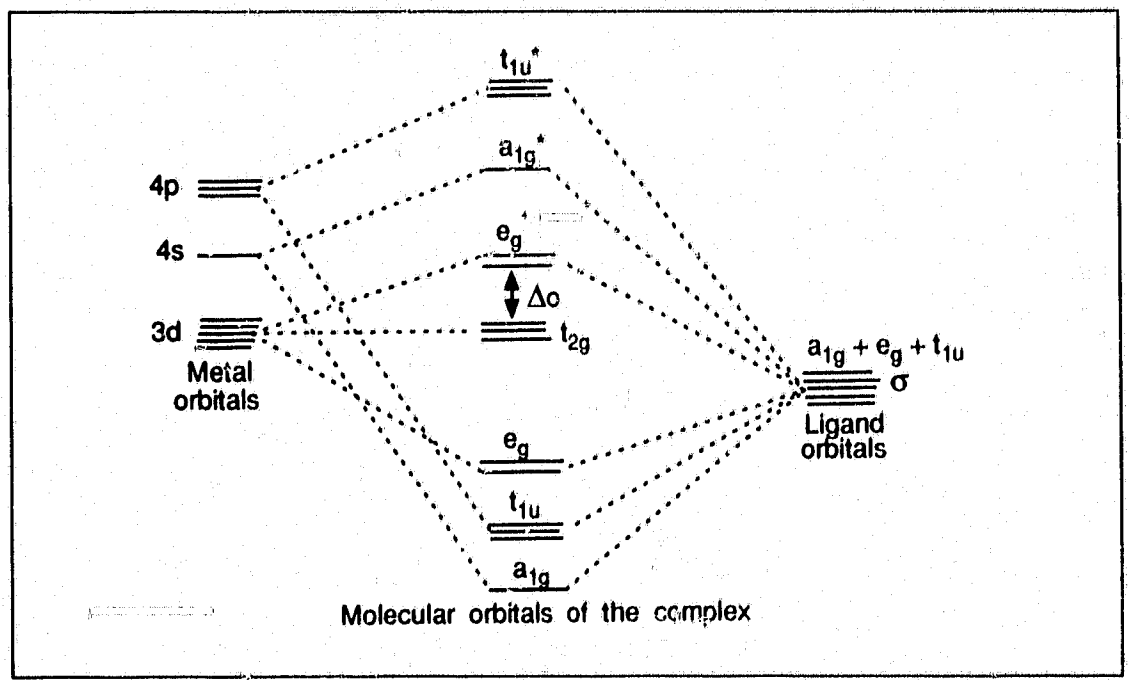

Figure 2 A schematic molecular orbital energy level diagram for octahedral complexes.

between the ligand and metal orbitals are neglected. For instance, in an octahedral complex, electrons in the d_z2 and $d_x2_{-y}2$ are repelled more strongly by the ligands than those in the d_{xy}, d_{xz}, d_{yz} orbitals and the energy difference between these two sets of orbitals are denoted by Δ_o (Figure 1).

Later, a more comprehensive approach to the bonding in transition metal complexes, now called ligand field theory[10], slowly emerged. This theory treats the metal-ligand σ bond as being formed by the combination of metal d_z2, $d_x2_{-y}2$, s, p_x, p_y or p_z orbitals (which have lobes lying along the metal-ligand bond direction) and the σ orbitals of the ligands. For complexes with ligands that do not have π bonding, six electron pairs from the ligand orbitals are filled into these orbitals (a_{1g}, t_{1u}, e_g) and electrons of the metal ions are then placed in the t_{2g} and e_g* orbitals as shown in Figure 2. Here, the energy difference between e_g* and t_{2g} orbitals arises from the strength of the metal-ligand bond and **not** by electrostatic effects as in crystal field theory.

For complexes having ligands with π orbitals, e.g., Cl^-, CN^- and pyridine, the metal t_{2g} orbitals (i.e., d_{xy}, d_{xz} and d_{yz}) interact with the π orbitals to form a new set of molecular orbitals (also with t_{2g} symmetry) in the complex. In the case of ligands with empty π orbitals of higher energy than the metal t_{2g} orbitals, e.g., in ligands such as phosphine, the newly formed t_{2g} orbitals in the complex are stabilized relative to the original non-bonding t_{2g} orbitals in a complex that does not have any π bonding (Figure 3). As a result, Δ_o increases. However, when the metal t_{2g} orbitals interact with filled π orbitals of lower

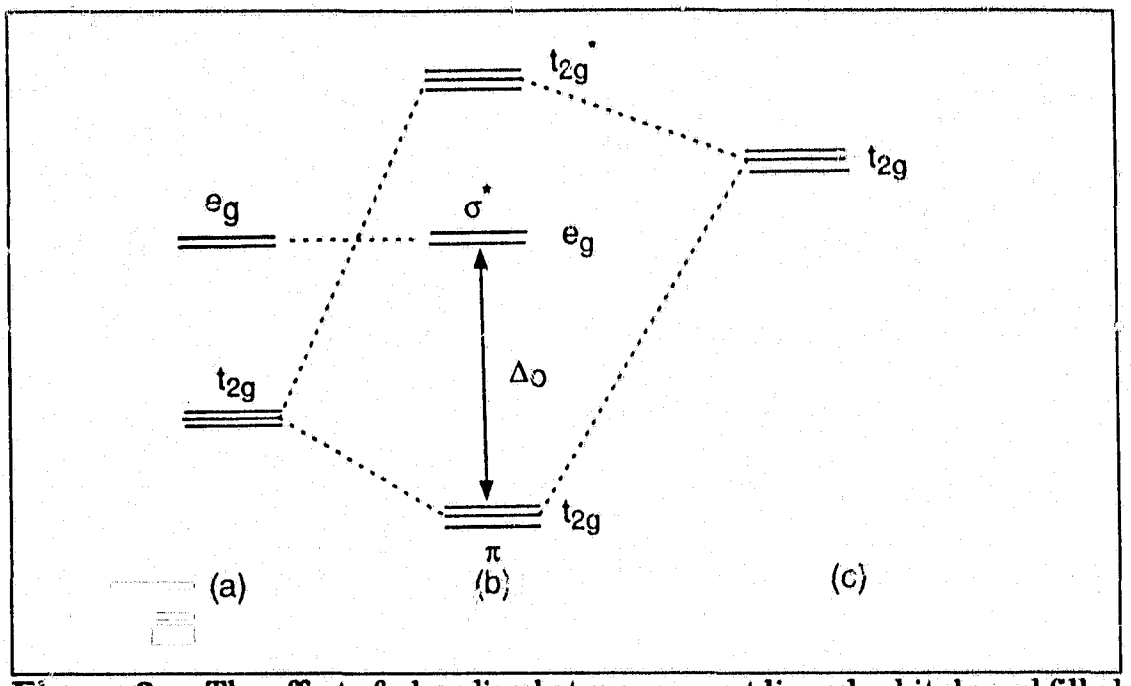

Figure 3 The effect of π bonding between vacant ligand orbitals and filled metal d orbitals on the MO of a metal complex . (a) Filled metal d orbitals, (b) MO of the complex, (c) vacant ligand orbitals.

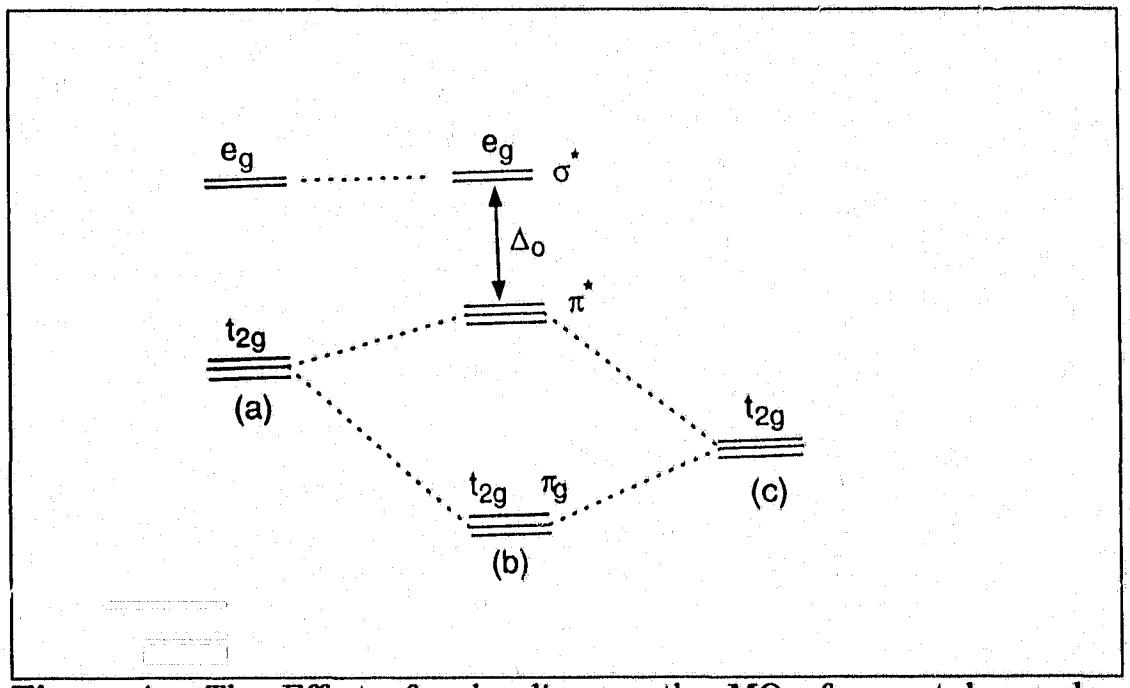

Figure 4 The Effect of π bonding on the MO of a metal complex. (a) Vacant or partially filled metal d orbitals, (b) MO of the complex, (c) Filled ligand orbitals.

energy than that of the metal t_{2g} orbitals, e.g., in ligands such as CO, the interaction destabilizes the metal t_{2g} orbitals and Δ_o decreases (Figure 4).

Although this theory is still far from perfect in describing the true nature of bonding in transition metal complexes, it combines the ideas of molecular orbital theory developed by Mulliken[11] and crystal field theory developed by Bethe[8] and is now widely used in the interpretation of the electronic spectra of transition metal complexes[12].

In the past few decades, the rapid development of various spectroscopic methods such as NMR[13], ESR[14], Mössbauer spectroscopy[15] (which provide specific information about the electronic environment at the nucleus of an atom) and computerized X-ray diffraction methods[15] for detailed structural analysis have undoubtedly contributed towards a better understanding of the nature of bonding in coordination compounds.

1.2 Stability of Complex Ions in Aqueous Solution[1, 16]

When dissolved in water, metal ions generally exist as aqua complexes, $[M(H_2O)_x]^{n+}$, with water molecules directly bonded to the metal ion. Therefore the process of complex formation in aqueous solution involves the displacement of water molecules by another set of ligands. The degree of complexation observed when the system has reached equilibrium is governed by the differences in the strength of the metal ion-ligand interactions and metal ion-solvent (usually water) interactions.

For a solution containing aqueous metal ions M and unidentate ligands L, the system at equilibrium may be described by the stepwise formation constant K_i or the overall formation constant β_n as shown by the following sets of equations.

Stepwise

$$M + L \rightleftharpoons ML \qquad K_1 = \frac{[ML]}{[M][L]}$$

$$ML + L \rightleftharpoons ML_2 \qquad K_2 = \frac{[ML_2]}{[ML][L]}$$

$$ML_{n-1} + L \rightleftharpoons ML_n \qquad K_n = \frac{[ML_n]}{[ML_{n-1}][L]}$$

Overall

$$M + L \rightleftharpoons ML \qquad \beta_1 = \frac{[ML]}{[M][L]}$$

$$M + 2L \rightleftharpoons ML_2 \qquad \beta_2 = \frac{[ML_2]}{[M][L]^2}$$

$$M + nL \rightleftharpoons ML_n \qquad \beta_n = \frac{[ML_n]}{[M][L]^n}$$

The number n represents the maximum coordination number or the metal ion for the ligand L. The overall formation constant β_n is related to the stepwise ones by the expression:

$$\beta_n = K_1K_2K_3.....K_n$$

A ligand for which K_n is large is one that binds more tightly than water. For the same ligand, the value of K_n decreases as n increases. This is due to the following reasons: (i) statistical factors related to the number of ligands (coordinated water molecules versus coordinated ligands) available for replacement as n increases; (ii) increase in steric hindrance as the number of ligands increases if they are bulkier than water molecules; (iii) coulombic factors if the ligands are charged. However, in some cases, when there is a major change in the structure and bonding at the metal center as more ligands are added, the stepwise formation constant may change abruptly. As an example, the tris(bipyridine) complex of Fe(II) is far more stable than the bis complex. This is attributed to a change from a weak field $t_{2g}^4e_g^2$ to a strong field t_{2g}^6 configuration.

The magnitude of the stability constant K_n depends on the nature of the metal ions and the ligands. The Hard and Soft Acid Base (HSAB) principle[17] has been widely used to provide a rough guideline for rationalizing the stabilities of complexes in aqueous solution. According to this principle, hard acids and bases are ions that have high charge densities and are bind together primarily by ionic bonds. Early transition metal ions of high oxidation states (e.g., Sc^{3+}, Cr^{3+}, Fe^{3+}), are "hard" and bind strongly to F^- and OH^-. The trend in stability constants for these ions follows the hardness of the donor atoms:

$F^- > Cl^- > Br^- > I^-$ $\qquad$ O > S $\qquad$ N > P > As

On the other hand, soft acids bind bases by covalent bonds which are strongest when the atoms are similar in size and electronegativity. Late transition metal ions with low oxidation numbers (e.g., Pd^{2+}, Pt^{2+} Ag^{+}, Hg^{2+}) are soft and form π bonds by donation to suitable ligands such as CO and phosphines. The stability constants for these ions follows an opposite trend compared to those of the hard ions:

$I^- > Br^- > Cl^- > F^-$ $\quad$ $S > O$ $\quad$ $As > P > N$

For the first row divalent transition metal ions (i.e., from V^{2+} to Zn^{2+}), however, the variation in the stability constants depends on crystal field stabilization energies and can be summarized by the "Irving-Williams series":[16]

Mn^{2+} (d^5) < Fe^{2+} (d^6) < Co^{2+} (d^7) < Ni^{2+} (d^8) < Cu^{2+} (d^9) > Zn^{2+} (d^{10})

The fact that the stability constants of Cu(II) complexes are greater than those of Ni(II) despite the presence of an electron in the antibonding e_g orbital in Cu(II) is due to an additional stabilization from Jahn-Teller distortion.

1.3 Chelate Effect[18]

In general, for a metal ion M^{n+}, the stability constant K_1 for the formation of a polydentate complex containing chelate rings (e.g., $[M(en)_n]^{n+}$, where en is ethylene diamine) is greater than the overall stability constant β_n for the corresponding monodentate ligand complex (e.g., $[M(NH_3)_n]^{n+}$). Such an increase in stability of a complex containing five or six membered chelate rings compared to their nonchelated analogs is called the **chelate effect**. For example[19],

$$[Cu(H_2O)_6]^{2+} + en \rightleftharpoons [Cu(H_2O)_4(en)]^{2+} + 2\,H_2O$$

$\log \beta_1 = 10.6$, $\Delta H^o = -54\ kJmol^{-1}$, $\Delta S^o = +23\ JK^{-1}mol^{-1}$

$$[Cu(H_2O)_6]^{2+} + 2\,NH_3 \rightleftharpoons [Cu(H_2O)_4(NH_3)_2]^{2+} + 2\,H_2O$$

$\log \beta_2 = 7.7$, $\Delta H^o = -46\ kJmol^{-1}$, $\Delta S^o = -8.4\ JK^{-1}mol^{-1}$

For the above system in equilibrium, the overall stability constant β_2 is related to the free energy change ΔG^o by the following expression:

$$\Delta G^o_n = -RT\ ln\ \beta_n$$

$$\Delta G^o = \Delta H^o - T\Delta S^o$$

The chelate effect arises mainly from the favourable entropic contribution. Whereas there is no net change in the number of independent molecules in solution with monodentate ligands, there is an increase in the chelation reaction. Only one molecule of ethylenediamine is required to displace two water molecules and there is a net gain of one unbound water molecule. Alternatively, the chelate effect can be viewed as an increase in translational entropy. This had led to several simple semi-quantitative approach to the chelate effect which has been discussed elsewhere[18].

1.4 Macrocyclic Ligands

A macrocyclic ligand is usually defined[20] as a polydentate ligand which contains three or more donor atoms in a cyclic array consisting of at least nine atoms (including the heteroatoms). This class of ligand complexes has long been recognized in several biological systems. For example, the importance of the porphyrin ring **1** complexed to iron in heme to the transport of oxygen

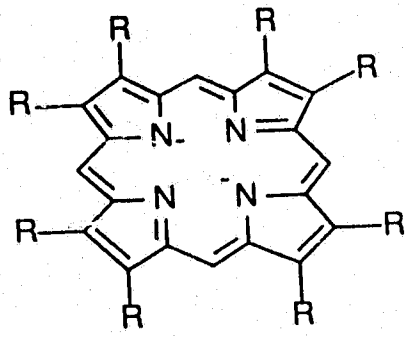

1

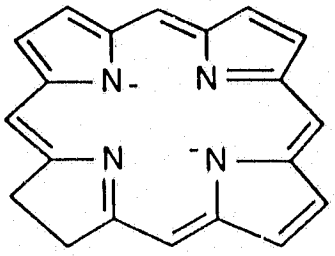

2

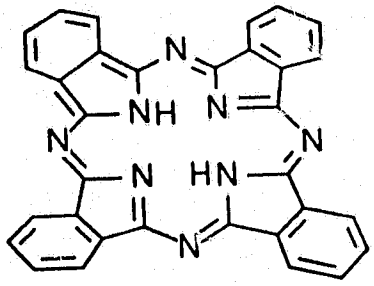

3

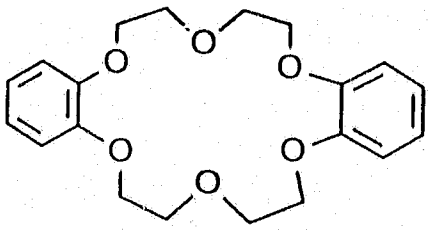

4

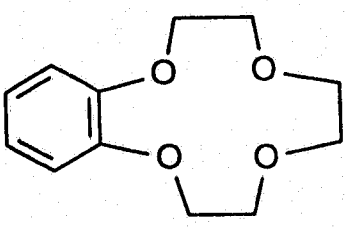

5

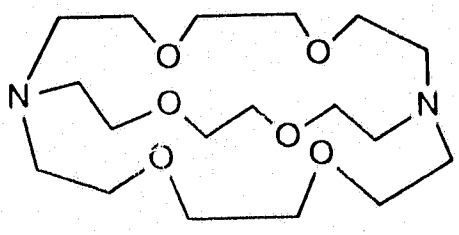

6

in mammalian and other respiratory systems[1] and the partially reduced porphyrin **2** (namely, a chlorin derivative) coordinated to magnesium in chlorophyll[1] to the mechanism of photosynthesis.

The realization that synthetic macrocyclic compounds may provide attractive model systems for many metalloproteins has provided an impetus for further research in this area. Prior to 1960, metal complexes of the highly conjugated phthalocyanines **3** were the only well-established class of synthetic macrocycles[20]. This is in part due to the strong resemblance between phthalocyanines and its derivatives to the naturally occurring porphyrin systems and also to their commercial importance as pigments and dyestuff.

In 1967, Pederson[21] synthesized a series of cyclic polyethers (now commonly known as crown ethers) with different ring sizes and substituent groups (e.g., **4** and **5**) having the ability to coordinate alkali metal and alkaline earth ions strongly in non-aqueous solutions. This discovery broadened the field of macrocyclic chemistry to include metal ions not previously studied. Shortly afterwards, Lehn and coworkers[22] reported the synthesis of the first macropolycyclic ligand **6** (now known as cryptand) which can accommodate a metal ion of suitable size and to form an inclusion complex. Since then, a large number of synthetic macrocycles with N, S, P and Se as donor atoms have been synthesized[20]. This undoubtedly has increased the interest in all aspects of the chemistry of macrocyclic systems.

1.5 Special Properties of Macrocyclic Complexes

Perhaps the most important factor that has escalated the interest in macrocyclic complexes for the last three decades is the realization of the unusual properties these ligands impose on their metal complexes when compared to their open chain analogues.

(a) Enhanced thermodynamic stability

Macrocyclic ligands form metal complexes of considerably greater thermodynamic stability and they are much more inert with respect to ligand dissociation. This permits the study of reactivities of many metal ions in strongly acidic or alkaline media. The "Macrocyclic Effect" is a term coined by Cabbiness and Margerum[23] to describe the additional stability of complexes containing macrocyclic ligands when compared to those formed with open chain ligands of similar structure. The thermodynamic parameters for the complexation reactions of 2,3,2-tet (1,4,8,11-tetraazaundecane) and cyclam (1,4,8,11-tetraazatetradecane) and those of 18-crown-6 and pentaglyme in 100% methanol[24] are shown in Tables1 and 2, respectively. These results suggest that the macrocyclic effect arises mainly from a more favourable enthalpic contribution from the macrocyclic complexes.

The microscopic nature of macrocyclic effect, however, is still a topic of current discussion[18a]. From the Born-Haber cycle shown in Figure 5 for both the formation of the macrocyclic complex and its open chain analog, some of the factors that may be important are: (i) less ligand desolvation enthalpies

Table 1

Thermodynamic parameters for the complexation of 2,3,2-tet and cyclam[18a]

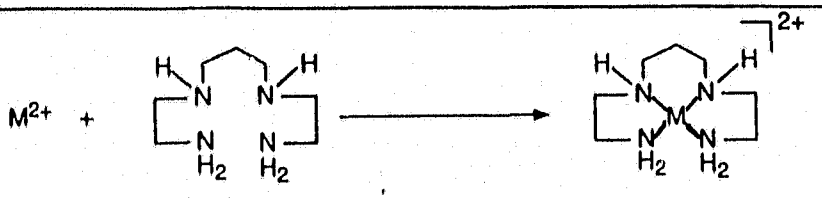

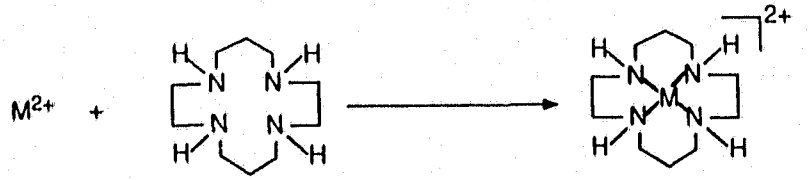

		Cu(II)	Ni(II)	Zn(II)
log K_1	cyclam	26.5	19.4	15.5
	2,3,2-tet	23.2	15.9	12.6
ΔH	cyclam	-32.4	-24.1	-14.8
	2,3,2-tet	-27.7	-18.6	-11.9
ΔS	cyclam	13	8	21
	2,3,2-tet	13	10	18

Table 2

Thermodynamic parameters for the complexation of 18-crown-6 and pentaglyme ($CH_3(OCH_2CH_2)_5OCH_3$) in 100% methanol[24]

		Na^+	K^+	Ba^{2+}
logK_1	18-crown-6	4.36	6.06	7.04
	pentaglyme	1.44	2.1	2.3
ΔH	18-crown-6	-8.4	-13.4	-10.4
	pentaglyme	-4.0	-8.7	-5.69
ΔS	18-crown-6	-8	-17	-3
	pentaglyme	-7	-20	-8

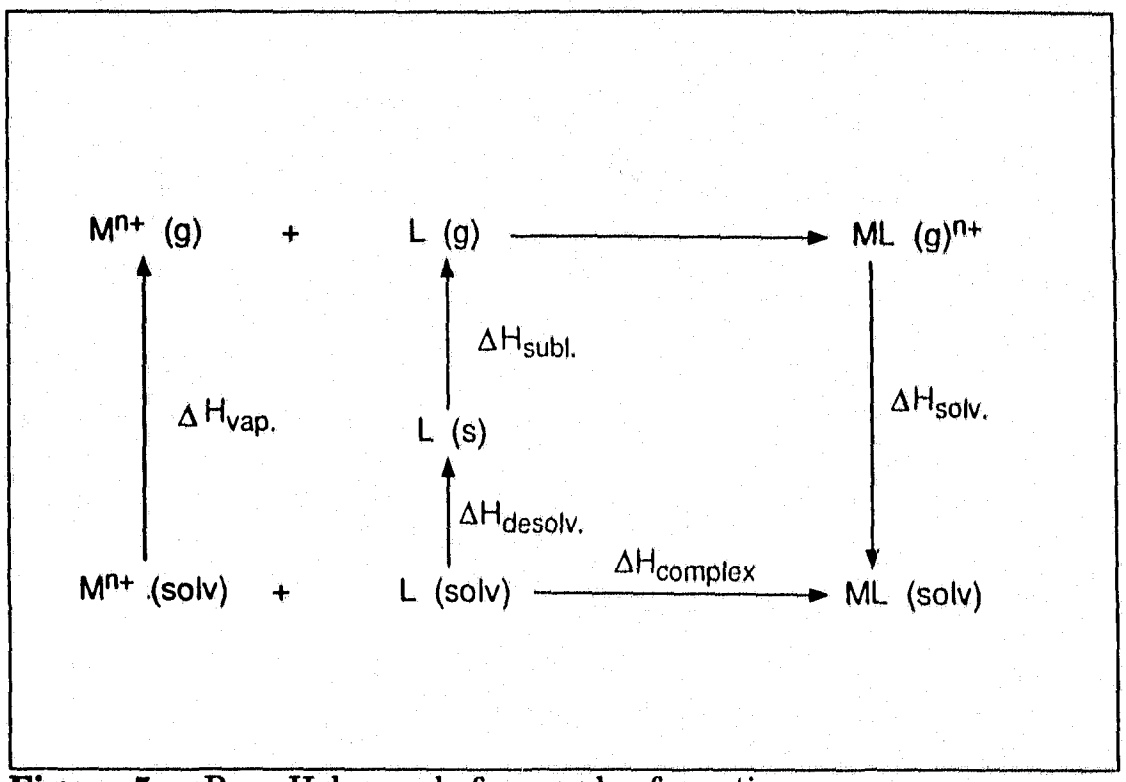

Figure 5 Born-Haber cycle for complex formation.

for macrocyclic ligands than the open chain analogues[23,25]; (ii) less geometrical change on coordination for macrocyclic ligand than the open chain analogues and therefore there is a less loss of internal entropy[26]; (iii) greater basicity of the donor atoms of the macrocyclic ligands[27].

The macrocyclic effect involving complexes of thioether donor atoms has also been studied. For these systems in general, a significantly smaller macrocyclic effect is observed compared to their amine analogs. For example, the stability constant of the Cu(II) complex of [14]aneS_4 is only a hundred times more stable in water than its open chain analog[28] (Figure 6). This is

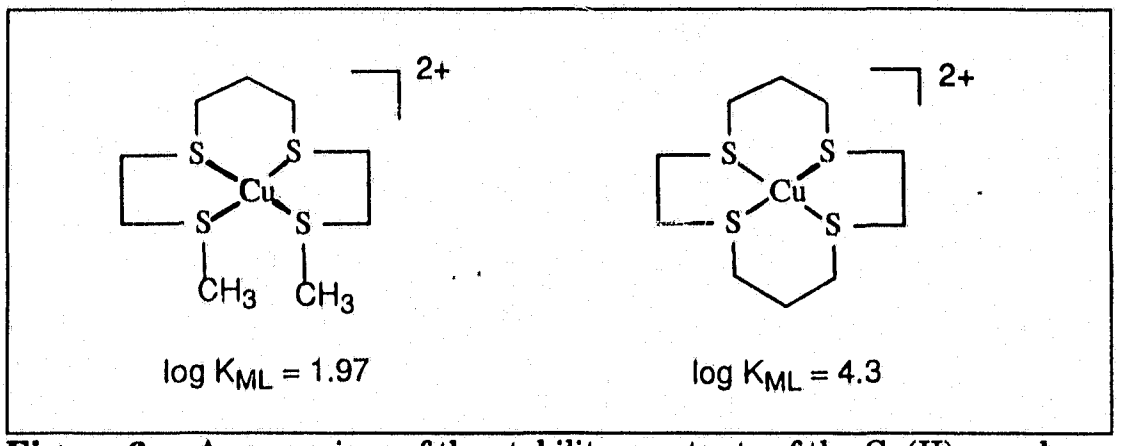

Figure 6 A comparison of the stability constants of the Cu(II) complexes of [14]aneS_4 and its open chain analog in water at 25 °C.

because the free ligand adopts a conformation in which the lone pairs of the S atoms are directed out of the ring[29]. Consequently, more reorganization energy is required prior to the complexation reaction.

(b) Enhanced kinetic stability

Busch and coworkers[30] attributed the enhanced stabilities of macrocyclic complexes to their kinetic inertness towards ligand dissociation. Relative to the corresponding open chain complexes, macrocyclic complexes are inert towards demetallation even in strong acidic media. This can be illustrated by the following example,

$$Ni(2,3,2\text{-tet})^{2+} \xrightleftharpoons{H^+/H_2O} [Ni(H_2O)_6]^{2+} + 2,3,2\text{-tet}(H^+)_n$$

$$Ni(cyclam)^{2+} \xrightleftharpoons{H^+/H_2O} \text{No Reaction}$$

The dissociation of $[Ni(2,3,2\text{-tet})]^{2+}$ in 0.5 M acid[31] has a rate constant of 0.38 s^{-1} whereas that of $[Ni(cyclam)]^{2+}$ has a half-life of over 30 years[32].

One hypothesis[20,30] for the enhanced kinetic stability is that straight chain ligand can undergo successive S_N1 replacement steps of the nitrogen donors by solvent molecules starting at one end of the ligand. In acidic media, the dissociated groups are quickly protonated and not available for complexation afterwards. On the other hand, a cyclic ligand has no terminal for the dissociation to begin. It may require unfavourable rearrangement such as folding within the coordination sphere before dissociation can occur.

(c) Stabilization of less common oxidation states

Macrocyclic ligands have the ability to stabilize unusual oxidation states of metal ions. In early studies, Cook and Curtis[33] reported the preparation of the first authentic Ni(III) complex by the addition of nitric acid to a Ni(II) complex of a cyclic tetramine (eq. 1). Soon afterwards, Olson and Vasilevskis[34] reported the electrochemical generation of Ni(III) and Cu(III) complexes of these cyclic tetramines.

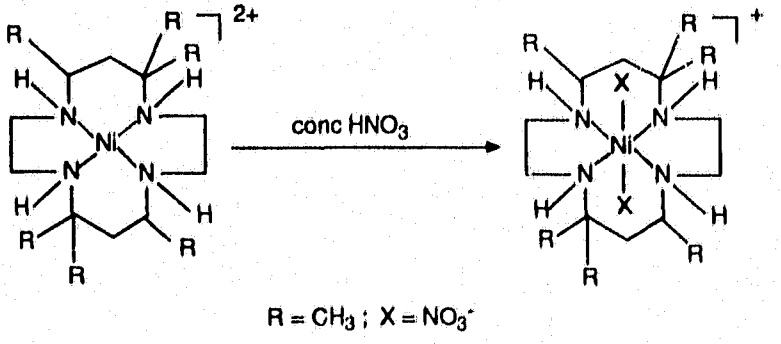

(1)

In 1974, Busch and coworkers[35] published an extensive study of the electrochemical behavior of twenty-seven low spin Ni(II) complexes of tetraaza macrocycles. Their study suggested that the overall redox properties of a given system depends on the ring size, the charge on the ligand, the nature of ligand substituents and the extent of unsaturation in the ligand framework. However, it appears that the ligand cyclam most favours the oxidation of Ni(II) to Ni(III)[36]. This has been attributed to the extremely large in-plane ligand field imposed by cyclam on the metal ion. Consequently, the energy level of the d_{x2-y2} orbital is raised and the removal of an electron from this orbital is easier.

Other examples of macrocyclic complexes with uncommon oxidation states are: (i) the disproportion of Ag(I) cyclam to produce a silver mirror and a stable Ag(II) complex of the ligand[37]; (ii) the stabilization of monomeric Pd(III) by 1,4,7-triazacyclononane[38] (**7**) and 1,4,7-trithiacyclononane[39] (**8**); (iii) the stabilization of Pd(I) by 1,4,8,11-tetramethyl-1,4,8,11-tetra-azacyclotetradecane[40] (**9**) and 7,16-dimethyl-1,4,10,13-tetrathia-7,16-diazacyclooctadecane[41] (**10**).

In summary, the ability of macrocyclic ligands in stabilizing unusual oxidation states of metal ions may be attributed to the structural constraint the ligand framework imposed on the metal ions which results in their immobilization[30]. Therefore oxidation states that have been rare may be more accessible.

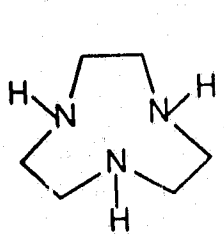

7

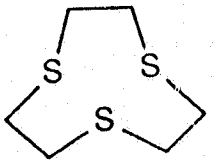

8

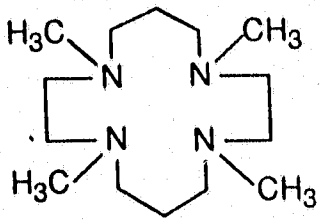

9

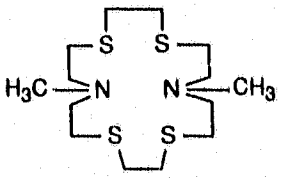

10

1.6 General Synthetic Methods For Macrocyclic Ligands

In general, macrocyclic ligands can be prepared[20,42] by a template reaction around a metal ion or direct synthesis.

(a) Template syntheses

The template synthesis with a suitable metal ion usually gives a reasonable yield of the required product (Table 3). However, the removal of the coordinated metal ion from the macrocycle usually requires vigorous conditions such as refluxing the macrocyclic complex in strong acidic medium (e.g., H_2SO_4) or in the presence of a strongly competing ligand (e.g., S^{2-}, CN^- or $EDTA^{4-}$) for several days. In the case of kinetically inert complexes such as Cr(III) and Co(III), a reduction may be required to reduce the metal ion into a more labile state before any demetallation reaction can take place.

Historically, the first synthetic macrocyclic complex, an Fe(II) complex of phthalocyanine, was obtained as a side product during the preparation of phthalimide by the reaction of phthalic anhydride and ammonia in an iron vessel[43]. This was followed by Curtis[44] who isolated a pair of isomeric Ni(II)

Table 3
A comparison of the synthesis of cyclam by different methods.

	Yield
template synthesis[47(a)]	
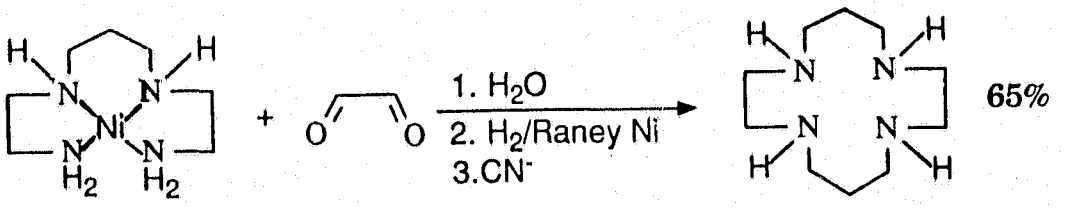	65%
high dilution[47(b)]	
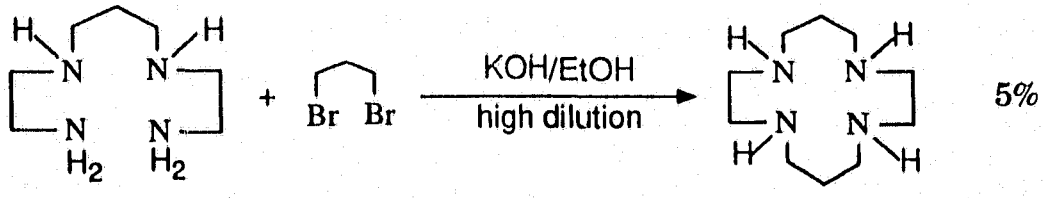	5%
Richman/Atkins synthesis[54]	
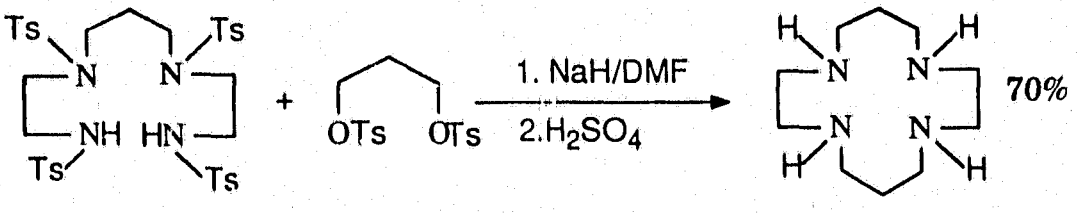	70%

macrocyclic complexes by the reaction between *tris*-ethylenediaminenickel(II) perchlorate and acetone (eq. 2).

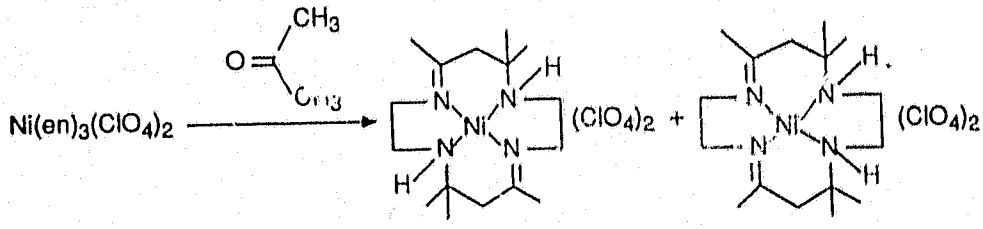

(2)

Two possible roles for the metal ion in a template synthesis have been suggested[45]. According to the kinetic coordination template hypothesis, the coordination sphere of the metal ion may serve as a template to hold reactive groups in proper position so that the formation of cyclic product is facilitated. According to the thermodynamic (or equilibrium) coordination template effect, the metal ion promotes the formation of macrocycle by removing the cyclic product from an equilibrium mixture of reactants and products via the formation of metal complexes. The metal ion may also stabilize a ligand structure which might otherwise be unstable in the pure organic chemical system at equilibrium by the formation of macrocyclic complex. As examples, Schiff base ligand such as bisacetyl bis(methylimine) **11** and the tetraaza macrocycle discovered by Curtis cannot be isolated as a pure compound without the metal ion.

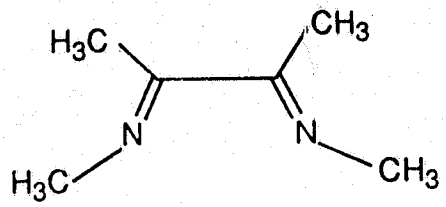

11

A typical template reaction which involves the formation of a macrocyclic ligand that completely encloses a planar metal ion can be represented in eq. 3[42]. It is clear that in order to conduct template reactions of this kind, the original ligand must be tetradentate and chelates in a planar or other suitable

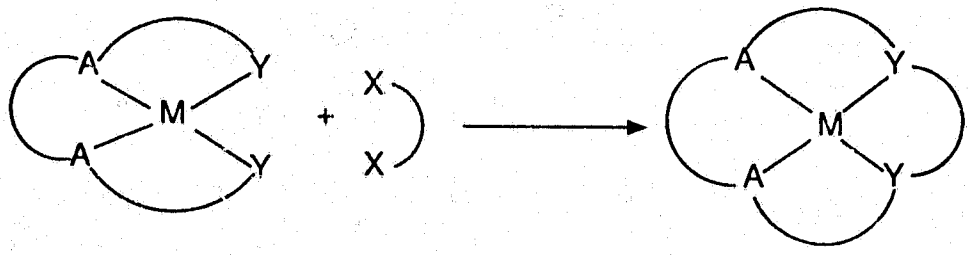

(3)

fashion and the end groups (Y) must undergo an addition reaction with the ring-forming groups. In practice, nucleophilic reactions between the ligating atoms of the coordinated tetradentate ligand and the ring forming groups have been widely utilized. The commonly used reactions are those involving coordinated mercaptide ions and alkyl halides and also the Schiff base condensation between coordinated ammines and aldehydes (or ketones). Examples which may be cited include the reaction of the complexed mercaptoimine **12** and α,α-dibromo-o-xylene[45,46] which results in the formation of a macrocycle with both nitrogen and sulphur as donor atoms as shown in eq. 4 , the condensation of 2,3,2-tet and gloxal in the presence of

Ni(II)[47] (Table 3) and the self-condensation of o-aminobenzaldehyde in the presence of metal ions[48] as shown in eq. 5.

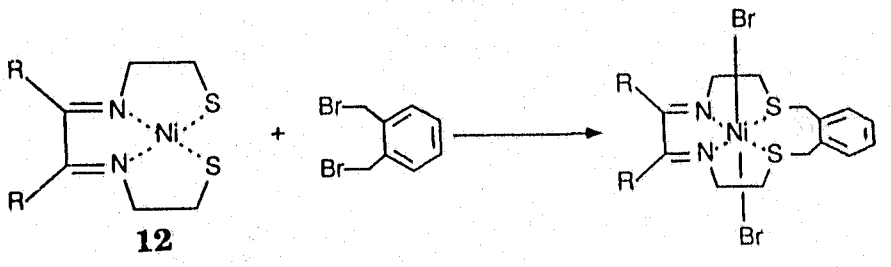

(4)

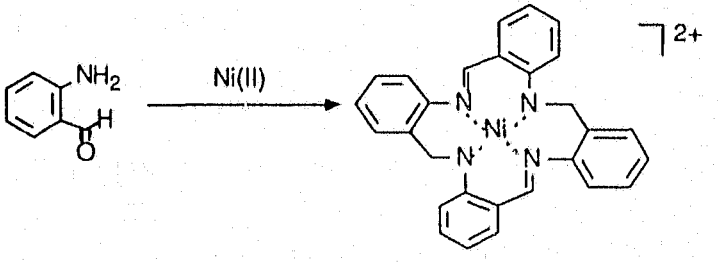

(5)

In principle, an encapsulation reaction in which a metal ion is wrapped by a poly-macrocyclic ligand is also feasible by the use of template process. Perhaps the most elegant species obtained so far is Co(III) sepulchrates **13** prepared by Sargeson and coworkers[49]. Another remarkable example of a new family of macrocyclic ligands made accessible by template reactions is the

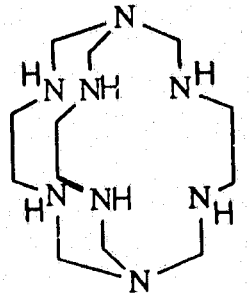

13

catenanes synthesized by Sauvage and coworkers[50] in which two macrocyclic rings are isolated as an interlocking ligand system by the use of Cu(I) during the synthesis (Scheme 1).

Scheme 1

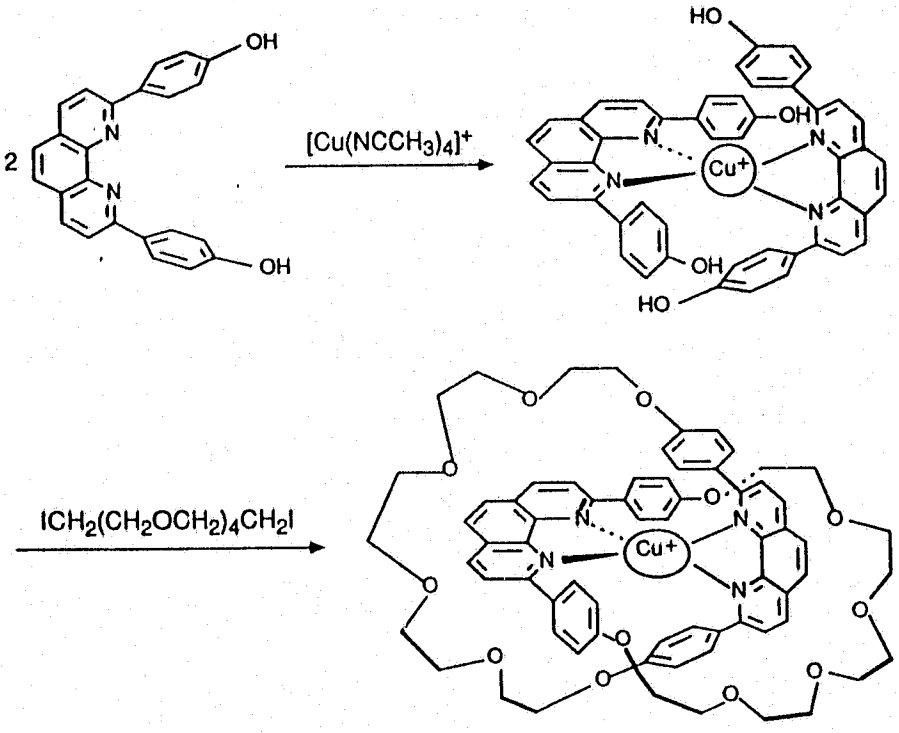

Finally, the ability of a particular ion to act as a template is affected by the compatibility between the size of the metal ion and the macrocyclic cavity formed in the product. For example, the condensation of 2,6-diacetylpyridine with bis(3-aminopropane)amine[51] in the presence of small ions such as Co(II), Ni(II) and Cu(II) results in the formation of a 14-membered macrocyclic

complex **14**. On the contrary, when larger Ag(I) ion is used, a 28-membered macrocyclic complex **15** is isolated.

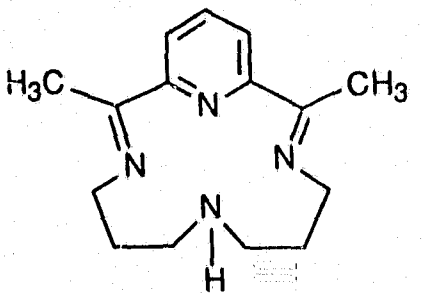

14

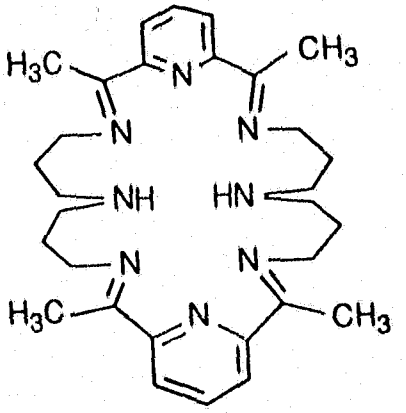

15

(b) direct syntheses

The direct synthesis of macrocyclic ligands usually gives variable yields due to a lack of stereochemical control during the cyclization process. However, this method provides the advantage that the macrocyclic ligand can be isolated, purified and characterized before the synthesis of the complex. In addition, any changes in the macrocyclic ligand upon complexation can also be detected by comparing the physical properties of the free ligand.

The direct synthesis of a macrocyclic ligand usually requires the use of the two reagents consisting of the required fragment of the target in equimolar concentrations. This is to ensure the occurrence of a 1:1 condensation. Moreover, a high dilution condition[52] (final concentration of reagents ca. 0.001 M) is necessary to enhance the prospect of an intramolecular reaction in which a "half-condensed" moiety reacts with itself in a "head-to-tail" fashion

Scheme 2

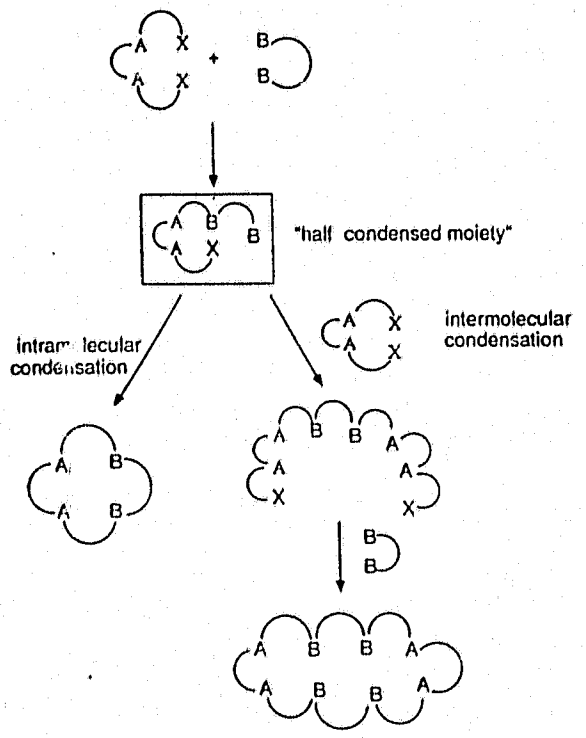

instead of an intermolecular reaction with another fragment to give oligomers (Scheme 2).

In practice, during the preparation of the macrocycle, two precision dropping funnels are used to dispense measured amounts of reagents into the solvent at a very slow rate (ca. 5 mL/hr). This establishes a low and stationary concentration of the reactants and steers the cyclization reaction in such a way that ideally the same amount of starting material is flowing into the reaction flask per unit time as the amount reacted and therefore optimizing the formation of the target macrocycle[52]. Such reactions normaliy require several

Scheme 3

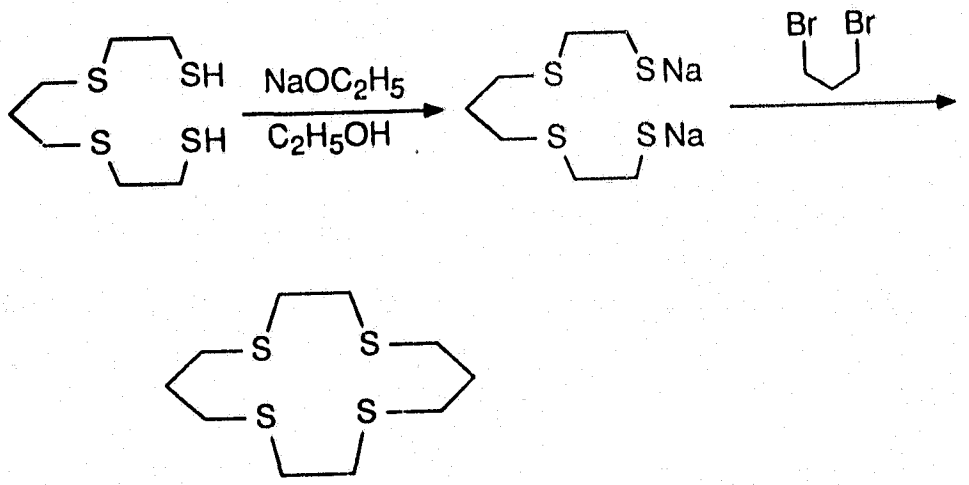

days to complete but for some systems, there is a dramatic improvement in product yield. For example, the yield of [14]aneS_4 is improved from 7½ % to 55 % when the reaction is performed under high dilution conditions[53] (Scheme 3).

In the mid-1970's, an alternative general synthesis of polyaza macrocycles was reported by Richman and Atkins[54]. This procedure makes use of pre-tosylated reactants to achieve cyclization in high yields (usually better than 50 %, see Table 3) without the use of high dilution conditions. The bulky tosyl groups decrease the number of conformational degress of freedom (e.g. bond rotation) in the reactants and intermediates so that cyclization instead of polymerization is favored.

Another significant improvement in the cyclization reaction includes the use of cesium salts introduced by Kellogg and coworkers[55]. For example, in the synthesis of [14]ane S_4, the use of a suspension of Cs_2CO_3 in N,N-dimethylformaide (DMF) has increased the product yield to 62%[56] (eq. 6). The cesium ion promotes the cyclization by forming weak ion pairs with the thiolate ion RS^-, which would make them extremely nucleophilic and under dilution conditions, this would favor intramolecular S_N2 reactions of the "half-condensed" halo-thiolate intermediate.

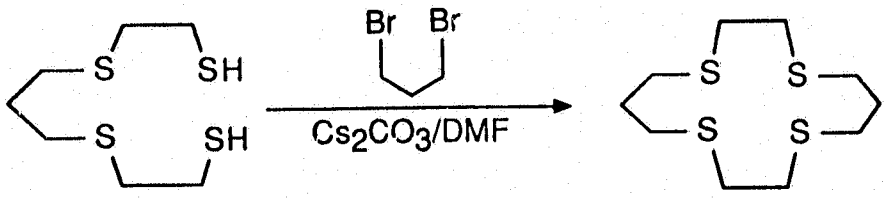

(6)

1.7 Objectives of the research

Macrocyclic ligands containing sulphur and nitrogen donor atoms have been studied in this project. The structures of these ligands are shown in Figure 7. At the beginning of this work, there were relatively few studies of metal complexes containing both of these donor atoms in the literature[57]. This is in part due to the synthetic demand in the preparation of the ligand. Our interest in these systems arises from the presence of similar coordination

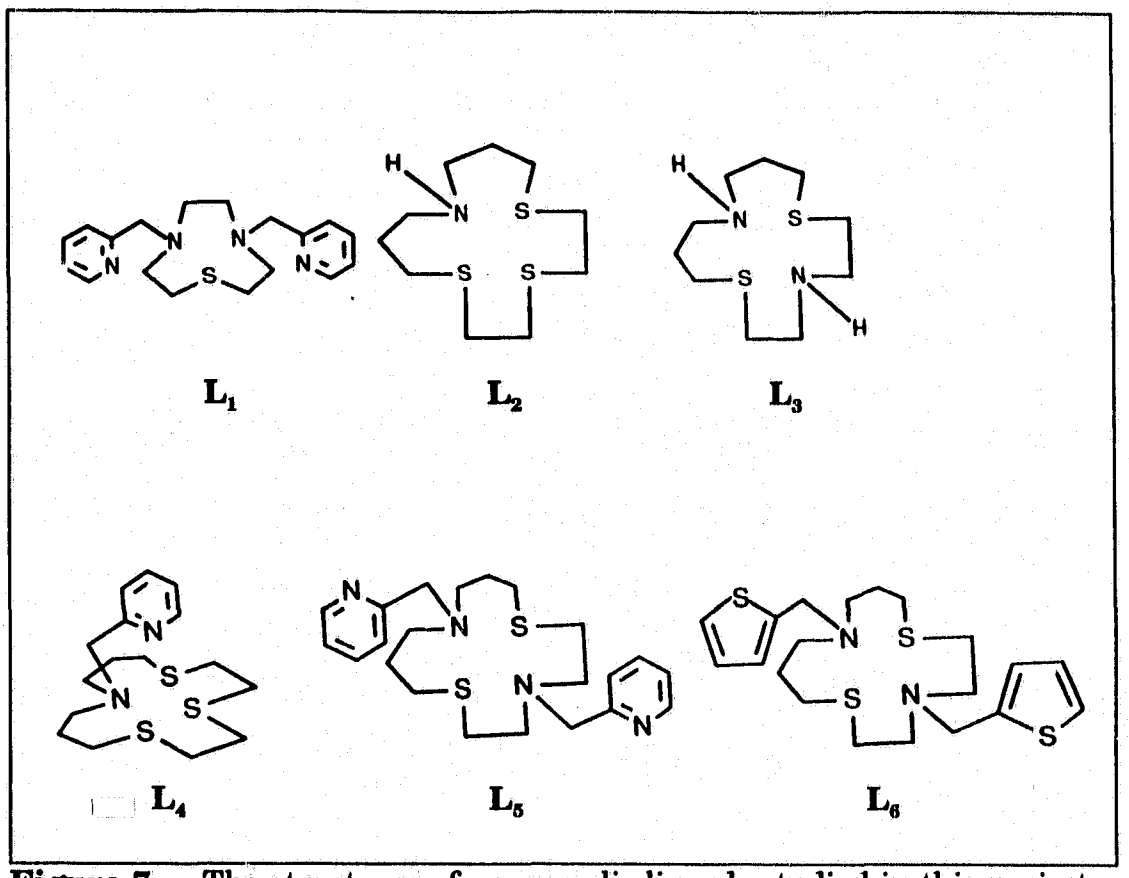

Figure 7 The structures of macrocyclic ligands studied in this project.

environment around metal centres in copper proteins[58] and the possibility that these systems may combine the complex properties of aza and thia macrocycles to stabilize high and low oxidation states of a metal centre.

A number of pendant arm ligands with pyridine and thiophene moieties, L_4 - L_6 have also been included in this study. These ligands not only increase the number of possible coordination sites, but also may act as powerful binding sites for soft and heavy transition metal ions.

In the following chapter, the crystal structure and solution studies of Pd(II) complex of L_1 will be discussed. The solid state structures and solution studies of Pd(II) complexes of L_2 - L_4 will be presented in Chapter 3, with special emphasis on the fluxional behavior of the Pd(II) complex of L_4 studied by variable temperature NMR spectroscopy. This is followed by the study of the solution behavior and crystal structures of Co(II), Ni(II) and Cu(II) complexes of L_2 - L_5. The solid state structures and solution chemistry of a Pd(II) macrocyclic complex with thiophene pendant arm (L_6) will be discussed in Chapter 5. Finally, the experimental details for the syntheses of these ligands and their metal complexes will be presented in Chapter 7.

CHAPTER 2

SYNTHESIS, STRUCTURE AND SOLUTION STUDIES OF THE PD(II) COMPLEX OF 1-THIA-4,7-BIS(2-PYRIDYLMETHYL)-DIAZACYCLONONANE

2.1 Introduction

The element palladium has an electronic configuration of [Kr]$4d^{10}$. Due to the high third ionization potential, the chemistry[1,59] of this metal is dominated by the +(II) oxidation state, which has an electronic configuration of d^8. Second and third row transition metal ions (e.g., Pd(II) and Pt(II)) exhibit a larger crystal field stabilization energy than the first row elements[10]. In the case of a d^8 ion, this stabilization energy outweighs the pairing energy and the two electrons in the e_g orbitals pair up and occupy the d_{z2} orbital, leaving the d_{x2-y2} orbital empty (Figure 8). This causes a distortion away from an octahedral geometry towards square-planar, where a net stabilization of the d_{z2} orbital is obtained from $\Delta_{sq.pl.}$.

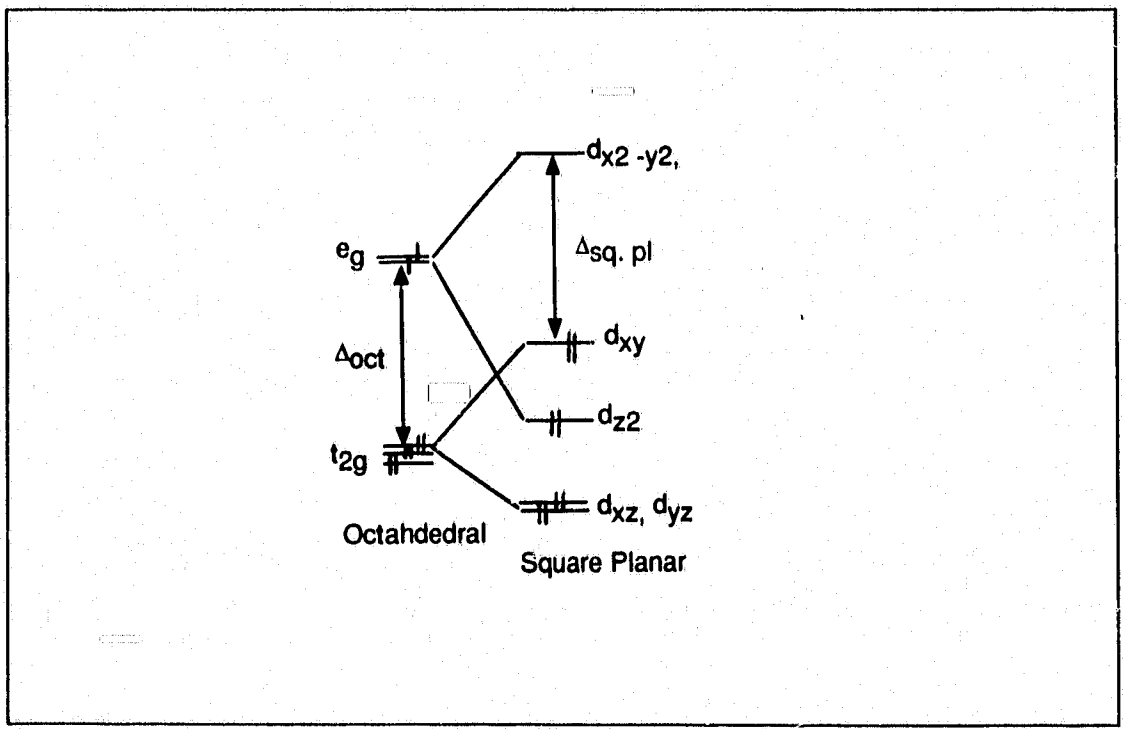

Figure 8 Energy level diagram for octahedral and square planar complexes of a d^8 ion.

In +(I) and +(III) oxidation states, the formation of binuclear compounds[1,59] with a M-M bond, e.g., $[(Cl)Pd(PPh_2CH_2PPh_2)]_2$, is observed, while mononuclear compounds[38] are very rare. The (0) oxidation state is represented by organometallic complexes[10] and metal clusters involving tertiary phosphines and/or carbonyl species[1], e.g., $Pd(PPh_3)_3$, $Pd_{23}(CO)_{22}(PEt_3)_{10}$.

Macrocyclic ligands have the ability to impart thermodynamic and kinetic stability to a variety of unusual oxidation states of metal ions[20]. This is exemplified by the ligand cyclam and the smaller macrocyclic compounds 1,4,7-triazacyclononane ([9]aneN_3, **7**)[60]; 1,4,7-trithiacyclononane ([9]aneS_3, **8**)[61], 1-thia-4,7-diazacyclononane ([9]aneN_2S, **16**)[62] and 7-aza-1,4-dithiacyclonane ([9]aneNS_2, **17**)[63]. The solution chemistry of these ligands involving Ni(III)[64] and Pd(III)[38,39] have been studied extensively. As a part of a continuing investigation of the chemistry of macrocyclic complexes of palladium, a macrocyclic ligand (L_1) with two pyridine pendant arms attached to the nitrogen atoms of [9]aneN_2S, has been synthesized. The nine-membered macrocyclic rings do not have a hole size large enough to accommodate a transition metal ion. They usually coordinate facially in octahedral complexes, although other geometry have been obtained[60]. In this investigation, the intention was that the combination of this mode of coordination of a nine-membered macrocycle, together with two strongly binding pyridine moieties in L_1 would favor penta-coordination. This in turn may lead to the stabilization

of the less accessible oxidation states and the formation of dimeric species upon oxidation to Pd(III) or reduction to Pd(I).

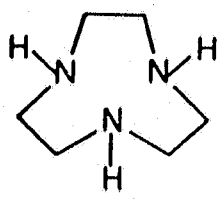

7

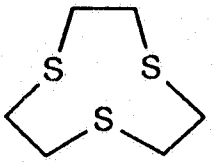

8

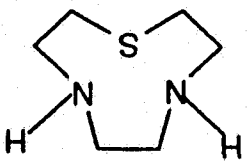

16

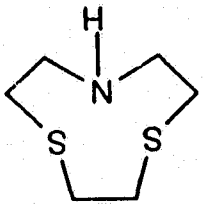

17

2.2 Synthesis

The synthetic route leading to the ligand (L_1) and its Pd(II) complex is outlined in Scheme 4. The dihydrobromide salt of 1-thia-4,7-diazacyclononane ([9]aneSN$_2$.2HBr) was prepared according to a literature method[62]. The pyridine moiety was introduced by reacting [9]aneSN$_2$ with two equivalents of 2-(chloromethyl)pyridine hydrochloride in the presence of a base in absolute ethanol. The ligand was isolated as a pale yellow oil in 60% yield.

Ligand L_1 was characterized by ^{1}H and ^{13}C NMR, as well as mass spectroscopy (MS). The ^{13}C NMR of L_1 exhibits nine lines which corresponds to the nine inequivalent carbon atoms in the molecule (Figure 9). The ^{1}H NMR is consistent with the ^{13}C NMR, exhibiting two singlets (δ 2.65 and 3.83) from the NCH$_2$CH$_2$N protons and the benzylic protons adjacent to the pyridine moiety, respectively. Two multiplets at δ 2.95 and 3.05 correspond to the

Scheme 4

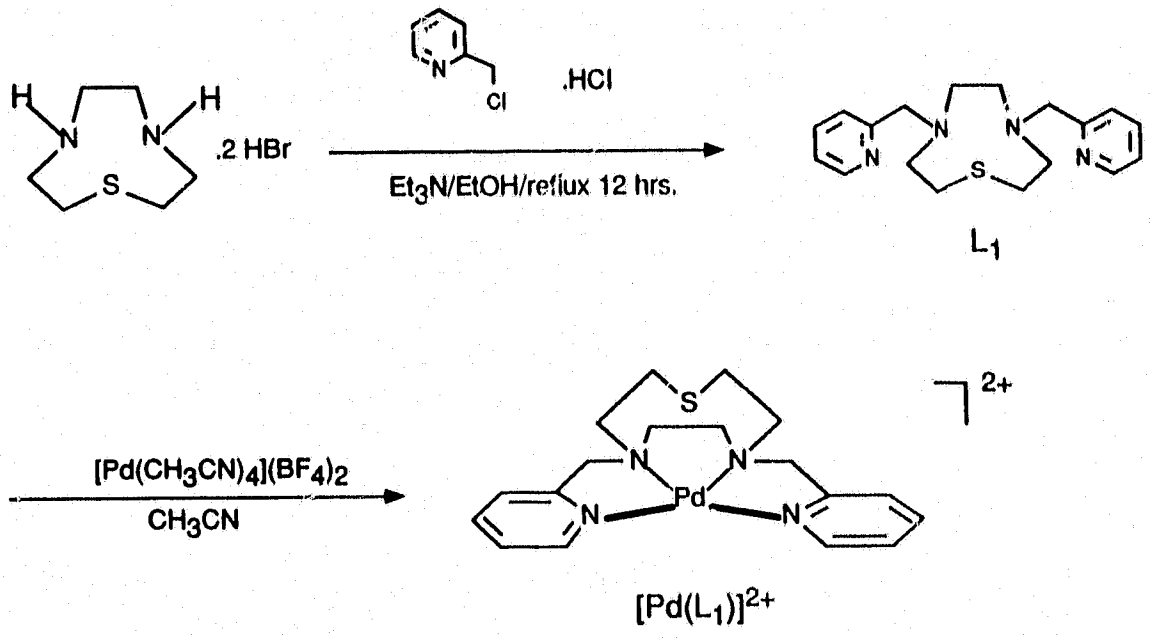

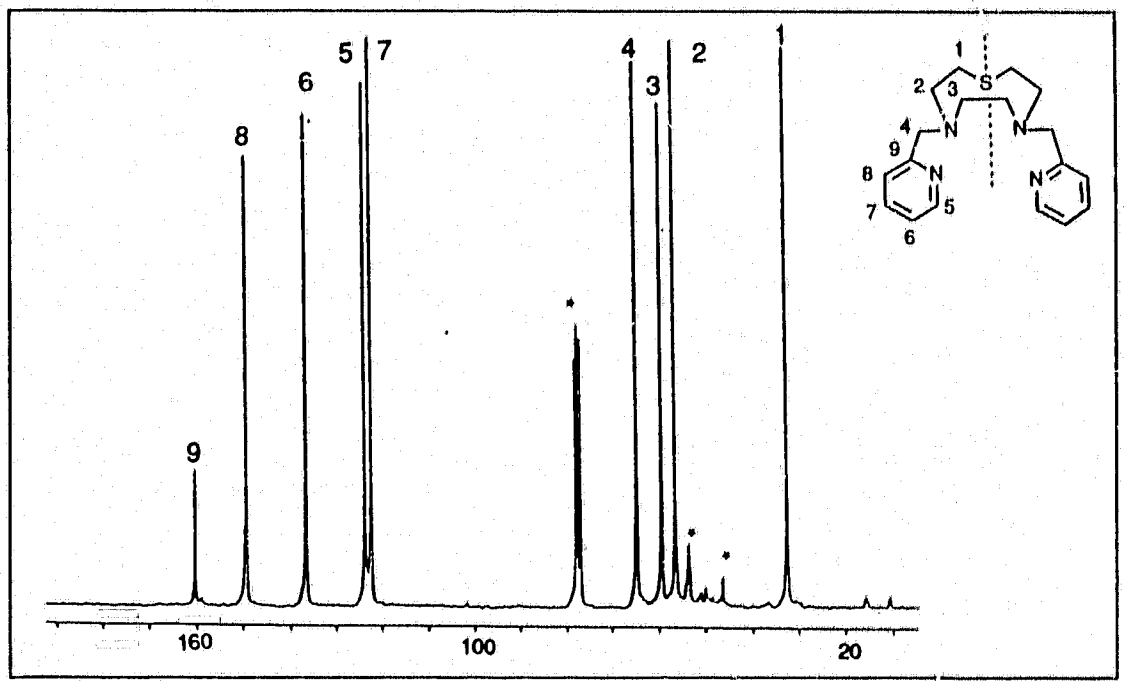

Figure 9 ^{13}C NMR spectrum of L_1 in $CDCl_3$. (* denotes solvent or impurity).

protons in the NCH_2 and SCH_2 fragments, respectively. Pyridine proton resonances are observed in the region of δ 7.12 - 8.48.

If exposed to in air and in the presence of light, $\mathbf{L_1}$ turned progressively darker in color. The degradation product was not characterized but to avoid the loss of ligand the metal complexes of $\mathbf{L_1}$ were prepared immediately after ligand isolation. The palladium(II) complex was prepared by the reaction of equimolar quantities of the ligand with $[Pd(CH_3CN)_4](BF_4)_2$ in dry CH_3CN under an atmosphere of nitrogen. X-ray quality crystals were obtained by slow diffusion of diethyl ether into an acetonitrile solution of $[Pd(\mathbf{L_1})]^{2+}$.

2.3 Crystal Structure

The Pd(II) complex of $\mathbf{L_1}$ has been characterized by crystallography and the molecular structure is shown in Figure 10, along with the atomic labelling scheme. The crystallographic parameters are given in Table 4. The fractional atomic coordinates, interatomic distances and bond angles are shown in Tables 5 - 7.

The Pd(II) center is in a distorted square-pyramidal environment. It is coordinated by nitrogen atoms from the two tertiary amines and two pyridine moieties, with an average bond distance of 2.04 Å. The five-membered chelate rings in the equatorial plane adopt an envelope conformation. The chelate bite angle N(1)-Pd(1)-N(2) is 87° which is comparable to the value of 86° observed in the palladium(II) complex of trien (triethylenetetraamine)[65] (Figure 11).

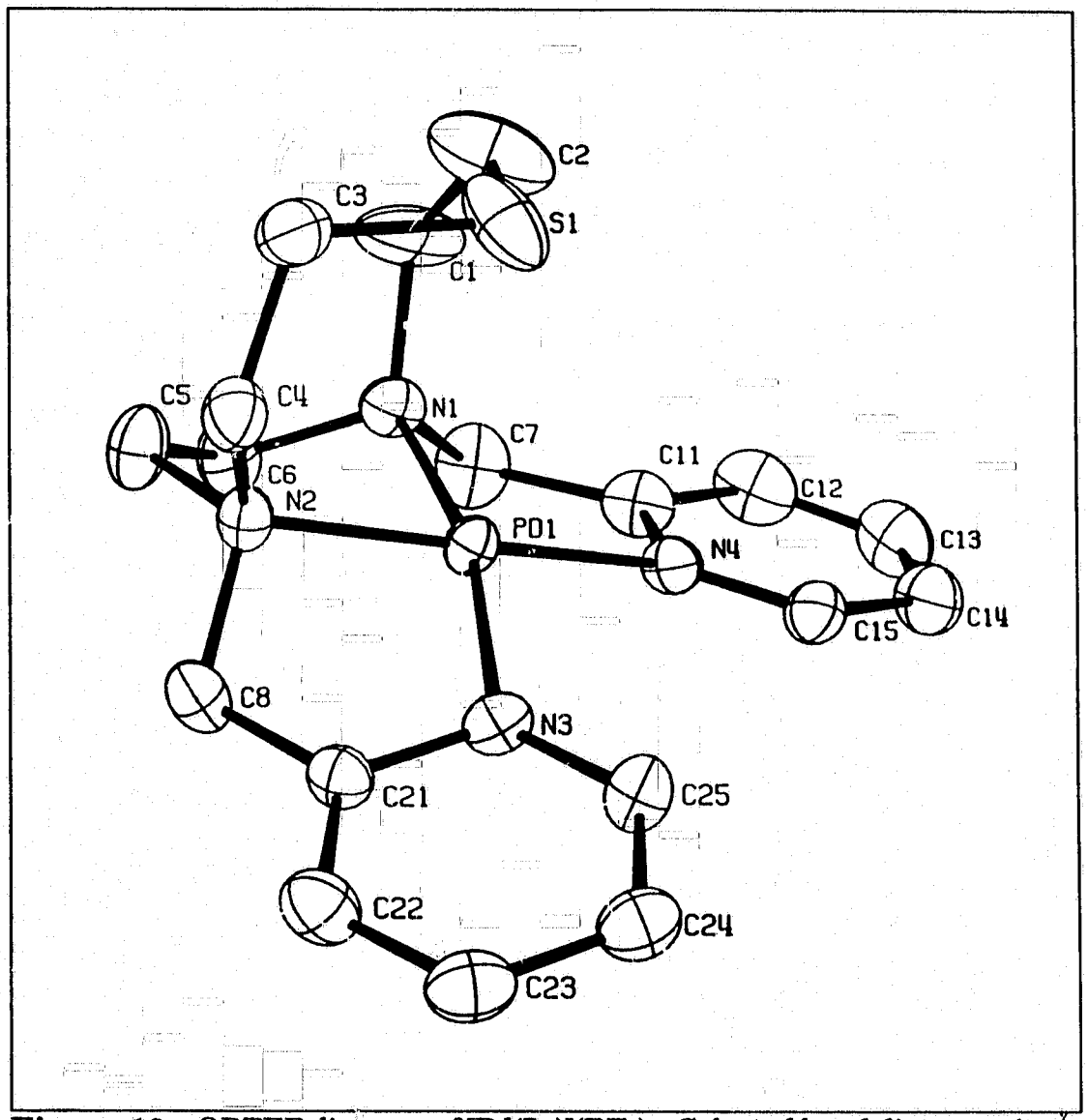

Figure 10 ORTEP diagram of $[Pd(L_1)](BF_4)_2$. Selected bond distances in Å: Pd...S(1) = 2.915(3), Pd-N(1) = 2.044(6), Pd-N(2) = 2.028(6), Pd-N(3) = 2.041(6), Pd-N(4) = 2.041(6).

Table 4
Experimental crystallographic data for $[Pd(L_1)](BF_4)_2$

Formula:	$PdC_{18}H_{24}N_4SB_2F_8$
F.W.:	608.5
Crystal colour:	reddish brown
Crystal system:	monoclinic
Space group:	$P2_1/n$ (No. 14)
Cell dimensions:	
	a = 10.233(4) Å $\quad \alpha = 90°$
	b = 11.484(5) Å $\quad \beta = 94.03(4)°$
	c = 19.913(6) Å $\quad \gamma = 90°$
V_{cell} :	2334 Å^3
Z:	4 molecules/cell
Temperature:	20 °C
Crystal dimensions:	0.61 x 0.64 x 0.24 mm^3
$D_{calcd.}$:	1.731 g/cm^3
$D_{meas.}$:	1.721 g/cm^3
Radiation:	Mo, K_α 0.71069 Å
μ:	8.64 cm^{-1}
Transmission range:	0.7[illegible] - 0.88
Measurement:	2θ(0-55°)
No. of reflections collected:	5356
No. of reflections $I \geq n\sigma(I)$:	3790 (n = 2)
No. of parameters:	367
Residual electron density:	0.2 e/Å^3
Maximum final shift/error:	0.005
Refinement method:	SHELX least squares
R:	0.0705
R_w:	0.0759

Table 5

Fractional atomic coordinates and temperature parameters for $[Pd(L_1)](BF_4)_2$

Atom	x/a	y/b	z/c	Ueq
Pd(1)	9182(5)	24179(4)	43892(3)	440(2)
S(1)	4950(31)	49140(25)	42078(14)	935(11)
N(1)	2840(5)	2927(6)	4469(4)	56(2)
N(2)	999(6)	2554(5)	3376(3)	54(2)
N(3)	-841(5)	1646(5)	4118(3)	53(2)
N(4)	1203(7)	2216(5)	5413(3)	52(2)
C(1)	3091(9)	4196(9)	4501(8)	122(6)
C(2)	2195(14)	5057(11)	4529(9)	155(8)
C(3)	534(9)	4747(7)	3314(5)	69(3)
C(4)	182(9)	3537(7)	3068(4)	63(3)
C(5)	2424(9)	2661(9)	3213(5)	76(3)
C(6)	3321(8)	2370(8)	3845(5)	74(3)
C(7)	3449(8)	2308(9)	5056(5)	81(4)
C(8)	369(8)	1422(7)	3120(4)	66(3)
C(11)	2508(9)	2323(7)	5614(5)	66(3)
C(12)	2898(12)	2364(9)	6304(6)	87(4)
C(13)	1985(13)	2260(9)	6766(6)	89(4)
C(14)	722(11)	2139(9)	6545(5)	78(4)
C(15)	353(9)	2139(7)	5865(4)	64(3)
C(21)	-828(7)	1251(6)	3473(4)	53(2)
C(22)	-1977(9)	714(8)	3156(5)	74(3)
C(23)	-3069(9)	572(8)	3511(6)	76(4)
C(24)	-3039(8)	976(8)	4186(5)	70(3)
C(25)	-1930(7)	1515(8)	4449(4)	61(3)
B(1)	6260(9)	4329(10)	3560(5)	64(3)
B(2)	1735(10)	3967(12)	1238(6)	74(4)
F(1)	6127(6)	3905(7)	4180(3)	119(3)
F(2)	7404(6)	4668(8)	3418(4)	147(4)
F(3)	5809(16)	3536(13)	3153(5)	265(9)
F(4)	5398(9)	5112(11)	3425(8)	244(8)
F(5)	1646(14)	4578(9)	1825(5)	213(7)
F(6)	2722(7)	4484(8)	961(5)	153(4)
F(7)	730(9)	4251(11)	884(8)	242(8)
F(8)	1803(16)	2869(9)	1334(10)	284(11)

Estimated standard deviations are given in parentheses.

Coordinates x 10^n where n = 5,5,4,4,4,4 for Pd,S,N,C,B,F.

Temperature parameters x 10^n where n = 4,4,3,3,3,3 for Pd,S,N,C,B,F.

U_{eq} = the equivalent isotropic temperature parameter.

$U_{eq} = \frac{1}{3}\Sigma_i\Sigma_j U_{ij} a_i^* a_j^* (a_i a_j)$ $T = \exp-(8\pi^2 U_{iso} \sin^2\theta/\lambda^2)$

Table 6
Interatomic Distances (Å) for $[Pd(L_1)](BF_4)_2$

Atoms	Distance	Atoms	Distance
S(1)-Pd(1)	2.915 (3)	C(5)-C(6)	1.538 (14)
N(1)-Pd(1)	2.044 (6)	C(11)-C(7)	1.519 (14)
N(2)-Pd(1)	2.028 (6)	C(21)-C(8)	1.467 (11)
N(3)-Pd(1)	2.041 (6)	C(11)-C(12)	1.402 (14)
N(4)-Pd(1)	2.041 (6)	C(12)-C(13)	1.361 (17)
C(2)-S(1)	1.815 (13)	C(13)-C(14)	1.341 (15)
C(3)-S(1)	1.791 (10)	C(14)-C(15)	1.377 (12)
C(1)-N(1)	1.480 (12)	C(22)-C(21)	1.431 (11)
C(6)-N(1)	1.507 (11)	C(22)-C(23)	1.373 (14)
C(7)-N(1)	1.466 (12)	C(23)-C(24)	1.420 (14)
C(4)-N(2)	1.506 (10)	C(24)-C(25)	1.362 (11)
C(5)-N(2)	1.520 (11)	F(1)-B(1)	1.341 (11)
C(8)-N(2)	1.521 (10)	F(2)-B(1)	1.282 (11)
C(21)-N(3)	1.361 (10)	F(3)-B(1)	1.281 (13)
C(25)-N(3)	1.342 (10)	F(4)-B(1)	1.274 (13)
C(11)-N(4)	1.370 (10)	F(5)-B(2)	1.369 (14)
C(15)-N(4)	1.297 (11)	F(6)-B(2)	1.324 (13)
C(2)-C(1)	1.351 (16)	F(7)-B(2)	1.245 (14)
C(3)-C(4)	1.506 (12)	F(8)-B(2)	1.276 (15)

Estimated standard deviations are given in parentheses.

Table 7
Bond Angles (deg) for $[Pd(L_1)](BF_4)_2$

Atoms	Angles	Atoms	Angle
N(1)-Pd(1)-S(1)	82.1(2)	C(1)-C(2)-S(1)	123.7(9)
N(2)-Pd(1)-S(1)	79.5(2)	C(4)-C(3)-S(1)	113.5(6)
N(2)-Pd(1)-N(1)	87.0(3)	C(3)-C(4)-N(2)	116.7(7)
N(3)-Pd(1)-S(1)	105.9(2)	C(6)-C(5)-N(2)	109.3(7)
N(3)-Pd(1)-N(1)	165.3(3)	C(5)-C(6)-N(1)	111.7(7)
N(3)-Pd(1)-N(2)	82.5(3)	C(11)-C(7)-N(1)	108.8(6)
N(4)-Pd(1)-S(1)	104.1(2)	C(21)-C(8)-N(2)	107.5(6)
N(4)-Pd(1)-N(1)	83.6(3)	C(7)-C(11)-N(4)	116.2(8)
N(4)-Pd(1)-N(2)	169.3(3)	C(12)-C(11)-N(4)	119.3(10)
N(4)-Pd(1)-N(3)	105.8(3)	C(12)-C(11)-C(7)	124.4(9)
C(2)-S(1)-Pd(1)	85.1(4)	C(13)-C(12)-C(11)	119.8(10)
C(3)-S(1)-Pd(1)	90.2(3)	C(14)-C(13)-C(12)	118.7(10)
C(3)-S(1)-C(2)	105.6(7)	C(15)-C(14)-C(13)	120.6(10)
C(1)-N(1)-Pd(1)	116.6(5)	C(14)-C(15)-N(4)	122.1(9)
C(6)-N(1)-Pd(1)	100.6(5)	C(8)-C(21)-N(3)	118.1(7)
C(6)-N(1)-C(1)	112.8(8)	C(22)-C(21)-N(3)	119.7(7)
C(7)-N(1)-Pd(1)	105.8(5)	C(22)-C(21)-C(8)	122.2(8)
C(7)-N(1)-C(1)	112.3(9)	C(23)-C(22)-C(21)	119.7(9)
C(7)-N(1)-C(6)	107.8(7)	C(24)-C(23)-C(22)	119.0(8)
C(5)-N(2)-Pd(1)	109.1(5)	C(24)-C(25)-N(3)	124.0(8)
C(5)-N(2)-C(4)	111.4(6)	F(2)-B(1)-F(1)	117.8(9)
C(8)-N(2)-Pd(1)	102.7(5)	F(3)-B(1)-F(1)	105.5(10)
C(8)-N(2)-C(4)	107.1(6)	F(3)-B(1)-F(2)	111.7(11)
C(8)-N(2)-C(5)	112.7(6)	F(4)-B(1)-F(1)	109.6(10)
C(21)-N(3)-Pd(1)	108.9(5)	F(4)-B(1)-F(2)	111.5(10)
C(25)-N(3)-Pd(1)	131.7(6)	F(4)-B(1)-F(3)	99.0(12)
C(25)-N(3)-C(21)	119.3(7)	F(6)-B(2)-F(5)	103.0(10)
C(11)-N(4)-Pd(1)	110.2(6)	F(7)-B(2)-F(5)	104.2(12)
C(15)-N(4)-Pd(1)	130.0(6)	F(7)-B(2)-F(6)	105.7(13)
C(15)-N(4)-C(11)	119.4(7)	F(8)-B(2)-F(5)	112.6(14)
C(2)-C(1)-N(1)	127.3(9)	F(8)-B(2)-F(6)	118.0(12)
		F(8)-B(2)-F(7)	112.1(13)

Estimated standard deviations are given in parentheses.

Table 8
Mean plane for $[Pd(L_1)](BF_4)_2$

The equation of the plane containing the four nitrogens is:
0.3821X - 0.9207Y - 0.0792Z + 2.9751 = 0

Atoms	X	Y	Z	P
N(1)	2.8212	3.3610	8.8763	0.0490
N(2)	0.5497	2.9332	6.7066	-0.0469
N(3)	-1.4366	1.8897	8.1805	0.0381
N(4)	0.4737	1.8897	8.1805	0.0381
Pd(1)	0.3254	2.7767	8.7186	-0.1479
S(1)	-0.0823	5.6432	8.3583	-2.9144
C(4)	-0.2427	4.0615	6.094	-1.3400
C(5)	-2.0312	3.0557	6.3824	0.4323

where P is the perpendicular distance between the atom and the mean plane, given in Å.

However, the chelate bite angles N(2)-Pd(1)-N(3)pyr and N(1)-Pd(1)-N(4)pyr are significantly smaller (82.5 and 83.6°). This is a consequence of the partial double bond character of the C-N bonds of the pyridine moieties which have an average bond distance of 1.36 Å, closing the bite distance between the atoms N(1) and N(4) to 2.73 Å and that of N(2) and N(3) to 2.68 Å (Figure 10).

The bond distance between palladium and sulphur atom in the apical position is 2.92 Å, which is consistent with that of $[Pd([9]aneS_3)_2](PF_6)_2$ reported in the literature[66]. However, this bond distance is less than the sum of the van der Waals' radii (3.40 Å) of palladium and sulphur[67]. Since the geometry of the $[9]aneN_2S$ moiety does not restrict the axial ligand to be coordinated to the metal centre, as has been shown by the crystal structure of $[Pd([9]aneN_3)_2]^{2+}$ (Figure 12)[68] in which the apical nitrogen atoms oriented away from the axial coordination sites of the palladium, this suggests the existence of significant interaction between Pd and S atoms in $[Pd(\mathbf{L_1})]^{2+}$. A close examination also indicates that the apical sulphur atom is tilted away by 18° (Figure 13) from the perpendicular position directly above the palladium center. This suggests that for the $[9]aneN_2S$ moiety, there is considerable strain involved in reaching over fully to cap the palladium ion in the axial site.

The mean plane calculation of the molecular structure of $[Pd(\mathbf{L_1})]^{2+}$ (Table 8) indicates that the palladium centre is 0.15 Å above the basal plane

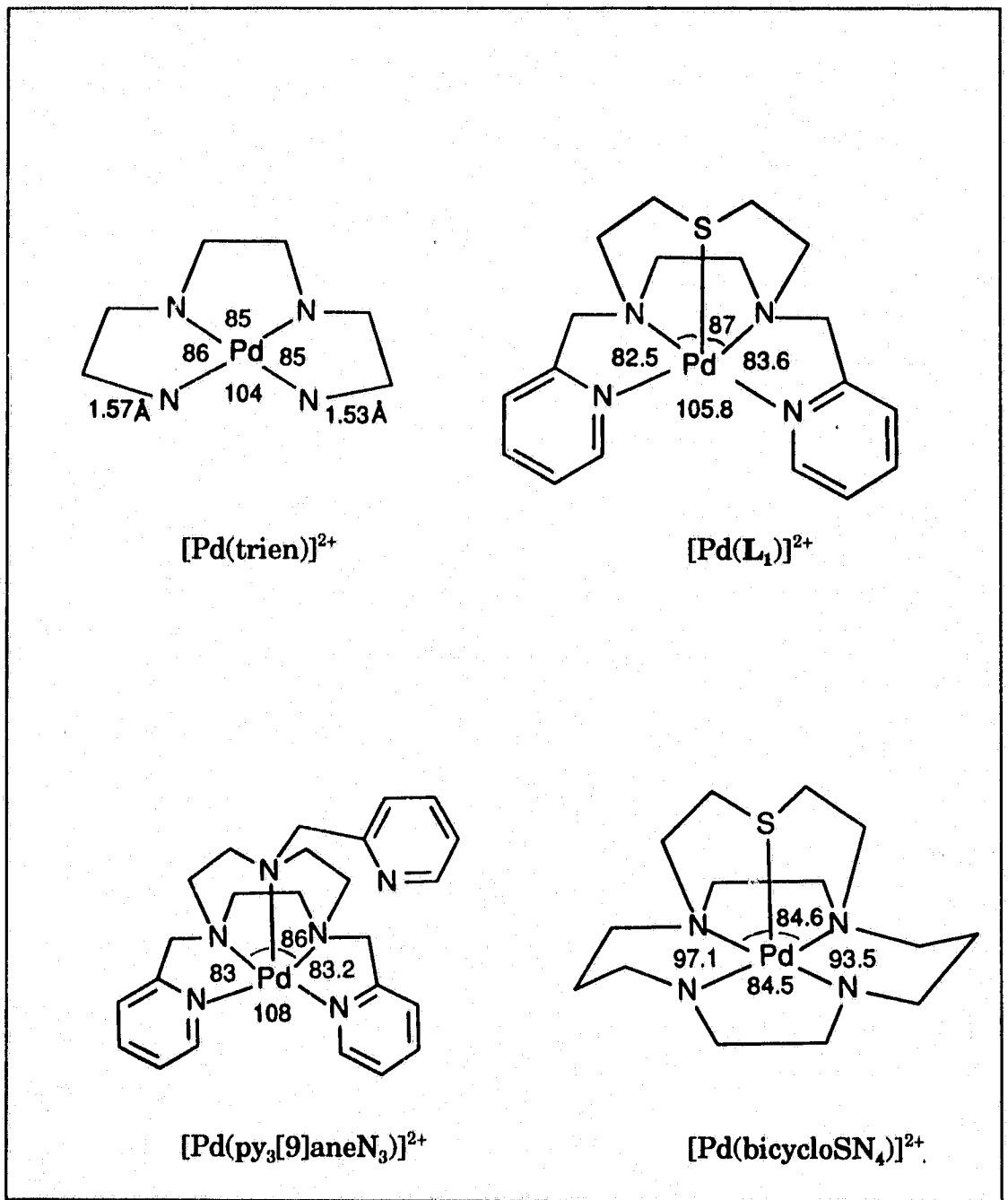

Figure 11 Comparison of the in-plane geometry of $[Pd(L_1)]^{2+}$ with structurally analogous species.

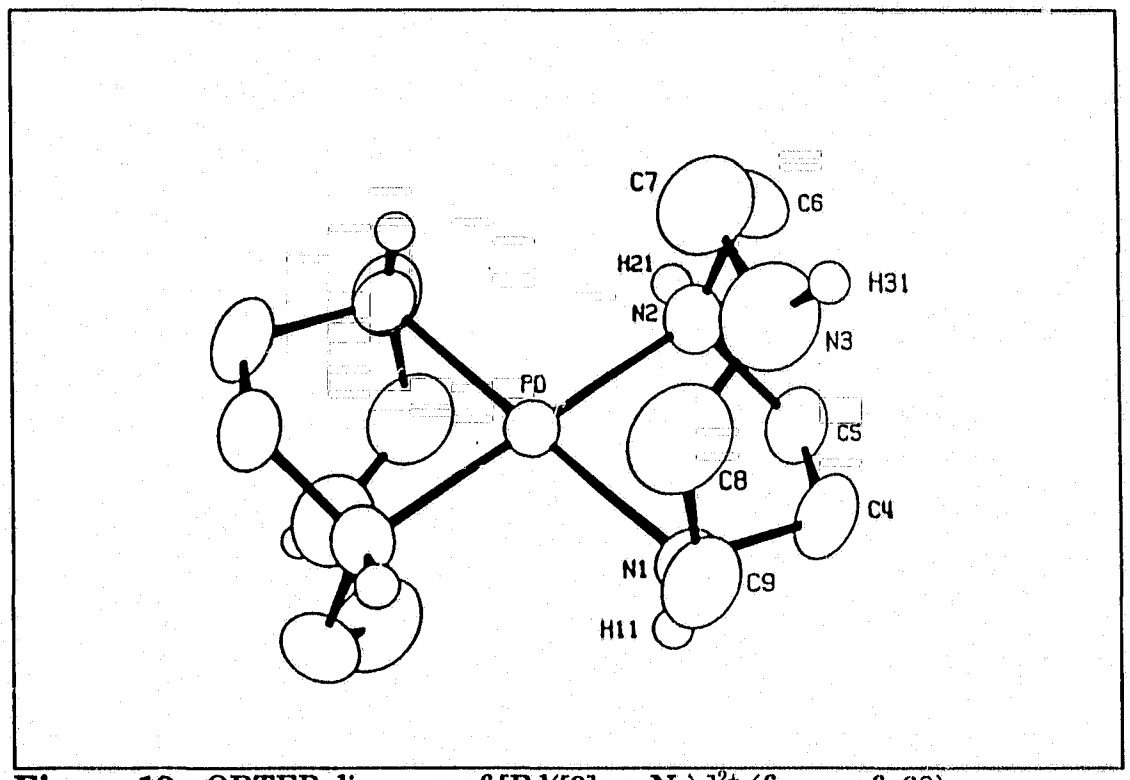

Figure 12 ORTEP diagram of $[Pd([9]aneN_3)_2]^{2+}$ (from ref. 68).

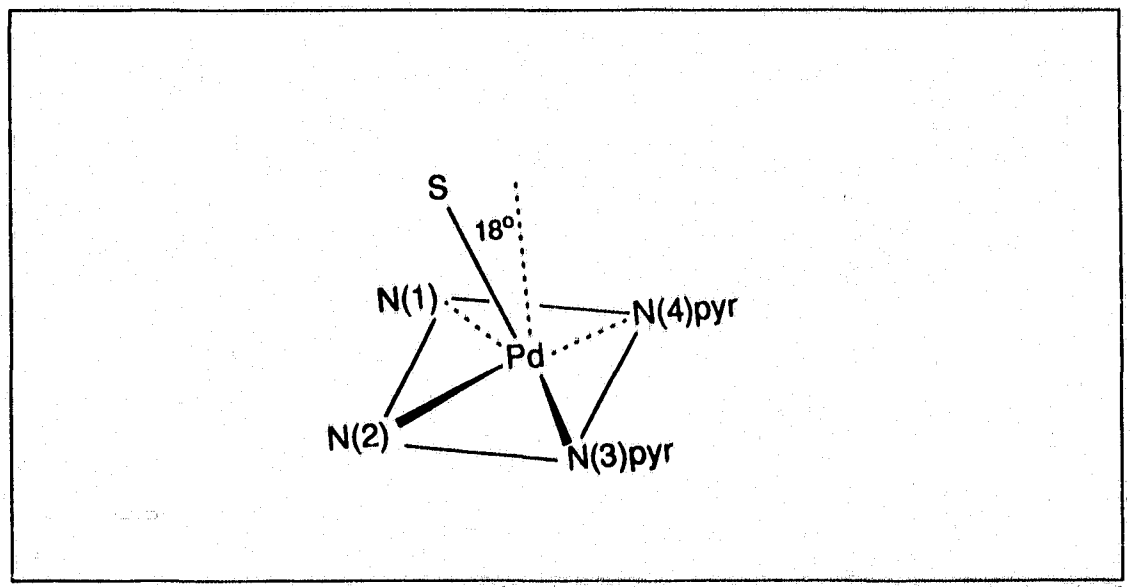

Figure 13 A diagram showing the deviation from perpendicularity of apical sulphur atom in $[Pd(L_1)]^{2+}$.

defined by the four coordinating nitrogen atoms. In addition, the bite distance between N(3) and N(4) is 3.27 Å (Figure 10), which is larger than the average distance spanned between the nitrogen atoms in five membered chelate rings (2.85 Å) of similar geometry as observed in the metal complexes of daptacn (**18**)[69]. These observations can be explained partially by the fact that the cavity defined by the ethylene linkage and the pyridine moieties in the basal plane does not provide the "best fit" for a Pd(II) ion. However, in $[Pd(trien)]^{2+}$, the palladium ion is only 0.06 Å above the plane defined by the four nitrogen atoms[67] despite the "hole" size of trien being similar to $\mathbf{L_1}$. This provides further evidence that in $[Pd(\mathbf{L_1})]^{2+}$, there is significant interaction between the sulphur atom in the axial position and the palladium ion, pulling the latter above the palladium ion further out of the equatorial plane.

Hoffman et al[70] have calculated the optimal L_{basal}-M-L_{basal} angle θ for ML_5 systems adopting a square-pyramidal geometry. For d^8 ions, the optimal θ is 164°. The basal angles for N(3)-Pd(1)-N(1) and N(2)-Pd(1)-N(4) in $[Pd(\mathbf{L_1})]^{2+}$ are 165° and 169° which are consistent with the theoretical value for a d^8 ion.

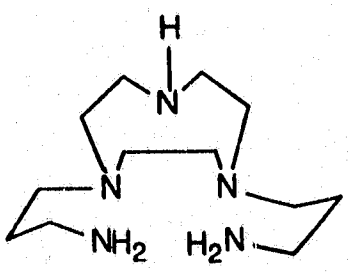

18

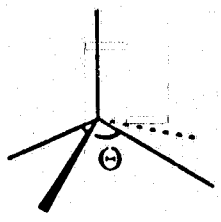

The existence of five-coordinate complexes of palladium(II) is well-documented[71], especially those containing phosphorus, sulphur and selenium as ligands[72]. Several palladium complexes containing 2,2'-bipyridine and o-phenanthroline (phen) ligands have also been reported[73]. However, very few examples of five-coordinate Pd(II) complexes with macrocyclic ligands structurally similar to $\mathbf{L_1}$ have been reported in the literature[74]. In the crystal structure of the five coordinate py_3[9]aneN_3 (1,4,7-tris(2-pyridylmethyl)-1,4,7-triazacyclononane) complex of Pd(II)[74], the average in-plane bond

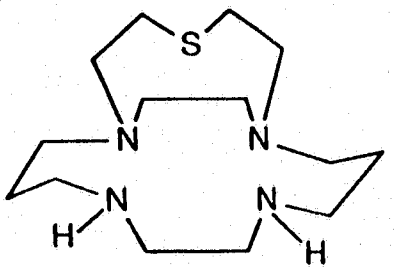

19

distances of Pd-N(amine) and Pd-N(pyridine) are 2.03 and 2.04 Å, respectively, which are comparable to those observed in $[Pd(\mathbf{L_1})]^{2+}$. However, the bond distance of Pd-N(amine) in the apical position is 2.58 Å which is shorter than the Pd-S bond distance observed in $[Pd(\mathbf{L_1})]^{2+}$. This results from the increased covalent radius of sulphur relative to that of nitrogen.

A structurally-related ligand, bicycloSN_4 (**19**) has been prepared[75] and the crystal structure of its Pd(II) complex[76] (Figure 14) demonstrates that the palladium ion is also in a square-pyramidal environment. The average in

palladium ion is also in a square-pyramidal environment. The average in plane Pd-N bond distance is 2.07 Å, which is longer than those observed in $[Pd(L_1)]^{2+}$. The bond distance of Pd-S in the axial site is 2.88 Å and the palladium centre is 0.148 Å above the basal plane defined by the four coordination nitrogen atoms. These structural data are comparable to those observed in $[Pd(L_1)]^{2+}$. The only exception is the apical sulphur atom which is only tilted away by 13° from the perpendicular position directly above the metal centre in $[Pd(bicycloSN_4)]^{2+}$ compared to an angle of 18° in $[Pd(L_1)]^{2+}$.

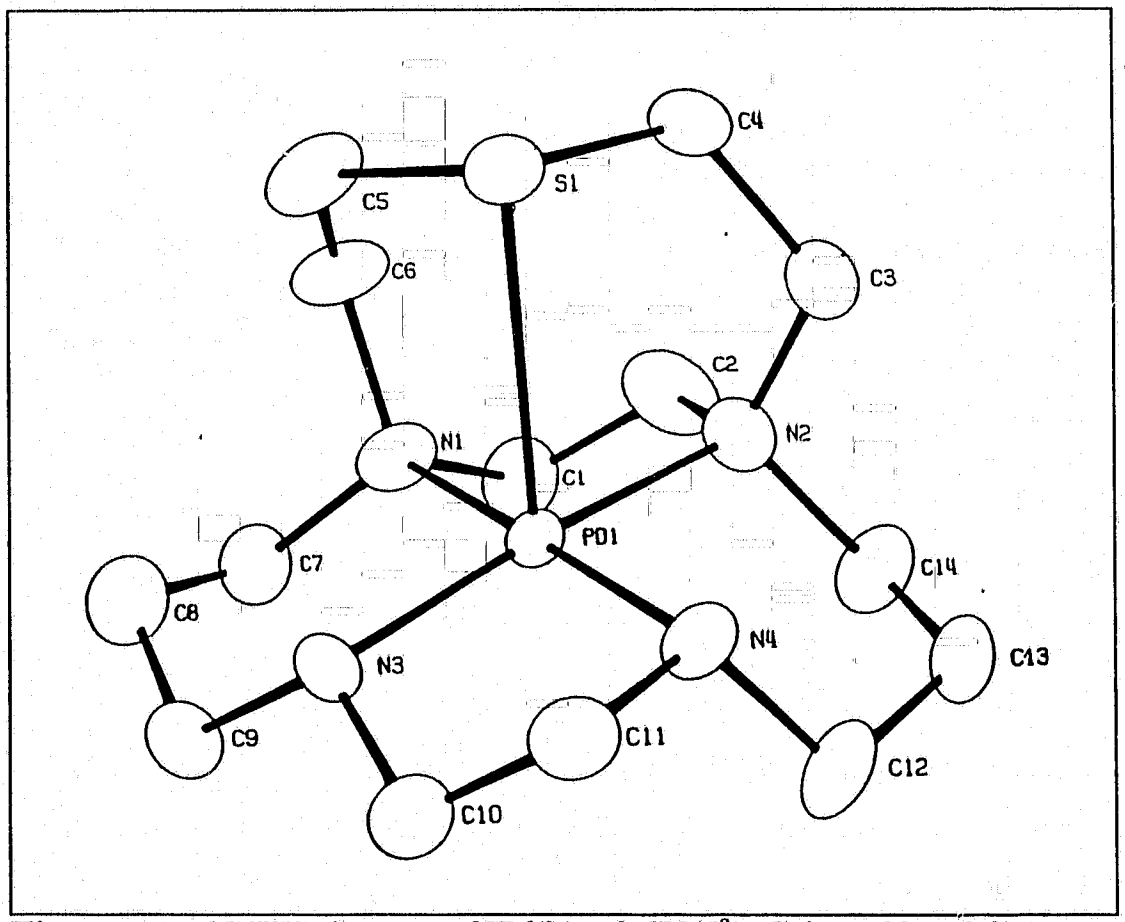

Figure 14 ORTEP diagram of $[Pd(bicycloSN_4)]^{2+}$. Selected bond distances in Å: Pd...S(1) = 2.875(3), Pd-N(1) = 2.068(9), Pd-N(2) = 2.088(8), Pd-N(3) = 2.063(8), Pd-N(4) = 2.064(8).

2.4 Solution Studies

(a) NMR spectroscopy

^{1}H and ^{13}C NMR spectra of $[Pd(L_1)]^{2+}$ at room temperature in CD_3CN were shown in Figure 15 and Figure 16, respectively, both of which suggest that the solution structure of $[Pd(L_1)]^{2+}$ is the time average of the solid state structure (Figure 10). The ^{13}C NMR spectrum shows nine lines and they are attributed to the nine distinct carbon atoms in the complex. A detailed assignment of each of these carbon resonances was aided by the ^{13}C-^{1}H correlated spectrum (Figure 17). The resonance at 32.8 ppm corresponds to carbons attached to the sulphur atom and the signals at 62.0 and 63.0 ppm correspond to carbons attached to the nitrogen atoms in the [9]aneN_2S moiety. The resonance at 69.6 ppm is attributed to the carbon atom next to the pyridine moiety and the resonances from 118.4 to 163.1 ppm are attributed to aromatic carbons in pyridine. The peak at 163.1 ppm is not correlated to any protons and is attributed to the α-position of the pyridine.

The analysis of the ^{1}H NMR is more complicated. This is in part due to the strong coupling between methylene protons adjacent to nitrogen and sulphur atoms in the cyclononane moiety. The aliphatic region of the spectrum can be divided into three subspectra: an AB pattern at δ 4.30 and 5.48 due to methylene protons next to the pyridine moiety; an AA'BB' pattern at δ 3.55 and 3.97 due to protons in the chelating ethylene-diamino portion in the

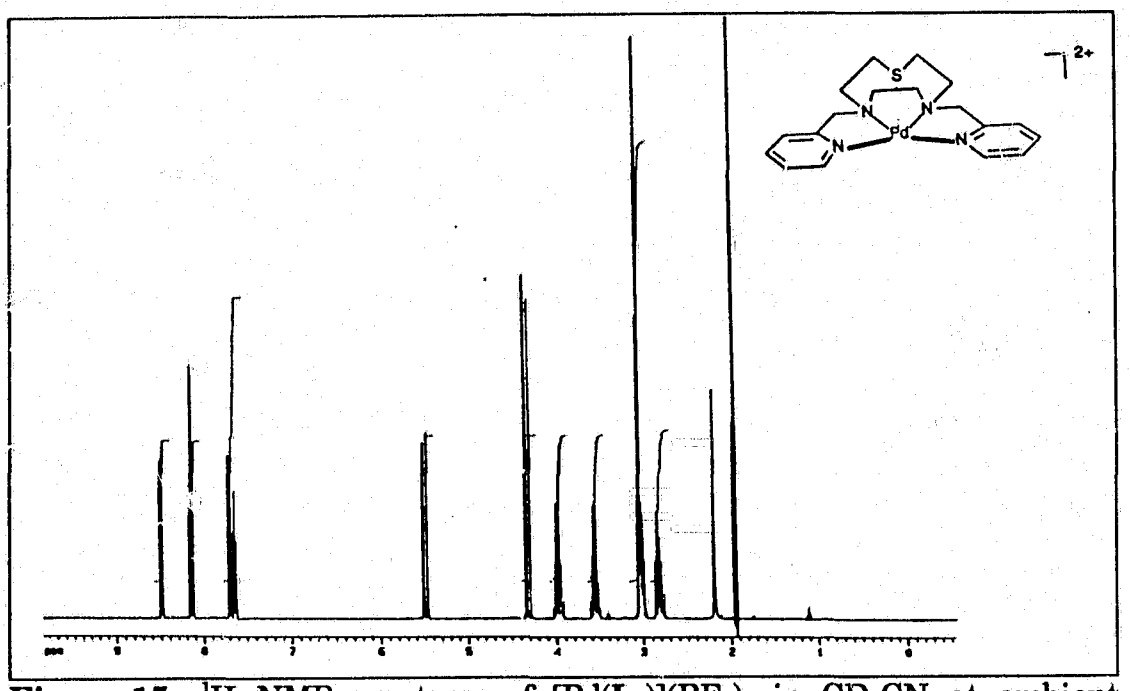

Figure 15 ^{1}H NMR spectrum of $[Pd(L_1)](BF_4)_2$ in CD_3CN at ambient temperture.

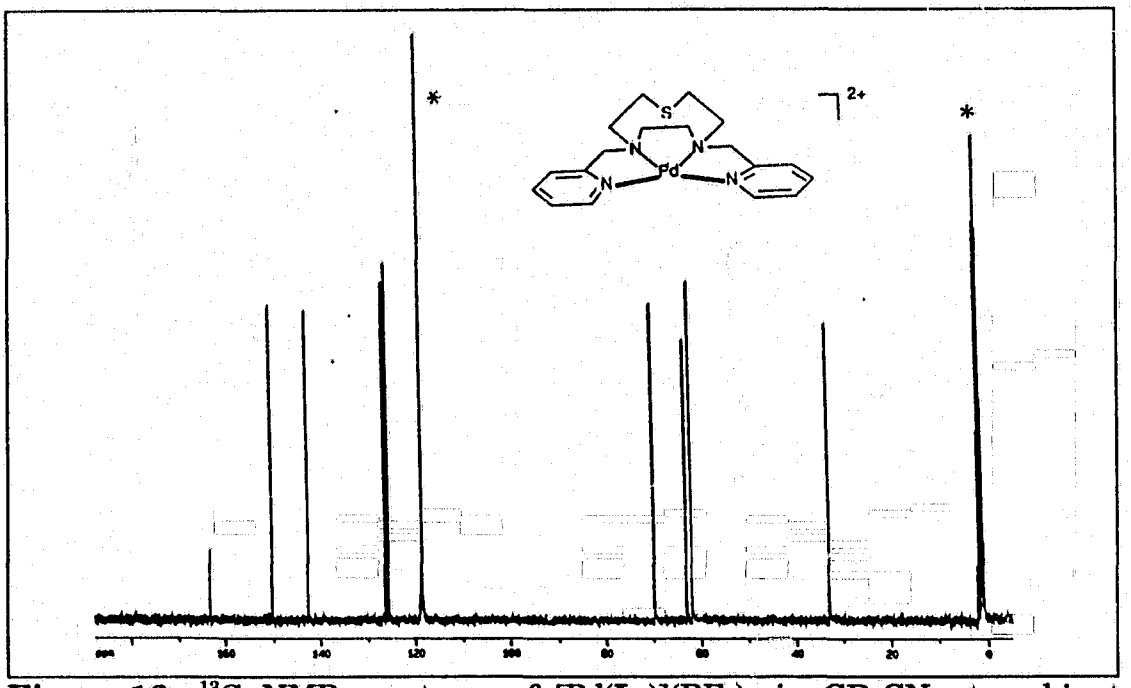

Figure 16 ^{13}C NMR spectrum of $[Pd(L_1)](BF_4)_2$ in CD_3CN at ambient temperature. (* denotes solvent peak)

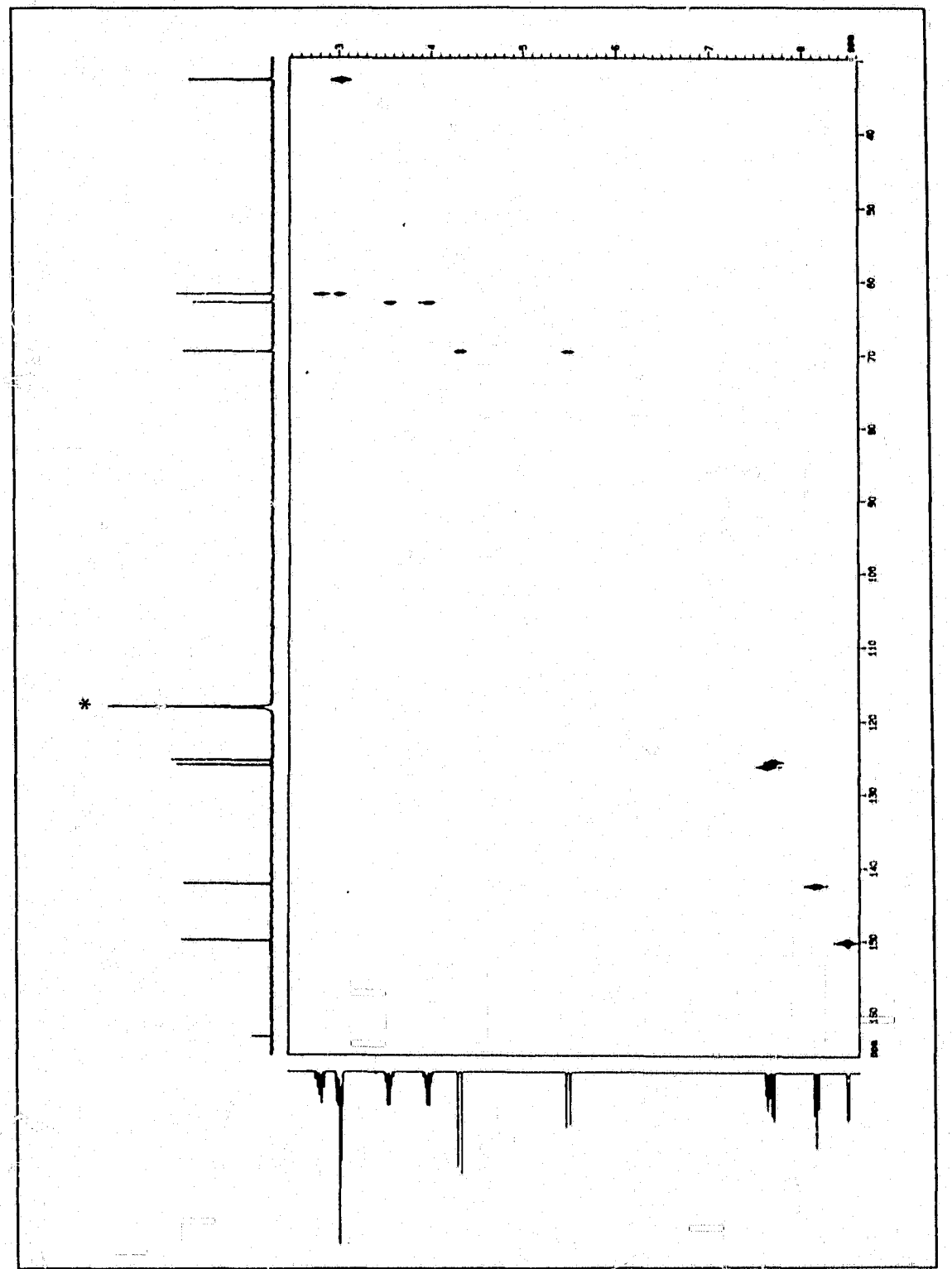

Figure 17 ^{1}H-^{13}C correlated NMR spectrum of $[Pd(L_1)](BF_4)_2$ in CD_3CN. (* denotes solvent peak)

Table 9
^{1}H NMR Parameters for $[Pd(L_1)](BF_4)_2$ in CD_3CN.

a. AA'BB' Subspectrum: Chelating diamino portion

$\delta_a = \delta_{a'} = 3.97$ ppm
$\delta_b = \delta_{b'} = 3.55$ ppm
$J_{aa'} = 6.58$ Hz
$J_{ab} = J_{a'b'} = -14.64$ Hz
$J_{ab'} = J_{a'b} = 7.20$ Hz
$J_{bb'} = 5.35$ Hz

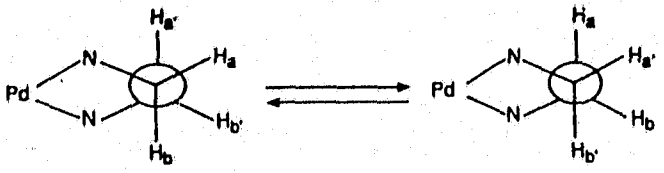

b. ABCC' Subspectrum: Chelating thia-amino portion

$\delta_a = 2.81$ ppm
$\delta_b = 3.00$ ppm
$\delta_c = \delta_{c'} = 3.03$ ppm
$J_{ab} = -10.34$ Hz
$J_{ac} = 0.727$ Hz
$J_{bc} = 5.64$ Hz
$J_{bc'} = 6.56$ Hz
$J_{cc'} = -15.17$ Hz

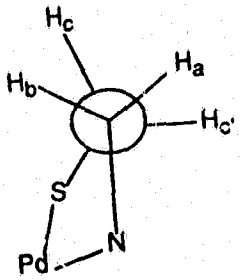

c. ABCDX Subspectrum: Chelating pyridylmethyl portion

$\delta_a = 8.49$ ppm
$\delta_b = 7.63$ ppm
$\delta_c = 8.14$ ppm
$\delta_d = 7.69$ ppm
$\delta_x = 5.48$ ppm
$\delta_y = 4.30$ ppm
$J_{ab} = 5.89$ Hz
$J_{ac} = 1.04$ Hz
$J_{ad} = 0.00$ Hz
$J_{ax} = 0.80$ Hz
$J_{bc} = 8.03$ Hz
$J_{bd} = 0.12$ Hz
$J_{bx} = 0.00$ Hz
$J_{cd} = 7.93$ Hz
$J_{cx} = 0.00$ Hz
$J_{dx} = 0.00$ Hz

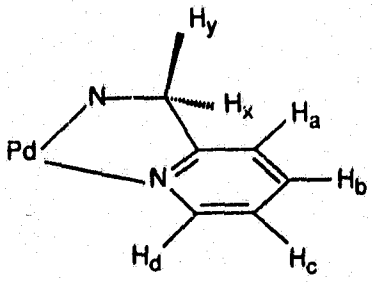

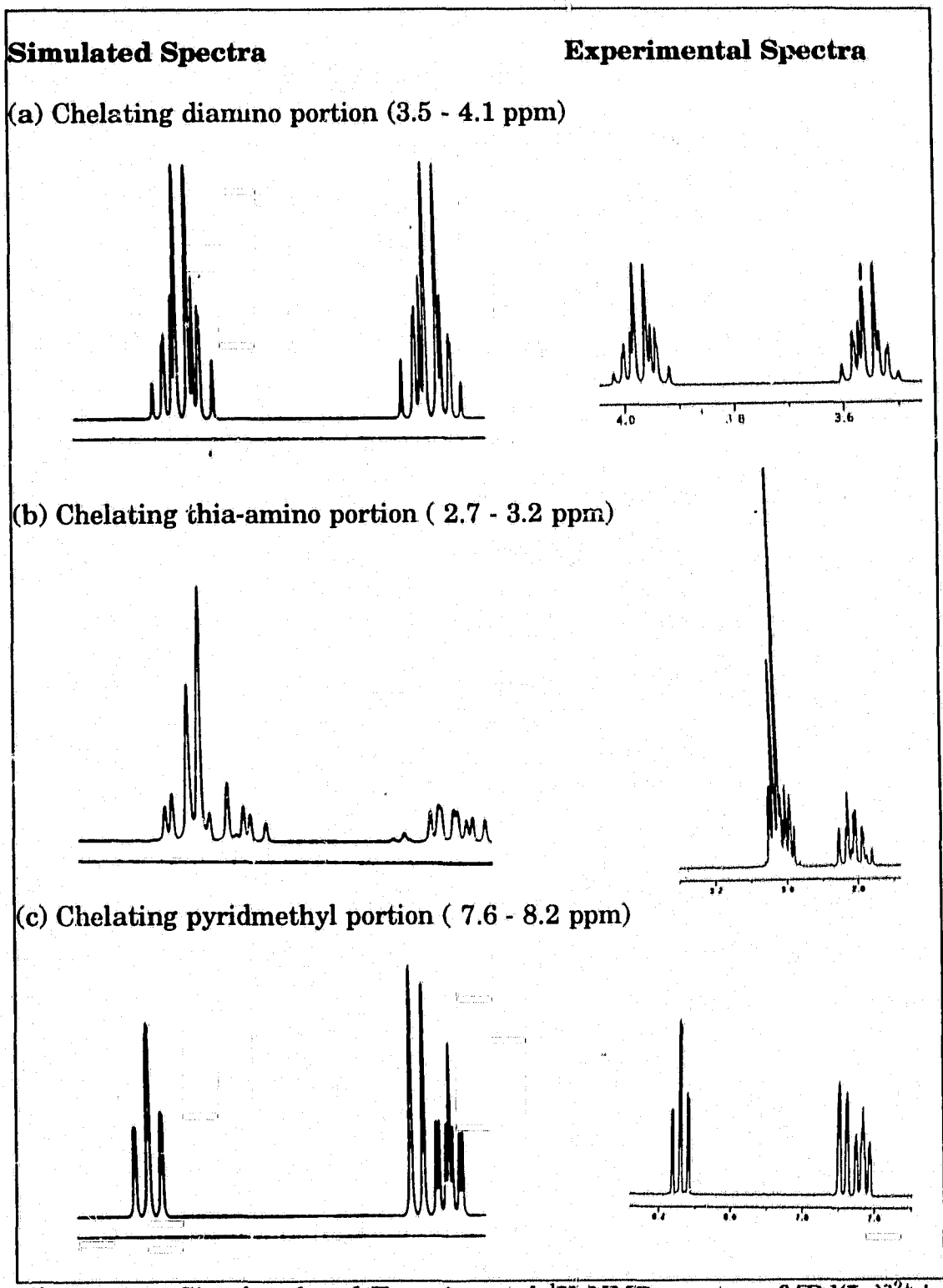

Figure 18 Simulated and Experimental ^1H NMR spectra of $[Pd(L_1)]^{2+}$ in CD_3CN.

equatorial plane and an ABCC' pattern at δ 2.81 - 3.03 due to methylene protons adjacent to sulphur and nitrogen near the apical region of the cation complex. The simulated spectroscopic parameters are summarized in Table 9 and Figure 18.

The Karplus equation[77] has been utilized in the structural analysis of organic molecules by providing a relationship between torsional angles and observed coupling constants. In the present case, the application of this equation provides a basis for determining the geometry in the chelate rings in solution. In the AABB' subspectrum which is generated by the ethylene protons of the NCH_2CH_2N portion of the ligand (Figure 18), the structure has an envelope shape (Figure 10). It is interesting to note that the coupling constants J_{ab} and $J_{a'b}$ are of the same magnitude (Table 9). This is due to rapid interconversion between two envelope conformations in the five membered chelate ring in solution. As a result, the solution structure of the chelating NCH_2CH_2N portion of the cation complex is the time average of the two conformers shown in Table 9. If the conformation in the five-membered chelate ring were locked in any one envelope conformation, $J_{a'b}$ (or $J_{ab'}$) would be greater than J_{ab} (or $J_{a'b}$). In addition, it would be expected to have a value close to 14 Hz since $H_{a'}$ (or H_a) and H_b (or $H_{b'}$) are essentially 180° apart. The other coupling constants $J_{aa'}$ and $J_{bb'}$ within the AA'BB' pattern are typical of two CH bonds with a dihedral angle of ≈ 60°.

For the thioamino portion of the molecule, the coupling constant observed for J_{ac} has a value of 0.73 Hz (Table 9), indicating that the dihedral angle between CH_a and CH_c bonds is essentially 90°. In addition, the five-membered chelate ring is not as flexible as that of the diamino portion of the complex in the equatorial position. This may be a consequence of the interaction between the sulphur atom and palladium as determined by the crystal structure, which results in a degree of rigidity in the thioamino portion of the complex.

The AB pattern due to pyridyl-methylene protons is complicated by the existence of long range coupling between the proton H_x at the equatorial plane with those in the pyridine moiety. Such coupling causes the second doublet at δ 5.48 within the AB pattern to be splitted into a doublet of a doublet, which was not resolved in the observed spectrum. As a result, the peak height of the doublet at δ 5.48 is only half of that observed at δ 4.25 (Figure 15). The pyridine portion of the spectrum at δ 7.63 to 8.49 was analyzed as an ABCDX pattern, X being the methylene proton which shows a long range coupling with the pyridine moiety. The corresponding coupling constants are tabulated in Table 9 and their values are typical of benzenoid aromatic compounds[78].

(b) UV/Vis spectroscopy

The electronic spectral data for $[Pd(L_1)](BF_4)_2$ and other analogous Pd(II) complexes are summarized in Table 10. The UV/Vis spectrum of $[Pd(L_1)]^{2+}$ exhibits two absorption bands at 264 nm (ε = 6220 $M^{-1}cm^{-1}$) and 301 nm (ε =

Table 10
Electronic spectral data for $[Pd(L_1)](BF_4)_2$ and analogous species

Complex	solvent	color	λ_{max}/nm (ε_{max}, $M^{-1}cm^{-1}$)	ref.
$[Pd(L_1)]^{2+}$	CH_3CN	orange-brown	264 (6220) 301 (3510)	present work
$[Pd(py_3[9]aneN_3)]^{2+}$	CH_3CN	red	453 (76)	74
$[Pd(trien)]^{2+}$	H_2O	---	296 (1000)	65
$[Pd(bicyloSN_4)]^{2+}$	CH_3CN	yellow	290	76
$[Pd([9]aneS_3)_2]^{2+}$	CH_3CN	blue	296 (15000) 615 (55)	66

3510 $M^{-1}cm^{-1}$). There are no distinctive absorption bands above 350 nm even when a concentrated (0.01 M) solution of $[Pd(L_1)]^{2+}$ in acetonitrile was recorded. It is possible that the high ligand-field effects of pyridines and amines combine to move the low energy d-d transition under the charge transfer absorption bands. However, it is interesting to note that the absorption maximum near 301 nm is also observed in analogous Pd(II) complexes such as $[Pd(trien)]^{2+}$ and $[Pd(bicycloSN_4)]^{2+}$ (Table 10). It is possible that this absorption is a ligand to metal transfer band which arises from the amine nitrogen to the palladium metal centre.

(c) Electrochemistry

The electrochemical data for the $[Pd(L_1)]^{2+}$ ion and related palladium complexes are summarized in Table 11. The cyclic voltammograms (CV) of $[Pd(L_1)]^{2+}$ in CH_3CN containing 0.1 M Bu_4NPF_6 as supporting electrolyte exhibited an irreversible reduction wave at -1.25 V vs Fc/Fc^+ when scanned from the potential range of 0.0 to -2.0 V (Figure 19). This reduction potential is comparable with the value of -1.3 V observed in $[Pd(bicycloSN_4)]^{2+}$. This reduction wave remained irreversible even when the scan rate was increased from 100 to 1000 mVs^{-1}, indicating that the Pd(I) species generated is unstable in the time scale of the CV experiment. The inability of L_1 to stabilize Pd(I) despite the presence of soft S atoms and pyridine moieties in its ligand framework (which can act as π acceptors and therefore stabilizing low oxidation states) may be due to the fact that the cavity defined by the ligand is too small to fit the larger Pd(I) ion. No $d\pi$-$p\pi^*$ backbonding which will delocalize some of the excess electron density at the palladium centre upon reduction can take place. As a result, the transient $[Pd(L_1)]^+$ formed which is substitution labile undergoes further reaction (possibly disproportionation to Pd(II) and Pd(0), followed by demetallation) rapidly and cannot be detected on the reverse scan in the CV experiment.

It is interesting to note that no oxidation wave was observed in the $[Pd(L_1)]^{2+}$ in the range of potential (0.0 - 2.0 V) investigated. On the other hand, a reversible metal-based oxidation wave was observed at 0.8 V vs Fc/Fc^+

Table 11
Redox potentials of Pd(II) complexes

Complex	E (vs Fc/Fc^+), V	Ref.
Pd(II) to Pd(I):		
$[Pd(L_1)]^{2+}$	-1.25[a]	present work
$[Pd(bicycloSN_4)]^{2+}$	-1.30[a]	76
Pd(II) to Pd(III):		
$[Pd(L_1)]^{2+}$	not observed	present work
$[Pd(bicyloSN_4)]^{2+}$	$E_{1/2}$ = 0.80 (ΔE_p = 120 mV)	76
$[Pd([9]aneS_3)]^{2+}$	$E_{1/2}$ = 0.60 (ΔE_p = 84 mV)	66

[a] irreversible reduction

for $[Pd(bicycloSN_4)]^{2+}$ and another related thia complex of Pd(II) (Table 11). Such an oxidative inactivity of the $[Pd(L_1)]^{2+}$ may again arise from the stereochemical inflexibility of L_1 upon coordination to Pd(II). A distorted octahedral stereochemistry, which is the preferred coordination for a d^7 ion[79] can be achieved by ligands such as bicylcoSN_4 and [9]aneS_3 but not by L_1 due to structural constraint in the ligand framework.

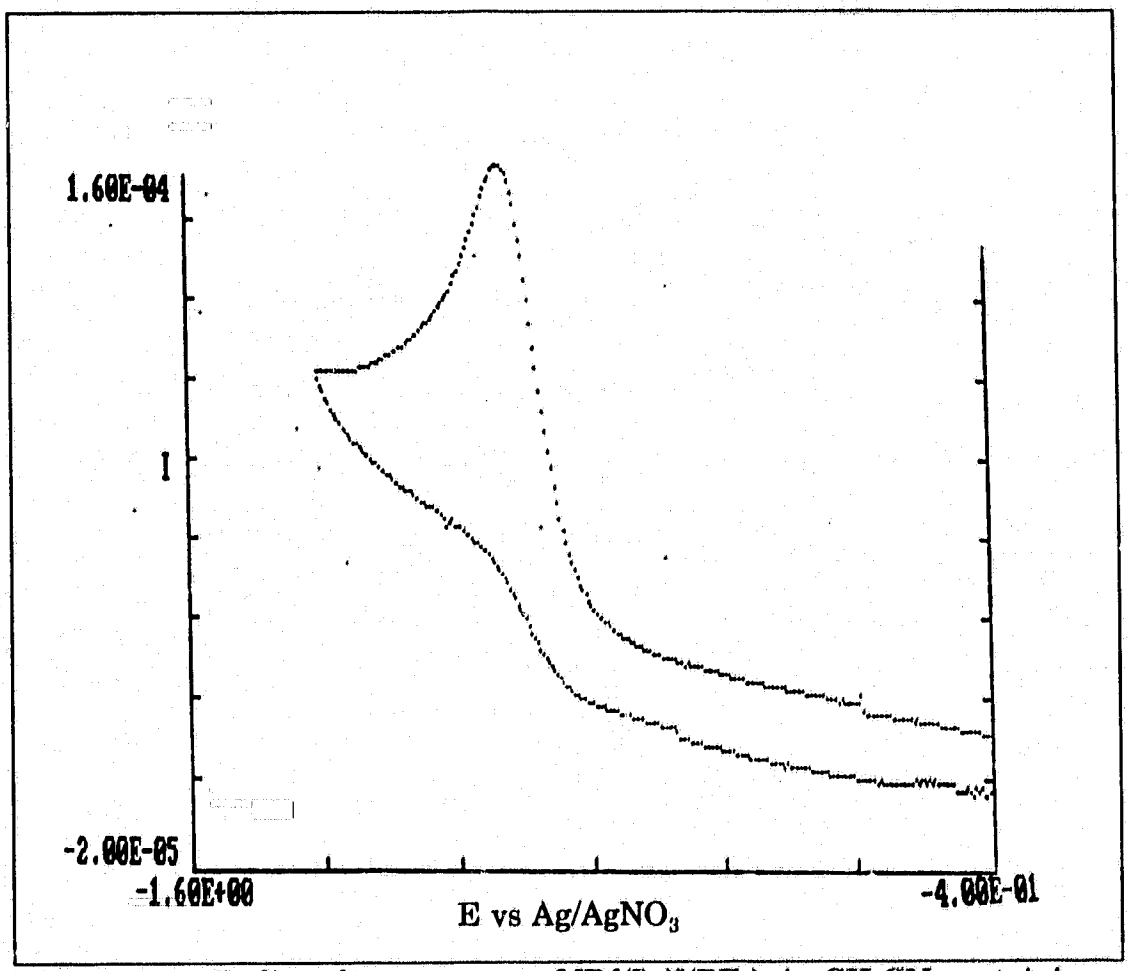

Figure 19 Cyclic voltammogram of $[Pd(L_1)](BF_4)_2$ in CH_3CN containing 0.1 M Bu_4NPF_6. Fc/Fc^+ occurs at 0.096 V.

2.5 Conclusions

In summary, the palladium(II) complex of $\mathbf{L_1}$ was synthesized and its solid state structure characterized by X-ray crystallography. This complex cation has a distorted square-pyramidal structure both in solution and in the solid state as confirmed by ^1H and ^{13}C NMR in CD_3CN. The CV study of this cation in acetonitrile under argon atmosphere indicated that it did not form stable monomeric $[Pd(\mathbf{L_1})]^+$ upon reduction despite the presence of soft S and pyridine N atoms in the ligand framework. In addition, no oxidation to a Pd(III) species was detected in the CV study in the range of potential (0 - 2.0 V vs $Ag/AgNO_3$) investigated. Such redox behavior was rationalized as due to the structural constraints imposed by the ligand framework, which is unable to sustain a tetragonally-distorted octahedral environment preferred by a d^7 Pd(III) or a d^9 Pd(I) ion. As a continuing attempt to isolate stable monomeric Pd(I) and Pd(III) species, several 14-membered tetradentate macrocyclic ligands containing nitrogen and sulphur donor atoms with pyridine pendant arms ($\mathbf{L_2}$ - $\mathbf{L_5}$) have been synthesized. The chemistry of their palladium(II) complexes in solution will be discussed in the next chapter.

CHAPTER 3

SYNTHESES AND SOLUTION STUDIES OF PALLADIUM(II) MACROCYCLIC COMPLEXES WITH NITROGEN AND SULPHUR MIXED DONOR LIGANDS

3.1 Introduction

Historically[20], the most commonly studied macrocyclic ligands are tetradentate with four nitrogen donor atoms. A typical example is the ligand 1,4,8,11-tetraazacyclotetradecane, commonly known as cyclam. Complexes of this ligand reported in the literature[20] generally have central metal ions from the latter half of the first transition metal series.

X-ray diffraction studies[80] show that most of these complexes have square-planar geometry in which the ligand cyclam encircles the metal ion in the equatorial plane. Five or six-coordinated species are formed in the presence of coordinating solvent molecules or counterions which show axial coordination (Figure 20). However, when the metal ion is too large to fit into the available macrocyclic cavity, the ligand may fold and coordinate to two axial sites and two equatorial sites of an octahedron. This mode of coordination is usually referred as "cis" (Figure 20).

In the "trans" coordination, the most favourable conformation for cyclam is the *trans-III*[80] (Figure 21). In such a configuration, it is possible for both of the five-membered chelate rings to adopt the optimum gauche conformation and the six-membered chelate rings to adopt the chair conformation. In the "cis" or folded coordination, however, the most favourable conformation for cyclam is the *cis-V* in which the NH groups along the N-M-N fold-line are on the same side of the molecular plane and the other trans pair of NH groups on the opposite side of the molecular plane[20].

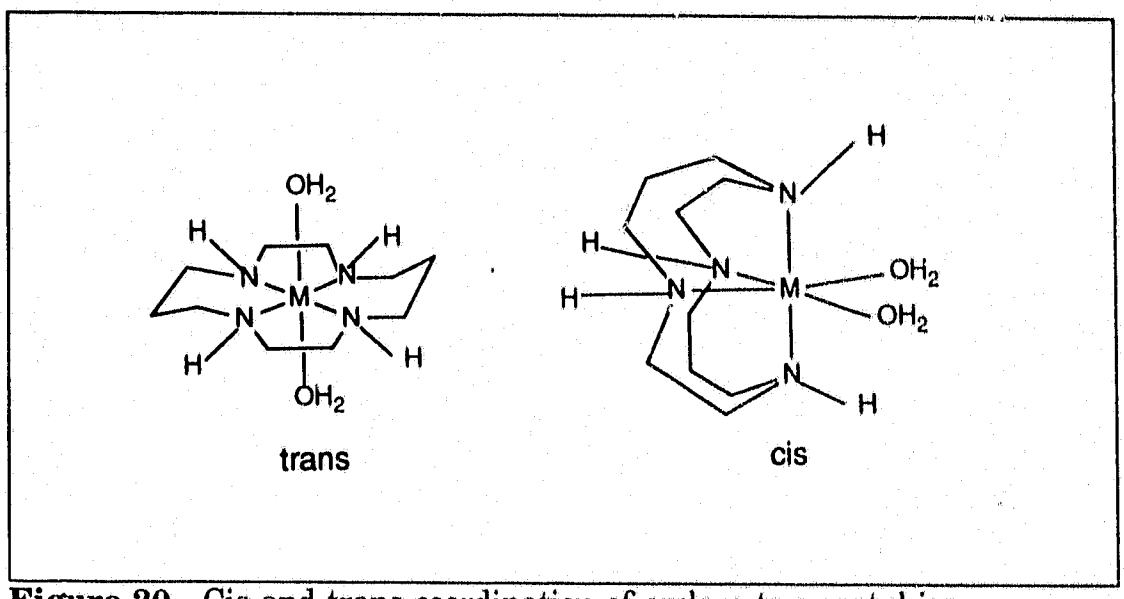

Figure 20 Cis and trans coordination of cyclam to a metal ion

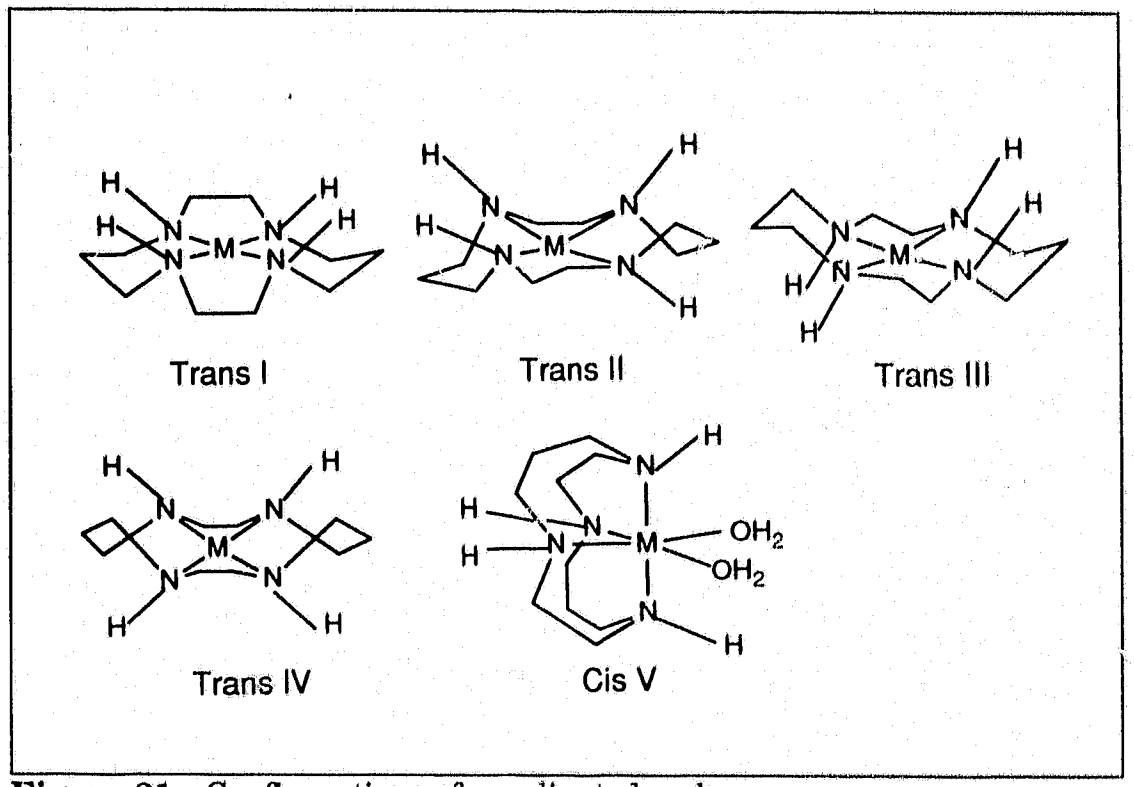

Figure 21 Configurations of coordinated cyclam.

In general, aza macrocycles are more selective towards hard ions, they tend to stabilize the high oxidation states of the first row transition metal ions[38,60,64]. In solution, the ligand cyclam forms metal complexes which exhibit a high degree of kinetic and thermodynamic stability, even with metal ions which give labile complexes, e.g. Ni(III)[64], thus permitting these metal complexes to be studied under common experimental conditions.

The coordination chemistry of the thia analogue of cyclam (i.e., [14]aneS_4), however, has been studied extensively only recently[81]. Solid state studies[82] showed that the free ligand, [14]aneS_4, crystallized in three conformations, α, β_1 and β_2. These isomorphs exhibit exo conformations with the lone pairs of electrons of the sulphur atoms pointing out of the macrocyclic ring (Figure 22). As a result, tetrathia macrocycles have a tendency to bind

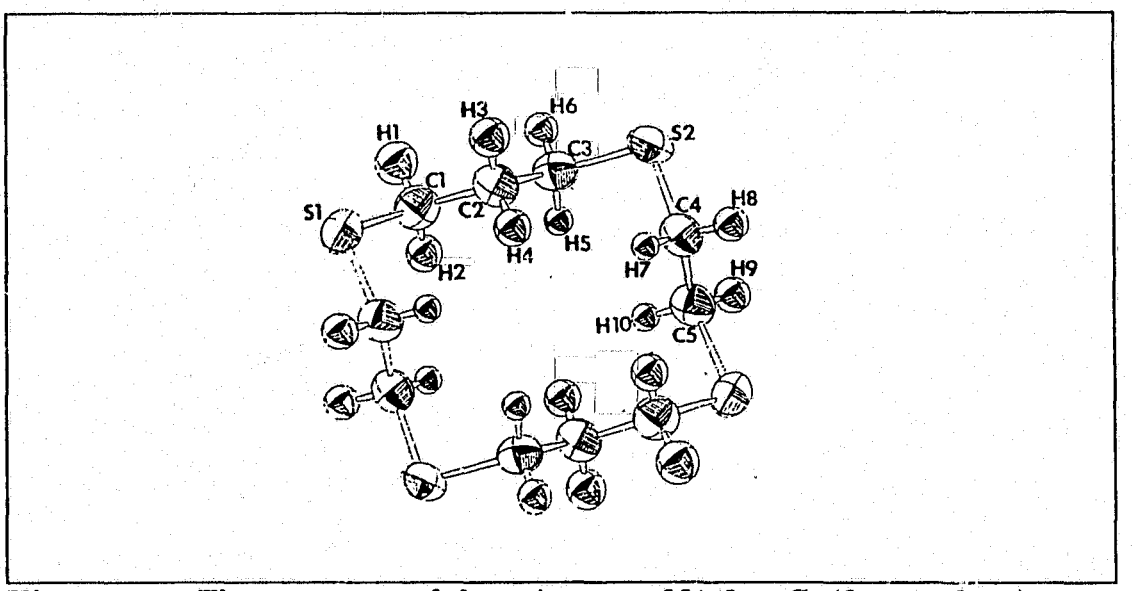

Figure 22 The structure of the α-isomer of [14]aneS_4 (from ref. 82)

to metal ions in an exo manner, causing bridging between two metal fragments, e.g., $[NbCl_5]_2[14]aneS_4$[83] (Figure 23). Complexation in an endo fashion in which the metal ion is complexed within the macrocyclic cavity, e.g., in $[Ni([14]aneS_4)]^{2+}$ as shown in Figure 23, requires reorganization of ligand.

The chemistry of thioether ligands has been reviewed recently[61,81]. In general, these ligands can serve as π-donors via donation of the second lone pair in sulphur to the metal and also as π-acceptors using the empty d orbitals on sulphur. The π-acceptor ability of the sulphur atoms can be demonstrated by their ability to stabilize the lower oxidation states of a given metal ion, e.g. in the Rh(I) complex[84], $[Rh[14]aneS_4)]^+$.

In contrast to the N_4 and S_4 donor sets, there have been relatively few studies on macrocyclic ligands involving sulphur and nitrogen mixed donor sets[57]. Black and coworkers[85] synthesized $[18]aneN_2S_4$ and the Co(II) and Ni(II) complexes. Lehn and coworkers[57] have prepared $[12]aneN_2S_2$ and

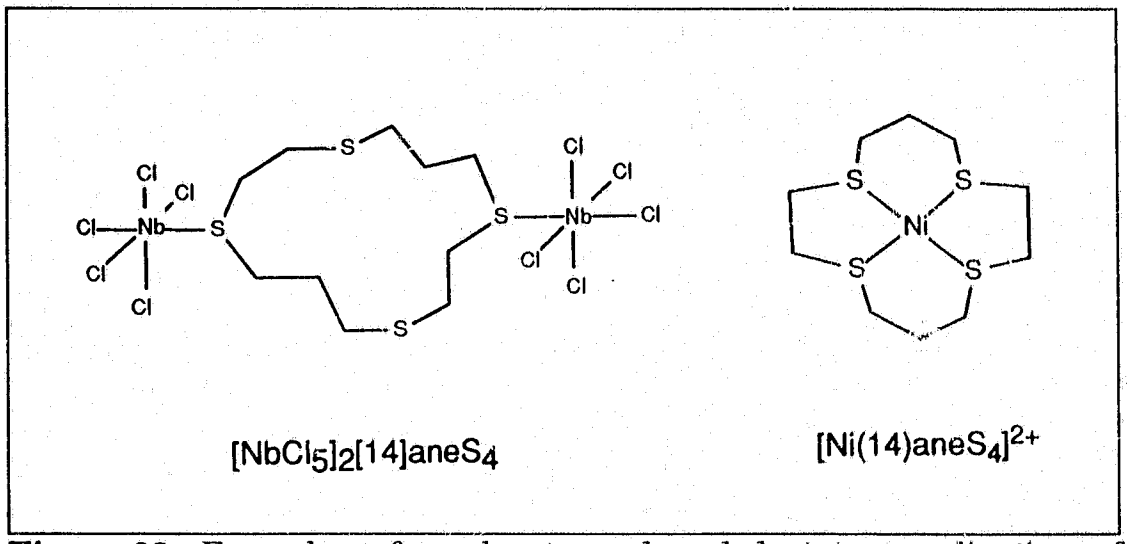

Figure 23 Examples of exodenate and endodentate coordination of $[14]aneS_4$ to transition metal ions.

studied the Cu(II) complex. Rorabacher et al[58,86] have prepared a series of 14-membered macrocyclic ligands containing N_xS_{4-x} donor sets (where x = 1, 2, 3) with alternating ethylene and propylene bridging groups. They have also studied the protonation constants, stability constants and kinetics of complex formation for these ligands with Cu(II) ion in aqueous medium[86]. The growing interest in the coordination chemistry of these systems arises from the potential similarity of coordination environment around metal centres in copper proteins[58]. In addition, the possibility exists that these systems may combine the hard and soft donor properties of aza and thia macrocycles and therefore stabilize both high and low oxidation states of a given metal centre.

This chapter describes the syntheses of a series of 14-membered macrocyclic ligands, $\mathbf{L_2}$ - $\mathbf{L_5}$, with special emphasis on the crystal structures and solution studies of Pd(II) complexes of $\mathbf{L_4}$. The characterization and solution studies of the Co(II), Ni(II) and Cu(II) complexes of $\mathbf{L_4}$ will be discussed in Chapter 4.

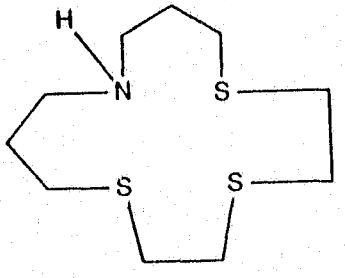

$\mathbf{L_2}$

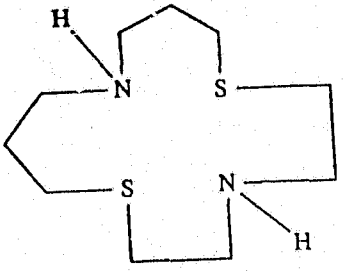

$\mathbf{L_3}$

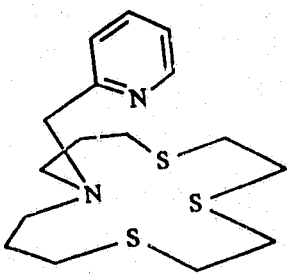

L_4

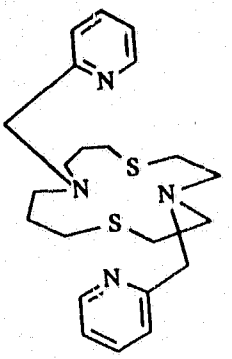

L_5

3.2 Syntheses

The synthetic route leading to ligands L_2 and L_3 are summarized in Schemes 5 and 6, respectively, with experimental details being provided in Chapter 7. For both ligands, the first step (from **20** to **21**, or from diethanolamine to **23**) involves the protection of the amino functional group by the formation of a sulphonamide. This is necessary as the secondary amino functional groups are nucleophilic and interfere with the cyclization reaction in the following step. The protection of the amine was achieved in good yields by the reaction with three equivalences of p-toluene sulphonyl chloride in dichloromethane. This process not only masks the nucleophilic property of the amino group but also converts the hydroxy into a better leaving group. The tosylates formed (**21** and **23**) were characterized by NMR, MS and melting point determination.

The tosylated amines (**21** and **23**) can be used directly for the cyclization (Scheme 5) or converted to dibromides (Scheme 6) via nucleophilic substitution of tosyl oxy groups by NaBr in N,N-dimethylformamide (DMF). Both the tosyl

Scheme 5

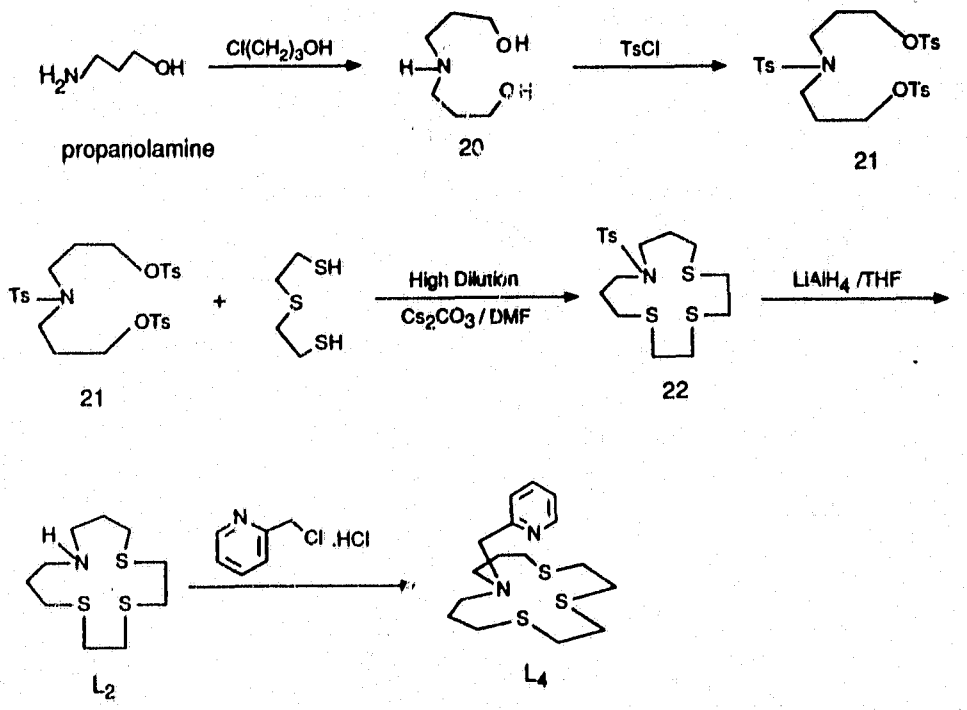

oxy group and bromide can serve as the leaving groups in the formation of C-S bonds in the cyclization.

The dithiol **25** required for the cyclization was obtained in good yield (ca. 85%) by refluxing an ethanolic solution of **21** and thiourea for 12 hours, followed by the base hydrolysis of the isothiuronium salt, as summarized in Scheme 7. The cyclization reaction leading to tosylated macrocycles **22** and **26**

Scheme 6

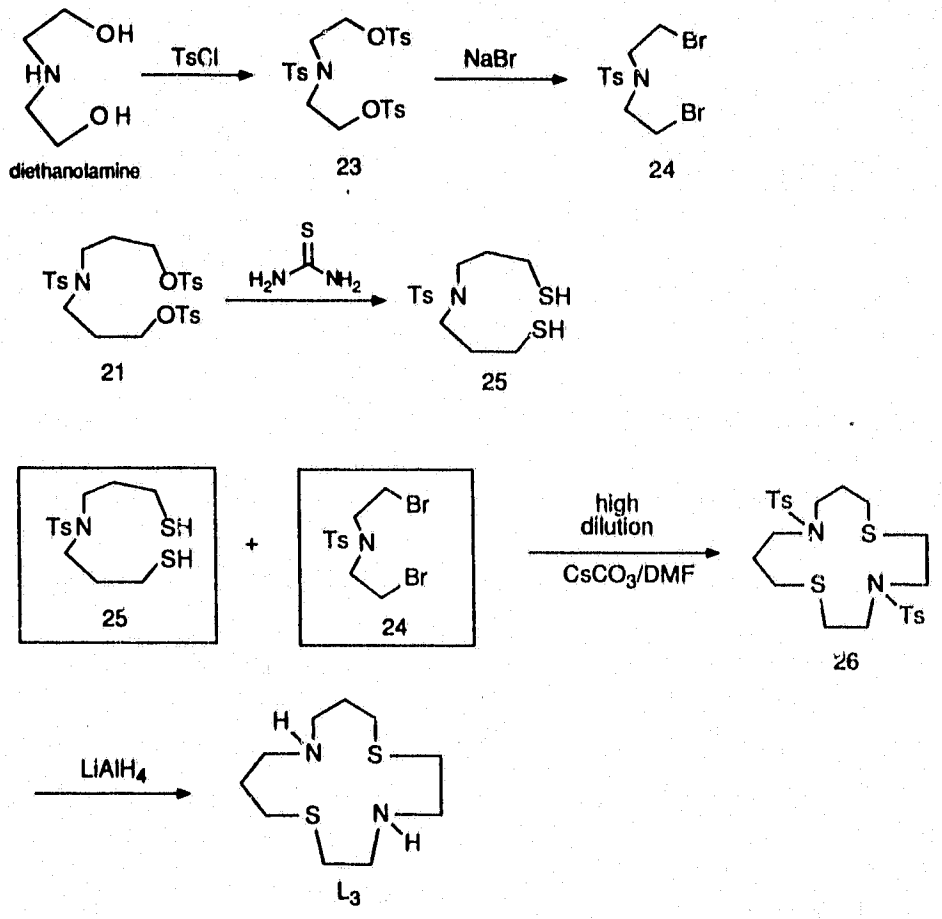

(Scheme 5 and 6) is achieved by the reaction of the corresponding dithiol and dibromide or ditosylate in equimolar concentration under medium dilution conditions (final concentration of reagents ca. 0.01 M) using Cs_2CO_3 as the base in dry DMF.

The detosylation of **22** and **26** was complicated by the presence of thioether functional groups. The thioether linkages were prone to cleavage when acidic procedures sufficient to remove tosyl groups were used (H_2SO_4 at 105 °C for 2 days[54] or 30% HBr/acetic acid[87] heated at refluxed for 2 days).

Scheme 7

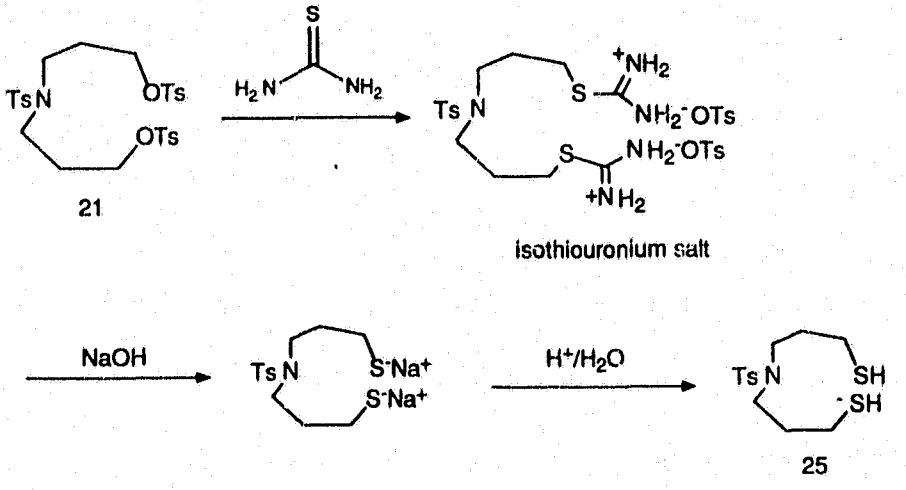

To avoid this problem, a reductive detosylation involving $LiAlH_4$ was employed[88]. Ligands $\mathbf{L}_2$ and $\mathbf{L}_3$ were obtained in satisfactory yields (ca. 70%). The pyridine moiety was introduced into $\mathbf{L}_2$ and $\mathbf{L}_3$ by the reaction of chloromethylpyridine as shown in Schemes 5 and eq. 7, respectively.

Palladium(II) complexes of $\mathbf{L}_2$ and $\mathbf{L}_4$ were prepared by the reaction of equimolar quantities of the ligand with $[Pd(CH_3CN)_4](BF_4)_2$ or $[Pd(PhCN)_2]Cl_2$ in dry CH_3CN under an atmosphere of nitrogen. The platinum(II) complex $[Pt(\mathbf{L}_4)Cl]^+$ was prepared by the reaction of $[Pt(PhCN)_2Cl_2]$ with the free ligand in dry acetonitrile.

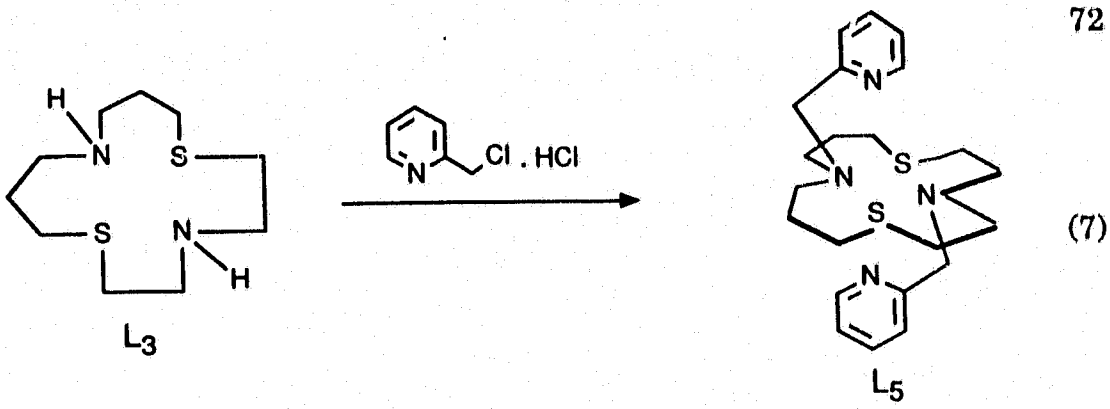

(7)

3.3 Crystal Structures

(a) Crystal structure of $[Pd(\mathbf{L_2})](Cl)(PF_6)$

The palladium(II) complex of L_2 has been characterized by crystallography and the molecular structure is shown in Figure 24, along with the atomic labelling scheme. The crystallographic parameters are listed in Table 12. The fractional atomic coordinates, interatomic distances and bond angles are shown in Tables 13 - 15. As illustrated in Figure 24, the palladium atom is in a square-planar environment. It is coordinated to three sulphur atoms and one nitrogen atom from the ligand.

The average Pd-S bond distance is 2.29 Å, which is similar to those observed in $[Pt(14)aneS_4]^{2+}$ (mean Pt-S = 2.28 Å)[89] and $[Pd(14)aneS_4]^{2+}$ (mean Pd-S = 2.27 Å)[61]. For S(2) which is trans to N(1), the Pd-S(2) bond distance is 0.04 Å shorter than the other two Pd-S bond distances. This is because the trans-influence of a sulphur ligand is greater than that of a nitrogen ligand[1]. The two anions Cl^- and PF_6^- are beyond the bonding distance to palladium (Pd...Cl = 3.396 Å and Pd...F = 4.040 Å).

The five-membered ring chelate bite angles of S(1)-Pd-S(2) and S(2)-Pd-S(3) are 88.6° and 87.1°, respectively. These values are typical of five-membered chelate rings with gauche conformations[65,74,76,89]. The six-membered chelate ring defined by the atoms Pd, N(1), C(8), C(9), C(10) and S(1) adopts a chair conformation with the bite angle of N(1)-Pd-S(1) being 90.4°. The other six-membered chelate ring defined by atoms Pd, S(3), C(5), C(6),C(7) and N(1) adopts a twist-boat conformation with the chelate bite angle N(1)-Pd-S(3) being 93.4°. The bond angles of N(1)-Pd-S(2) and S(1)-Pd-S(3) are 173.6° and 173.2°, respectively. These values are close to the ideal value (180°) for square-planar geometry.

The mean plane calculation for the nitrogen and sulphur donor atoms in the molecular structure of $[Pd(\mathbf{L_2})]^{2+}$ indicates that all three sulphur atoms of the ligand framework lie on the same plane whereas the nitrogen atom is 0.04 Å below the plane (Table 16). The palladium atom, on the other hand, is 0.106 Å above the "plane" defined by the nitrogen and three sulphur atoms. It is interesting to note that when coordinated to palladium, the ligand $\mathbf{L_2}$ adopted a "puckered crown" shape similar to the *Trans-I* geometry observed with transition metal complexes of cyclam (Figure 21). The lone pairs on sulphur atoms and the hydrogen on the nitrogen atom in $[Pd(\mathbf{L_2})]^{2+}$ are oriented above the ligand-metal plane. This configuration puts carbon bridges below the nitrogen and sulphur donor plane. A similar configuration is also adopted by [14]aneS_4 when coordinated to Rh(I)[84], Pd(II)[61] and Pt(II)[89]. This

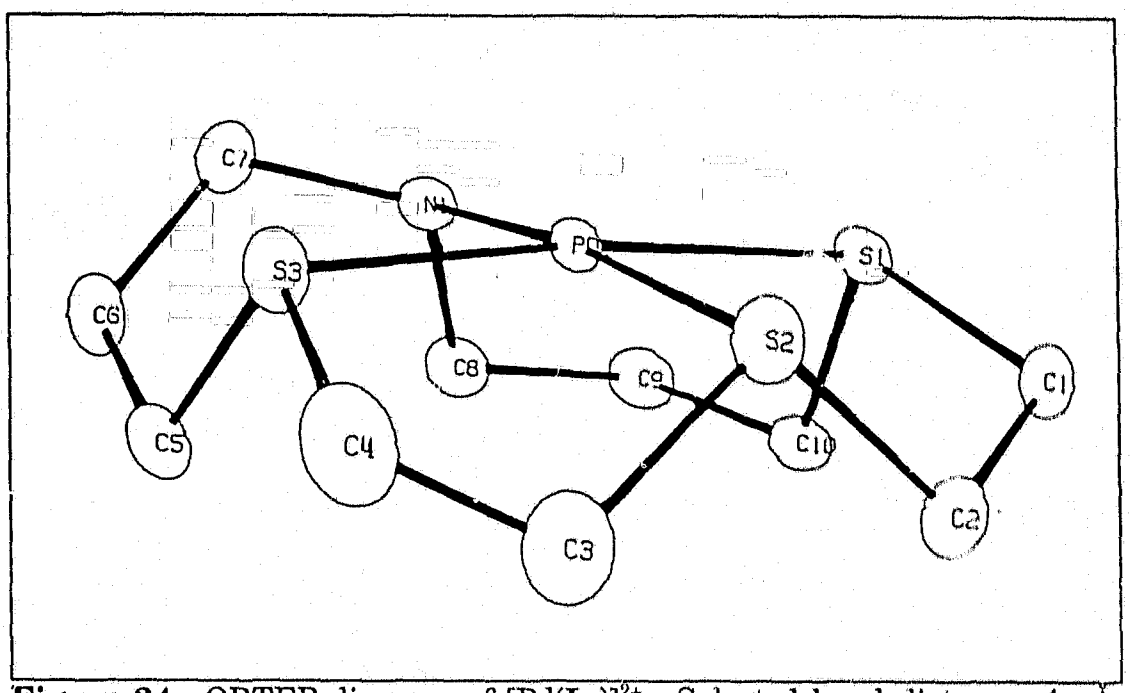

Figure 24 ORTEP diagram of $[Pd(L_2)]^{2+}$. Selected bond distances in Å: Pd-N(1) = 2.088(4), Pd-S(1) = 2.302(1), Pd-S(2) = 2.269(1), Pd-S(3) = 2.309(1).

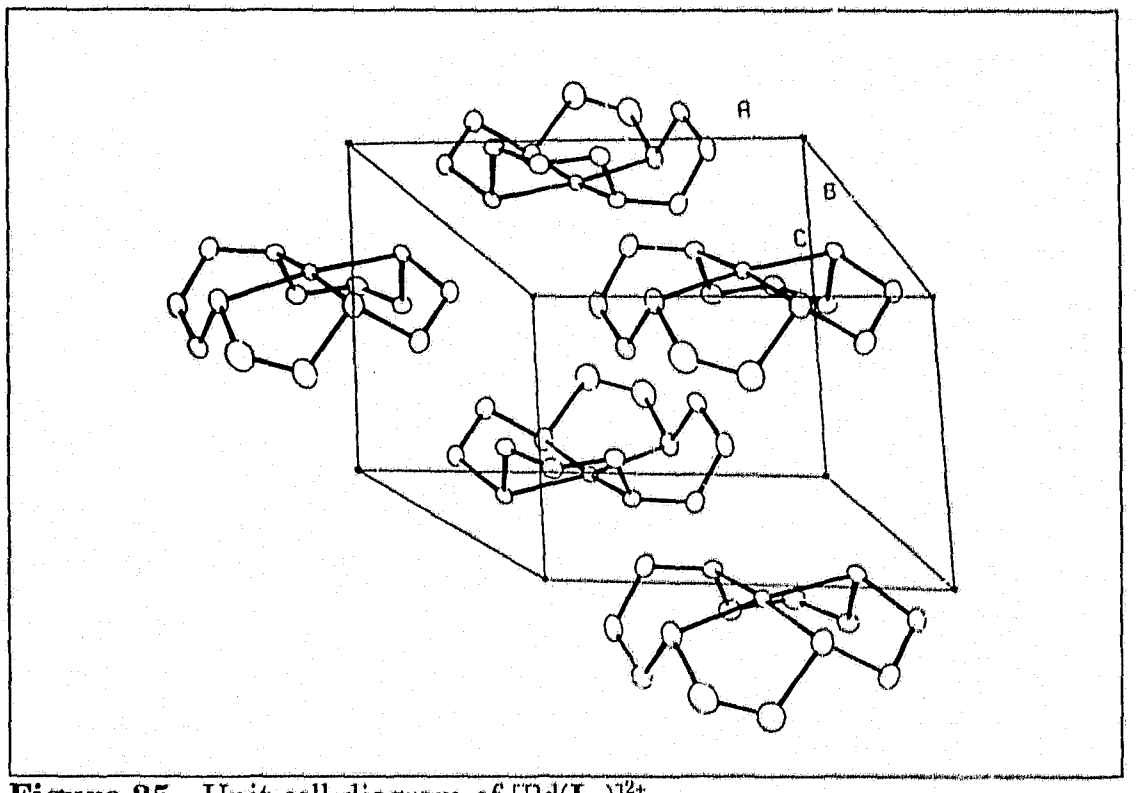

Figure 25 Unit cell diagram of $[Pd(L_2)]^{2+}$

Table 12
Experimental Crystallographic Data for $[Pd(L_2)](Cl)(PF_6)$

Formula:	$PdC_{10}H_{20}NS_3ClPF_6$	
F.W.:	537.3	
Crystal colour:	yellow	
Crystal system:	triclinic	
Space Group:	$P\bar{1}$ (No. 2)	
Cell dimensions:		
	a = 10.127(2) Å	α = 87.99 (2)°
	b = 12.568(4) Å	β = 95.55 (2)°
	c = 7.141(2) Å	γ = 91.02 (2)°
V_{cell}:	904.0 Å^3	
Z:	2 molec./cell	
Temperature:	20 °C	
Crystal dimensions:	0.2 x 0.7 x 0.25 mm^3	
$D_{calcd.}$:	1.974 g/cm^3	
$D_{meas.}$:	1.959 g/cm^3	
Radiation:	Mo, K_α 0.71069 Å	
μ:	15.14 cm^{-1}	
transmission range:	0.805 - 1.00	
Measurement:	2θ(0-50°)	
No. of reflections collected:	3079	
No. of reflections $I \geq n\sigma(I)$:	2806 (n = 4)	
No. of parameters:	208	
No. of standards:	0100, 007, 700	
Residual electron density:	0.16 e/Å^3	
Maximum final shift/error:	0.030	
Refinement method:	SHELX least squares	
R:	0.0422	
R_w:	0.0486	

Table 13
Fractional atomic coordinates and temperature parameters for $[Pd(L_2)](Cl)(PF_6)$

Atom	x/a	y/b	z/c	U_{eq}
Pd(1)	22313(3)	25294(3)	27459(5)	270(2)
Cl(1)	26357(15)	42146(12)	73560(19)	430(5)
S(1)	5400(13)	36453(11)	16040(18)	340(4)
S(2)	7401(15)	15534(11)	42823(24)	437(5)
S(3)	38451(15)	14309(12)	42195(24)	451(5)
P(1)	7675(2)	1020(1)	-842(2)	43(1)
F(1)	7691(7)	1085(4)	1349(6)	94(2)
F(2)	7617(7)	975(5)	-3042(7)	106(3)
F(3)	7329(7)	2241(4)	-1023(9)	110(3)
F(4)	6161(6)	755(5)	-1008(10)	115(3)
F(5)	7938(8)	-186(4)	-655(9)	123(3)
F(6)	9159(5)	1357(7)	-638(10)	134(3)
N(1)	3615(4)	3550(4)	1601(6)	34(1)
C(1)	-778(6)	3223(5)	3058(9)	43(2)
C(2)	-248(6)	2668(5)	4903(3)	45(2)
C(3)	1828(9)	1332(8)	6532(11)	85(4)
C(4)	3044(8)	867(8)	6207(13)	82(3)
C(5)	4921(6)	2489(5)	5203(9)	45(2)
C(6)	5690(6)	2984(5)	3621(10)	50(2)
C(7)	4955(6)	3114(5)	1666(9)	48(2)
C(8)	3649(6)	4643(4)	2486(8)	39(2)
C(9)	2394(6)	5272(4)	1888(8)	41(2)
C(10)	1140(6)	4876(4)	2714(8)	37(2)

Estimated standard deviations are given in parentheses.
Coordinates x 10^n where n = 5,5,5,4,4,4,4 for Pd, Cl, S, P, F, N, C.
Temperature parameters x 10^n where n = 4,4,4,3,3,3,3 for Pd, Cl, S, P, F, N, C.
U_{eq} = the equivalent isotropic temperature parameter.
$U_{eq} = \frac{1}{3}\Sigma_i\Sigma_j U_{ij} a_i^* a_j^* (a_i . a_j)$
$T = \exp-(8\pi^2 U_{iso} \sin^2\theta/\lambda^2)$

Table 14
Interatomic Distances in Å for $[Pd(L_2)](Cl)(PF_6)$

Atoms	Distance	Atoms	Distance
N(1)-Pd(1)	2.088(4)	S(2)-C(3)	1.873(8)
S(1)-Pd(1)	2.302(1)	S(3)-C(4)	1.819(8)
S(2)-Pd(1)	2.269(1)	S(3)-C(5)	1.821(6)
S(3)-Pd(1)	2.309(1)	C(1)-C(2)	1.524(8)
N(1)-C(7)	1.468(7)	C(3)-C(4)	1.415(12)
N(1)-C(8)	1.531(7)	C(5)-C(6)	1.540(9)
S(1)-C(1)	1.829(6)	C(6)-C(7)	1.523(9)
S(1)-C(10)	1.830(5)	C(8)-C(9)	1.527(8)
S(2)-C(2)	1.827(6)	C(9)-C(10)	1.520(8)

Estimated standard deviations are given in parentheses.

Table 15
Bond Angles in degrees for $Pd(L_2)](Cl)(PF_6)$

Atoms	Angle	Atoms	Angle
N(1)-Pd(1)-S(1)	90.4 (1)	C(5)-S(3)-C(4)	104.8 (4)
N(1)-Pd(1)-S(2)	173.2 (1)	C(7)-N(1)-Pd(1)	114.3 (4)
N(1)-Pd(1)-S(3)	93.2 (1)	C(8)-N(1)-Pd(1)	111.3 (3)
S(2)-Pd(1)-S(1)	88.6 (1)	C(8)-N(1)-C(7)	110.9 (4)
S(3)-Pd(1)-S(1)	173.6 (1)	C(2)-C(1)-S(1)	112.7 (4)
S(3)-Pd(1)-S(2)	87.1 (1)	C(4)-C(3)-S(2)	111.4 (6)
C(1)-S(1)-Pd(1)	101.6 (2)	C(3)-C(4)-S(3)	115.8 (5)
C(10)-S(1)-Pd(1)	99.4 (2)	C(6)-C(5)-S(3)	108.3 (4)
C(10)-S(1)-C(1)	101.8 (3)	C(7)-C(6)-C(5)	117.7 (5)
C(2)-S(2)-Pd(1)	96.9 (2)	C(6)-C(7)-N(1)	115.5 (5)
C(3)-S(2)-Pd(1)	96.7 (3)	C(9)-C(8)-N(1)	112.1 (4)
C(3)-S(2)-C(2)	100.6 (4)	C(10)-C(9)-C(8)	116.1 (5)
C(4)-S(3)-Pd(1)	102.5 (3)	C(9)-C(10)-S(1)	110.0 (4)
C(5)-S(3)-Pd(1)	96.3 (2)		

Estimated standard deviations are given in parentheses.

Table 16
Mean plane for $[Pd(L_2)](Cl)(PF_6)$

The equation of the plane containing the three sulphurs and one nitrogen is:

$$-0.0375X - 0.5938Y - 0.8037Z + 3.6755 = 0$$

Atoms	X	Y	Z	P
S(1)	0.3545	4.6189	1.1394	0.0036
S(2)	0.4190	2.0540	3.0419	-0.0048
S(3)	3.5705	1.8986	2.9973	0.0051
N(1)	3.4712	4.4985	1.1376	-0.0404
Pd(1)	2.0134	3.2439	1.9506	0.1060
Cl(1)	2.0669	5.4713	5.2254	-3.8508
C(1)	-1.0709	4.1234	2.1723	-0.4788
C(2)	-0.6496	3.4692	3.4831	-1.1597
C(3)	1.3700	1.8293	4.6397	-1.1912
C(4)	2.6341	1.2376	4.4093	-0.7021

where P is the perpendicular distance between the atom and the mean plane, given in Å.

conformation has been associated with the increase in nucleophilicity in the $[Rh([14]aneS_4)]^+$ cation complex[84]. However, in the unit cell packing diagram (Figure 25) of $[Pd(\mathbf{L_2})]^{2+}$, the open coordination face of the complex is not associated with another molecule to form loose dimers as have been previously observed[84,89] in $[Rh([14]aneS_4)]^+$ and $[Pt([14]aneS_4)]^{2+}$.

(b) Crystal structures of $[Pd(\mathbf{L_4})Cl](PF_6)$ and $[Pt(\mathbf{L_4})Cl](BF_4)$

Both of the palladium(II) and platinum(II) complexes of $\mathbf{L_4}$ have been characterized by crystallography. The molecular structures, along with the atomic labelling schemes are shown in Figures 26 and 27, respectively. The crystallographic parameters are listed in Table 17. The fractional atomic coordinates, interatomic distances and bond angles of $[Pd(\mathbf{L_4})Cl]^+$ are shown in Tables 18 - 20, whereas those of $[Pt(\mathbf{L_4})Cl]^+$ are shown in Tables 22 - 24.

As shown in Figure 26, the ligand $\mathbf{L_4}$ adopts a "folded" conformation when coordinated to palladium, similar to the *cis-V* geometry observed in transition metal complexes of cyclam (Figure 21). This is in contrast to the "trans" conformation adopted by $\mathbf{L_2}$ in $[Pd(\mathbf{L_2})]^{2+}$, which is similar to the *trans-I* geometry observed in metal complexes of cyclam (Figure 21).

In the crystal structure of the $[Pd(\mathbf{L_4})Cl]^+$ ion, the palladium centre is in a square planar environment. It is coordinated to two nitrogen atoms: one of them is a tertiary amino nitrogen from the macrocycle and the other one is an aromatic amino nitrogen from the pyridine moiety, one chloride atom from the counterion and one thioether sulphur atom from the ligand. There are two

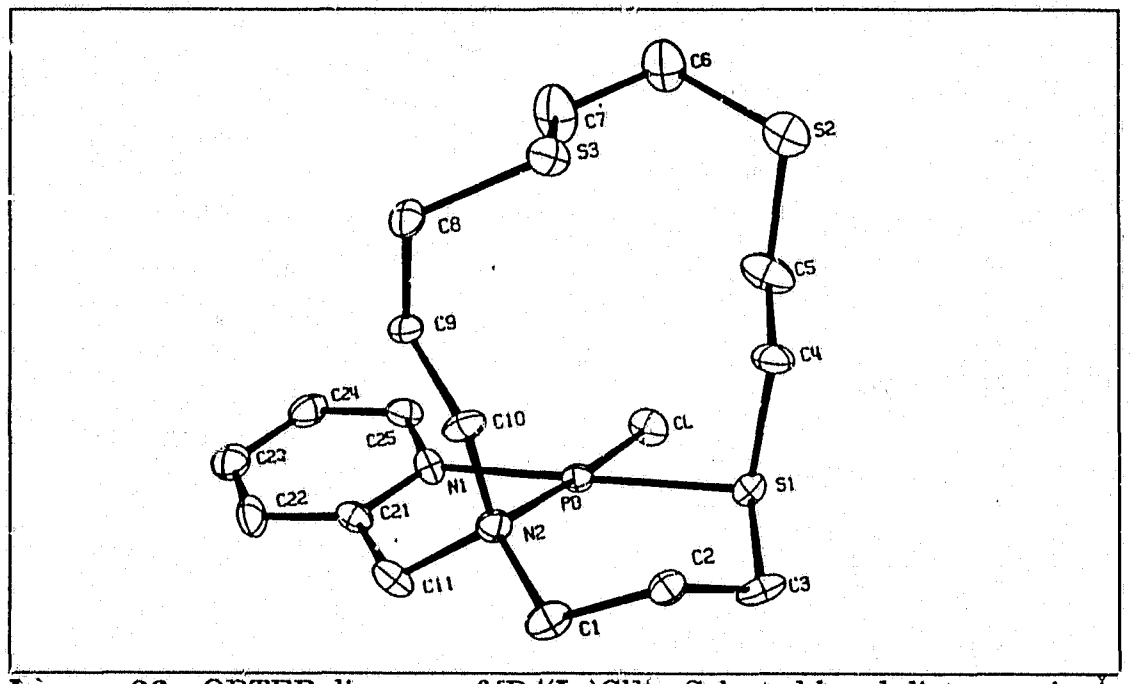

Figure 26 ORTEP diagram of $[Pd(L_4)Cl]^+$. Selected bond distances in Å: Pd-Cl, 2.287(3); Pd-S(1), 2.281(3); Pd-N(1)pyr, 2.035(8); Pd-N(2), 2.093(8); Pd...S(3), 4.77 Å.

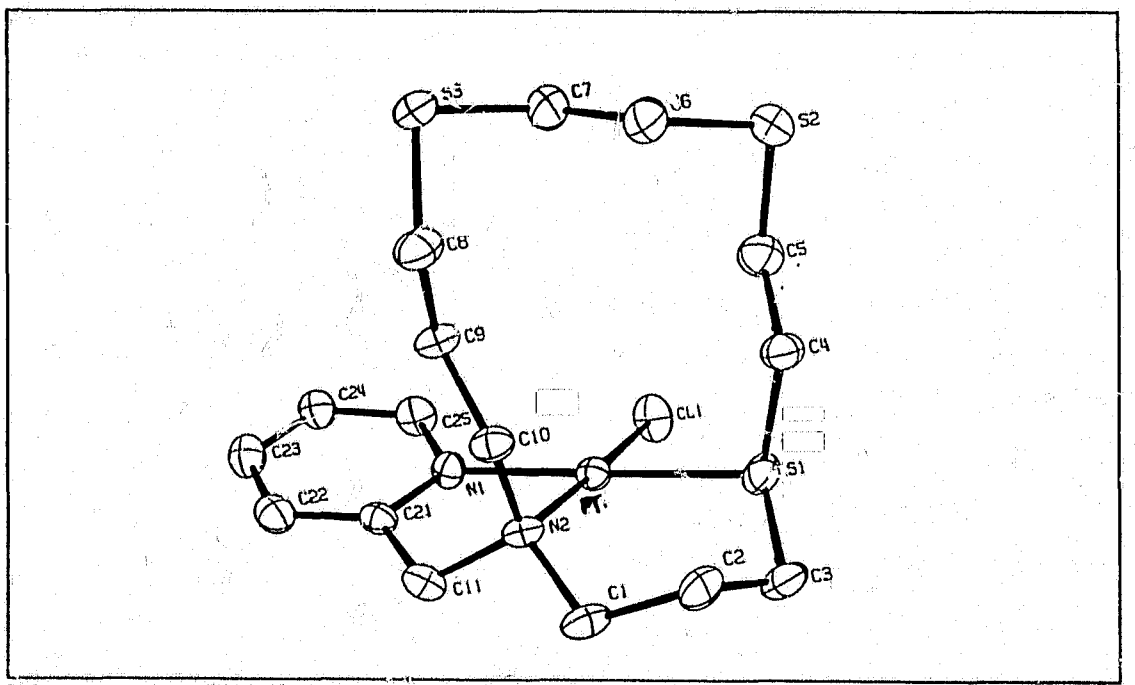

Figure 27 ORTEP diagram of $[Pt(L_4)Cl]^+$. Selected bond distances in Å: Pt-Cl = 2.298(2), Pt-S(1) = 2.268(2), Pt-N(1) = 2.033(7), Pt-N(2) = 2.093(7).

thioether sulphur atoms in the ligand which are not coordinated.

The Pd-N(1)pyr bond distance is 2.04 Å, which is comparable to $[Pdpy_3[9]aneN_3]^{2+}$ (2.03 Å)[74]. The bond length of Pd-N(2) is 2.09 Å, which is comparable to $[Pd(bicylcoSN_4)]^{2+}$ (2.07 Å)[76] and $[Pd(cyclam)]^{2+}$ (2.05 Å)[90]. The bond length of Pd-S(1) is 2.28 Å, which is typical of palladium(II) thioether complexes[61].

The five-membered chelate ring adopts an envelope conformation and the chelate bite angle N(1)pyr-Pd-N(2) is 81.8°, which is smaller than the angle N-Pd-N_{en} observed in $[Pd(cyclam)]^{2+}$ (83°)[90]. This is a consequence of the partial double bond character of the C-N bond of the pyridine moiety which decrease the bite distance between N(1)pyr and N(2) in $[Pd(\mathbf{L}_4)Cl]^+$. The six-membered chelate ring adopts a boat conformation and the chelate bite angle N(2)-Pd-S(1) is 98.7°. The other bond angles in the square plane are: S(1)-Pd-Cl = 85.5°, N(1)pyr-Pd-Cl = 93.9°. These are close to the ideal value of 90° for square planar geometry since there is no constraint imposed by the chloride ligand. The sulphur atom in the apical position, S(3), is pointed towards the palladium ion, with a bond angle C(8)-S(3)-C(7) equals to 100.1° and the interatomic distance Pd-S(3) being 3.30 Å. The other non-coordinated sulphur atom S(2) is oriented such that the bond angle of C(5)-S(2)-C(6) is 105.7°, indicating that the non-bonding electron pairs on the sulphur atom are directed out of the ring.

The mean plane calculations in Table 21 shows that the donor atoms Cl, S(1), N(1) and N(2) are in the same plane, with the palladium centre being 0.009 Å below the plane. The fact that $\mathbf{L_4}$ did not use all its donor atoms to coordinate to palladium to form a five-coordinate complex may due to the presence of chloride which forms stronger bonds than thiother sulphur atoms to Pd(II); or the non-bonding electron pair in the nitrogen atom of the pyridine is already set up for complexation even in the free ligand and little or no reorganization energy is required.

In view of the fact that chloride ions form strong bonds with Pd(II) and Pt(II), the Pt(II) complex was prepared by the reaction of $AgBF_4$ with $Pt(PhCN)_2Cl_2$ in CH_2Cl_2/CH_3CN, followed by the addition of $\mathbf{L_4}$. By doing so, the chloride ions coordinated in $Pt(PhCN)_2Cl_2$ would be removed through the formation of the highly insoluble AgCl and therefore it may be possible to force Pt(II) to coordinate to all of the donor atoms in $\mathbf{L_4}$. Unfortunately, not all of the chloride ions were precipitated as AgCl. Fair amount of $Pt(PhCN)_2Cl_2$ were still present when the free ligand $\mathbf{L_4}$ was added in the complexation reaction. As a result, the more insoluble $[Pt(\mathbf{L_4})Cl](BF_4)$ crystals were isolated when acetonitrile was used as a solvent instead of the anticipated $[Pt(\mathbf{L_4})](BF_4)_2$.

In a broad sense, the structure of $[Pt(\mathbf{L_4})Cl]^+$ is isostructural to its palladium analogue (Figure 27). The platinum metal is in a square planar environment. It is coordinated to two nitrogen atoms, one chloride atom from

the counterion and thioether atom from the ligand. Once again, there are two thioether sulphur atoms in the ligand which are not coordinated.

The Pt-N(1)pyr and Pt-N(2) bond distances are 2.04 Å and 2.09 Å, respectively. The latter is longer than those observed in $[Pt(NH_3)]^{2+}$ (2.06 Å)[91] and $[Pt(en)_2]^{2+}$ (2.04 Å)[92]. The bond distance between Pt-Cl is 2.30 Å and that of Pt-S(1) is 2.26 Å, which is comparable to $[Pt[14]aneS_4]^{2+}$ (2.28 Å)[89]. Due to the partial double bond character of the C-N bond in the pyridine moiety, the bite distance between N(1)pyr and N(2) is decreased. As a consequence, the five-membered chelate bite angle, N(1)pyr-Pt-N(2), is only 81.9°. The six-membered chelate ring adopts a boat conformation and the chelate bite angle N(2)-Pt-S(1) is 98.5°. The other bond angles in the square plane are: S(1)-Pt-Cl = 85.6°, N(1)pyr-Pt-Cl = 94.0°, N(1)pyr-Pd-S(1) = 178.6°, N(2)-Pd-Cl = 175.7°.

A close examination indicates that four donor atoms Cl, S(1), N(1)pyr and N(2) are not strictly coplanar (Table 25). In addition, the conformation of the ligand $\mathbf{L_4}$ in the $[Pt(\mathbf{L_4})Cl]$ ion is slightly different from its palladium analogue. In this case, the sulphur atoms S(2) and S(3) are oriented such that the bond angles C(5)-S(2)-C(6) and C(7)-S(3)-C(8) are 100.6° and 102.1°, respectively, indicating that the non-bonding electron pairs in both of S(2) and S(3) are pointing out of the ring (exodentate). These results from the molecular structures suggest that both Pd(II) and Pt(II) prefer to coordinate to the nitrogen atoms from the macrocycle and the pyridine pendant arm.

Perhaps the five-membered chelate ring formed by such coordination is very favourable thermodynamically and structurally.

Table 17

Experimental crystallographic data for $[Pd(L_4)Cl](PF_6)$ and $[Pt(L_4)Cl](BF_4)$

Formula:	$PdClPF_6C_{16}H_{26}N_2S_3$	$PtClBF_4C_{16}H_{26}N_2S_3$
F.W.:	620.39	659.9
Crystal colour:	yellow	clear(white)
Crystal system:	orthorhombic	triclinic
Space group:	$P2_12_12_1$(No. 19)	$P\bar{1}$(No. 2)
Cell dimensions:	a = 13.305(3) Å	a = 8.940(3)
	b = 12.413(4) Å	b = 14.478(6)
	c = 14.060(3) Å	c = 9.110(5)
	α = 90°	α = 94.59(6)
	β = 90°	β = 102.85(4)
	γ = 90°	γ = 94.83(5)
V_{cell}:	2322.1 Å^3	1139.6 Å^3
Z:	4 molecules/cell	2 molecules/cell
Temperature:	20 °C	20 °C
Crystal dimensions:	0.195 x 0.170 x 0.604 mm^3	0.49 x 0.20 x 0.29 mm^3
$D_{calc.}$:	1.800	1.923
$D_{meas.}$:	1.767	1.917
Radiation:	Mo, K_α 0.71069 Å	Mo, K_α 0.71069 Å
μ:	12.61 cm^{-1}	68.74 cm^{-1}
Transmission range:	0.777 - 0.817	0.151 - 0.292
Measurement:	2θ(0 - 50°)	2θ(25 - 50)
No. of reflections collected:	2333	4013
No. of reflections $I \geq n\sigma(I)$:	2075 (n = 2)	3661 (n = 6)
No. of parameters:	271	253
No. of standards:	0010, 0100, 1000	005, 070, 300
Residual electron density:	0.2 e/Å^3	0.2 e/Å^3
Maximum final shift/error:	0.01	0.004
Refinement method:	least squares	least squares
R:	0.0538	0.0507
R_w:	0.0529	0.0517

Table 18
Fractional atomic coordinates and temperature parameters for $[Pd(L_4)Cl](PF_6)$

Atom	x/a	y/b	z/c	U_{eq}
Pd	75391(6)	-486(6)	84102(5)	290(2)
Cl	86400(23)	-10773(25)	92679(22)	468(10)
S(1)	96448 (21)	7411(24)	77808(21)	381(9)
S(2)	96448(26)	81379(27)	57892(24)	543(11)
S(3)	72210(23)	-15259(24)	52913(22)	465(10)
N(1)	6301(6)	-773(7)	8969(6)	32(3)
N(2)	6445(6)	817(7)	7663(6)	31(3)
P	76779(29)	47254(26)	34584(30)	591(12)
F(1)	7522(16)	5132(12)	2459(10)	211(10)
F(2)	6798(9)	3878(11)	3289(11)	138(6)
F(3)	7806(11)	4268(10)	4458(8)	137(6)
F(4)	8533(12)	5552(13)	3609(15)	198(10)
F(5)	8407(10)	3879(10)	3069(10)	135(6)
F(6)	6955(11)	5627(10)	3844(11)	157(7)
C(1)	6660(9)	2000(9)	7498(9)	44(4)
C(2)	7610(9)	2193(8)	6850(8)	44(4)
C(3)	8613(11)	2097(9)	7364(10)	51(4)
C(4)	9148(9)	47(9)	6650(8)	46(4)
C(5)	9474(12)	-1097(12)	6873(9)	64(5)
C(6)	8730(10)	-2965(11)	5849(12)	67(5)
C(7)	7643(11)	-2661(11)	6004(13)	82(6)
C(8)	5950(9)	-1378(10)	5744(7)	43(4)
C(9)	5923(9)	-899(10)	6769(8)	45(4)
C(10)	6187(9)	283(8)	6737(7)	37(3)
C(11)	5559(8)	819(9)	8329(8)	42(4)
C(21)	5435(8)	-245(8)	8860(7)	36(3)
C(22)	4509(9)	-626(11)	9183(9)	52(4)
C(23)	4472(9)	-1608(10)	9638(8)	51(4)
C(24)	5377(11)	-2194(9)	9743(9)	54(4)
C(25)	6276(9)	-1769(9)	9405(7)	39(4)

Estimated standard deviations are given in parentheses.
Coordinates x 10^n where n = 5,5,5,4,4,4,4 for Pd,Cl,S,N,P,F,C
Temperature parameters x 10^n where n = 4,4,4,3,3,3,3 for Pd,Cl,S,N,P,F,C.
U_{eq} = the equivalent isotropic temperature parameter.
$U_{eq} = \frac{1}{3}\Sigma_i\Sigma_j U_{ij} a_i^* a_j^* (a_i.a_j)$
$T = \exp-(8\pi^2 U_{iso} \sin^2\theta/\lambda^2)$

Table 19
Interatomic Distances (Å) for $[Pd(L_4)Cl](PF_6)$

Atoms	Distance	Atoms	Distance
Cl-Pd	2.287(3)	F(2)-P	1.591(11)
S(1)-Pd	2.281(3)	F(3)-P	1.525(11)
N(1)-Pd	2.035(8)	F(4)-P	1.546(13)
N(2)-Pd	2.093(8)	F(5)-P	1.531(11)
C(3)-S(1)	1.833(12)	F(6)-P	1.572(11)
C(4)-S(1)	1.829(11)	C(2)-C(1)	1.576(17)
C(5)-S(2)	1.809(13)	C(3)-C(2)	1.523(18)
C(6)-S(2)	1.834(14)	C(5)-C(4)	1.518(16)
C(7)-S(3)	1.820(14)	C(7)-C(6)	1.504(19)
C(8)-S(3)	1.817(12)	C(9)-C(8)	1.558(15)
C(21)-N(1)	1.334(13)	C(10)-C(9)	1.509(15)
C(25)-N(1)	1.381(14)	C(21)-C(11)	1.526(15)
C(1)-N(2)	1.514(14)	C(22)-C(21)	1.396(15)
C(10)-N(2)	1.501(13)	C(23)-C(22)	1.377(17)
C(11)-N(2)	1.506(13)	C(24)-C(23)	1.413(18)
F(1)-P	1.508(13)	C(25)-C(24)	1.391(16)

Estimated standard deviations are given in parentheses.

Table 20
Bond Angles (deg) for $[Pd(L_4)Cl](PF_6)$

Atoms	Angle	Atoms	Angle
S(1)-Pd-Cl	85.5(1)	F(5)-P-F(1)	89.1(8)
N(1)-Pd-Cl	93.9(3)	F(5)-P-F(2)	87.7(7)
N(1)-Pd-S(1)	179.2(3)	F(5)-P-F(3)	90.1(7)
N(2)-Pd-Cl	175.7(3)	F(5)-P-F(4)	92.2(8)
N(2)-Pd-S(1)	98.7(2)	F(6)-P-F(1)	90.0(8)
N(2)-Pd-N(1)	81.8(3)	F(6)-P-F(2)	94.1(8)
C(3)-S(1)-Pd	109.1(5)	F(6)-P-F(3)	90.9(7)
C(4)-S(1)-Pd	105.1(4)	F(6)-P-F(4)	86.0(8)
C(4)-S(1)-C(3)	101.1(6)	F(6)-P-F(5)	178.0(8)
C(6)-S(2)-C(5)	105.7(7)	C(2)-C(1)-N(2)	112.8(9)
C(8)-S(3)-C(7)	100.1(6)	C(3)-C(2)-C(1)	114.6(9)
C(21)-N(1)-Pd	116.0(7)	C(2)-C(3)-S(1)	115.5(8)
C(25)-N(1)-Pd	125.9(7)	C(5)-C(4)-S(1)	107.8(8)
C(25)-N(1)-C(21)	118.0(9)	C(4)-C(5)-S(2)	110.7(9)
C(1)-N(2)-Pd	116.3(7)	C(7)-C(6)-S(2)	117.1(10)
C(10)-N(2)-Pd	111.6(6)	C(6)-C(7)-S(3)	114.4(11)
C(10)-N(2)-C(1)	109.8(8)	C(9)-C(8)-S(3)	112.6(8)
C(11)-N(2)-Pd	103.5(6)	C(10)-C(9)-C(8)	109.8(10)
C(11)-N(2)-C(1)	104.0(8)	C(9)-C(10)-N(2)	117.2(9)
C(11)-N(2)-C(10)	111.2(8)	C(21)-C(11)-N(2)	112.8(8)
F(2)-P-F(1)	88.9(10)	C(11)-C(21)-N(1)	112.8(9)
F(3)-P-F(1)	177.3(10)	C(22)-C(21)-N(1)	124.0(10)
F(3)-P-F(2)	88.5(8)	C(22)-C(21)-C(11)	123.2(10)
F(4)-P-F(1)	90.4(10)	C(23)-C(22)-C(21)	118.8(12)
F(4)-P-F(2)	179.3(11)	C(24)-C(23)-C(22)	118.3(11)
F(4)-P-F(3)	92.2(10)	C(25)-C(24)-C(23)	120.1(10)
		C(24)-C(25)-N(1)	120.8(10)

Estimated standard deviations are given in parentheses.

Table 21
Mean plane for $[Pd(L_4)Cl](PF_6)$

The equation of the plane containing Cl, S and two nitrogens is:
0.0167X - 0.6811Y - 0.7320Z + 8.4352 = 0

Atoms	X	Y	Z	P
Cl	11.4955	-1.3372	13.0307	0.0001
S(1)	11.8911	0.9199	10.9398	-0.0001
N(1)	8.3832	-0.9596	12.6101	-0.0013
N(2)	8.5749	1.0148	10.7739	0.0012
S(2)	12.8324	10.1016	8.1396	-4.1895
S(3)	9.6075	-1.8941	7.4396	4.4423
Pd	10.0308	-0.0603	11.8247	-0.0114
C(11)	7.3959	1.0164	11.711	-0.7056
C(21)	7.2315	-0.3044	12.4576	-0.3552

where P is the perpendicular distance between the atom and the mean plane, given in Å.

Table 22
Fractional atomic coordinates and temperature parameters for $[Pt(L_4)Cl](BF_4)$

Atom	x/a	y/b	z/c	U_{eq}
Pt(1)	32058(3)	20029(2)	28194(3)	393(1)
Cl(1)	27442(31)	4510(17)	31283(33)	637(9)
S(1)	7228(26)	18657(20)	14711(30)	547(8)
S(2)	16195(34)	7540(24)	-28792(33)	699(10)
S(3)	63887(31)	22011(27)	-17098(34)	765(12)
N(1)	5447(8)	2109(5)	3983(8)	42(2)
N(2)	3778(8)	3419(5)	2658(8)	43(2)
C(1)	2518(12)	4047(7)	2768(12)	59(4)
C(2)	1024(12)	3817(8)	1491(15)	72(4)
C(3)	-19(13)	3029(10)	1645(13)	70(4)
C(4)	759(11)	1768(7)	-543(10)	55(3)
C(5)	1432(13)	861(8)	-938(13)	66(4)
C(6)	3244(13)	1587(11)	-2754(13)	75(5)
C(7)	4763(12)	1310(9)	-1913(14)	72(4)
C(8)	5785(13)	3174(8)	-675(12)	61(4)
C(9)	5484(10)	2962(6)	844(10)	47(3)
C(10)	4310(10)	3599(6)	1252(10)	46(3)
C(11)	5056(11)	3725(6)	4018(10)	52(3)
C(21)	6140(10)	2975(6)	4359(9)	42(3)
C(22)	7691(11)	3169(7)	5000(10)	52(3)
C(23)	8568(11)	2421(8)	5256(11)	58(3)
C(24)	7897(11)	1538(8)	4890(11)	58(3)
C(25)	6316(11)	1384(6)	4243(11)	53(3)
B(1)	1972(14)	4407(8)	7275(14)	59(4)
F(1)	1463(14)	3628(7)	7780(11)	130(5)
F(2)	3314(14)	4284(8)	6830(13)	136(6)
F(3)	2397(16)	5027(10)	8537(18)	198(8)
F(4)	1030(19)	4707(15)	6171(19)	250(12)

Estimated standard deviations are given in parentheses.
Coordinates x 10^n where n = 5,5,5,4,4,4,4 for Pt,Cl,S,N,C,B,F.
Temperature parameters x 10^n where n = 4,4,4,3,3,3,3 for Pt,Cl,S,N,C,B,F.
U_{eq} = the equivalent isotropic temperature parameter.
$U_{eq} = \frac{1}{3} \Sigma_i\Sigma_j U_{ij} a_i^* a_j^* (a_i.a_j)$ $T = \exp-(8\pi^2 U_{iso} \sin^2\theta/\lambda^2)$

Table 23
Interatomic Distances (Å) for $[Pt(L_4)Cl](BF_4)$

Atoms	Distance	Atoms	Distance
Cl(1)-Pt(1)	2.298(2)	C(2)-C(1)	1.555(16)
S(1)-Pt(1)	2.268(2)	C(3)-C(2)	1.444(18)
N(1)-Pt(1)	2.033(7)	C(5)-C(4)	1.538(14)
N(2)-Pt(1)	2.093(7)	C(7)-C(6)	1.506(16)
C(3)-S(1)	1.868(13)	C(9)-C(8)	1.515(13)
C(4)-S(1)	1.835(9)	C(10)-C(9)	1.538(11)
C(5)-S(2)	1.806(12)	C(21)-C(11)	1.520(12)
C(6)-S(2)	1.783(13)	C(22)-C(21)	1.374(13)
C(7)-S(3)	1.824(13)	C(23)-C(22)	1.392(15)
C(8)-S(3)	1.817(11)	C(24)-C(23)	1.348(15)
C(21)-N(1)	1.333(11)	C(25)-C(24)	1.396(14)
C(25)-N(1)	1.361(11)	F(1)-B(1)	1.322(14)
C(1)-N(2)	1.520(11)	F(2)-B(1)	1.368(16)
C(10)-N(2)	1.494(11)	F(3)-B(1)	1.362(17)
C(11)-N(2)	1.494(11)	F(4)-B(1)	1.290(16)

Estimated standard deviations are given in parentheses.

Table 24
Bond Angles for $[Pt(L_4)Cl](BF_4)$

Atoms	Angle	Atoms	Angle
S(1)-Pt(1)-Cl(1)	85.6(1)	C(2)-C(3)-S(1)	115.5(7)
N(1)-Pt(1)-Cl(1)	94.0(2)	C(5)-C(4)-S(1)	109.1(7)
N(1)-Pt(1)-S(1)	178.6(2)	C(4)-C(5)-S(2)	111.6(8)
N(2)-Pt(1)-Cl(1)	175.8(2)	C(7)-C(6)-S(2)	114.9(11)
N(2)-Pt(1)-S(1)	98.5(2)	C(6)-C(7)-S(3)	114.1(10)
N(2)-Pt(1)-N(1)	81.9(3)	C(9)-C(8)-S(3)	114.1(8)
C(3)-S(1)-Pt(1)	108.0(4)	C(10)-C(9)-C(8)	109.0(7)
C(4)-S(1)-Pt(1)	107.4(3)	C(9)-C(10)-N(2)	115.7(7)
C(4)-S(1)-C(3)	99.8(5)	C(21)-C(11)-N(2)	111.4(7)
C(6)-S(2)-C(5)	100.6(5)	C(11)-C(21)-N(1)	113.8(7)
C(8)-S(3)-C(7)	102.1(5)	C(22)-C(21)-N(1)	122.9(8)
C(21)-N(1)-Pt(1)	115.5(6)	C(22)-C(21)-C(11)	123.3(8)
C(25)-N(1)-Pt(1)	125.6(6)	C(23)-C(22)-C(21)	118.0(9)
C(25)-N(1)-C(21)	118.5(7)	C(24)-C(23)-C(22)	120.4(9)
C(1)-N(2)-Pt(1)	115.6(6)	C(25)-C(24)-C(23)	119.0(9)
C(10)-N(2)-Pt(1)	113.4(5)	C(24)-C(25)-N(1)	121.2(9)
C(10)-N(2)-C(1)	107.3(7)	F(2)-B(1)-F(1)	109.8(12)
C(11)-N(2)-Pt(1)	104.7(5)	F(3)-B(1)-F(1)	104.0(12)
C(11)-N(2)-C(1)	105.6(7)	F(3)-B(1)-F(2)	104.9(11)
C(11)-N(2)-C(10)	109.8(7)	F(4)-B(1)-F(1)	116.0(13)
C(2)-C(1)-N(2)	114.5(8)	F(4)-B(1)-F(2)	107.9(14)
C(3)-C(2)-C(1)	116.5(11)	F(4)-B(1)-F(3)	113.6(16)

Estimated standard deviations are given in parentheses.

Table 25
Mean plane for $[Pt(L_4)Cl](BF_4)$

The equation of the plane containing Cl, S and two nitrogen atoms is:
0.5190X - 0.1670Y - 0.8383Z + 1.4583 = 0

Atoms	X	Y	Z	P
Cl(1)	1.7645	0.3682	2.7641	-0.0033
S(1)	0.1207	2.5588	1.2998	0.0053
N(1)	3.8056	2.6824	3.5195	0.0448
N(2)	2.4225	4.6920	2.3486	-0.0266
S(2)	1.9391	1.3476	-2.5431	4.3710
S(3)	5.7896	3.3298	-1.5108	5.1843
Pd	2.0506	2.6350	2.4912	-0.0057
C(11)	3.2516	5.0116	3.5501	-0.6669
C(21)	4.2431	3.8984	3.8515	-0.2191

where P is the perpendicular distance between the atom and the mean plane, given in Å.

(c) Crystal structure of $[Pd(L_4)](BF_4)_2$

In order to obtain a Pd(II) complex without a coordinated anion, $[Pd(CH_3CN)_4](BF_4)_2$ was used as a starting material to react with the free ligand L_4, yielding the cation complex $[Pd(L_4)]^{2+}$. The molecular structure of this cation, along with the atomic labelling scheme is shown in Figure 28. The crystallographic parameters are listed in Table 26. The fractional atomic coordinates, interatomic distances and bond angles are shown in Tables 27-29.

In the molecular structure of $[Pd(L_4)]^{2+}$ (Figure 28), the palladium centre is in a square planar environment. It is coordinated to two nitrogen atoms and two thioether sulphur atoms. The ligand L_4 adopts a "folded" conformation, similar to the *cis-V* geometry observed in transition metal complexes of cyclam (Figure 21). Such a ligand conformation has also been observed previously in the cation complex $[Pd(L_4)Cl]^+$ and the platinum analogue (Figures 26 and 27).

The five membered chelate rings in $[Pd(L_4)]^{2+}$ adopt an envelope conformation with bite angles N(1)pyr-Pd-N(2) = 81.7° and S(1)-Pd-S(2) = 86.8°. The six membered chelate ring adopts a chair conformation with a bite angle N(2)-Pd-S(1) being 94.2°. The Pd-N(1)pyr distance is 2.08 Å, which is longer than those observed in the chloro complex $[Pd(L_4)Cl]^+$ (Pd-N(pyr) = 2.03 Å). On the other hand, the bond distance of Pd-N(2) is 2.07 Å, which is slightly shorter than those in $[Pd(L_4)Cl]^+$ (Pd-N = 2.09 Å). For S(1) which is trans to the nitrogen atom N(1) of the pyridine ring, the Pd-S(1) distance is 2.26 Å, which is 0.05 Å shorter than Pd-S(2). This is attributed to the trans-influence

of a sulphur ligand being stronger than an amine nitrogen, which in turn is stronger than nitrogen from the pyridine moiety. The non-coordinated S(3) atom is pointing towards the palladium ion, with Pd-S(3) interatomic distance being 3.12 Å.

The donor atoms S(1), S(2), N(1) and N(2) do not lie in the same plane (Table 30). However, the palladium centre, S(1) and S(2) are almost coplanar. A comparison with the structure of $[Pd(L_4)Cl]^+$ indicates that in the absence of a chloride anion, the sulphur atom S(2) in L_4 is forced to coordinate to the palladium metal centre. This in effect has shortened the Pd...S(3) distance by 0.2 Å and increased the angle between C(8)-S(3)-C(7) from 100.1° in $[Pd(L_4)Cl]^+$ to a value of 105.3° in $[Pd(L_4)]^{2+}$. A comparison of the coordination geometry for the three complexes, $[Pd(L_4)Cl]^+$, $[Pt(L_4)Cl]^+$ and $[Pd(L_4)]^{2+}$ is summarized in Figure 29.

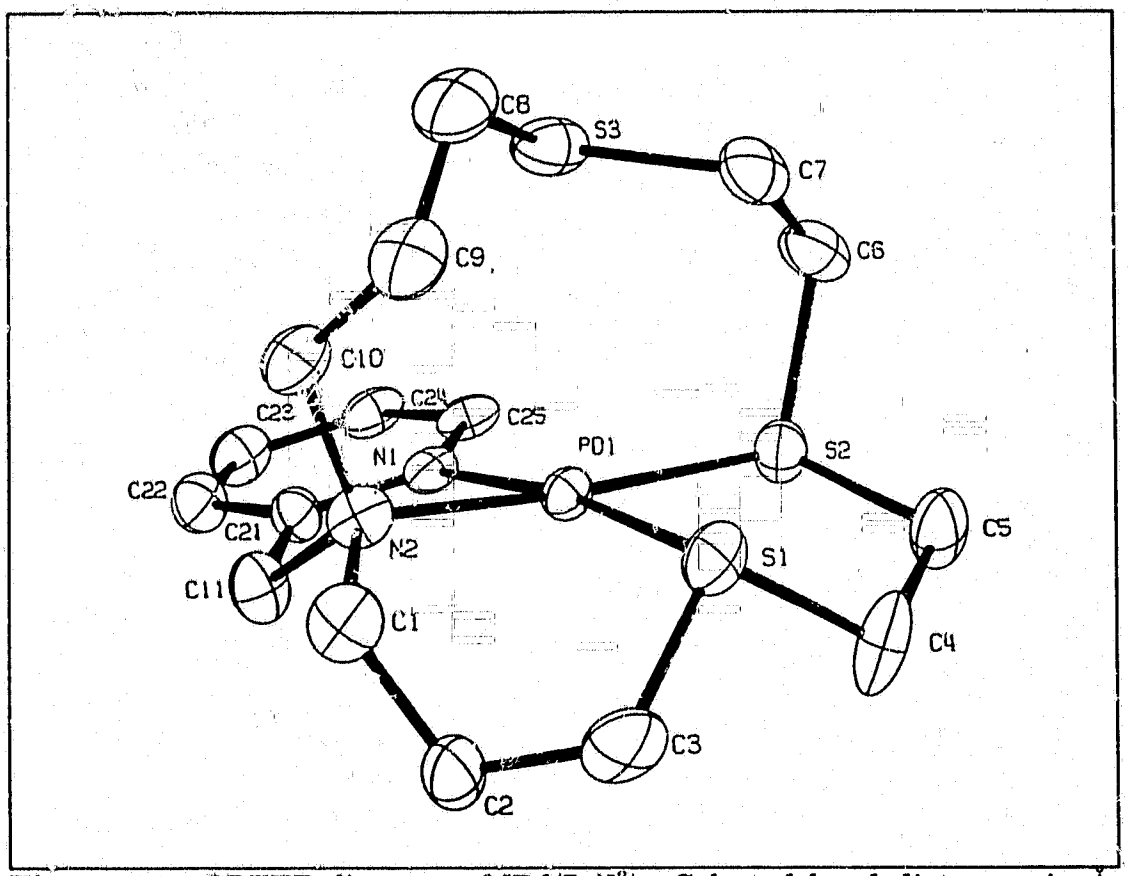

Figure 28 ORTEP diagram of $[Pd(L_4)]^{2+}$. Selected bond distances in Å: Pd-N(1)pyr, 2.078(8); Pd-N(2), 2.067(8); Pd-S(1), 2.260(3); Pd-S(2), 2.308(3); Pd...S(3), 3.12 Å.

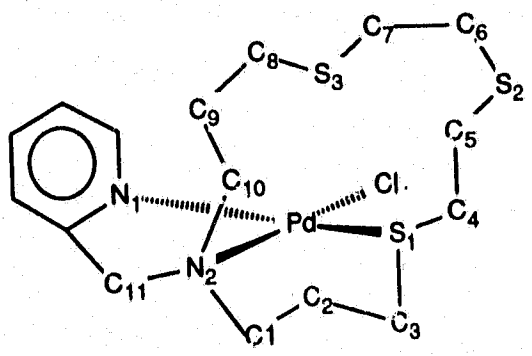

Pd-N(1) = 2.03 Å
Pd-N(2) = 2.09 Å
Pd-S(1) = 2.28 Å
Pd-Cl = 2.29 Å
N(1)-Pd-Cl = 93.9°
N(2)-Pd-S(1) = 98.7°
N(1)-Pd-N(2) = 81.8°
S(1)-Pd-Cl = 85.5°
C(6)-S(2)-C(5) = 105.7°
C(10)-N(2)-Pd = 111.6°
C(10)-N(2)-C(11) = 111.2°
C(4)-S(1)-Pd = 105.1°

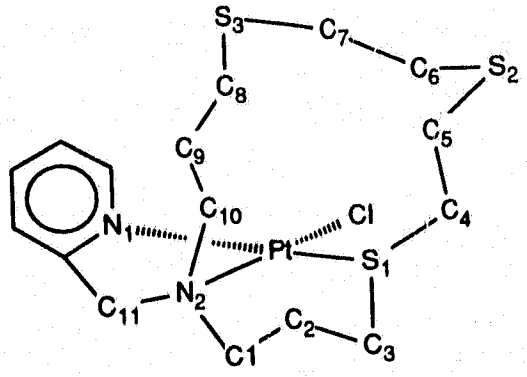

Pt-N(1) = 2.03 Å
Pt-N(2) = 2.09 Å
Pt-S(1) = 2.27 Å
Pt-Cl = 2.30 Å
N(1)-Pt-Cl = 94.0°
N(1)-Pt-N(2) = 81.9°
N(2)-Pt-S(1) = 98.5°
S(1)-Pt-Cl = 85.6°
C(10)-N(2)-Pt = 113.4°
C(10)-N(2)-C(11) = 109.8°
C(4)-S(1)-Pt = 107.4°
C(6)-S(2)-C(5) = 100.6°

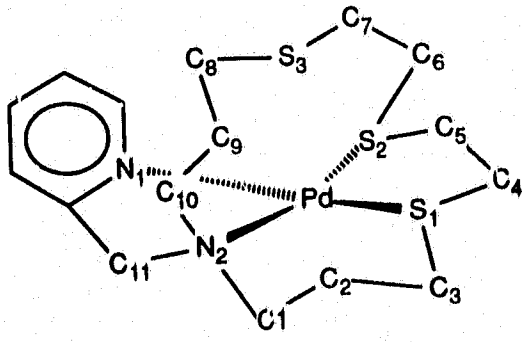

Pd-N(1) = 2.08 Å
Pd-N(2) = 2.07 Å
Pd-S(1) = 2.26 Å
Pd-S(2) = 2.31 Å
N(1)-Pd-N(2) = 81.7°
N(1)-Pd-S(2) = 97.9°
N(2)-Pd-S(1) = 94.2°
S(1)-Pd-S(2) = 86.8°
C(10)-N(2)-Pd = 108.5°
C(10)-N(2)-C(11) = 109.7°
C(4)-S(1)-Pd = 101.4°
C(6)-S(2)-Pd = 105.8°
C(5)-S(2)-Pd = 103.6°

Figure 29 Comparison of coordination geometry for $[Pd(L_4)Cl]^+$, $[Pt(L_4)Cl]^+$ and $[Pd(L_4)]^{2+}$.

Table 26
Experimental crystallographic data for $[Pd(\mathbf{L}_4)](BF_4)_2$

Formula:	$PdB_2F_8C_{16}H_{26}N_2S_3.H_2O$	
F.W.:	640.6	
Crystal color:	orange-yellow	
Crystal system:	monoclinic	
Space group:	I2/a (No. 15)	
Cell dimensions:	a = 19.045(8)	$\alpha = 90°$
	b = 16.952(4)	$\beta = 113.47$ (3)
	c = 16.635(6)	$\gamma = 90°$
V_{cell}:	4926.3 Å^3	
Z:	8 molecules/cell	
Temperature:	20 °C	
Crystal dimensions:	0.152 x 0.368 x 0.501 mm^3	
D_{calcd}:	1.727	
$D_{meas.}$:	1.723	
Radiation:	Mo, K_α 0.71069 Å	
μ:	10.85 cm^{-1}	
Transmission range:	0.680 - 0.856	
Measurement:	$2\theta(0 - 45°)$	
No. of reflections collected:	3214	
No. of reflection $I \geq n\sigma(I)$:	2106 (n = 6)	
No. of parameters;	298	
No. of standards:	080, 006, 600	
Residual electron density:	0.20 e/Å^3	
Maximum final shift/error:	0.05	
Refinement method:	least squares SHELX76	
R:	0.0532	
R_w:	0.056	

Table 27
Fractional atomic coordinates and temperature parameters for $[Pd(L_4)](BF_4)_2$

Atoms	x/a	y/b	z/c	U_{eq}
Pd(1)	-2776(5)	32853(5)	19608(5)	440(3)
S(1)	-67(19)	45570(18)	23767(22)	658(14)
S(2)	7741(16)	33126(18)	16007(20)	606(13)
S(3)	8354(20)	22629(19)	35004(22)	795(16)
N(1)	-682(5)	2175(5)	1462(5)	43(3)
N(2)	-1169(5)	3214(5)	2369(6)	56(4)
C(1)	-1547(7)	3992(7)	2457(9)	80(7)
C(2)	-1608(8)	4567(7)	1751(10)	80(7)
C(3)	-916(8)	5105(8)	1972(12)	96(8)
C(4)	361(8)	4912(8)	1579(11)	95(8)
C(5)	1029(7)	4373(7)	1671(11)	95(8)
C(6)	1577(6)	2926(8)	2564(9)	76(6)
C(7)	1481(7)	3028(7)	3422(10)	81(6)
C(8)	510(9)	2613(8)	4333(9)	94(7)
C(9)	-181(9)	3186(8)	3965(8)	85(7)
C(10)	-883(7)	2789(7)	3249(8)	71(6)
C(11)	-1781(7)	2720(7)	1680(9)	72(6)
C(21)	-1385(6)	2054(7)	1441(7)	52(5)
C(22)	-1765(7)	1335(7)	1131(7)	64(5)
C(23)	-1401(8)	762(7)	824(8)	71(6)
C(24)	-669(7)	906(6)	849(7)	62(5)
C(25)	-327(6)	1622(6)	1177(7)	51(4)
B(1)	1666(10)	685(10)	1130(12)	73(8)
B(2)	6303(9)	3806(10)	516(10)	71(7)
F(1)	996(5)	308(6)	848(7)	139(6)
F(2)	2222(6)	220(7)	1471(9)	170(7)
F(3)	1662(8)	1248(8)	1609(12)	250(12)
F(4)	1771(9)	956(8)	445(10)	216(11)
F(5)	6452(7)	4484(6)	196(7)	150(7)
F(6)	6567(6)	3198(6)	223(6)	151(6)
F(7)	5514(5)	3783(6)	244(6)	124(5)
F(8)	6611(4)	3819(4)	1415(5)	89(4)
O(1)	2297(8)	3664(8)	488(12)	212(12)

Estimated standard deviations are given in parentheses.
Coordinates x 10^n where n = 5,5,4,4,4,4,4 for Pd,S,N,C,B,F,O.
Temperature parameters x 10^n where n = 4,4,3,3,3,3,3 for Pd,S,N,C,B,F,O.
U_{eq} = the equivalent isotropic temperature parameter.
$U_{eq} = \frac{1}{3} \Sigma_i \Sigma_j U_{ij} a_i^* a_j^* (a_i . a_j)$ $\quad T = \exp-(8\pi^2 U_{iso} \sin^2\theta/\lambda^2)$

Table 28
Interatomic Distances (Å) for $[Pd(L_4)](BF_4)_2$

Atoms	Distance	Atoms	Distance
S(1)-Pd(1)	2.260(3)	C(5)-C(4)	1.524(18)
S(2)-Pd(1)	2.308(3)	C(7)-C(6)	1.519(20)
N(1)-Pd(1)	2.078(8)	C(9)-C(8)	1.552(19)
N(2)-Pd(1)	2.067(8)	C(10)-C(9)	1.546(17)
C(3)-S(1)	1.840(14)	C(21)-C(11)	1.498(15)
C(4)-S(1)	1.831(14)	C(22)-C(21)	1.405(15)
C(5)-S(2)	1.853(12)	C(23)-C(22)	1.402(17)
C(6)-S(2)	1.840(12)	C(24)-C(23)	1.399(16)
C(7)-S(2)	1.828(13)	C(25)-C(24)	1.384(14)
C(8)-S(3)	1.827(16)	F(1)-B(1)	1.334(16)
C(21)-N(1)	1.341(13)	F(2)-B(1)	1.259(17)
C(25)-N(1)	1.346(12)	F(3)-B(1)	1.247(19)
C(1)-N(2)	1.539(13)	F(4)-B(1)	1.315(19)
C(10)-N(2)	1.525(14)	F(5)-B(2)	1.343(18)
C(11)-N(2)	1.520(14)	F(6)-B(2)	1.322(17)
C(2)-C(1)	1.496(18)	F(7)-B(2)	1.387(17)
C(3)-C(2)	1.523(18)	F(8)-B(2)	1.371(16)

Estimated standard deviations are given in parentheses.

Table 29
Bond Angles (deg) for $[Pd(L_4)](BF_4)_2$

Atoms	Angle	Atoms	Angle
S(2)-Pd(1)-S(1)	86.8(1)	C(4)-C(5)-S(2)	112.8(9)
N(1)-Pd(1)-S(1)	171.7(2)	C(7)-C(6)-S(2)	114.1(9)
N(1)-Pd(1)-S(2)	97.9(2)	C(6)-C(7)-S(3)	108.8(9)
N(2)-Pd(1)-S(1)	94.2(3)	C(9)-C(8)-S(3)	113.2(9)
N(2)-Pd(1)-S(2)	175.6(3)	C(10)-C(9)-C(8)	111.7(11)
N(2)-Pd(1)-N(1)	81.7(3)	C(9)-C(10)-N(2)	113.7(10)
C(3)-S(1)-Pd(1)	107.6(5)	C(21)-C(11)-N(2)	107.4(9)
C(4)-S(1)-Pd(1)	101.4(5)	C(11)-C(21)-N(1)	118.8(9)
C(4)-S(1)-C(3)	98.3(7)	C(22)-C(21)-N(1)	120.3(10)
C(5)-S(2)-Pd(1)	103.6(5)	C(22)-C(21)-C(11)	120.7(10)
C(6)-S(2)-Pd(1)	105.8(5)	C(23)-C(22)-C(21)	118.5(11)
C(6)-S(2)-C(5)	100.6(6)	C(24)-C(23)-C(22)	120.0(11)
C(8)-S(3)-C(7)	105.3(7)	C(25)-C(24)-C(23)	118.0(11)
C(21)-N(1)-Pd(1)	110.9(7)	C(24)-C(25)-N(1)	121.8(10)
C(25)-N(1)-Pd(1)	127.8(7)	F(2)-B(1)-F(1)	112.0(14)
C(25)-N(1)-C(21)	121.4(9)	F(3)-B(1)-F(1)	110.0(16)
C(11)-N(2)-Pd(1)	117.3(7)	F(3)-B(1)-F(2)	114.2(17)
C(10)-N(2)-Pd(1)	108.5(7)	F(4)-B(1)-F(1)	108.5(15)
C(10)-N(2)-C(1)	108.3(9)	F(4)-B(1)-F(2)	102.7(16)
C(11)-N(2)-Pd(1)	105.6(7)	F(4)-B(1)-F(3)	109.2(16)
C(11)-N(2)-C(1)	107.2(9)	F(6)-B(2)-F(5)	110.5(15)
C(11)-N(2)-C(10)	109.7(9)	F(7)-B(2)-F(5)	105.5(13)
C(2)-C(1)-N(2)	112.1(10)	F(7)-B(2)-F(6)	112.3(13)
C(3)-C(2)-C(1)	114.3(12)	F(8)-B(2)-F(5)	110.6(12)
C(2)-C(3)-S(1)	112.6(9)	F(8)-B(2)-F(6)	110.8(13)
C(5)-C(4)-S(1)	105.9(10)	F(8)-B(2)-F(7)	107.0(13)

Estimated standard deviations are given in parentheses.

Table 30
Mean plane for $[Pd(L_4)](BF_4)_2$

The equation of the plane containing the palladium(II) ion, two nitrogens and two sulphurs is:

$$-0.2365X + 0.3138Y + -0.9196Z + 0.5688 = 0$$

Atoms	X	Y	Z	P
Pd(1)	-1.8278	5.5692	2.9919	-0.0023
S(1)	-1.5874	7.7250	3.6265	0.0338
S(2)	0.4138	5.6155	2.4425	-0.0192
N(1)	-2.2680	3.6867	2.2302	0.1530
N(2)	-3.7948	5.4484	3.6145	-0.2065
S(3)	-0.7281	3.8361	5.3412	-3.0036

where P is the perpendicular distance between the atom and the mean plane, given in Å.

3.4 NMR Studies

(a) $[Pd(L_2)]^{2+}$

Both of the free ligand L_2 and the cation complex $[Pd(L_2)]^{2+}$ were characterized by ^{13}C NMR and the assignment of the observed peaks are presented in Figure 30. In the ^{13}C NMR spectrum of $[Pd(L_2)]^{2+}$ in CD_3CN at room temperature, there are five ^{13}C resonances corresponding to five distinctive carbon atoms in the complex. This indicates that in solution, there is rapid tumbling of $[Pd(L_2)]^{2+}$ and the NMR spectrum is a time average spectrum in which only five components similar to the crystal structure (Figure 24) are observed.

When complexed to palladium, several configurations can be adopted by the ligand L_2 (Figure 31). These arise from the relative orientation of the NH proton and the sulphur lone pairs with respect to the ring plane. The interconversion between different configurations is possible via an inversion at the sulphur atom. The energy barrier for such a pyramidal inversion is significantly reduced to about 20 - 100 kJ mole^{-1} when sulphur atoms (or other Group VIB atoms) are coordinated to transition metals with d orbitals available for π-backbonding[93]. This can be demonstrated by the variable temperature (VT) NMR study of $[PtCl_2(MeSCH_2CH_2SMe)]$[94], which were able to detect the varying rate of inversion of the coordinated sulphur atoms.

VT NMR study has been also conducted for $[Pd(L_2)]^{2+}$ in the temperature range of (-40) °C - (+75) °C. However, no temperature dependence was

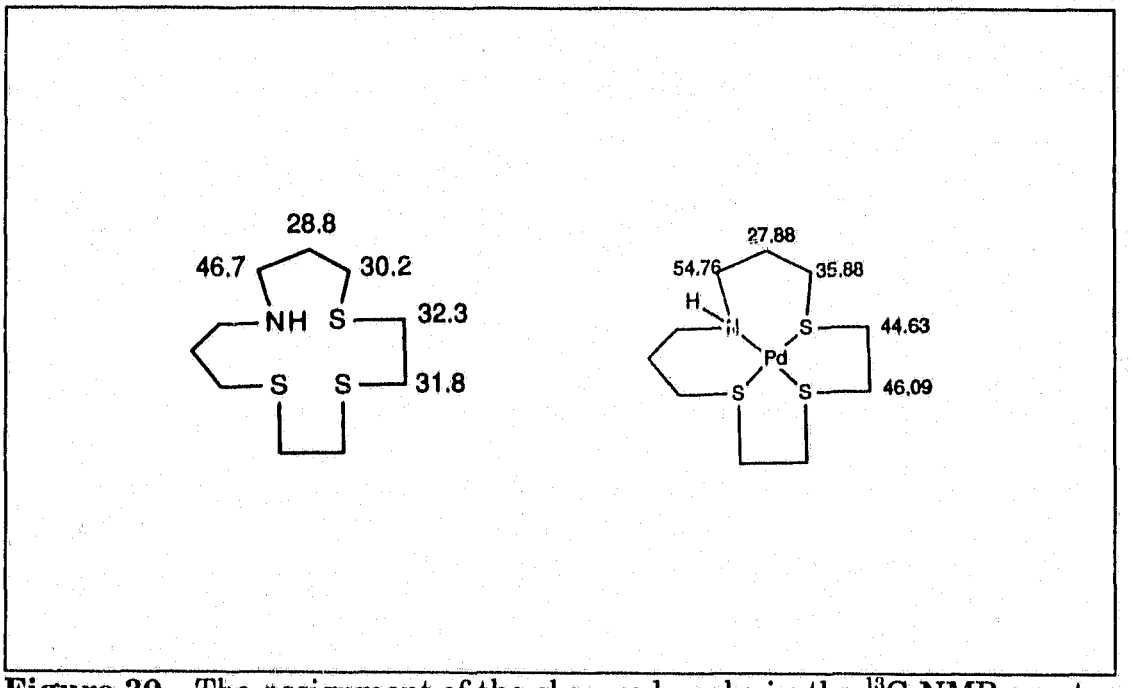

Figure 30 The assignment of the observed peaks in the ^{13}C NMR spectra of $\mathbf{L_2}$ and $[Pd(\mathbf{L_2})]^{2+}$.

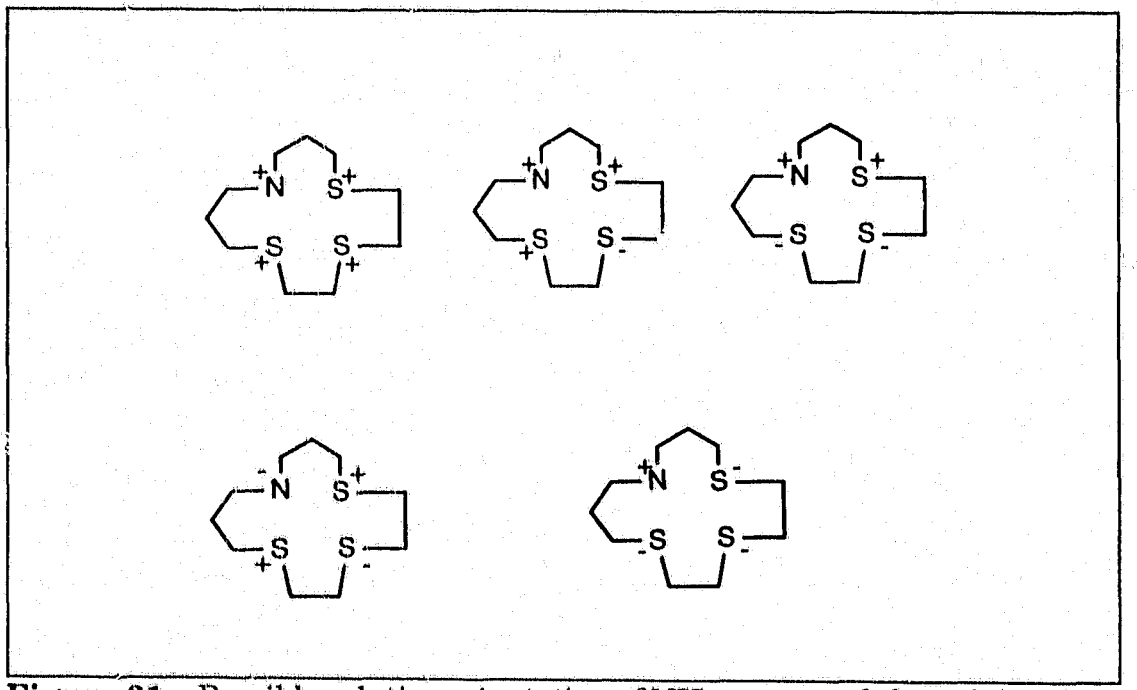

Figure 31 Possible relative orientation of NH proton and the sulphur lone pairs with respect to the ring plane in $\mathbf{L_2}$ when acting as a tetradentate ligand (+: up; -: down).

detected from the series of ^{1}H NMR spectra recorded. This may suggest that pyramidal inversion at the sulphur atoms in the coordinated L_2 is not occurring in the temperature range studied. Only one isomer which has sulphur lone pairs and NH proton pointing above the metal-ligand plane (same as the solid state structure) is present in solution. Alternatively, the equilibration is occurring rapidly and the other isomer (-,-,-,-) generated, which has sulphur lone pairs and NH proton pointing below the metal-ligand plane, is indistinguishable by ^{1}H NMR from the initial isomer (+,+,+,+). Such an equilibration is unlikely because a series of sulphur inversions and deprotonation-inversion-reprotonation at nitrogen are required to generate the (-,-,-,-) isomer from the (+,+,+,+) isomer (Scheme 8).

Scheme 8

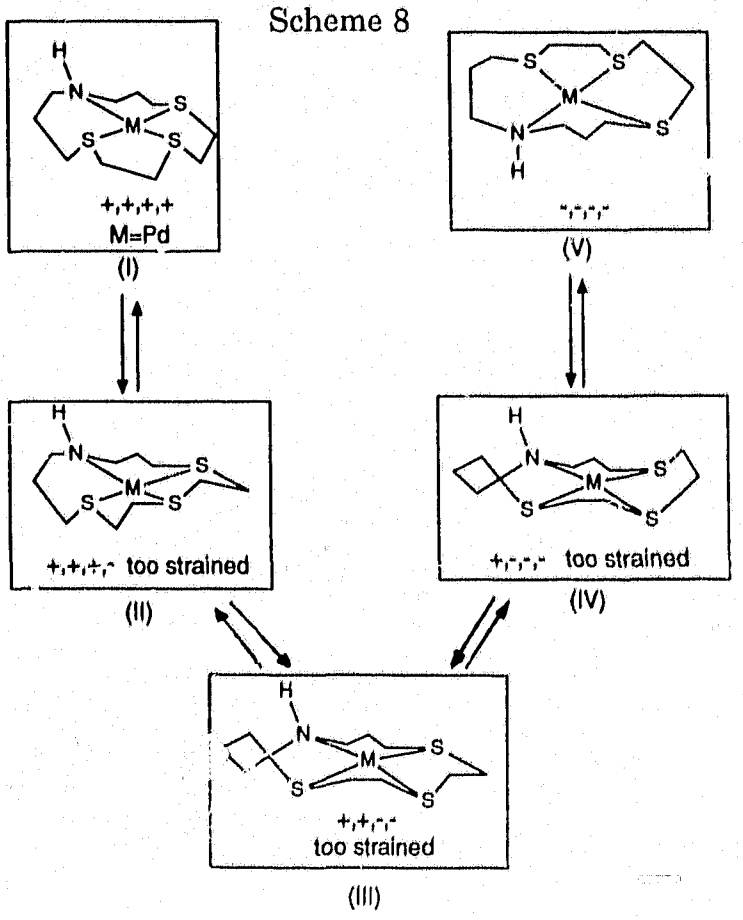

(b) $[Pd(\mathbf{L_4})Cl](PF_6)$

Ligand $\mathbf{L_4}$ has been characterized by ^1H and ^{13}C NMR in $CDCl_3$ and the assignment of the peaks in the ^{13}C NMR spectrum was aided by a ^1H-^{13}C correlated spectrum. As shown in Figure 32, there is a one to one correlation between the peaks observed in the ^{13}C and ^1H NMR. The ^{13}C resonances at δ 121.84 - 148.80 correlates to the peaks at δ 7.09 - 8.44 in ^1H NMR, which are due to the aromatic carbons in the pyridine ring. The ^{13}C peak at δ 61.71 is tied to the peak at δ 3.64 in the ^1H NMR and is attributed to the "benzylic" carbon. The signals at δ 30.81 and 31.20 are related to the ^1H peak at δ 2.70, which arise from the carbons in the $S\underline{C}H_2\underline{C}H_2$ portion of the free ligand. Finally, the ^{13}C peak responsible for the $\underline{C}H_2N$ fragment of the ligand is observed at δ 52.81, which is tied to the ^1H signal at δ 2.50.

On complexation with $Pd(PhCN)_2Cl_2$, at room temperature in CD_3CN and D_2O, all ^1H and ^{13}C resonances are somewhat displaced and very broad compared to those of the free ligand. This suggests the possibility of fluxional rearrangement in the $[Pd(\mathbf{L_4})Cl]^+$ cation. An exchange process which involves the commutation of the metal-coordinated and -uncoordinated sulphur atoms of the ligand takes place in solution.

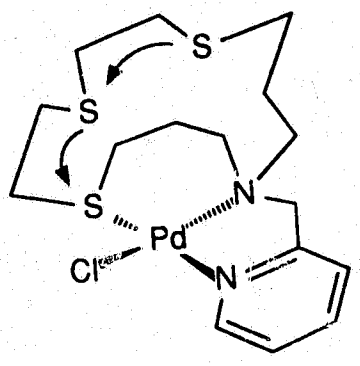

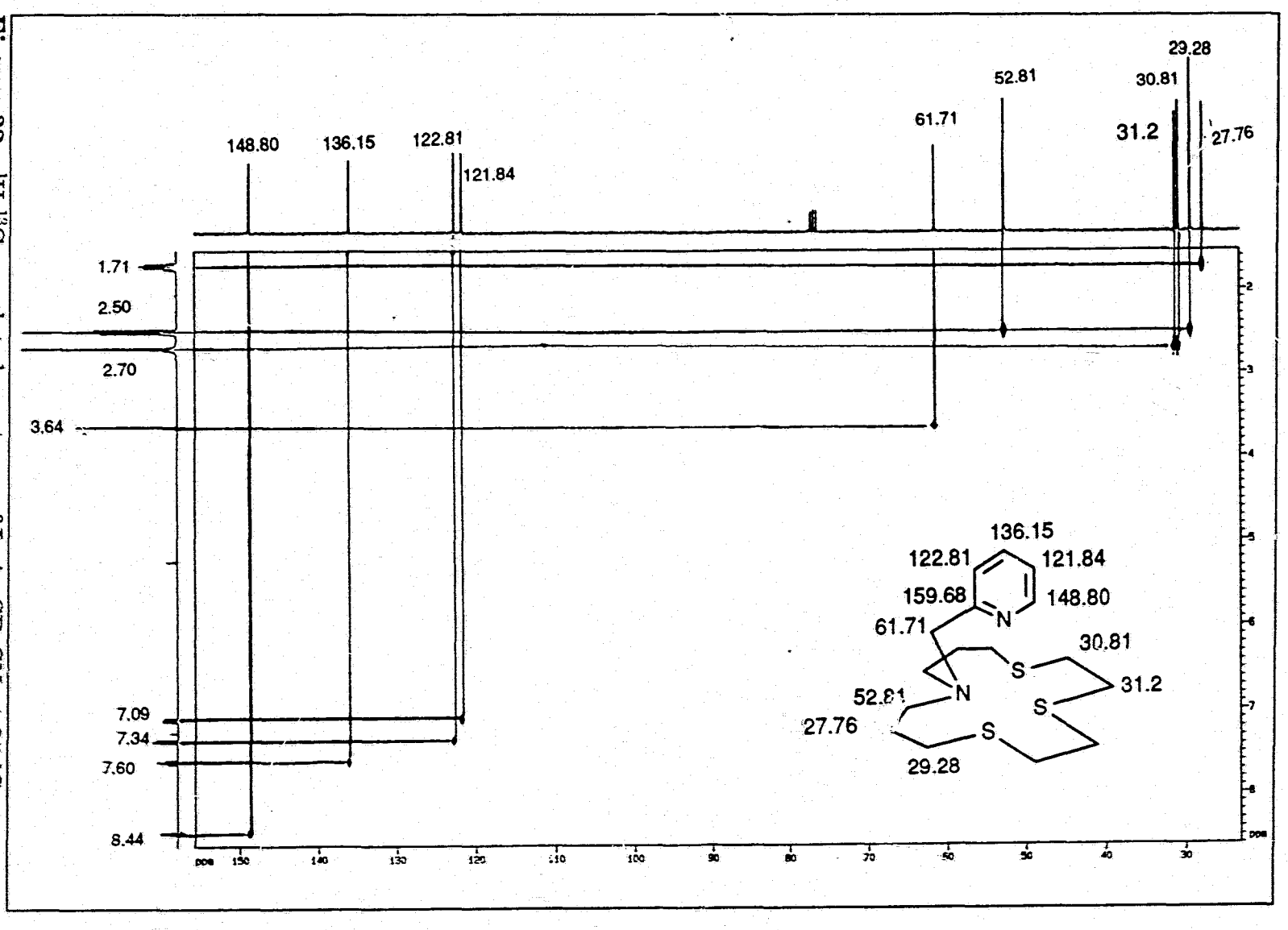

Figure 32 ^{1}H-^{13}C correlated spectrum of $\mathbf{L_4}$ in CD_3CN at 25 °C.

To study the fluxional process involved, variable temperature (VT) ^1H NMR of $[Pd(L_4)Cl]^+$ were recorded in CD_3CN at a temperature range of -40 °C to +70 °C (Figures 33 - 36). At temperatures of -20 °C and -40 °C, the ^{13}C NMR spectra obtained (Figure 37) were consistent with the solid state structure (Figure 26). Five carbon resonances were observed in the aromatic region corresponding to the carbons in the pyridine moiety. In the aliphatic region, eleven resonances were observed corresponding to the eleven distinct carbon centres in the macrocycle when coordinated.

The ^1H NMR spectra recorded at -20 °C and -40 °C (Figure 33) exhibit a very complicated splitting pattern in the aliphatic region of 2 - 3.5 ppm but are consistent with the ^{13}C NMR spectra and the solid state structure. In particular, the singlet at 3.64 ppm which is observed in the free ligand (Figure 32) due to "benzylic" hydrogens are split into an AB quartet in the palladium complex. This indicates the loss of rotational freedom at the "benzylic" C-N bond upon coordination to palladium.

In an attempt to assign some of the peaks in the aliphatic region of the ^1H NMR at -20 °C and -40 °C, two-dimensional NMR spectra such as ^1H-^{13}C correlation and ^1H COSY were recorded (Figures 38 and 39). From the ^1H-^{13}C correlated spectrum (Figure 38), it can be seen that the ^{13}C peaks at δ 62.28 and 61.46, which arise from carbons in the CH_2N portion of the cation complex, are tied to the peaks at δ 3.22, 2.88. 3.60 and 2.26 in the ^1H NMR. The ^1H COSY spectrum also shows correlation between multiplets at δ 1.25 and 2.55,

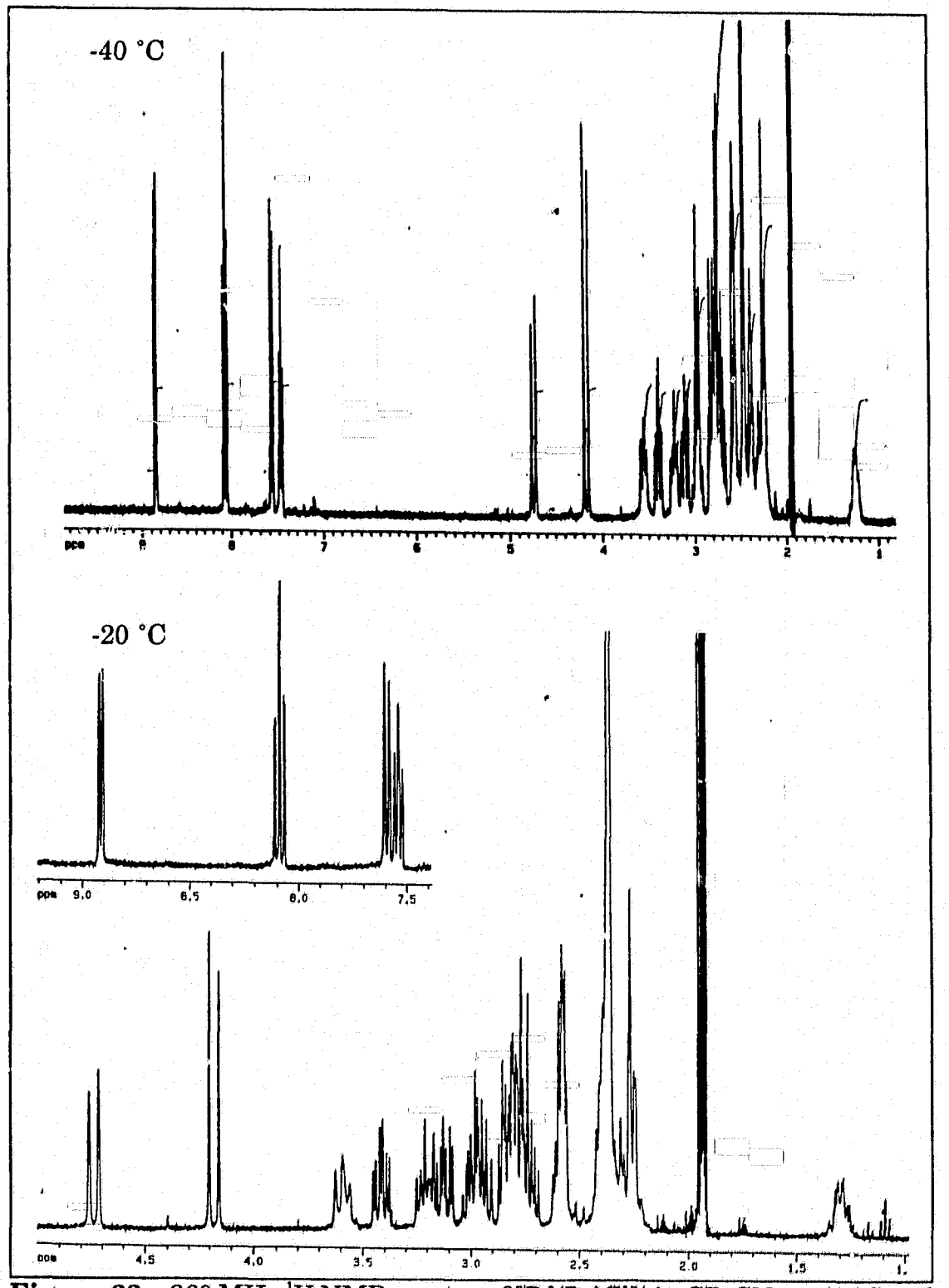

Figure 33 360 MHz ^{1}H NMR spectra of $[Pd(L_4)Cl]^+$ in CD_3CN at -40 °C and -20 °C.

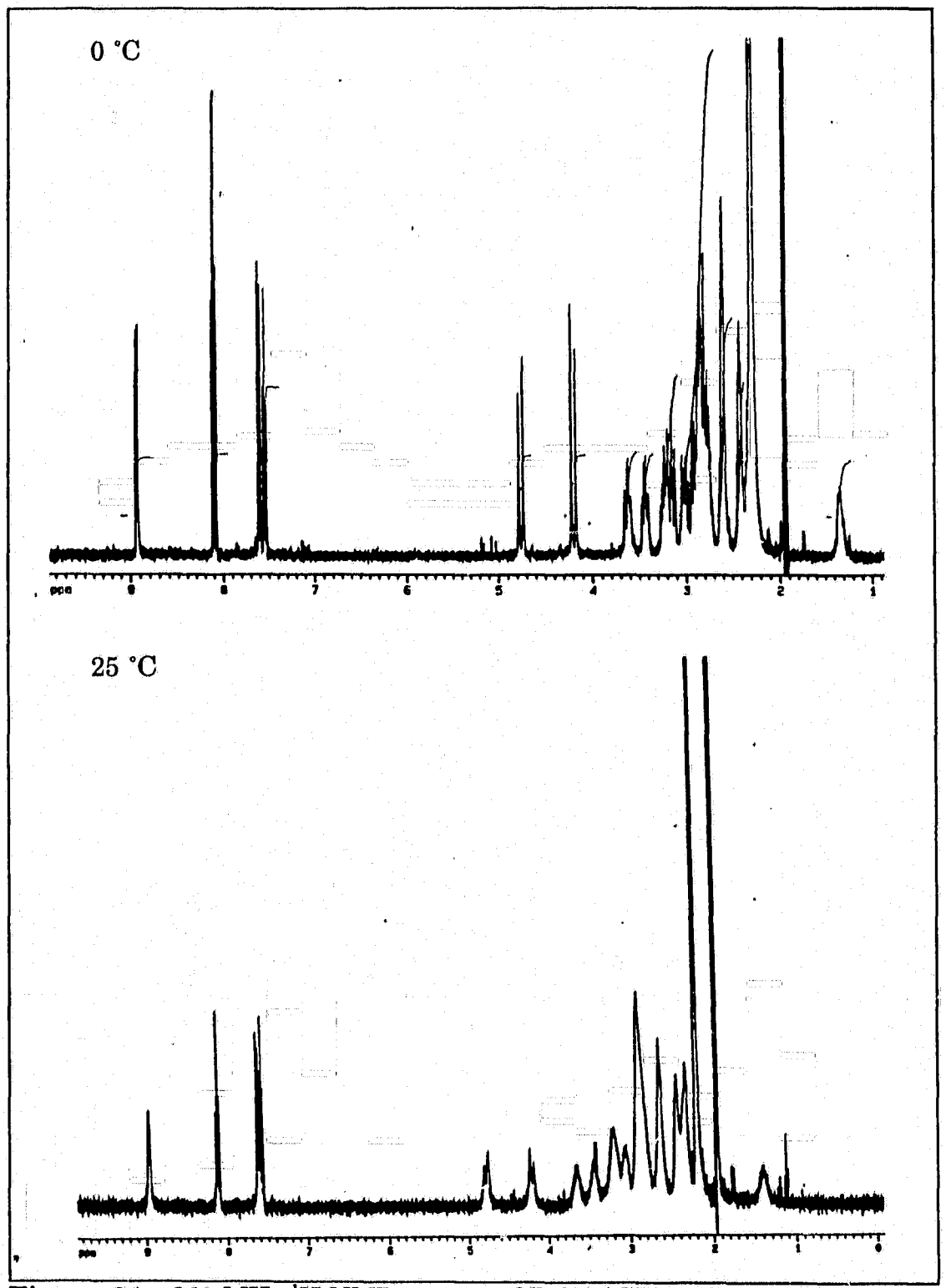

Figure 34 360 MHz ^{1}H NMR spectra of $[Pd(L_4)Cl]^+$ in CD_3CN at 0 °C and 25 °C.

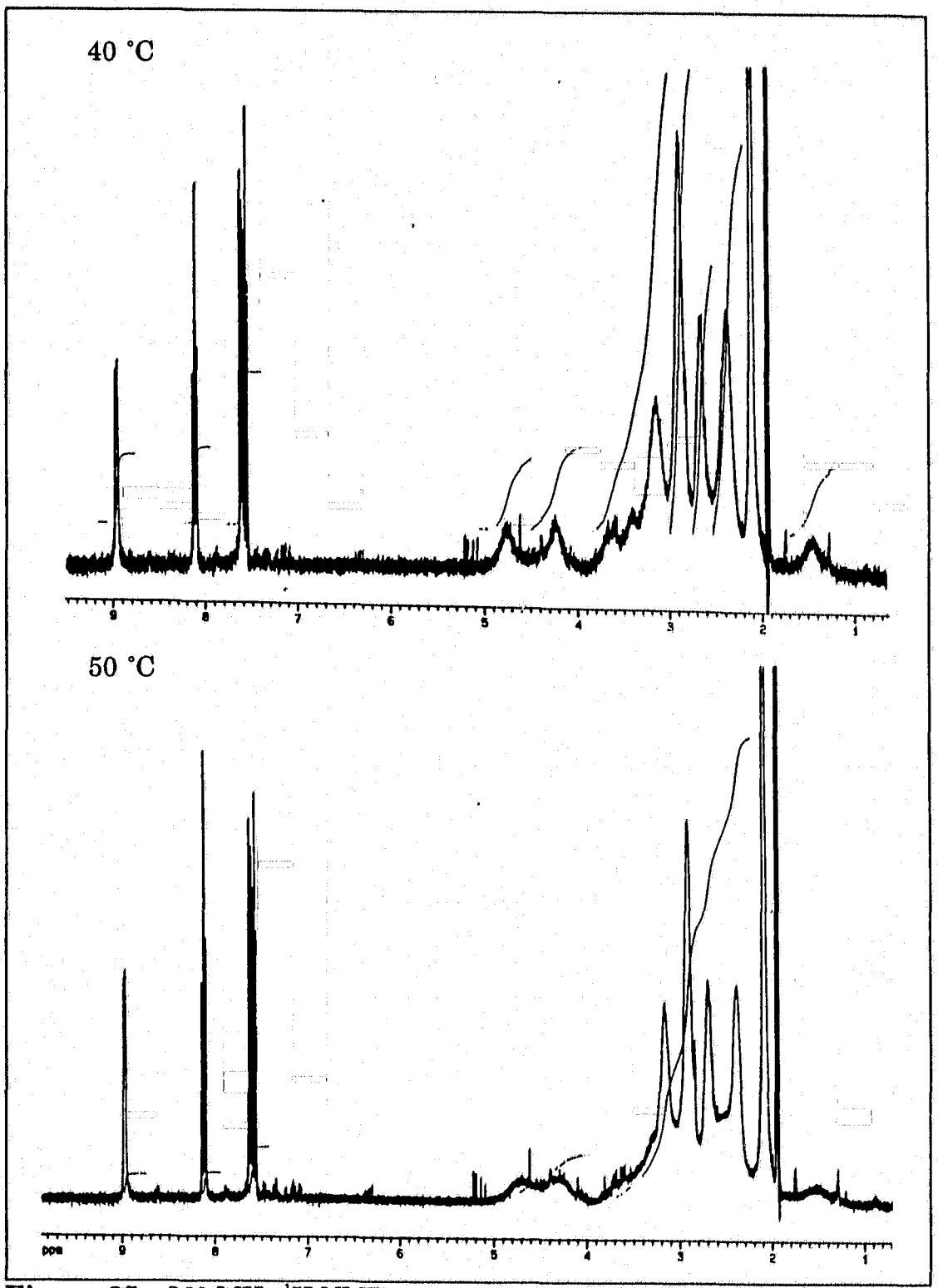

Figure 35 360 MHz ^{1}H NMR spectra of $[Pd(L_4)Cl]^+$ in CD_3CN at 40 °C and 50 °C.

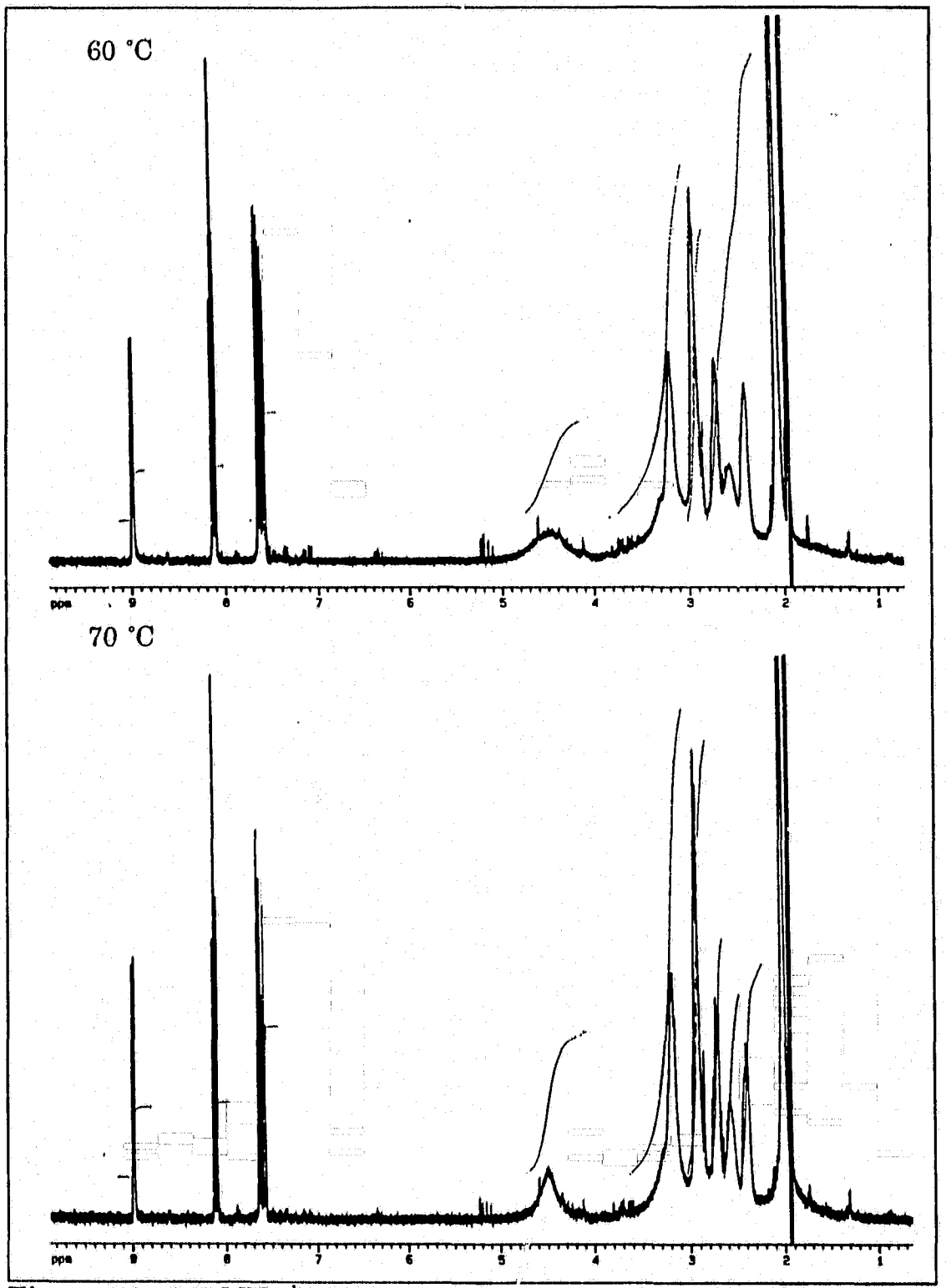

Figure 36 360 MHz ^{1}H NMR spectra of $[Pd(L_4)Cl]^+$ at 60 °C and 70 °C.

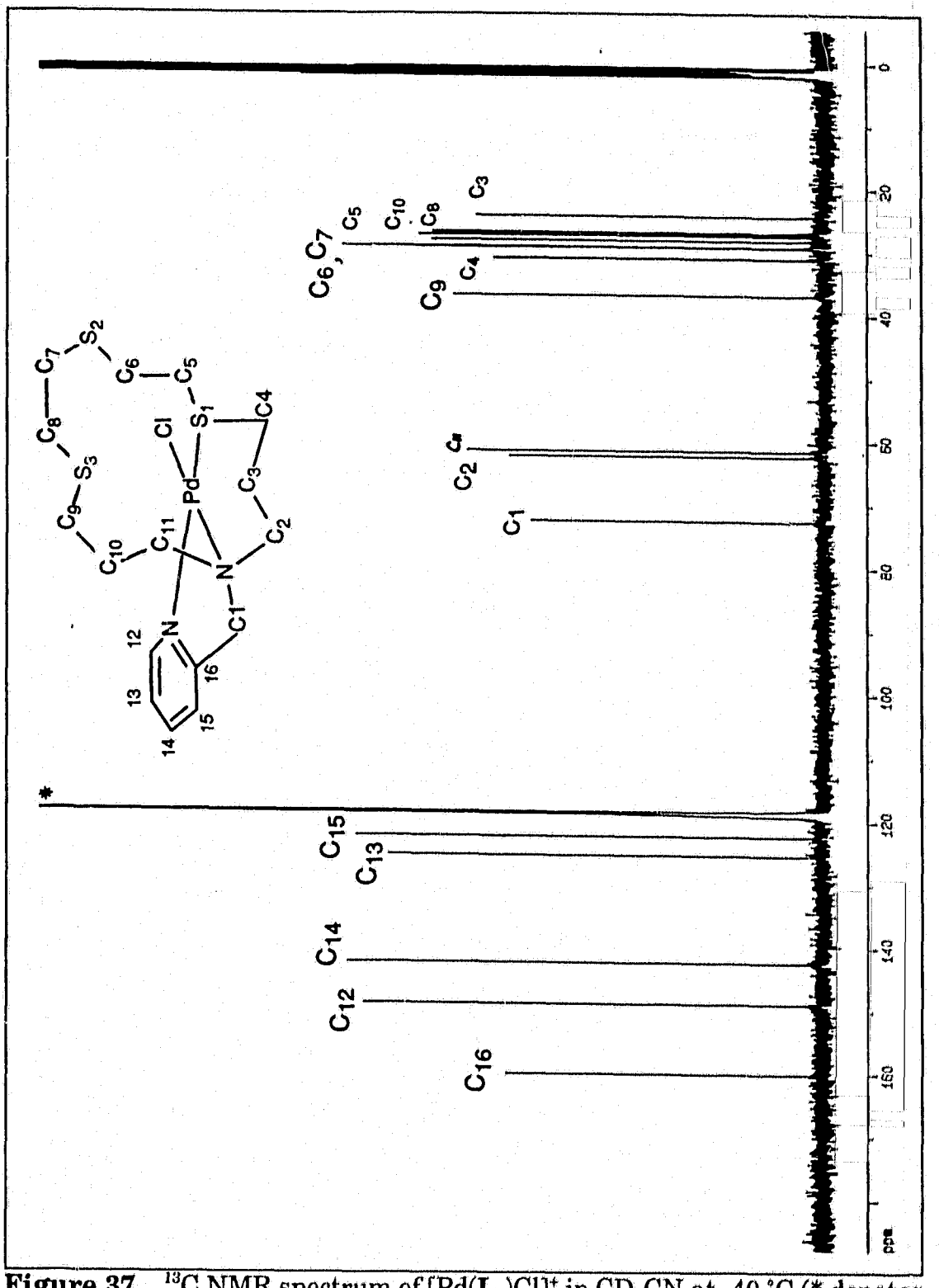

Figure 37 ^{13}C NMR spectrum of $[Pd(L_4)Cl]^+$ in CD_3CN at -40 °C (* denotes peaks from the solvent).

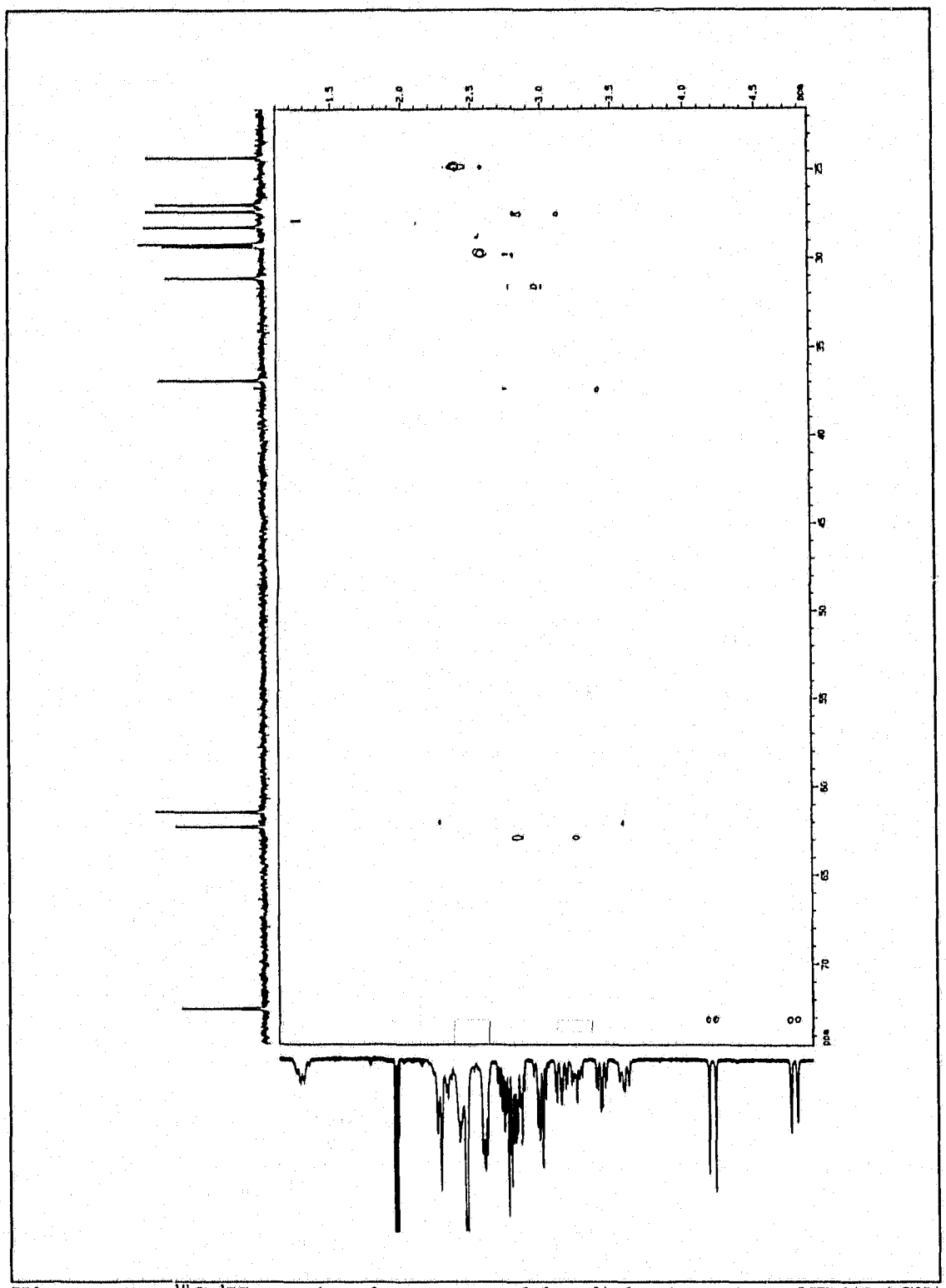

Figure 38 ^{13}C-^{1}H correlated spectrum of the aliphatic region of $[Pd(L_4)Cl]^+$ in CD_3CN at -40 °C.

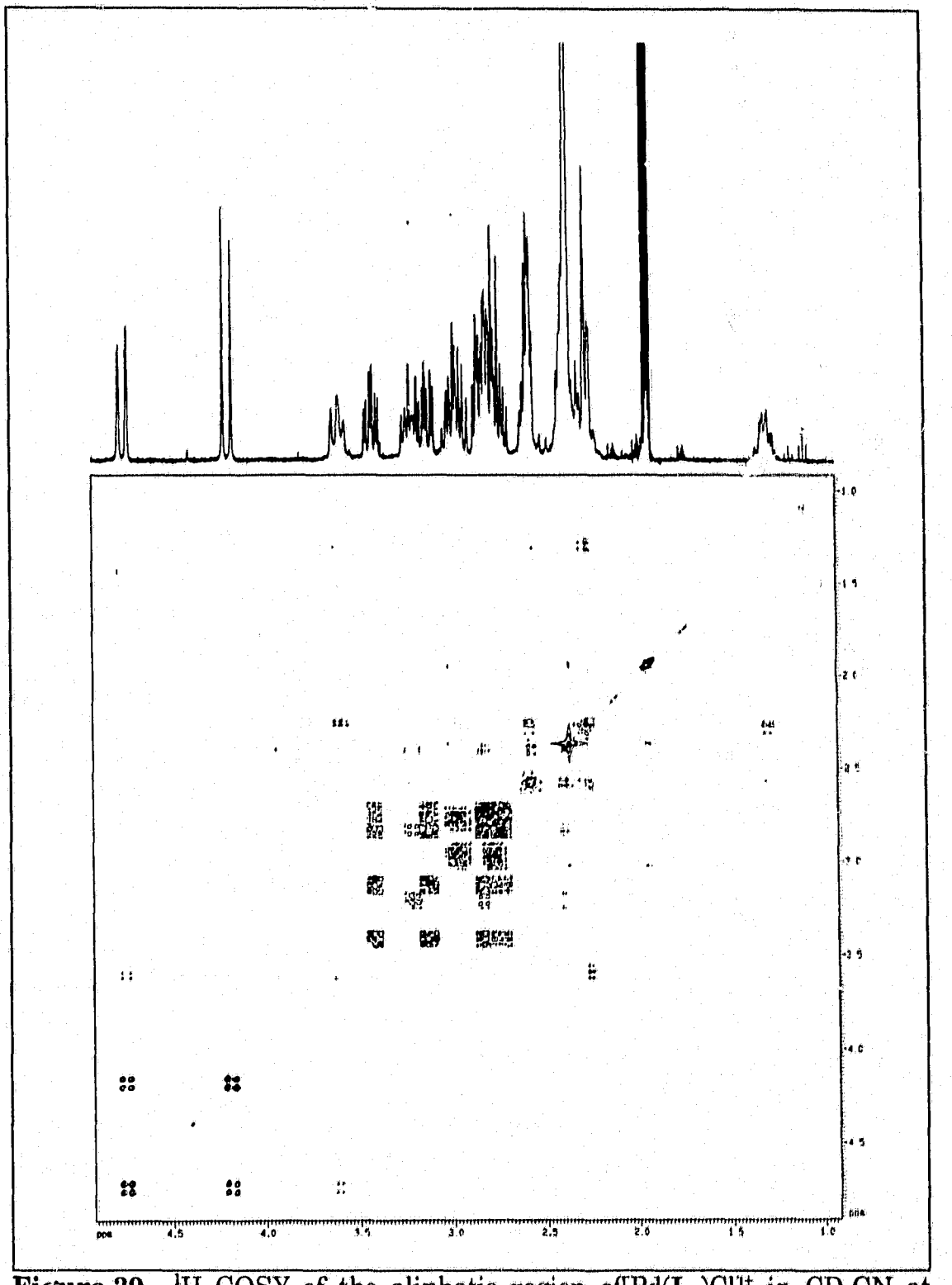

Figure 39 ^{1}H COSY of the aliphatic region of$[Pd(L_4)Cl]^+$ in CD_3CN at -20 °C.

Table 31
Tentative assignment of some of the chemical shifts in the aliphatic region of the NMR spectra of $[Pd(L_4)Cl]^+$ at - 40 °C

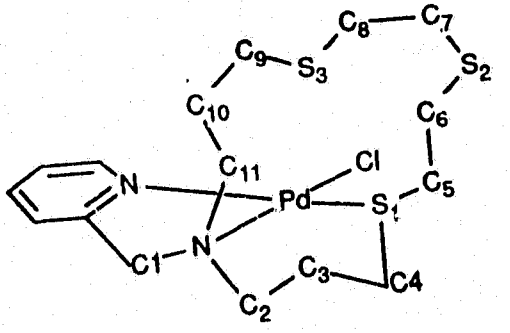

^{13}C NMR, δ in ppm	^{1}H NMR, δ in ppm	Assignment
72.55	4.18(d), 4.74(d)	C_1, H_1, $H_{1'}$
62.28	3.22(m), 2.88(m)	C_2, H_2, $H_{2'}$
61.46	3.60(t), 2.26(m)	C_{11}, H_{11}, $H_{11'}$
36.81	3.40(td), 2.7(m)	C_4, H_4, $H_{4'}$
30.94	3.10(m), 2.85(m)	C_9, H_9, $H_{9'}$
29.14	2.75(m)	C_6, H_6, $H_{6'}$

δ2.65 and 2.45 and they are tentatively assigned as methylene protons in the CH_2-CH_2-CH_2 fragment. The remaining peaks are methylene protons attached to thioethers. The assignment of some of the peaks in the aliphatic region of the ^{1}H and ^{13}C NMR spectra of $[Pd(L_4)Cl]^+$ at -40° are presented in Table 31.

For temperatures above 0 °C, a striking feature of the ^{1}H NMR spectra recorded (Figures 34 - 36) is that the signal for the "benzylic" protons (an AB quartet at temperature below 0 °C) started to broaden as the temperature

increased and collapsed into a broad singlet at 70 °C. In addition, ^{1}H resonances in the region of 2 - 4 ppm also become increasingly broad as the temperature is increased. The pyridine portion of the complex, however, remained unchanged in the temperature range of (-40)°C - (+70)°C. These observations suggest that there is a fluxional process that shifts the site of ligand-metal attachment from S1 to S3 with the Pd-N(pyr) bond remained intact. This process interchanges the equatorial and axial hydrogens in the pyridyl methyl segment of the complex. It also renders equivalent hydrogens on C2 and C11, C3 and C10, C4 and C9, C5 and C8, C6 and C7. As a result, only five broad singlets were observed in the aliphatic region of the ^{1}H NMR spectrum at 70 °C.

The fluxional process observed in the $[Pd(\mathbf{L}_4)Cl]^+$ complex can be rationalized by either a two-site exchange in which the palladium ion "hops" from S1 to S3 directly (Scheme 9); or a three-site exchange with the palladium centre moving from S1 to S2 and then from S2 to S3 (Scheme 10). In both mechanisms, the exchange of ligand to metal attachment from the sulphur atom S1 to S3 is accompanied by the exchange of equatorial and axial hydrogens in the "benzylic" position. The rate constant for the fluxional process can be obtained from the computer simulation of the "benzylic" protons in the variable temperature ^{1}H NMR spectra and the activation barrier for the exchange can be estimated afterwards.

Scheme 9

Two-site exchange mechanism:

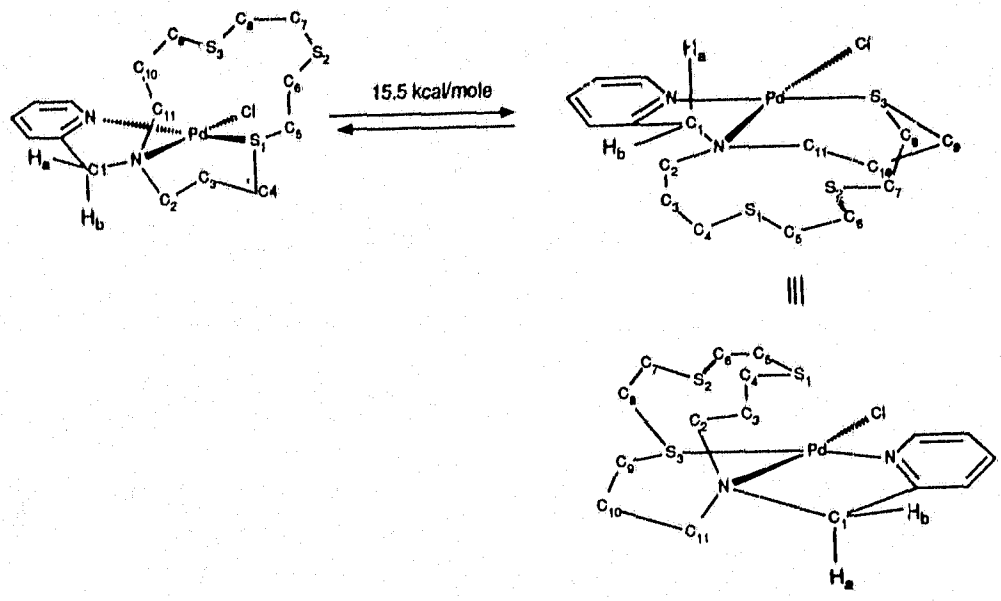

Scheme 10

Three-site exchange mechanism:

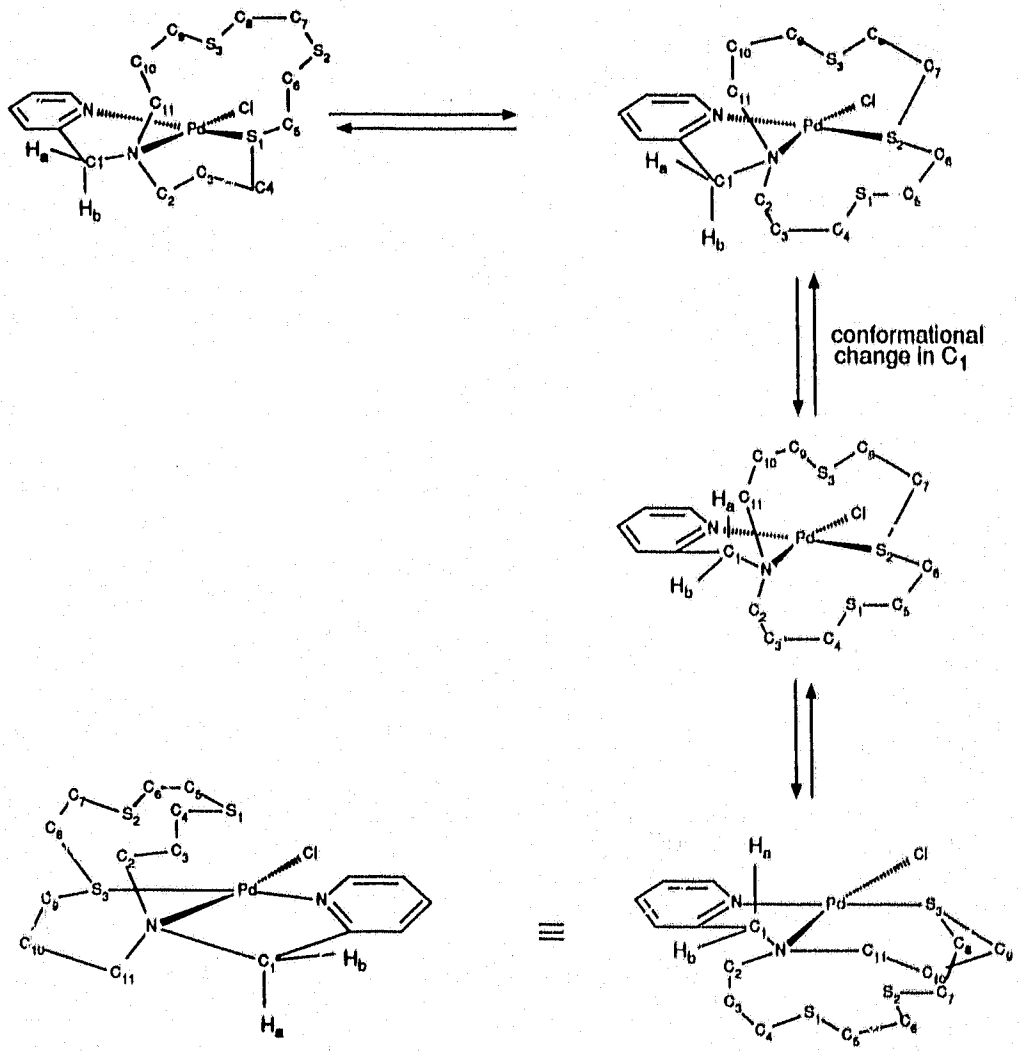

Fluxional processes involving heteroatoms are well-documented in the literature[93], especially those involving a 1,3 or 1,5 metallotropic shift. As examples, the stereo-nonrigidity observed in group V metal pentacarbonyl complexes of β-2,4,6-trimethyl-1,3,5-trithiacyclohexane **27** and bimetallic complexes of $[(PtClMe_3)_2L]$, **28**, where L is 1,3,5,7-tetrathiacyclooctane, have been reported to proceed via a 1,3 and 1,5 shift, respectively. Fluxional processes involving 1,4-metallotropic shift in a transition metal complex of a macrocyclic thioether ligand are not very common. Only two examples, the palladium(II) complex of a thiophene macrocycle[95] **29**, and the trimethyl platinum(IV) complex of [12]aneS_4[96] **30**, have been reported recently. Unfortunately, the present VT ^{1}H NMR data did not distinguish whether the fluxional process occurred via a two-site or three-site exchange pathway. A more extensively study, for instance, by substituting the chloride ion in $[Pd(L_4)Cl]^+$ with an NMR active nucleus such as F^- and the analysis of the V.T. ^{19}F NMR of $[Pd(L_4)F]^+$ may shed some light to the exact mechanistic pathway involved. Alternatively, the study of V.T. ^{195}Pt NMR of the structurally similar complex, $[Pt(L_4)Cl]^+$ may also provide additional information.

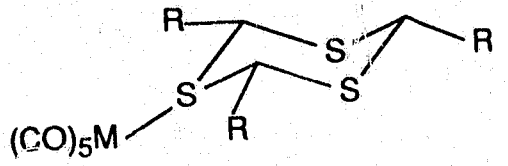

R = H, Me
M = Cr, W

27

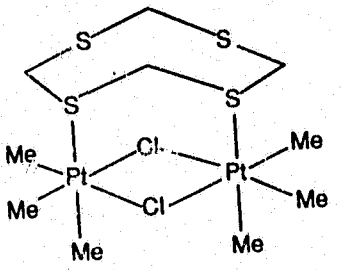

28

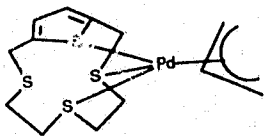

$[Pd(\eta^3\text{-allyl})(\mathbf{29})]^+$

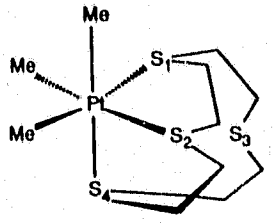

30

(c) $[Pd(\mathbf{L_4})](BF_4)_2$

^{1}H NMR spectra of $[Pd(\mathbf{L_4})](BF_4)_2$ in CD_3CN were recorded in the temperature range of (-40) °C to (+60) °C (Figures 40 - 43). A striking feature of the ^{1}H NMR spectrum of $[Pd(\mathbf{L_4})]^{2+}$ at -40 °C is that ^{1}H resonances from the pyridine moiety may be divided into two groups, which may indicate the presence of two isomers (A and B) in solution.

A COSY spectrum (Figure 44) at -45 °C indicates that ^{1}H resonances at δ 8.85, 7.88, 7.48 and 7.38, which are sharp and show distinctive superhyperfine splittings, belong to a pyridine moiety in a rigid environment (Isomer A). On the other hand, ^{1}H resonances at δ 8.28, 8.15, 7.75 and 7.58, which do not show superhyperfine splitting, belong to a pyridine moiety which is in a less rigid environment (Isomer B). It should be interesting to note that the splitting pattern of the pyridine protons from isomer B also resembles those observed in the ^{1}H NMR spectrum of the free ligand $\mathbf{L_4}$ (Figure 32). As the temperature increases to 40 °C or higher, ^{1}H resonances from the pyridine moiety in both isomers broaden and coalescence occurs at temperature above 60 °C.

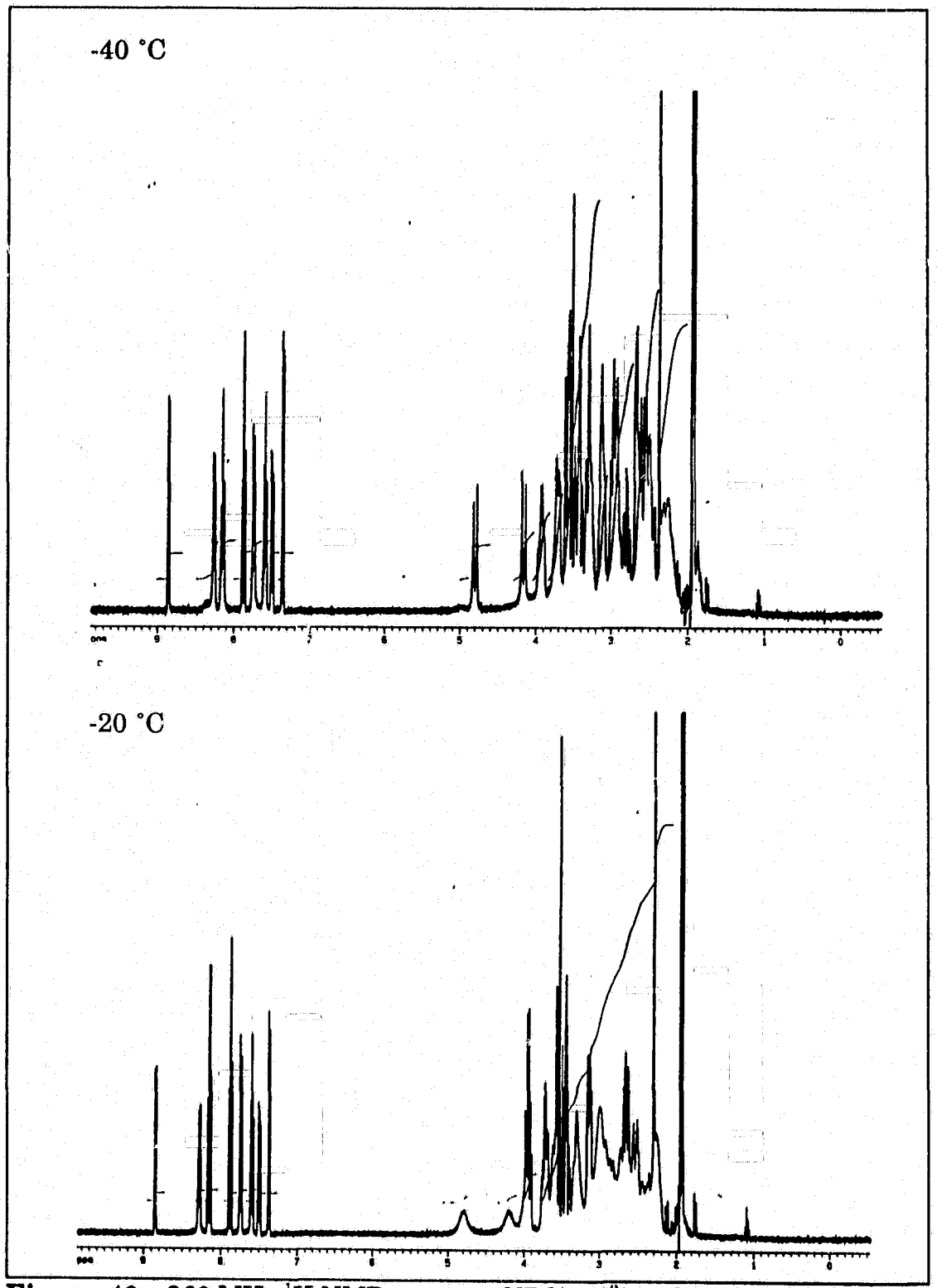

Figure 40 360 MHz ^{1}H NMR spectra of $[Pd(L_4)]^{2+}$ in CD_3CN at -40 °C and -20 °C

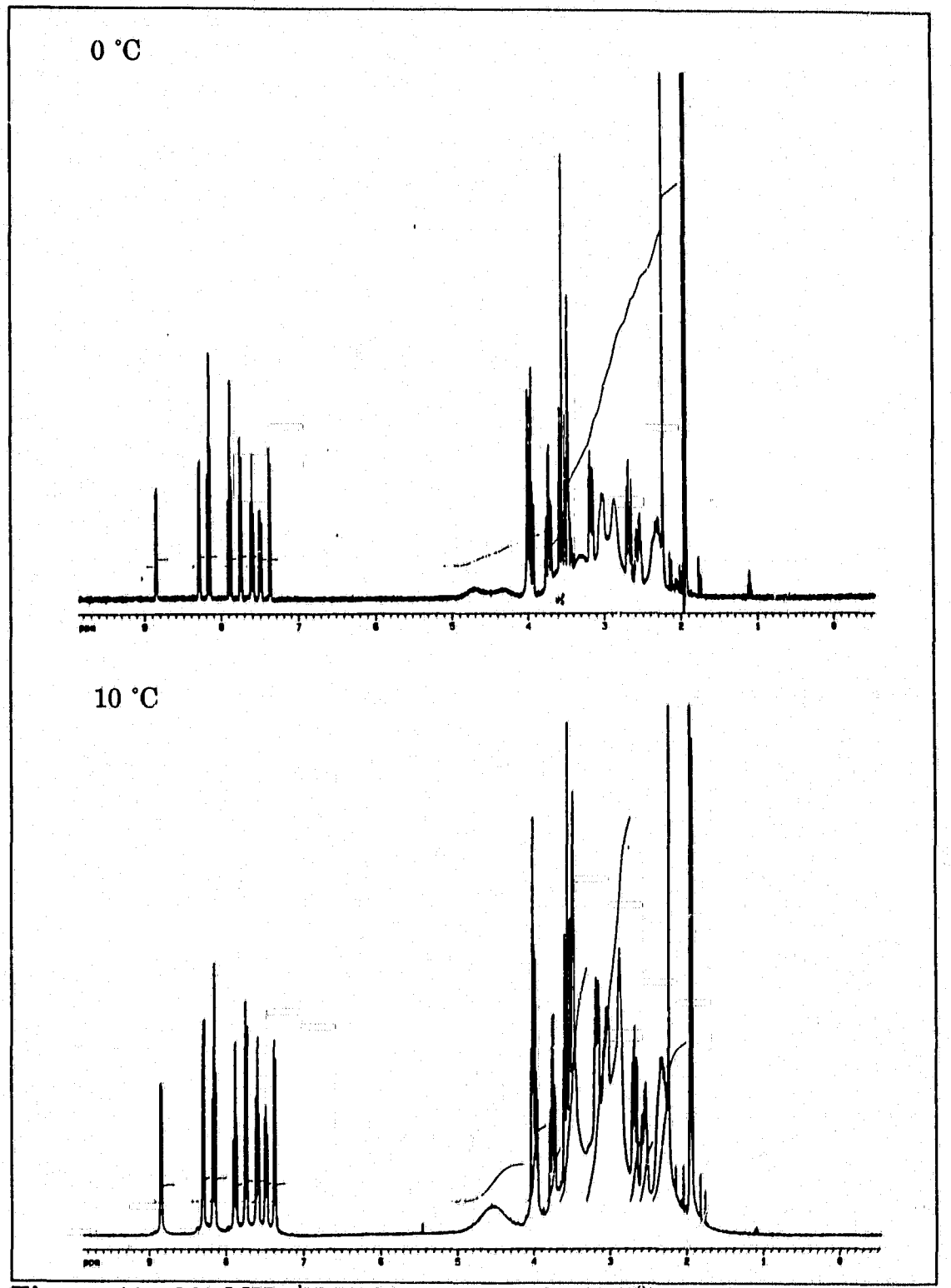

Figure 41 360 MHz ^{1}H NMR spectra of $[Pd(L_4)]^{2+}$ in CD_3CN at 0 °C and 10 °C

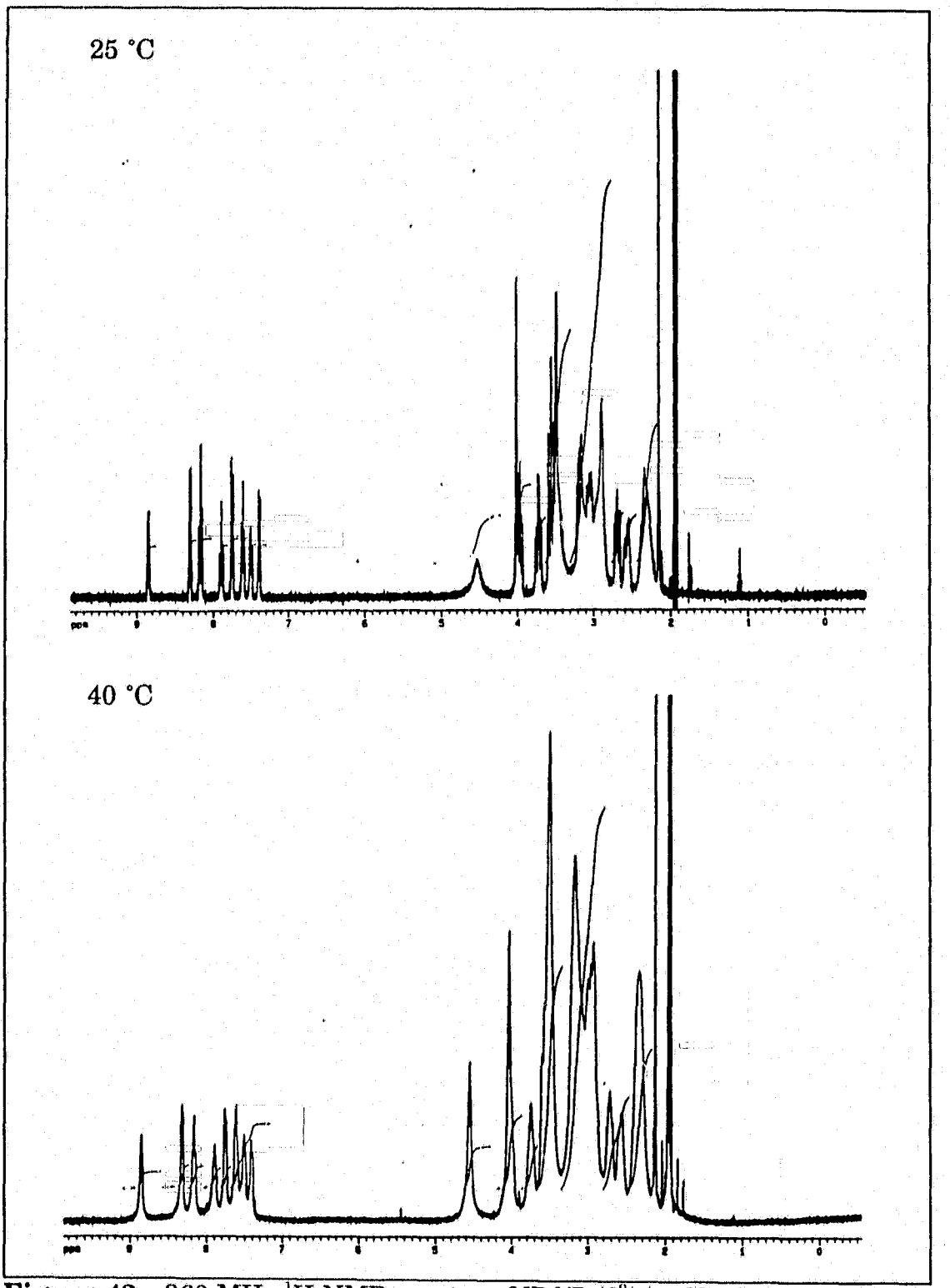

Figure 42 360 MHz ^{1}H NMR spectra of $[Pd(\mathbf{L}_4)]^{2+}$ in CD_3CN at 25 °C and 40 °C

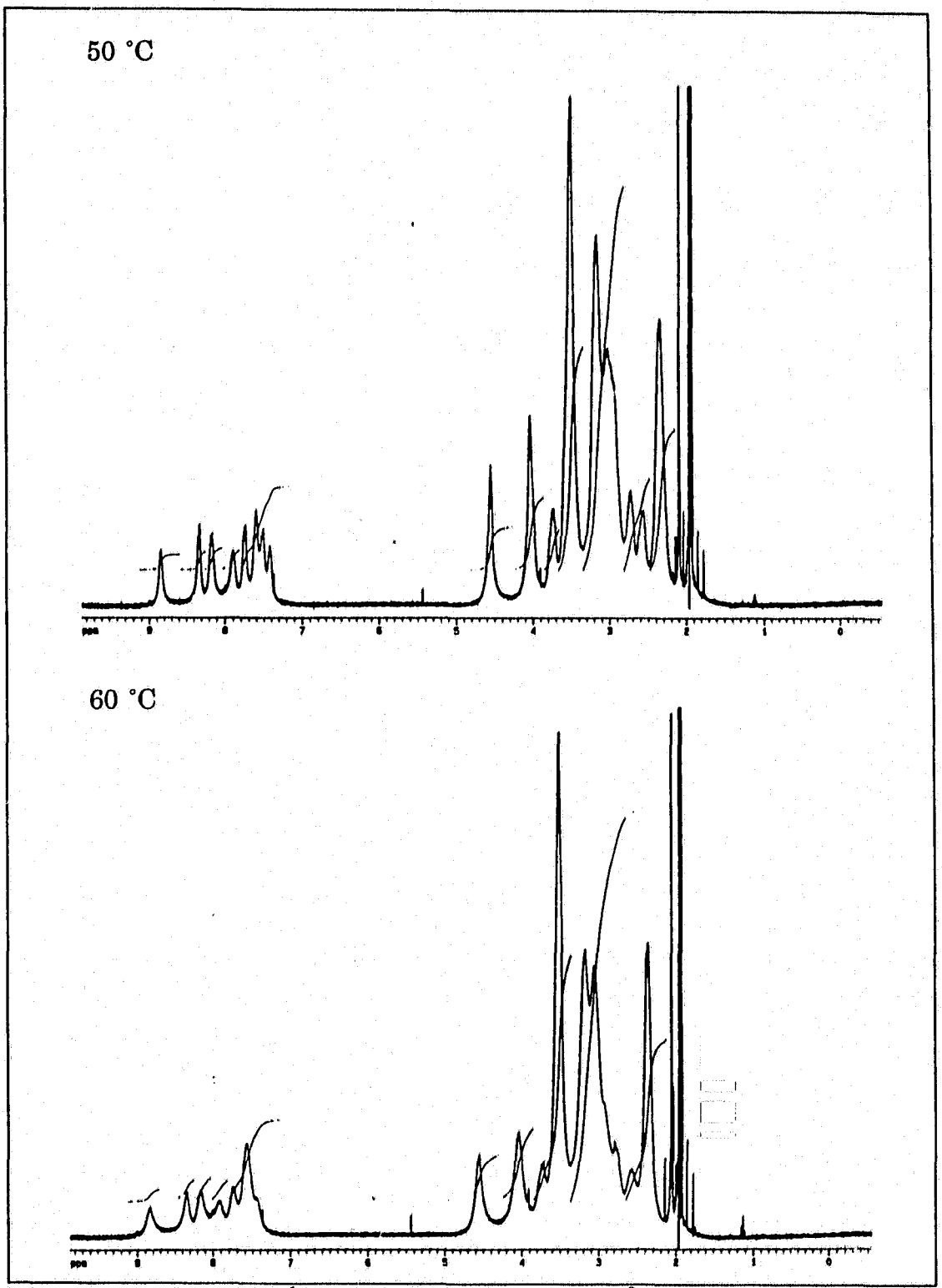

Figure 43 360 MHz ^{1}H NMR spectra of $[Pd(L_4)]^{2+}$ in CD_3CN at 50 °C and 60 °C

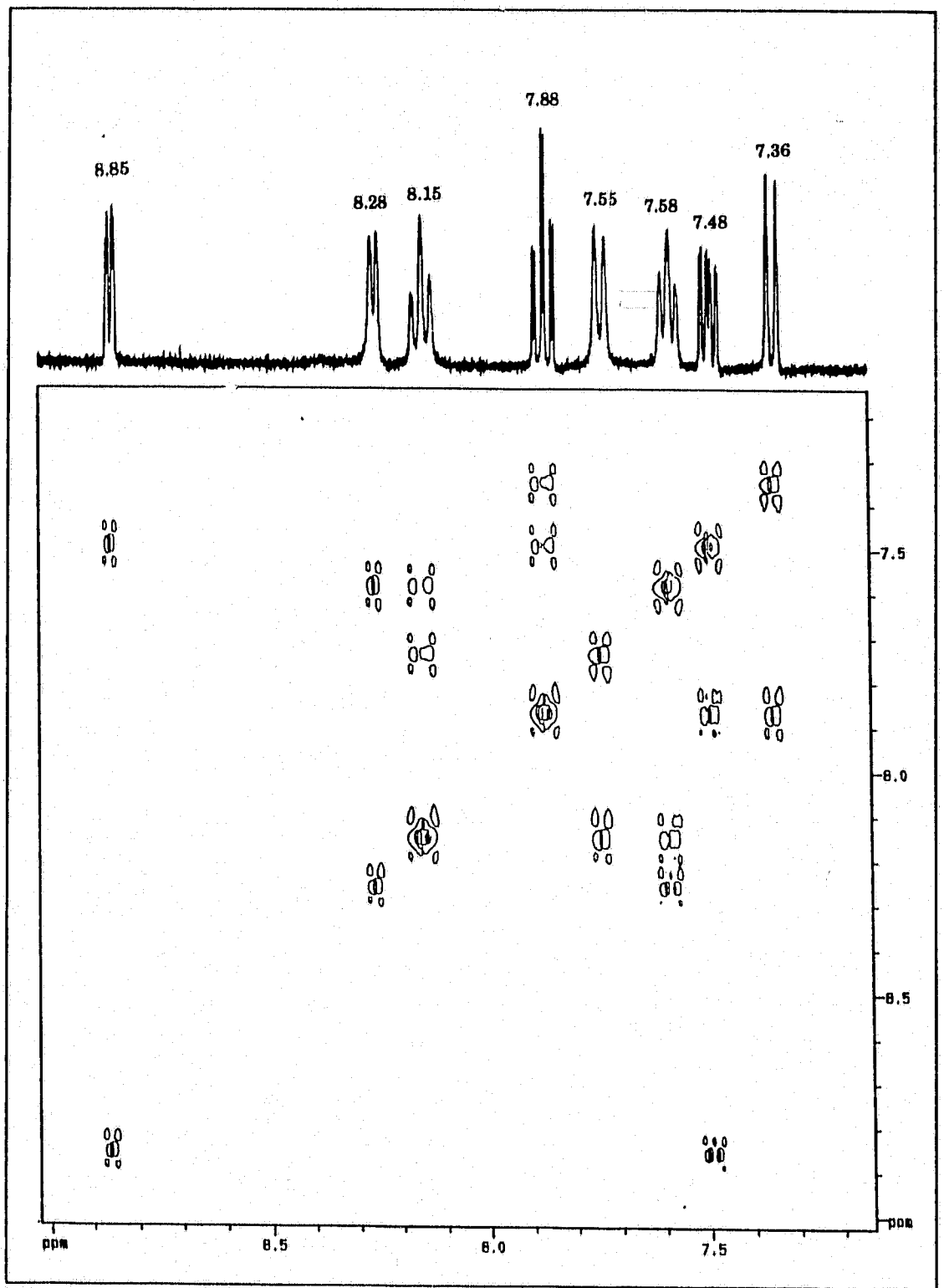

Figure 44 The aromatic portion of the ^{1}H COSY of $[Pd(L_4)]^{2+}$ in CD_3CN at -45 °C

Another interesting feature of the NMR spectra is the ^1H resonances due to "benzylic" protons. They appear as sharp AB quartet at δ 4.25 and 4.8 at -40 °C. However, these signals broaden at temperature above -20 °C and collapse to a broad singlet at 10 °C. These observations indicate that several exchange processes are present when $[Pd(\mathbf{L}_4)]^{2+}$ was dissolved in CD_3CN. One of these processes interchanges the "benzylic" protons in the axial and equatorial positions. This feature has a lower activation energy than the other process which changes the pyridine moiety from one chemical environment to the other.

A mechanistic pathway which may rationalize some of the temperature dependent NMR behavior of $[Pd(\mathbf{L}_4)]^{2+}$ in CD_3CN is summarized in Scheme 11. It is proposed that when dissolved in CD_3CN, $[Pd(\mathbf{L}_4)]^{2+}$ exists in two isomers. In isomer A, the complex has a structure similar to that observed in the crystalline state (Figure 28). The palladium ion is in a square-planar environment, it is coordinated to the nitrogen atoms from the pyridine and the macrocycle and also two thioether atoms. In isomer B, the palladium centre is coordinated to one nitrogen atom and three thioether atoms from the ligand in a square-planar environment (similar to the cation complex $[Pd(\mathbf{L}_2)]^{2+}$ as observed previously in Figure 24), with the nitrogen atom in the pyridine moiety uncoordinated but in close proximity. When dissolved in CD_3CN, one of the exchange processes involves the commutation between the metal coordinated S_1 and the non-coordinated S_3 atoms. This process occurs via a

metallotropic shift with the S_2-Pd-N(2) axis acting as the pivot and has a relatively low activation barrier (ca. ≈ 12.3 kcal/mol). At the temperature range of (-20) °C to (+25) °C, this exchange process is dominant in solution. The other process which involves the interchange of the two pyridine environments in isomers A and B, has a higher activation barrier (≥ 18 kcal/mole) and can be detected by NMR at temperature above 50 °C.

Scheme 11

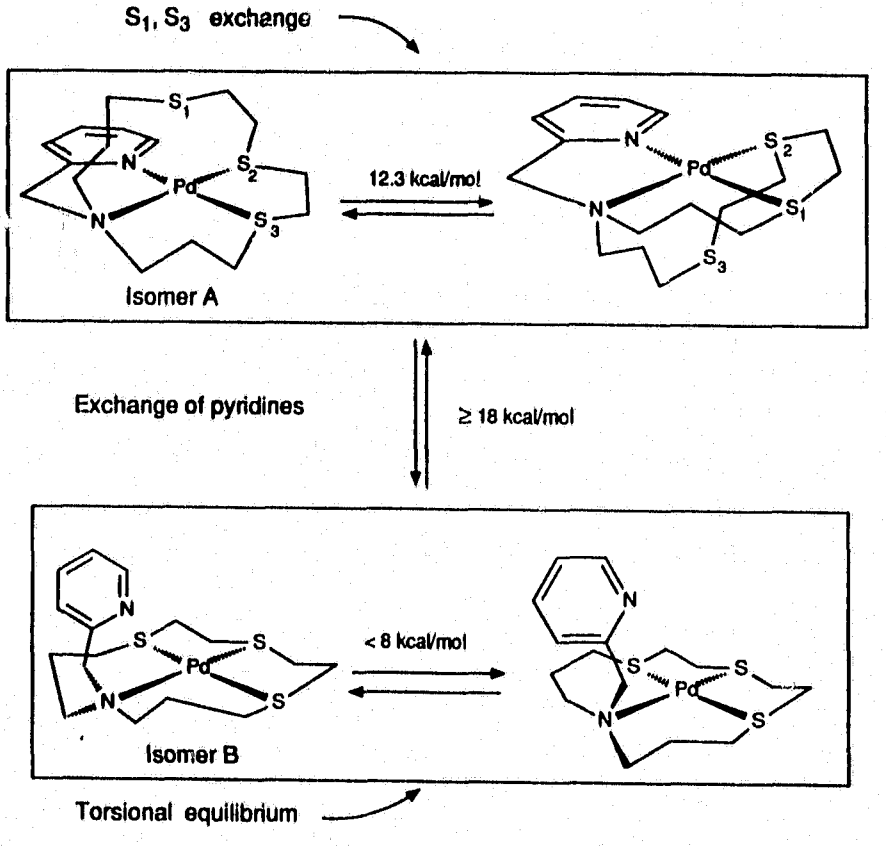

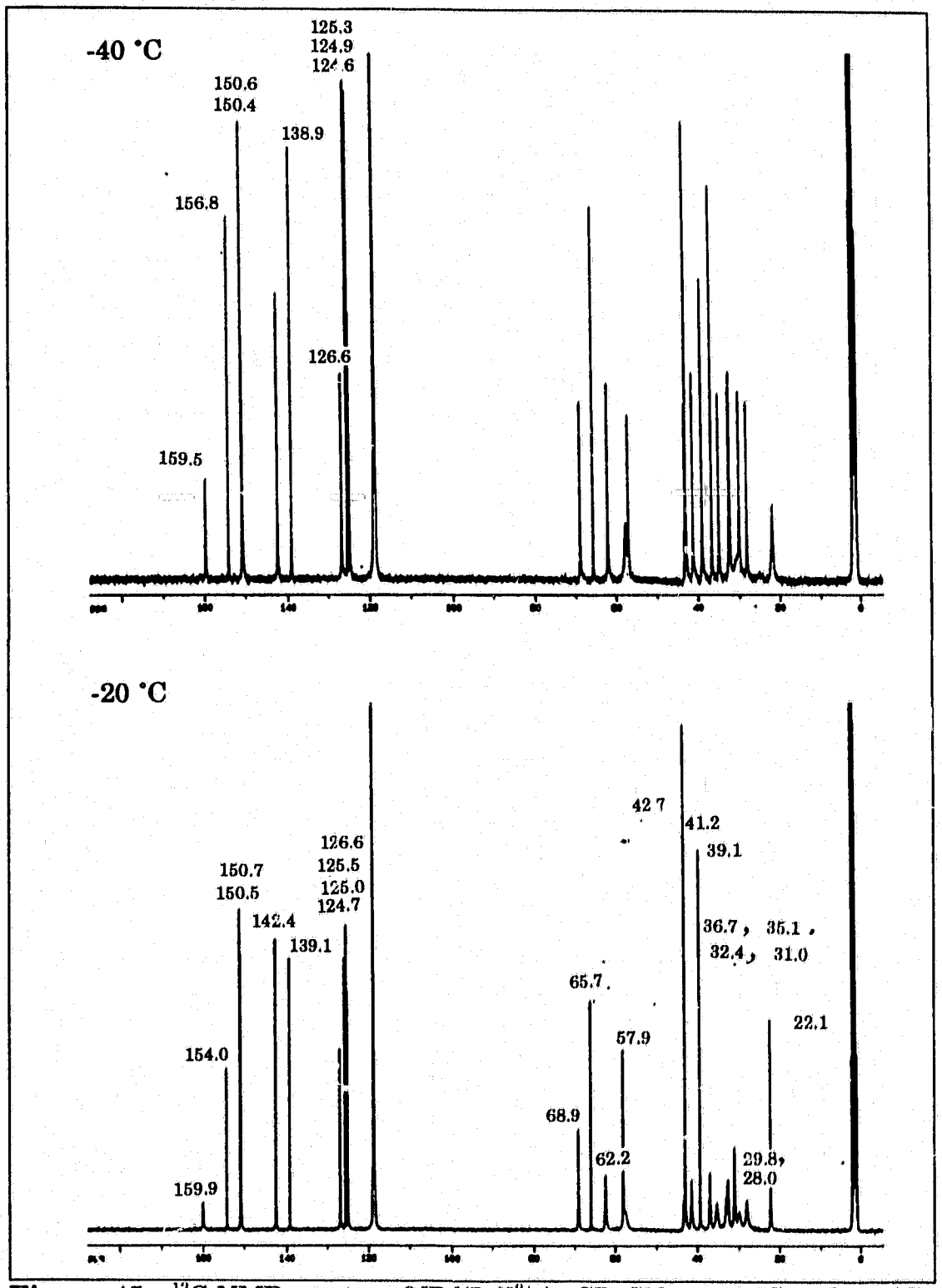

Figure 45 ^{13}C NMR spectra of $[Pd(L_4)]^{2+}$ in CD_3CN at -40 °C and -20 °C

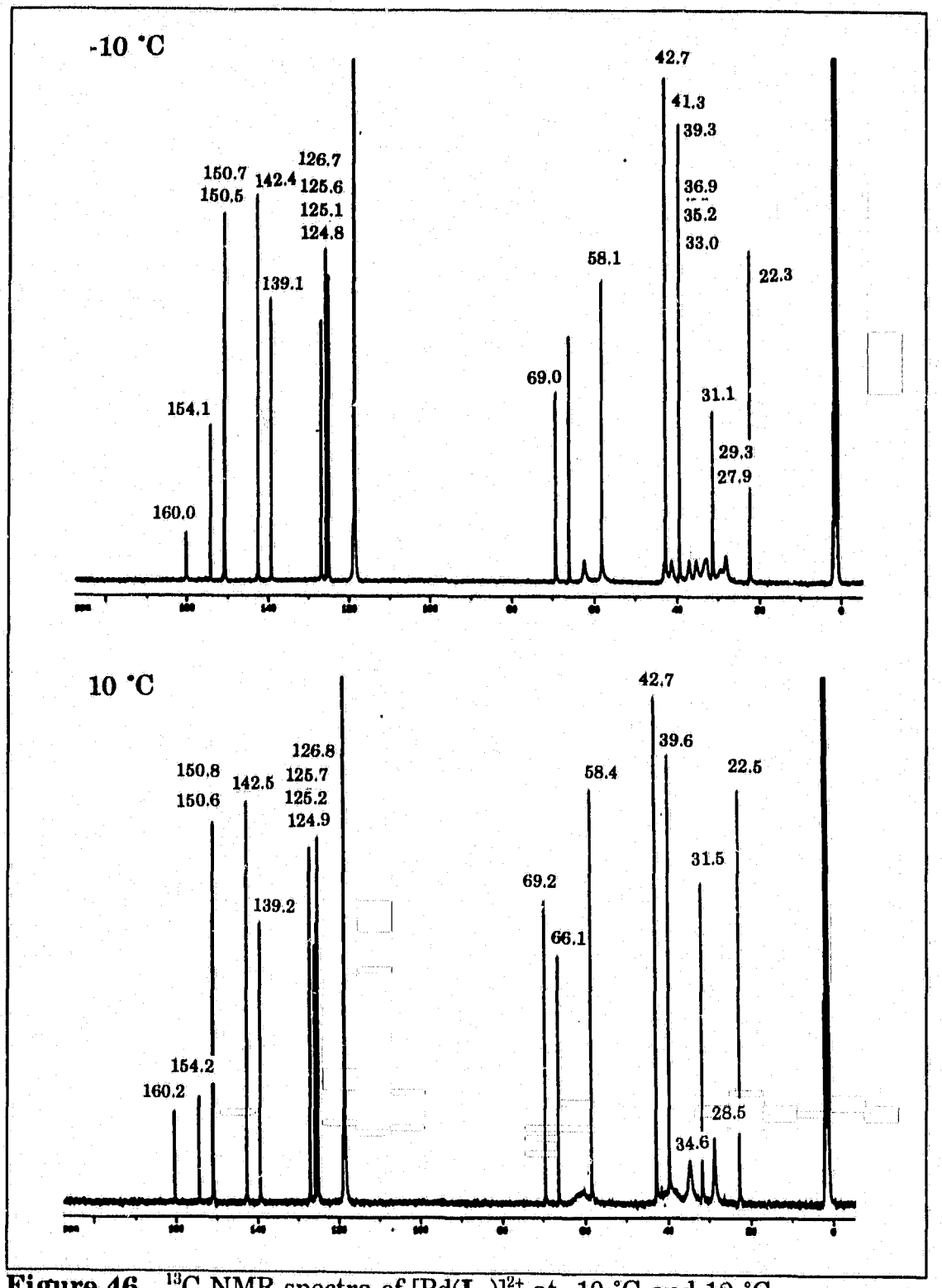

Figure 46 ^{13}C NMR spectra of $[Pd(\mathbf{L}_4)]^{2+}$ at -10 °C and 10 °C

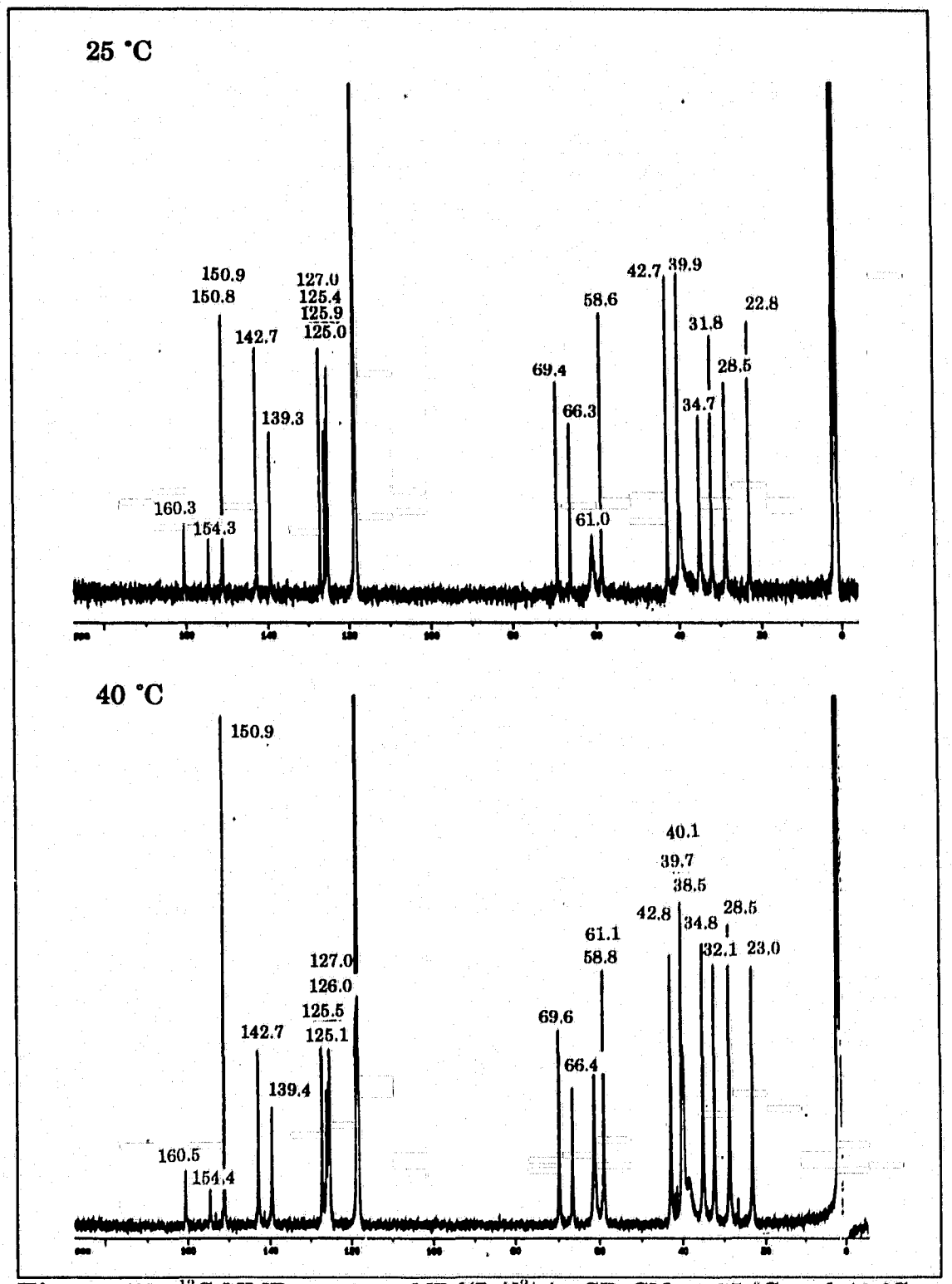

Figure 47 ^{13}C NMR spectra of $[Pd(\mathbf{L}_4)]^{2+}$ in CD_3CN at 25 °C and 40 °C

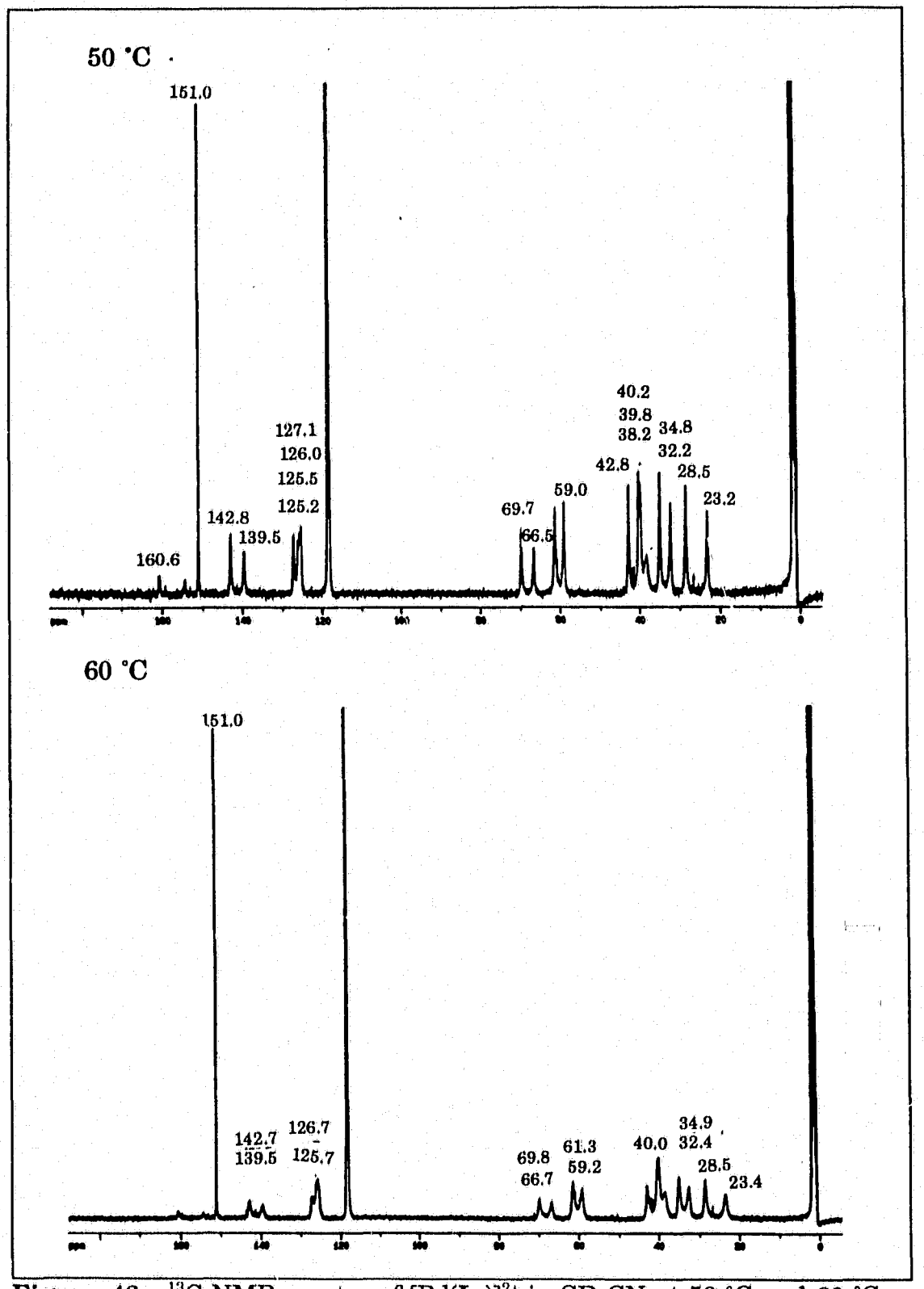

Figure 48 ^{13}C NMR spectra of $[Pd(L_4)]^{2+}$ in CD_3CN at 50 °C and 60 °C

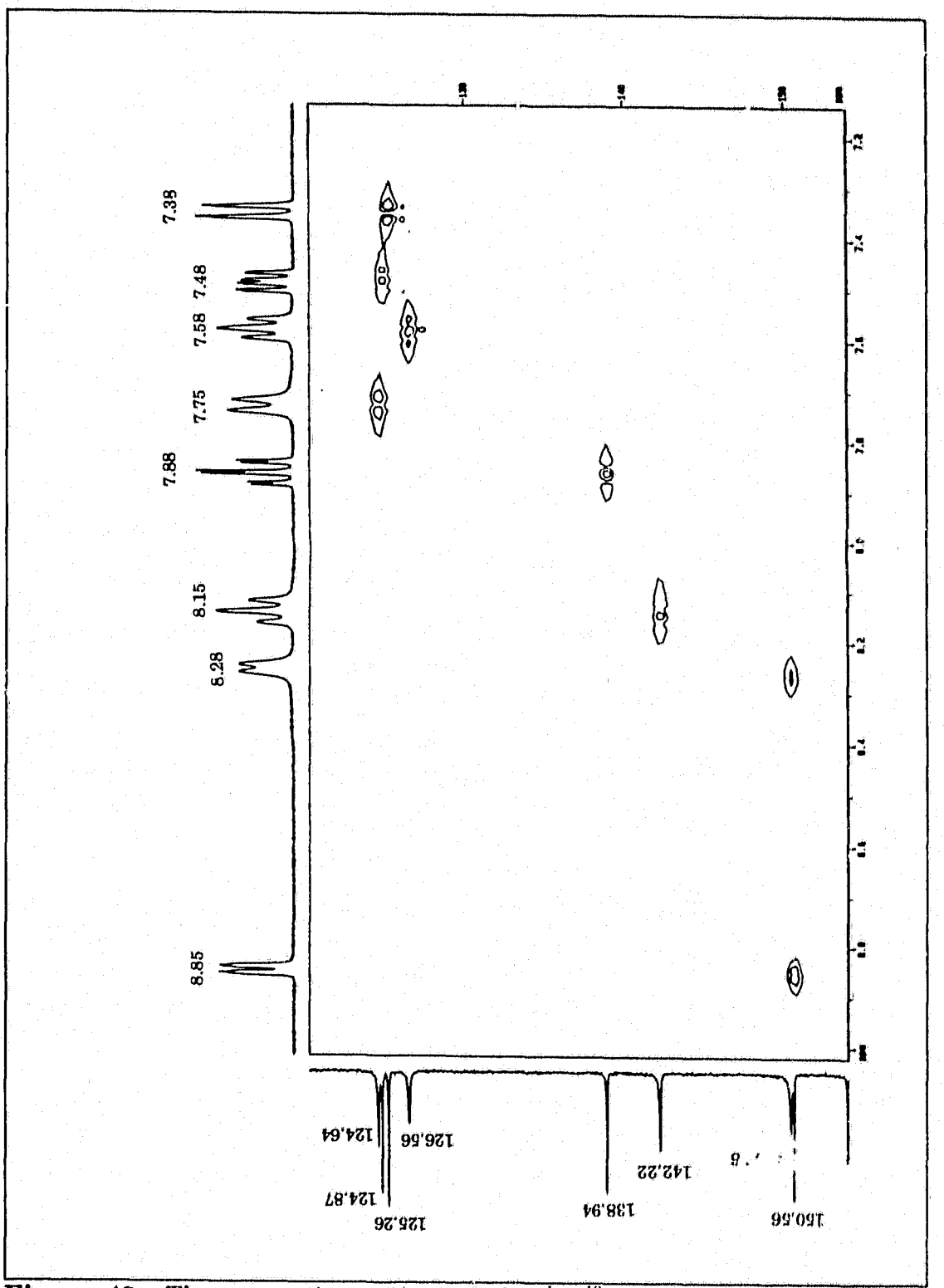

Figure 49 The aromatic portion of the ^{1}H-^{13}C correlated spectrum of $[Pd(L_4)]^{2+}$ in CD_3CN at -40 °C

The mechanism suggested in Scheme 11 is also supported by changes observed in the ^{13}C NMR spectra of $[Pd(\mathbf{L}_4)]^{2+}$ at different temperatures (Figures 45 - 48). At -40 °C, the ^{13}C NMR spectrum shows ten aromatic signals and sixteen aliphatic signals from isomers A and B in solution. With the aid of the ^{13}C-^{1}H correlated spectrum recorded at -40 °C (Figure 49), we tentatively assigned the ^{13}C resonances at δ 159.5, 150.6, 138.9, 124.9 and 125.3 correspond to the pyridine moiety in the isomer A of $[Pd(\mathbf{L}_4)]^{2+}$. The other set of ^{13}C resonances at δ 153.8, 150.4, 142.2, 124.6 and 126.6 correspond to isomer B of $[Pd(\mathbf{L}_4)]^{2+}$. The ^{13}C resonance at δ 68.7 and 65.7 correspond to the "benzylic" carbon in isomer A and B, respectively. The peaks at δ 58.1, 42.7, 39.3, 31.1 and 22.3, which remained sharp and unchanged between temperatures -40° to 40 °C are assigned to aliphatic carbons from isomer B. The remaining ^{13}C resonances correspond to the aliphatic carbons in the isomer A. At temperatures between -20 °C and 25 °C, when the commutation between metal-coordinated and uncoordinated thioether atoms in isomer A is the major exchange process in solution, the ^{13}C resonances at δ 28.0 and 29.8; 32.4, 35.1 and 36.7; 62.2 and 57.8 show broadening. They collapse to three singlets at δ 28.5, 34.7 and 61.0, respectively, at 25 °C. No change was observed in the aromatic carbons at these temperature ranges. This supports the proposal in Scheme 11 that the commutation of coordinated and uncoordinated thioether atoms in $[Pd(\mathbf{L}_4)]^{2+}$ occurs without the cleavage of the Pd-N(pyr) bond. At temperatures above 40 °C, when the exchange between the

two isomers of $[Pd(\mathbf{L_4})]^{2+}$ start to occur, both aliphatic and aromatic carbon signals start to broaden. This indicates that this process involves the rearrangement of all carbon atoms in the ligand framework as suggested by the mechanism shown in Scheme 11.

3.5 UV/Vis Spectroscopy

The UV/Vis spectral data of the palladium complexes of $\mathbf{L_2}$ and $\mathbf{L_4}$, are summarized in Table 32. For these complexes, no distinctive absorption bands were observed above 350 nm even when a more concentrated solution of the complex in acetonitrile was prepared. However, it is interesting to note that for $[Pd(\mathbf{L_4})Cl]^+$ and $[Pd(\mathbf{L_4})]^{2+}$, the addition of a pyridine pendant arm in the ligand does not shift the UV/Vis absorption bands significantly from those observed in the parent complex, $[Pd(\mathbf{L_2})]^{2+}$.

For square planar palladium complexes, the d-d transitions, ligand to metal charge transfer (LMCT) and metal to ligand charge transfer (MLCT) bands all overlap in the same region[97] and therefore no specific assignments have been made. However, a comparison with other similar complexes[41], $[Pd(\mathbf{10})]^{2+}$ and $[Pd(\mathbf{31})]^{2+}$ (Table 32) indicates that absorptions around λ = 320 - 370 nm are a common feature of palladium complexes with mixed sulphur and nitrogen donor systems.

Table 32
UV/Vis Spectral Data for Pd(II) complexes.

Complex	Anion	Solvent	λ_{max}[nm](ε_{max} in $M^{-1}cm^{-1}$)	Reference
$Pd(L_2)^{2+}$	Cl^-	H_2O	257(12,000); 326(4,600)	present work
$[Pd(L_4)Cl]^+$	Cl^-	H_2O	253(15,700); 340(2360)	present work
$Pd(L_4)^{2+}$	BF_4^-	CH_3CN	254(17,800); 345(2820)	present work
$[Pd(\mathbf{10})]^{2+}$	PF_6^-	CH_3CN	232(15,070) 298(14,460) 373(2175)	41
$[Pd(\mathbf{31})]^{2+}$	PF_6^-	CH_3CN	233(10,850) 266(10,000) 332(4250) 514(124)	41

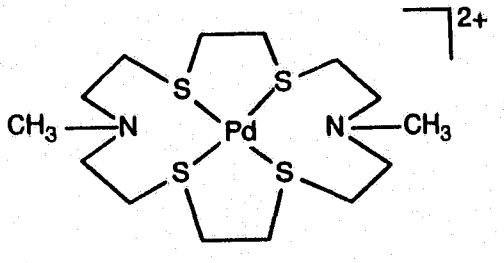

$[Pd(\mathbf{10})]^{2+}$

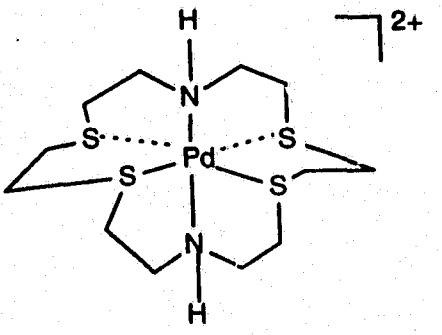

$[Pd(\mathbf{31})]^{2+}$

3.6 Electrochemistry

The redox chemistry of the Pd(II) complexes of $\mathbf{L_2}$ and $\mathbf{L_4}$ were studied by cyclic voltammetry and the results are summarized in Table 33. . In most cases, two irreversible reduction waves were observed (Figures 50 - 52). They are tentatively assigned as the reduction from Pd(II) to Pd(I); and Pd(I) to Pd(0).

For the complexes $[Pd(\mathbf{L_4})]^+$, the reduction of Pd(II) to Pd(I) occurred at a similar potential as $[Pd(\mathbf{L_2})]^{2+}$ (-0.96 V vs -0.90 V). However, for the complex $[Pd(\mathbf{L_4})Cl]^+$, such a reduction occurred at -1.2 V vs Fc/Fc^+. This may suggest that the reduction of Pd(II) to Pd(I) is more difficult in the chloro complex.

The stabilization of monomeric Pd(I) has been reported[40,41] in the square planar N_4 donor complex $[Pd(\mathbf{9})]^{2+}$ and also N_2S_2 donor complex $[Pd(\mathbf{10})]^{2+}$. The inability of ligands $\mathbf{L_2}$ and $\mathbf{L_4}$ to stabilize Pd(I) despite the presence of soft S atoms and a pyridine moiety in the ligand framework may due to the cavity of the ligand is not big enough to fit the larger Pd(I) ion. Alternatively, it may be attributed to the ligand $\mathbf{L_4}$ being coordinated to palladium in a folded fashion and the macrocyclic effect is very small compared to ligands such as cyclam which coordinated to a metal centre by wrapping around the cation in a square plane.

Table 33
Reduction potentials of Pd(II) complexes in acetonitrile.

Complex	Scan Rate (mV/s)	E_{red} vs Fc^+/Fc (V)	Ref.
$Pd(L_2)^{2+}$	100	-0.90 (Pd(II) - Pd(I)) -1.45 (Pd(I) - Pd(0))	present work
$Pd(L_4)Cl^+$	100	-1.2 -1.6	present work
$Pd(L_4)^{2+}$	50	-0.96 -1.62	present work
$[Pd(\mathbf{10})]^{2+}$	100	$E_{1/2}$ = -0.74	41
$[Pd(\mathbf{9})]^{2+}$	100	$E_{1/2}$ = -1.53	40

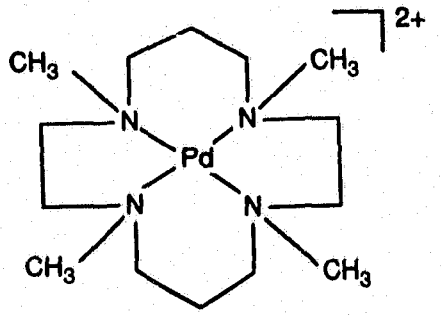

$[Pd(\mathbf{9})]^{2+}$

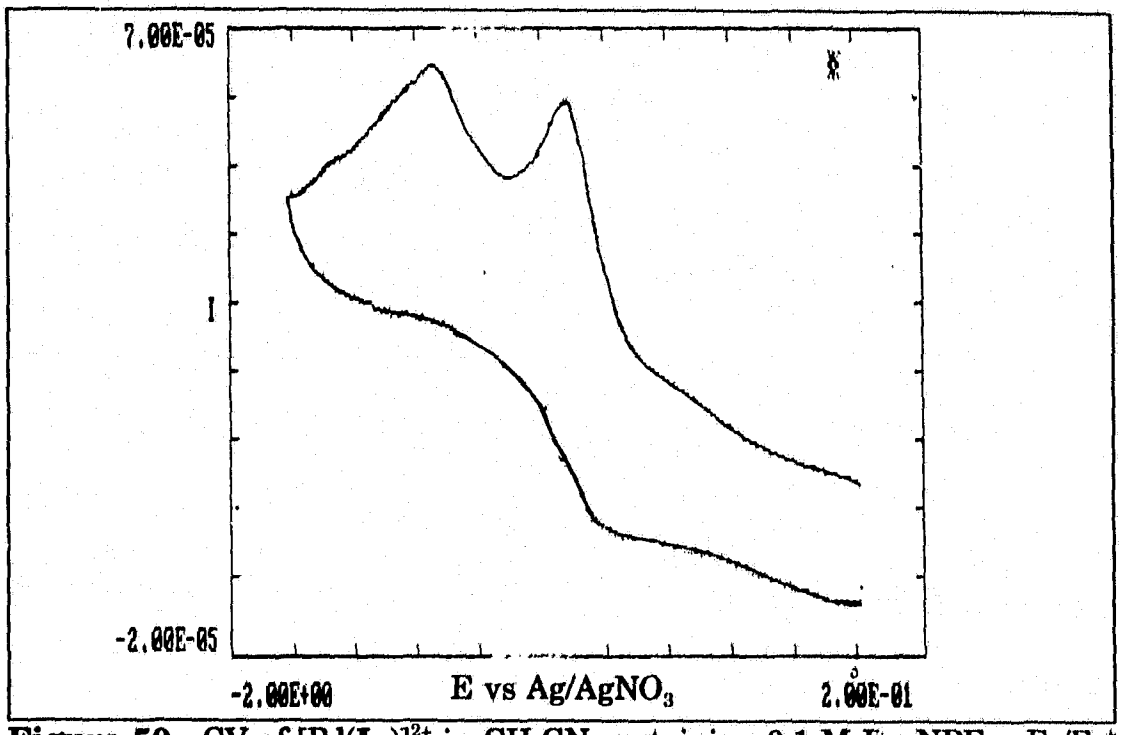

Figure 50 CV of $[Pd(L_2)]^{2+}$ in CH_3CN containing 0.1 M Bu_4NPF_6. Fc/Fc^+ occurs at 0.12 V.

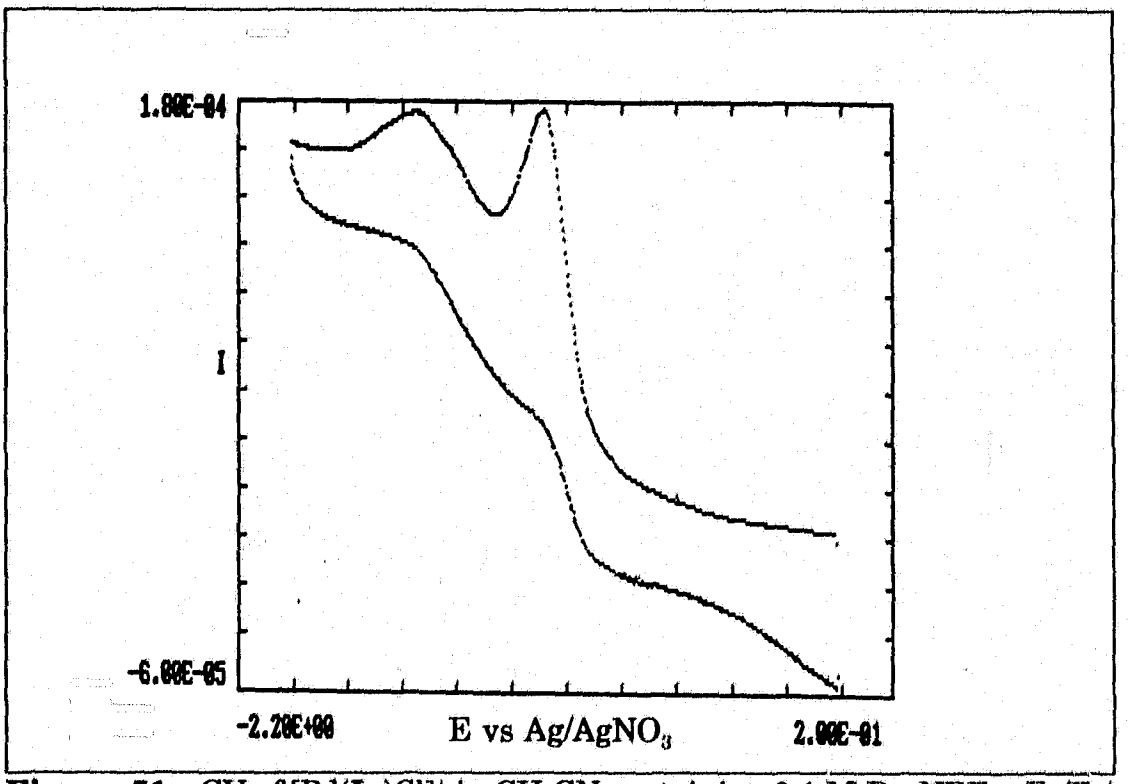

Figure 51 CV of $[Pd(L_4)Cl]^+$ in CH_3CN containing 0.1 M Bu_4NPF_6. Fc/Fc^+ occurs at 0.09 V.

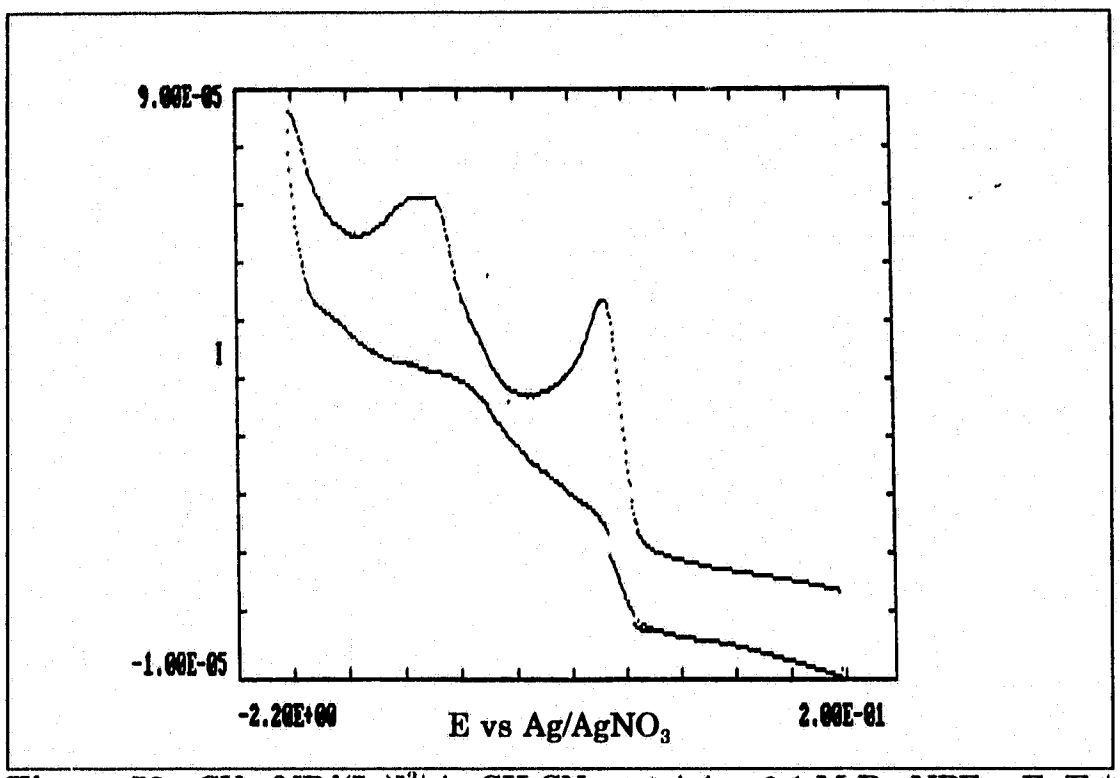

Figure 52 CV of $[Pd(L_4)]^{2+}$ in CH_3CN containing 0.1 M Bu_4NPF_6. Fc/Fc^+ occurs at 0.095 V.

3.7 Conclusion

In summary, the palladium(II) complexes of L_2 and L_4 were synthesized and their solid state structure characterized by X-ray crystallography. The complex $[Pd(L_2)]^{2+}$ has a square planar geometry both in the solid state and in solution, as confirmed by ^{13}C NMR in CD_3CN at room temperature. No temperature dependent NMR behavior was detected. Electrochemical reduction of this complex cation results in two irreversible reduction waves at -0.90 and -1.45 V vs Fc/Fc^+. In the complexes $[Pd(L_4)Cl]^+$ and $[Pd(L_4)]^{2+}$, the ligand was coordinated to the palladium in a folded fashion. The geometry

around the palladium atom is square planar. It is coordinated to two nitrogen atoms (one of which is from the pyridine moiety) and either two thioether sulphur atoms or one thioether atom and one chloride ion in the case of the chloro complex. In solution, both $[Pd(\mathbf{L}_4)]^{2+}$ and $[Pd(L_4)Cl]^{+}$ exhibited fluxional behavior due to the commutation of the metal coordinated and uncoordinated sulphur atoms of the ligand. By studying the NMR spectra of these two complexes at different temperatures, the mechanisms of the exchange processes involved were evaluated. The electrochemical reduction of $[Pd(\mathbf{L}_4)]^{2+}$ and its chloro complex also gave two irreversible reduction waves. The inability of ligands $\mathbf{L}_2$ and $\mathbf{L}_4$ to stabilize monomeric Pd(I) species was rationalized as due to either the cavity of the ligands being insufficiently large enough to accommodate a Pd(I) ion, or due to the folded conformation of the ligand when coordinated to palladium which reduced the macrocyclic effect.

CHAPTER 4

SYNTHESES AND SOLUTION STUDIES OF TRANSITION METAL COMPLEXES OF NITROGEN AND SULPHUR MIXED DONOR MACROCYCLES WITH PYRIDINE PENDANT ARMS

4.1 Introduction

As an ongoing study of nitrogen and sulphur mixed donor macrocycles with pyridine pendant arms, this chapter presents the syntheses, crystal structures and solution studies of the Co(II), Ni(II) and Cu(II) complexes of ligands $\mathbf{L_4}$ and $\mathbf{L_5}$. Our interest in these ligand systems arises partly from the recognition of similar coordination environment around metal centres in methanogenic bacterial enzymes[98] and in copper proteins[58,99].

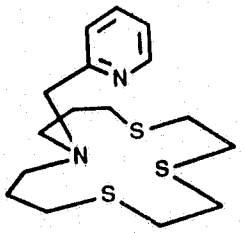

$\mathbf{L_4}$

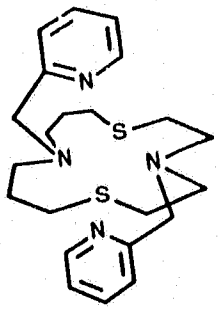

$\mathbf{L_5}$

4.2 Synthesis

The synthetic route leading to various transition metal complexes of $\mathbf{L_4}$ is outlined in Scheme 12 and to the Cu(II) complex of $\mathbf{L_5}$ is presented in eq. 8. The ligands were prepared according to the steps shown in Schemes 5 and 6 and also eq. 7 of chapter 3. In general, the nickel(II) and copper(II) complexes were prepared by the reaction of equimolar quantities of the ligand with $[Ni(H_2O)_6](ClO_4)_2$ or $[Cu(H_2O)_6](ClO_4)_2$ in dry CH_3CN under an atmosphere

Scheme 12

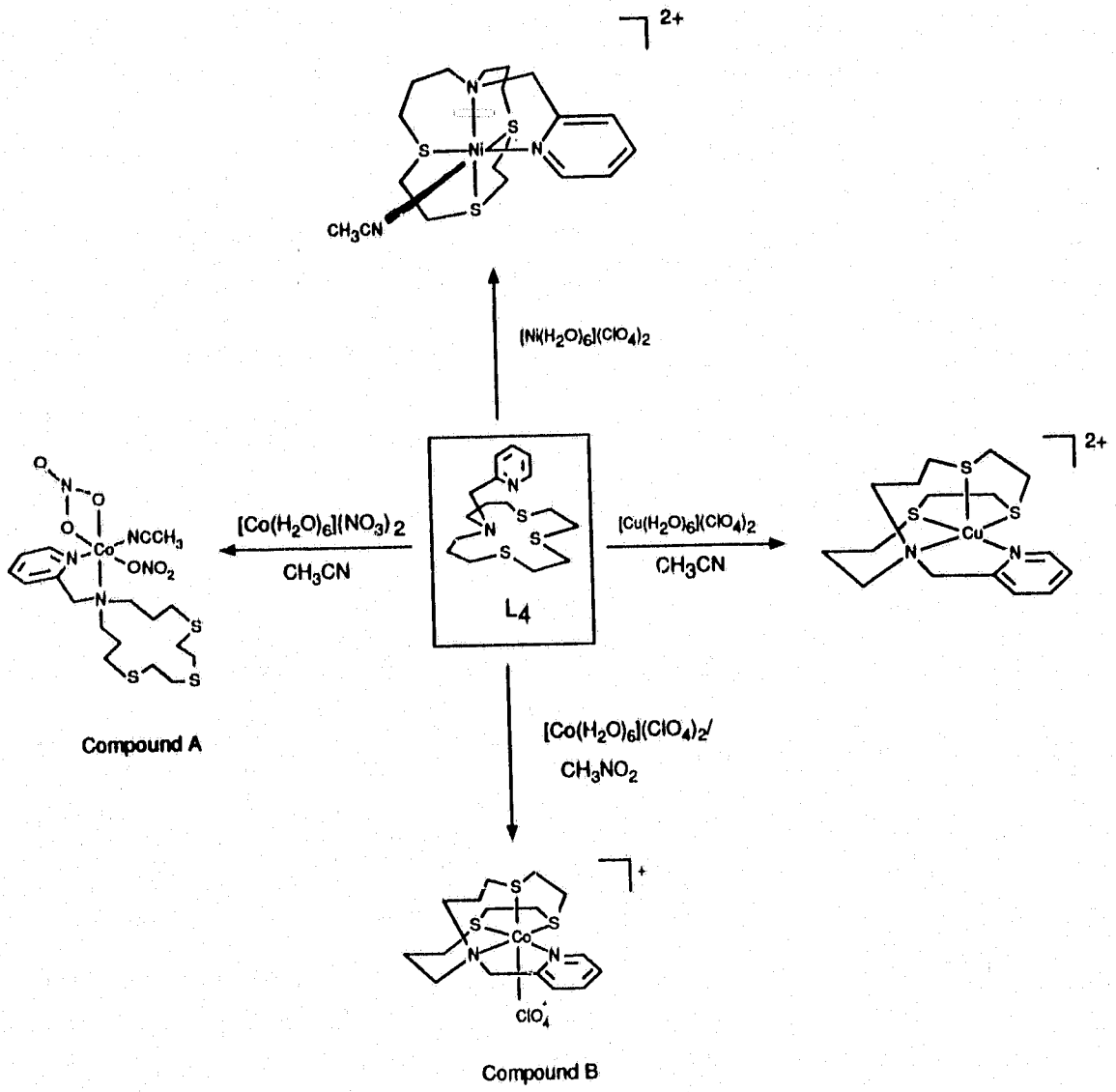
2+
CH3CN
[Ni(H2O)6](ClO4)2
[Co(H2O)6](NO3)2
CH3CN
L4
[Cu(H2O)6](ClO4)2
CH3CN
2+
NCCH3
ONO2
Compound A
[Co(H2O)6](ClO4)2/
CH3NO2
+
ClO4
Compound B

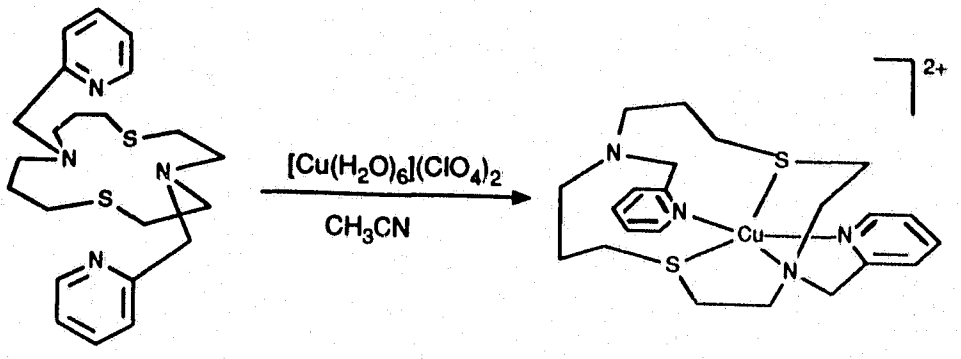

(8)

L_5

of nitrogen. X-ray quality crystals were obtained by slow diffusion of diethyl ether into the acetonitrile solution of the complexes.

In the case of the cobalt(II) complex of $\mathbf{L_4}$, two compounds were isolated. When the complex was prepared via the reaction of $[Co(H_2O)_6](NO_3)_2$ and $\mathbf{L_4}$ in dry acetonitrile, compound A was obtained. Its structure which has been determined by X-ray crystallography, will be discussed in section 4.3. In contrast, when the cobalt complex of $\mathbf{L_4}$ was prepared by the reaction of $[Co(H_2O)_6](ClO_4)_2$ in dry nitromethane, a different speicies (Compound B) was produced. Both of these compounds are stable in air and when dissolved in acetonitrile or nitromethane, yield different spectroscopic characteristics and electrochemical behavior. These aspects will be discussed in sections 4.4 and 4.6 of this chapter.

4.3 Crystal Structures

(a) Crystal structure of $[Ni(\mathbf{L_4})CH_3CN)](ClO_4)_2$

The nickel(II) complex of $\mathbf{L_4}$ has been characterized by crystallography. The molecular structure is shown in Figure 53, together with the atomic labelling scheme. Crystallographic parameters are listed in Table 34. The fractional atomic coordinates, interatomic distances and bond angles are given in Tables 35 - 37.

As illustrated in Figure 53, the nickel centre is located in a pseudo-octahedral environment. It is coordinated to three types of nitrogen atoms (one from the macrocycle, one from the pyridine ring and one from the solvent acetonitrile) and the three thioether sulphur atoms. Three different Ni-N bond lengths are observed, with the Ni-N(1)pyr being the shortest and has a value of 2.04 Å. This distance is slightly shorter than the ideal strain-free Ni-N bond length (2.10 Å)[26a]. However, this is close to the values found for related high spin mixed donor macrocyclic complexes reported in the literature[57,62,63,75]. For example, in the complexes $[Ni(bicycloSN_4)(ClO_4)]^{2+}$ and $[Ni(\mathbf{32})]^{2+}$, the mean Ni-N bond distance is 2.06 Å[75] and 2.08 Å[57i], respectively.

Three distinct Ni-S bond distances, ranging from 2.37 - 2.48 Å, are observed in the cation complex $[Ni(\mathbf{L_4})CH_3CN]^{2+}$. For the sulphur atom S(1) which is trans to the pyridine nitrogen N(1), the Ni-S bond is the shortest and has a distance of 2.37 Å. This is attributed to the trans influence of a sulphur atom being stronger than the nitrogen atom from pyridine. For the sulphur

atom S(3) which is trans to the nitrogen N(3) from acetonitrile, the bond length of Ni-S is 2.40 Å. This value is comparable to other mixed donor macrocyclic complexes such as $[Ni(\mathbf{32})]^{2+}$ (mean Ni-S = 2.41 Å)[57i] , $[Ni([9]aneSN_2)_2]^{2+}$ (2.42 Å)[62] and $Ni([9]aneNS_2)_2]^{2+}$ (2.41 Å)[63]. The longest Ni-S bond distance is observed for the sulphur atom S(2) trans to the tertiary amine, with a value of 2.48 Å. Earlier studies based on the Pd-S bond distances obtained from the crystal structures of $[Pd(\mathbf{L_2})]^{2+}$ (Figure 24) and $[Pd(\mathbf{L_4})]^{2+}$ (Figure 28) have established that the trans influence of a thioether sulphur atom is greater than a nitrogen atom from a tertiary amine, which in turn is greater than the nitrogen from pyridine. The very long Ni-S(2) bond distance observed in the present case is a consequence of a tetragonal elongation along the N(2)-Ni-S(2) axis. The d^8 Ni(II) ion has an electronic configuration of $t_{2g}^6 e_g^2$ in an octahedral field and in the presence of high crystal field, spin pairing of the two electrons in the e_g orbital occurs. The complex is then subjected to Jahn-Teller distortion and an elongation along the z-axis (the N(2)-Ni-S(2) axis in the present complex) is observed, which will lower the energy of the d_z^2 orbital.

A close examination at the structure of $[Ni(\mathbf{L_4})(CH_3CN)]^{2+}$ indicates that the ligand also adopts a "folded" conformation similar to the palladium and platinum analogues. The mean plane calculation (Table 38) indicates the S(1) atom is 0.1710 Å above the plane defined by the atoms S(2), N(1) and N(2). The nickel atom is also 0.0426 Å above this plane.

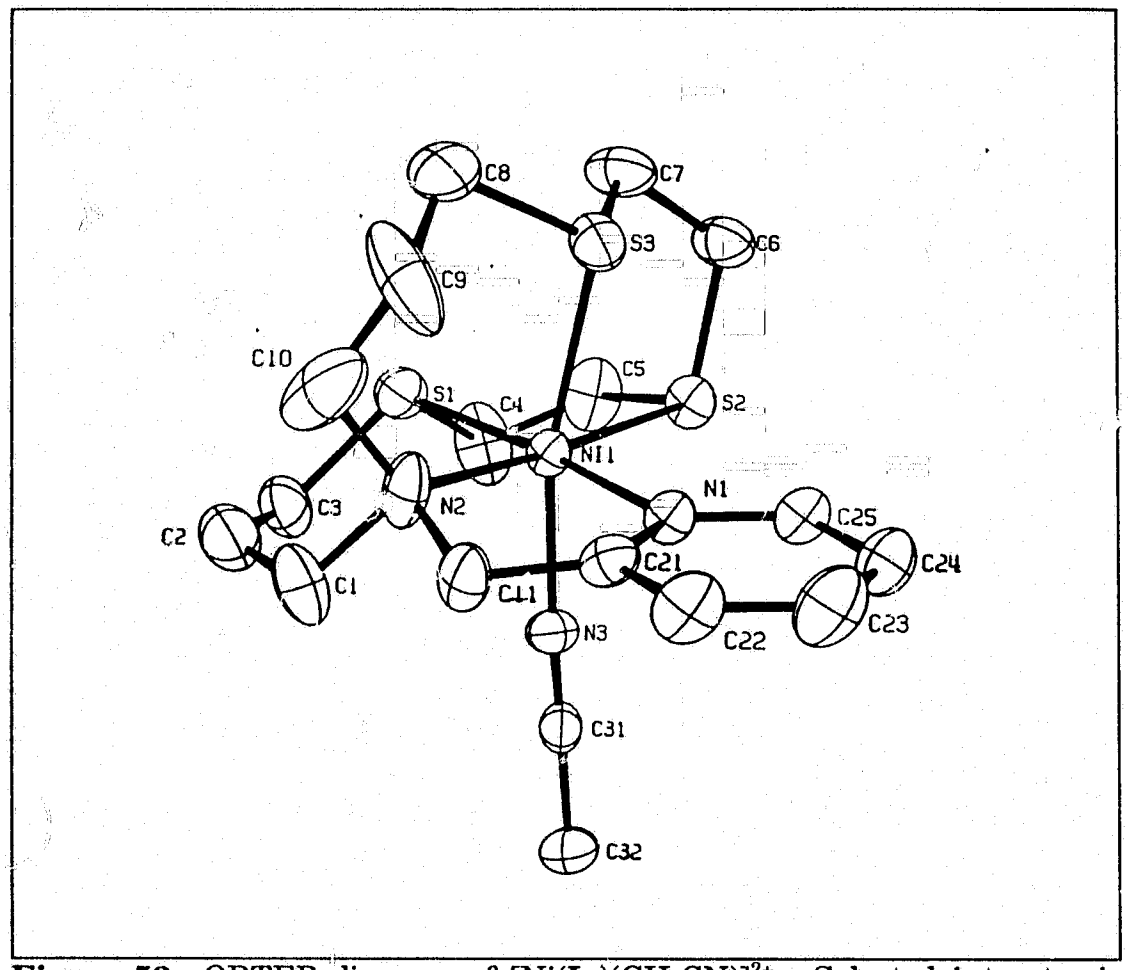

Figure 53 ORTEP diagram of $[Ni(L_4)(CH_3CN)]^{2+}$. Selected interatomic distances in Å: Ni-S(1) = 2.371(3); Ni-S(2) = 2.481(2); Ni-S(3) = 2.398(3); Ni-N(1) = 2.037(7); Ni-N(2) = 2.133(7); Ni-N(3) = 2.085(8).

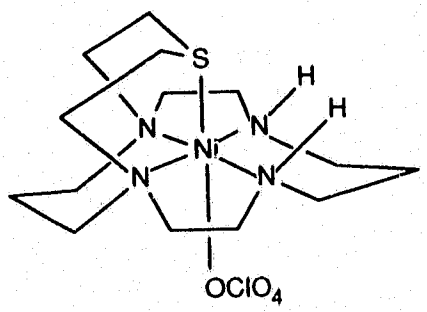

$[Ni(bicycloSN_4)(ClO_4)]^{2+}$

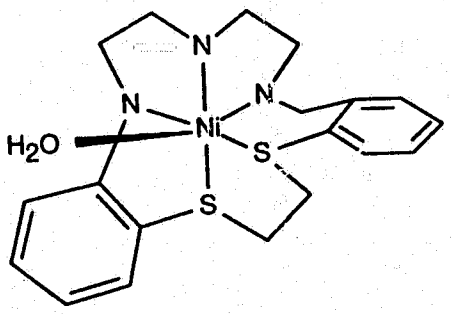

$[Ni(\mathbf{32})]^{2+}$

A nickel(II) complex of cyclam with pyridine pendant arm, $[Ni(\mathbf{33})]^{2+}$ has been prepared by Kimura and coworkers[100]. In such a system, the ligand cyclam adopts a *trans-I* configuration with pyridyl coordination in the axial position with Ni-N(pyr) bond distance being 2.124 Å. However, in the present complex cation $[Ni(\mathbf{L_4})(CH_3CN)]^{2+}$, the ligand $\mathbf{L_4}$ adopts a folded arrangement with pyridyl coordination in the equatorial position. Such a different coordination geometry can be rationalized by the constraint imposed by the ligand framework in the former case. In ligand **33**, the pyridine moiety is linked directly to the carbon framework of cyclam whereas in $\mathbf{L_4}$, the pyridine ring is linked to the macrocycle via a "benzylic" carbon on the tertiary amine. As a consequence, the five-membered chelate ring formed by the nitrogen atoms from the pyridine and the tertiary amine in **33** is not very flexible and will be too strain to coordinate to a metal ion in an equatorial position.

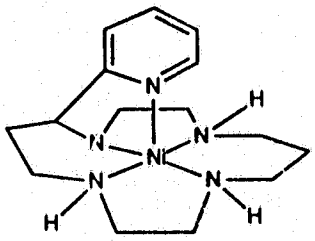

$[Ni(\mathbf{33})]^{2+}$

Table 34
Experimental crystallographic data for $[Ni(\mathbf{L_4}).CH_3CN](ClO_4)_2$

Formula:	$NiC_{20}H_{32}N_4S_3O_8Cl_2$
F.W.:	682.3
Crystal colour:	royal purple
Crystal system:	monoclinic
Space group:	$P2_1/n$ (No. 14)
Cell dimensions:	
	a = 12.152(5) Å α = 90°
	b = 14.445(2) Å β = 109.84(3)°
	c = 17.194(5) Å γ = 90°
V_{cell} :	2839.1 Å^3
Z:	4 molecules/cell
Temperature:	20 °C
Crystal dimensions:	0.64 x 0.20 x 0.25 mm^3
$D_{calcd.}$:	1.596 g/cm^3
$D_{meas.}$:	1.595 g/cm^3
Radiation:	Mo, K_α 0.71069 Å
μ:	11.07 cm^{-1}
transmission range:	0.598 -- 0.664
Measurement:	2θ(0-45°)
No. of reflections collected:	3828
No. of reflections n ≥ nσ(I):	2992 (n = 4)
No. of parameters:	343
Residual electron density:	0.2 e/Å^3
Maximum final shift/error:	0.03
Refinement method:	SHELX least squares
R:	0.078
R_w:	0.086

Table 35
Fractional atomic coordinates and temperature parameters for $[Ni(L_4).CH_3CN](ClO_4)_2$

Atom	x/a	y/b	z/c	U_{eq}
Ni(1)	12268(8)	4160(7)	31720(6)	500(4)
Cl(1)	-4408(22)	46178(19)	26411(16)	737(11)
Cl(2)	12942(29)	19799(25)	-2860(21)	955(14)
S(1)	18578(22)	19506(16)	30700(16)	684(10)
S(2)	33084(18)	1232(17)	39966(15)	641(10)
S(3)	10590(22)	5905(20)	45142(16)	783(12)
O(1)	473(10)	4449(9)	2340(10)	197(9)
O(2)	-614(15)	3841(7)	3052(9)	203(10)
O(3)	-202(24)	5281(8)	3173(9)	307(17)
O(4)	-1287(12)	4920(20)	2020(11)	329(16)
O(5)	1031(22)	2699(13)	83(10)	315(15)
O(6)	1875(17)	1484(10)	383(10)	234(11)
O(7)	1980(17)	2371(28)	-597(12)	441(25)
O(8)	418(11)	1668(10)	-903(10)	208(9)
N(1)	536(5)	-871(5)	3160(4)	56(3)
N(2)	-549(7)	763(6)	2500(6)	84(4)
N(3)	1606(6)	-12(5)	2132(5)	63(3)
C(1)	-631(12)	1257(12)	1631(8)	125(7)
C(2)	-103(11)	2127(10)	1663(8)	102(6)
C(3)	1165(11)	2274(7)	2000(7)	88(5)
C(4)	3342(10)	1664(10)	3055(10)	113(5)
C(5)	4016(10)	1144(8)	3754(9)	101(6)
C(6)	3876(9)	373(8)	5059(6)	86(5)
C(7)	2487(10)	1083(9)	5091(7)	97(5)
C(8)	-22(15)	1534(12)	4399(9)	152(9)
C(9)	-1136(11)	1116(16)	3649(12)	172(11)
C(10)	-1153(12)	1408(13)	2801(14)	185(11)
C(11)	-1143(8)	-95(7)	2195(7)	79(4)
C(21)	-614(7)	-905(7)	2724(6)	65(4)
C(22)	-1225(9)	-1736(8)	2694(8)	85(5)
C(23)	-667(11)	-2504(9)	3111(9)	103(7)
C(24)	513(10)	-2459(7)	3538(7)	82(5)
C(25)	1081(8)	-1633(7)	3576(6)	68(4)
C(31)	1808(8)	-299(6)	1585(6)	61(4)
C(32)	2042(10)	-669(7)	858(6)	84(5)
N(4)	6539(19)	1460(16)	317(15)	196(13)
C(41)	5644(29)	1173(28)	118(15)	243(22)
C(42)	4417(26)	736(45)	-168(24)	440(48)

Estimated standard deviations are given in parentheses. Coordinates x 10^n where n = 5,5,5,4,4,4 for Ni,Cl,S,O,N,C. Temperature parameters x 10^n where n = 3,3,3,3,2,3 for Ni,Cl,S,O,N,C.
U_{eq} = the equivalent isotropic temperature parameter. $U_{eq} = \frac{1}{3}\Sigma_i\Sigma_j U_{ij} a_i^* a_j^* (a_i.a_j)$.
Primed values indicate that U_{iso} is given. $T = \exp(-8\pi^2 U_{iso} \sin^2\theta/\lambda^2)$

Table 36
Interatomic Distances (Å) for $[Ni(L_4).CH_3CN](ClO_4)_2$

Atoms	Distance	Atoms	Distance
S(1)-Ni(1)	2.371(3)	C(21)-N(1)	1.344(10)
S(2)-Ni(1)	2.481(2)	C(25)-N(1)	1.357(11)
S(3)-Ni(1)	2.398(3)	C(1)-N(2)	1.629(17)
N(1)-Ni(1)	2.037(7)	C(10)-N(2)	1.390(16)
N(2)-Ni(1)	2.133(7)	C(11)-N(2)	1.441(13)
N(3)-Ni(1)	2.085(8)	C(31)-N(3)	1.129(10)
O(1)-Cl(1)	1.397(10)	C(2)-C(1)	1.403(19)
O(2)-Cl(1)	1.380(11)	C(3)-C(2)	1.466(16)
O(3)-Cl(1)	1.288(11)	C(5)-C(4)	1.419(16)
O(4)-Cl(1)	1.282(14)	C(7)-C(6)	1.505(15)
O(5)-Cl(2)	1.312(17)	C(9)-C(8)	1.635(25)
O(6)-Cl(2)	1.335(13)	C(10)-C(9)	1.512(26)
O(7)-Cl(2)	1.265(20)	C(21)-C(11)	1.488(14)
O(8)-Cl(2)	1.302(12)	C(22)-C(21)	1.403(13)
C(3)-S(1)	1.806(11)	C(23)-C(22)	1.369(17)
C(4)-S(1)	1.859(12)	C(24)-C(23)	1.372(15)
C(5)-S(2)	1.825(11)	C(25)-C(24)	1.368(13)
C(6)-S(2)	1.836(10)	C(32)-C(31)	1.474(14)
C(7)-S(2)	1.825(11)	C(41)-N(4)	1.105(28)
C(8)-S(3)	1.856(12)	C(42)-C(41)	1.537(40)

Estimated standard deviations are given in parentheses.

Table 37
Bond Angles (deg) for $[Ni(L_4).CH_3CN](ClO_4)_2$

Atoms	Angle	Atoms	Angle
S(2)-Ni(1)-S(1)	84.8(1)	C(7)-S(3)-Ni(1)	100.9(4)
S(3)-Ni(1)-S(1)	96.2(1)	C(8)-S(3)-Ni(1)	105.2(4)
S(3)-Ni(1)-S(2)	82.6(1)	C(8)-S(3)-C(7)	106.2(7)
N(1)-Ni(1)-S(1)	174.2(2)	C(21)-N(1)-Ni(1)	112.7(6)
N(1)-Ni(1)-S(2)	100.8(2)	C(25)-N(1)-Ni(1)	127.5(6)
N(1)-Ni(1)-S(3)	86.3(2)	C(25)-N(1)-C(21)	119.6(8)
N(2)-Ni(1)-S(1)	91.9(2)	C(1)-N(2)-Ni(1)	109.6(7)
N(2)-Ni(1)-S(2)	176.0(2)	C(10)-N(2)-Ni(1)	121.4(9)
N(2)-Ni(1)-S(3)	95.5(3)	C(10)-N(2)-C(1)	99.8(13)
N(2)-Ni(1)-N(1)	82.6(3)	C(11)-N(2)-Ni(1)	106.6(6)
N(3)-Ni(1)-S(1)	92.4(2)	C(11)-N(2)-C(1)	100.1(10)
N(3)-Ni(1)-S(2)	87.7(2)	C(11)-N(2)-C(10)	116.7(10)
N(3)-Ni(1)-S(3)	166.4(2)	C(31)-N(3)-Ni(1)	175.7(7)
N(3)-Ni(1)-N(1)	86.0(3)	C(2)-C(1)-N(2)	118.2(12)
N(3)-Ni(1)-N(2)	94.7(3)	C(3)-C(2)-C(1)	123.5(11)
O(2)-Cl(1)-O(1)	109.0(8)	C(2)-C(3)-S(1)	115.4(3)
O(3)-Cl(1)-O(1)	112.2(14)	C(5)-C(4)-S(1)	113.0(9)
O(3)-Cl(1)-O(2)	106.2(8)	C(4)-C(5)-S(2)	116.1(8)
O(4)-Cl(1)-O(1)	105.3(10)	C(7)-C(6)-S(2)	112.3(7)
O(4)-Cl(1)-O(2)	119.0(14)	C(6)-C(7)-S(3)	106.0(8)
O(4)-Cl(1)-O(3)	105.2(16)	C(9)-C(8)-S(3)	100.4(10)
O(6)-Cl(2)-O(5)	98.8(10)	C(10)-C(9)-C(8)	113.2(13)
O(7)-Cl(2)-O(5)	98.8(19)	C(9)-C(10)-N(2)	109.6(17)
O(8)-Cl(2)-O(6)	111.8(15)	C(21)-C(11)-N(2)	113.2(8)
O(8)-Cl(2)-O(5)	113.7(11)	C(11)-C(21)-N(1)	117.7(8)
O(8)-Cl(2)-O(6)	124.3(11)	C(22)-C(21)-N(1)	119.3(9)
O(8)-Cl(2)-O(7)	106.5(11)	C(22)-C(21)-C(11)	122.4(9)
C(3)-S(1)-Ni(1)	105.5(4)	C(23)-C(22)-C(21)	120.8(9)
C(4)-S(1)-Ni(1)	97.6(4)	C(24)-C(23)-C(22)	118.9(10)
C(4)-S(1)-C(3)	99.3(6)	C(25)-C(24)-C(23)	119.0(10)
C(5)-S(2)-Ni(1)	101.5(4)	C(24)-C(25)-N(1)	122.3(9)
C(6)-S(2)-Ni(1)	103.2(3)	C(32)-C(31)-N(3)	178.6(10)
C(6)-S(2)-C(5)	101.8(6)	C(42)-C(41)-N(4)	177.7(45)

Estimated standard deviations are given in parentheses.

Table 38
Mean plane for $[Ni(L_4)(CH_3CN)](ClO_4)_2$

The equation of the plane containing sulphur and nitrogen atoms is:
0.4931X - 0.1891Y - 0.8492Z + 4.6904 = 0

Atoms	X	Y	Z	P
S(2)	1.6881	0.1780	6.4639	0.000
N(1)	-1.1929	-1.2579	5.1108	0.000
N(2)	-2.1260	1.1016	4.0437	0.000
Ni(1)	-0.3602	0.6009	5.1302	0.0426
S(1)	0.4661	2.8176	4.9652	0.1710
S(3)	-1.3474	0.8530	7.3010	-2.3352
N(3)	0.7071	-0.0173	3.4488	2.1136

where P is the perpendicular distance between the atom and the mean plane, given in Å.

(b) Crystal structure of $[Co(L_4)(NO_3)_2.CH_3CN]$ (Compound A)

The complex $[Co(L_4)(CH_3CN)(NO_3)_2]$ has been characterized by crystallography. The molecular structure and atomic labelling scheme is shown in Figure 54. The crystallographic parameters, fractional atomic coordinates, interatomic distances and bond angles are listed in Tables 39 - 42.

As shown in Figure 54, the cobalt ion is in an octahedral environment. It is coordinated to three nitrogen atoms, one from the macrocycle, one from the pyridyl ring and one from the solvent acetonitrile. The remaining coordination sites are occupied by a monodentate and bidentate nitrate ion, NO_3^-. These two modes of coordination of the nitrate ions have also been established by IR spectroscopy. The IR spectrum of $[Co(L_4)(NO_3)_2(CH_3CN)]$ (KBr disc) shows NO stretches at 1360 and 1461 cm^{-1} which correspond to a monodentate nitrate ion[101]. In addition, NO stretches at 1285 and 1021 cm^{-1} were also observed, consistent with a bidentate nitrate.

In contrast to the structure of the nickel(II) complex of L_4 discussed in the previous section, none of the thioether sulphur atoms in the macrocycle L_4 is coordinated to the metal in Compound A. The ligand adopts a conformation similar to that observed in the free ligand [14]aneS_4 (Figure 22)[32], suggesting the lone pairs of electrons in the non-coordinating thioether atoms are directed out of the ring.

A detailed examination at the structure of $[Co(L_4)(CH_3CN)(NO_3)_2]$ indicates that the coordination geometry at the cobalt centre is best described

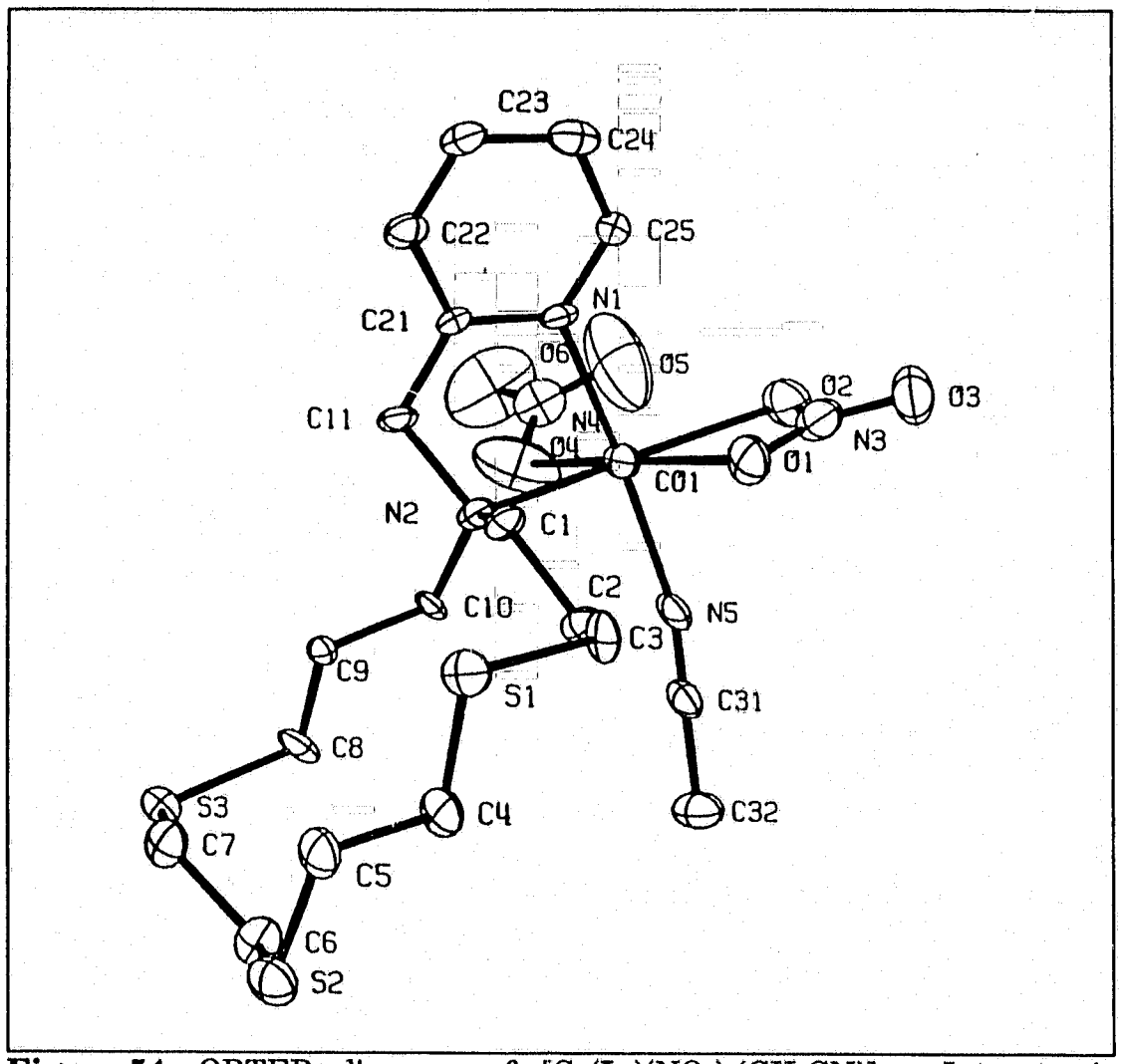

Figure 54 ORTEP diagram of $[Co(L_4)(NO_3)_2(CH_3CN)]$. Interatomic distances in Å: Co-O(1) = 2.245(15); Co-O(2) = 2.362(15); Co-O(4) = 2.217(22); Co-N(1) = 2.145(13); Co-N(2) = 2.354(13); Co-N(5) = 2.159(16).

as a distorted octahedron. The Co(II) centre, being a d^7 ion, has one unpaired electron in the e_g orbital in an octahedral field and is subjected to Jahn-Teller distortion. In the present complex, a tetragonal compression along the N(1)-Co-N(5) axis is observed. The mean Co-N bond distance in the axial position of $[Co(\mathbf{L}_4)(CH_3CN)(NO_3)_2]$ is 2.15 Å, which is about 0.2 Å shorter than that in the equatorial plane (Co-N(2) = 2.35 Å). The Co-N(1)pyr bond distance is the shortest of the three Co-N bonds. This is due to the steric strain imposed by the five membered chelate ring formed by the pyridyl nitrogen and the nitrogen in the macrocycle. Such strain is also manifested in the five membered chelate bite angle N(1)pyr-Co-N(2), which is only 76.6°, which is significantly smaller than that observed in the complexes $[Ni(\mathbf{L}_4)(CH_3CN)]^{2+}$ (N(1)pyr-Ni-N(2): 82.6°) and $[Pd(\mathbf{L}_4)]^{2+}$ (N(1)pyr-Pd-N(2): 81.7°), when the nitrogen atoms from the pyridyl ring and the macrocycle are coordinated to the metal centre in the equatorial plane.

The Co-O bond distances in the bidentate chelating nitrate ion are not identical, with Co-O(1) being 2.24 Å and Co-O(2) being 2.36 Å. The bite angle of the four-membered chelate O(1)-Co-O(2) is 54.4° and the bond angle of N(2)-Co-O(4) is 85.1°. The former value reflects the small spatial distribution of the oxygens in bidentate nitrate and the latter is smaller than the ideal value of 90° between two donors in the equatorial plane of a normal octahedron.

For some thioether macrocycles, e.g., [12]aneS$_4$ and [14]aneS$_4$, the conformation of the free ligand is such that the lone pairs of the sulphur atoms are directed out of the ring[82,102]. In these cases, complexation of metal ions occurs in an exo manner. It is not unusual that such thia macrocycles act only as mono-, bi- or tridentate ligands, and leave some of the thioether sulphur atoms uncoordinated. For example, in the complexes [Al(CH$_3$)$_3$[12]aneS$_4$][102] and [ReBr(CO$_3$)[14]aneS$_4$][61], the thia macrocycles act as a mono- or bidentate ligands, respectively. The complex [Co(**L**$_4$)(CH$_3$CN)(NO$_3$)$_2$] is unique in the sense that the metal centre prefers to bind to a bidentate and monodentate nitrate and the solvent molecule acetonitrile, rather than the thioether sulphur atoms in the macrocycle. This result is very interesting and the ion may be viewed as a precursor to the formation of the macrocyclic complex of [Co(**L**$_4$)]$^{2+}$.

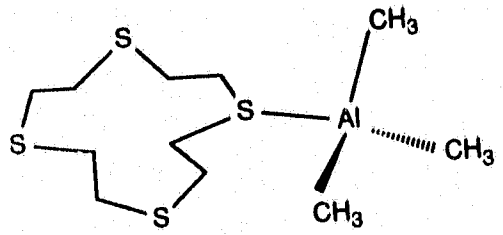

[Al(CH$_3$)$_3$[12]aneS$_4$]

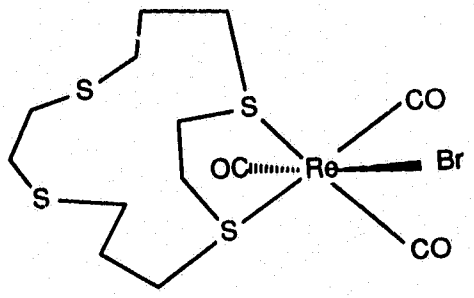

[ReBr(CO)$_3$[12]aneS$_4$]

Table 39
Experimental crystallographic data for $[Co(L_4).(NO_3)_2.CH_3CN]$

Formula:	$CoS_3O_6N_6C_{20}H_{32}$	
F.W.:	607.6	
Crystal color:	burgundy red	
Crystal system:	triclinic	
Space group:	$P\bar{1}$ (No. 2)	
Cell dimensions:	a = 8.419(1)	α = 109.38(1)°
	b = 13.165(2)	β = 101.37(1)°
	c = 14.524(2)	γ = 103.27(1)°
V_{cell}:	1411.06 Å^3	
Z:	2 molecules/cell	
Temperature:	20 °C	
Crystal dimensions:	0.4 x 0.2 x 0.05 mm^3	
D_{cald}:	1.430	
$D_{meas.}$:	1.435	
Radiation:	Cu, 1.542 Å	
μ:	65.5 cm^{-1}	
Transmission range:	N/A	
Measurement:	2θ(0 - 110°)	
No. of reflections collected:	3225	
No. of reflections $I \geq n\sigma(I)$:	1950 (n = 6)	
No. of parameters:	320	
No. of standards:	008, 500, 050	
Residual electron density:	0.20 e/Å^3	
Maximum final shift/error:	0.01	
Refinement method:	least squares SHELX76	
R:	0.1148	
R_w:	0.1129	

Table 40
Fractional atomic coordinates and temperature parameters for
$[Co(L_4).(NO_3)_2.CH_3CN]$

Atom	x/a	y/b	z/c	U_{eq}
Co(1)	14263(38)	28927(24)	30612(21)	448(16)
S(1)	80707(69)	54959(44)	24097(40)	619(29)
S(2)	76285(72)	85062(47)	18524(44)	708(32)
S(3)	20802(66)	66016(40)	3462(36)	533(26)
O(1)	3836(18)	3061(11)	4103(10)	69(8)
O(2)	1563(23)	2254(12)	4319(11)	78(9)
O(3)	4053(22)	2387(14)	5267(11)	94(10)
O(4)	-1094(26)	2695(17)	2141(20)	158(18)
O(5)	-1592(39)	1610(29)	2721(25)	227(30)
O(6)	-3594(30)	1686(22)	1624(22)	223(21)
N(1)	1540(17)	1380(10)	2020(10)	41(7)
N(2)	2550(17)	3545(10)	1998(10)	37(7)
N(3)	3142(29)	2566(14)	4596(14)	66(11)
N(4)	-2195(36)	1959(19)	2145(19)	90(14)
N(5)	1601(23)	4537(13)	4065(11)	66(10)
C(31)	1728(26)	5483(17)	4463(14)	53(11)
C(32)	1936(26)	6658(15)	4950(16)	68(12)
C(1)	4387(22)	3773(13)	2250(12)	42(9)
C(2)	5409(23)	4869(14)	3213(13)	48(9)
C(3)	7353(21)	5111(15)	3391(12)	47(10)
C(4)	7815(23)	6871(16)	2657(14)	61(11)
C(5)	8143(24)	7239(16)	1802(14)	62(11)
C(6)	5313(23)	8082(16)	1607(14)	59(11)
C(7)	4341(24)	7062(18)	541(15)	67(11)
C(8)	1828(23)	5990(14)	1287(13)	48(10)
C(9)	2443(25)	4977(14)	1149(13)	50(10)
C(10)	1900(20)	4492(12)	1934(12)	34(8)
C(11)	1769(21)	2518(12)	1007(12)	40(8)
C(21)	1858(20)	1477(13)	1179(12)	36(8)
C(22)	2261(23)	617(14)	476(14)	52(10)
C(23)	2268(25)	-358(16)	627(15)	60(11)
C(24)	1951(26)	-403(15)	1553(16)	67(12)
N(6)	7507(49)	1238(30)	6282(23)	169(25)
C(33)	7614(53)	748(31)	5530(39)	157(33)
C(34)	7239(73)	147(35)	4356(29)	261(39)
C(25)	1585(20)	457(15)	2217(12)	42(5)'

Estimated standard deviations are given in parentheses. Coordinates x 10^n where n = 5,5,4,4,4 for Co,S,O,N,C
Temperature parameters x 10^n where n = 3,3,3,2,2 for Co,S,O,N,C.
U_{eq} = the equivalent isotropic temperature parameter. $U_{eq} = \frac{1}{3}\Sigma_i\Sigma_j U_{ij} a_i^* a_j^* (a_i.a_j)$.
Primed values indicate that U_{iso} is given. $T = \exp-(8\pi^2 U_{iso} \sin^2\theta/\lambda^2)$

Table 41
Interatomic Distances (Å) for $[Co(\mathbf{L}_4)(NO_3)_2.CH_3CN]$

Atoms	Distance	Atoms	Distance
O(1)-Co(1)	2.245(15)	C(25)-N(1)	1.355(19)
O(2)-Co(1)	2.362(15)	C(1)-N(2)	1.451(20)
O(4)-Co(1)	2.217(22)	C(10)-N(2)	1.496(18)
N(1)-Co(1)	2.145(13)	C(11)-N(2)	1.563(20)
N(2)-Co(1)	2.354(13)	C(31)-N(5)	1.161(20)
N(5)-Co(1)	2.159(16)	C(32)-C(31)	1.429(24)
C(3)-S(1)	1.918(18)	C(2)-C(1)	1.596(22)
C(4)-S(1)	1.794(20)	C(3)-C(2)	1.543(22)
C(5)-S(2)	1.799(20)	C(5)-C(4)	1.608(24)
C(6)-S(2)	1.823(18)	C(7)-C(6)	1.642(26)
C(7)-S(3)	1.789(19)	C(9)-C(8)	1.505(21)
C(8)-S(3)	1.910(16)	C(10)-C(9)	1.644(22)
N(3)-O(1)	1.298(21)	C(21)-C(11)	1.496(21)
N(3)-O(2)	1.236(20)	C(22)-C(21)	1.446(22)
N(3)-O(3)	1.287(21)	C(23)-C(22)	1.378(23)
N(4)-O(4)	1.180(26)	C(24)-C(23)	1.531(28)
N(4)-O(5)	1.212(29)	C(25)-C(24)	1.397(24)
N(4)-O(6)	1.140(26)	C(33)-N(6)	1.164(46)
C(21)-N(1)	1.422(20)	C(34)-C(33)	1.659(53)

Estimated standard deviations are given in parentheses.

Table 42
Bond Angles (deg) for [Co($\mathbf{L}_4$)$(NO_3)_2$.CH_3CN]

Atoms	Angle	Atoms	Angle
O(2)-Co(1)-O(1)	54.5(5)	C(11)-N(2)-C(10)	108.5(13)
O(4)-Co(1)-O(1)	174.0(8)	O(2)-N(3)-O(1)	112.9(20)
O(4)-Co(1)-O(2)	119.8(8)	O(3)-N(3)-O(1)	121.6(21)
N(1)-Co(1)-O(1)	91.6(5)	O(3)-N(3)-O(2)	125.5(21)
N(1)-Co(1)-O(2)	96.4(5)	O(5)-N(4)-O(4)	108.2(30)
N(1)-Co(1)-O(4)	90.9(7)	O(6)-N(4)-O(4)	118.9(33)
N(2)-Co(1)-O(1)	100.8(5)	O(6)-N(4)-O(5)	132.9(36)
N(2)-Co(1)-O(2)	154.5(6)	C(31)-N(5)-Co(1)	167.0(15)
N(2)-Co(1)-O(4)	85.1(7)	C(32)-C(31)-N(5)	178.2(21)
N(2)-Co(1)-N(1)	76.6(5)	C(2)-C(1)-N(2)	113.3(14)
N(5)-Co(1)-O(1)	86.0(5)	C(3)-C(2)-C(1)	110.4(14)
N(5)-Co(1)-O(2)	88.3(5)	C(2)-C(3)-S(1)	111.1(12)
N(5)-Co(1)-O(4)	92.2(7)	C(5)-C(4)-S(1)	107.7(13)
N(5)-Co(1)-N(1)	172.2(6)	C(4)-C(5)-S(2)	113.1(14)
N(5)-Co(1)-N(2)	96.5(5)	C(7)-C(6)-S(2)	111.5(13)
C(4)-S(1)-C(3)	102.0(8)	C(6)-C(7)-S(3)	110.6(13)
C(6)-S(2)-C(5)	104.1(9)	C(9)-C(8)-S(3)	112.8(12)
C(8)-S(3)-C(7)	103.8(9)	C(10)-C(9)-C(8)	105.0(13)
N(3)-O(1)-Co(1)	98.2(13)	C(9)-C(10)-N(2)	114.5(12)
N(3)-O(2)-Co(1)	94.4(13)	C(21)-C(11)-N(2)	107.1(13)
N(4)-O(4)-Co(1)	111.7(21)	C(11)-C(21)-N(1)	118.7(14)
C(21)-N(1)-Co(1)	115.6(10)	C(22)-C(21)-N(1)	123.3(15)
C(25)-N(1)-Co(1)	121.7(12)	C(22)-C(21)-C(11)	118.0(16)
C(25)-N(1)-C(21)	121.8(14)	C(23)-C(22)-C(21)	117.2(19)
C(1)-N(2)-Co(1)	110.3(10)	C(24)-C(23)-C(22)	117.0(17)
C(10)-N(2)-Co(1)	108.3(9)	C(25)-C(24)-C(23)	123.6(17)
C(10)-N(2)-C(1)	117.4(12)	C(34)-C(33)-N(6)	162.6(51)
C(11)-N(2)-Co(1)	105.0(9)	C(24)-C(25)-N(1)	116.9(17)
C(11)-N(2)-C(1)	103.7(12)		

Estimated standard deviations are given in parentheses.

(c) Crystal structures of L_5 and $[Cu(L_5)](ClO_4)_2$

Both the free ligand L_5 and its Cu(II) complex have been characterized by crystallography. The molecular structures, along with the atomic labelling schemes are shown in Figures 55 and 56, respectively and crystallographic parameters are listed in Table 43. The fractional atomic coordinates, interatomic distances and bond angles of L_5 are shown in Tables 44 - 46, and those of $[Cu(L_5)](ClO_4)_2$ are presented in Tables 47 - 49.

For the free ligand L_5, the interatomic distances between the nitrogen and sulphur donor atoms inside the cavity of the macrocycle are: N(1)...S(1) = 3.011 Å, S(1)...N(2) = 4.511 Å, N(1)...S(2) = 4.099 Å, N(2)...S(2) = 4.737 Å, N(1)...N(2) = 5.762 Å and S(1)...S(2) = 5.905 Å. The average of the C-S bond distance is 1.833 Å, which is similar to that observed in [14]aneS_4[82]. The geometry of the ligand in the solid state suggests that the lone pairs of electrons on the sulphur atoms are exocyclic and the non-bonding electron pairs on all the nitrogen atoms are oriented in different directions such that no two sites may bond to the same metal simultaneously without any conformational changes of the ligand.

In the complex $[Cu(L_5)]^{2+}$, the copper ion is in a distorted square-pyramidal environment (Figure 56). It is coordinated by three nitrogen atoms and two thioether sulphur atoms. There is one nitrogen atom in the macrocycle which is not coordinated. The Cu-N bond distances range from 2.00 to 2.14 Å. The apical Cu-S(1) bond distance is 2.51 Å, which is very close to

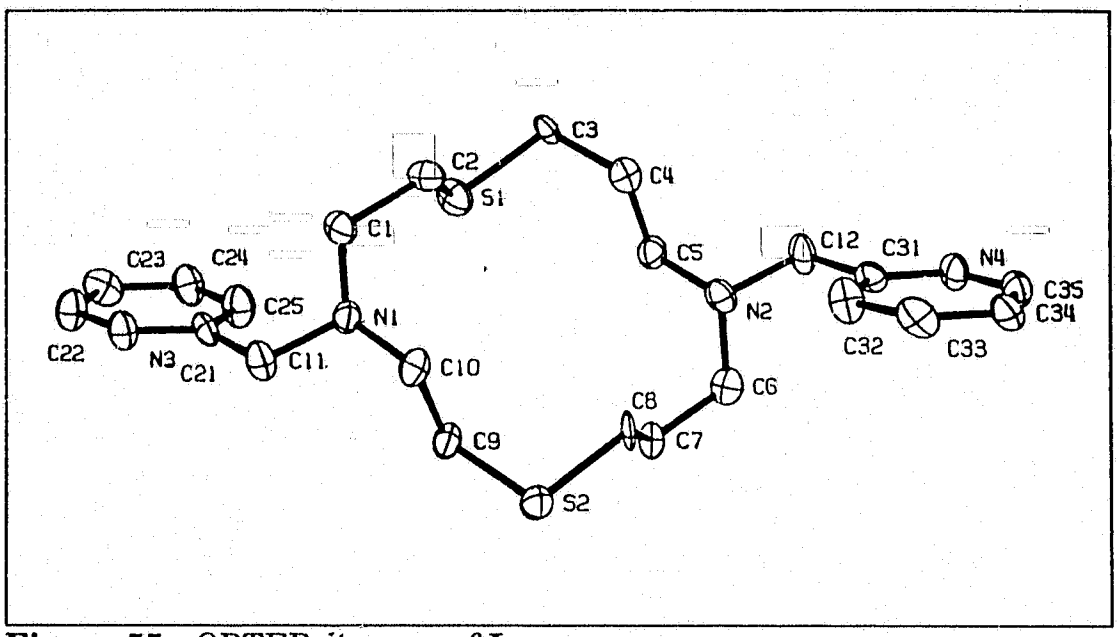

Figure 55 ORTEP diagram of $\mathbf{L_5}$

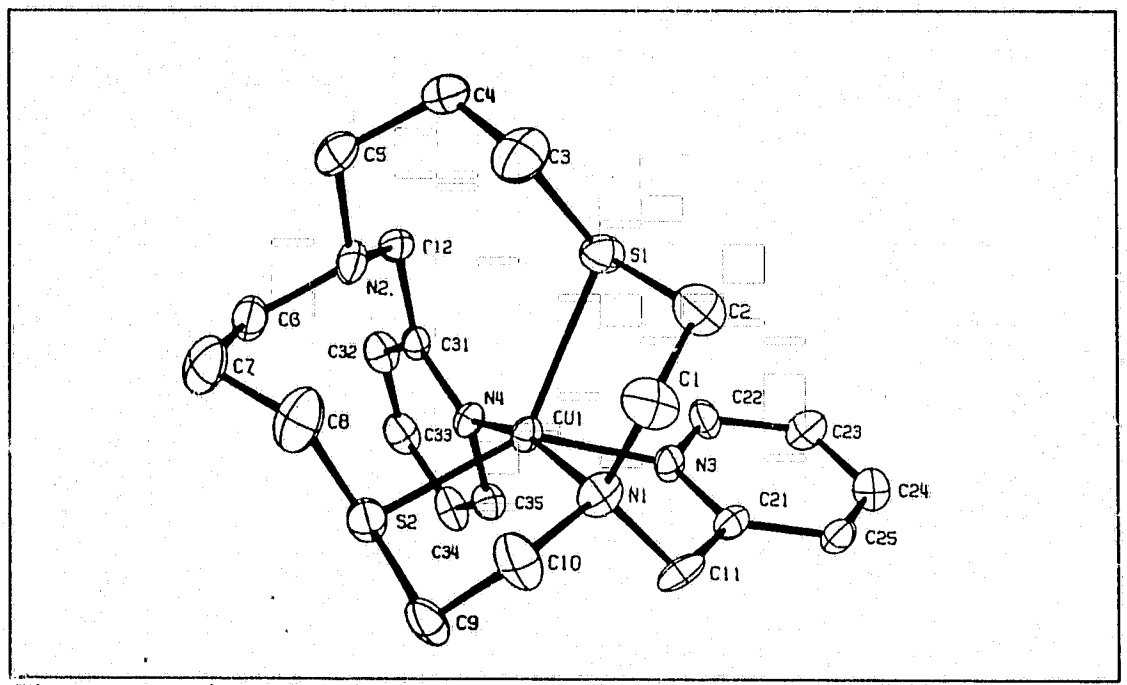

Figure 56 ORTEP diagram of $[Cu(\mathbf{L_5})](ClO_4)_2$. Selected Interatomic distances in Å: Cu-S(1) = 2.511(4); Cu-S(2) = 2.339(4); Cu-N(1) = 2.135(11); Cu-N(3) = 2.066(11); Cu-N(4) = 2.000(11).

the value in $[Cu(bicycloSN_4)]^{2+}$ (2.55 Å)[69]. The basal Cu-S(2) bond distance is 2.34 Å, which is comparable to that observed in $[Cu[14]aneS_4]^{2+}$ (mean Cu-S = 2.30 Å)[103]. A comparison with the interatomic bond distances in $\mathbf{L_5}$ indicates that there is no major change in bond lengths within the macrocycle upon coordination to copper.

From the mean plane calculation (Table 50), the copper ion is 0.258 Å above the plane defined by the basal atoms N(1), N(3) and N(4). In addition, S(2) is 0.9059 Å below this plane. A consequence of the non-planarity between the copper ion and the nitrogen and sulphur donor atoms is that the bond angle S(1)-Cu-S(2) is 130.5°. The copper centre is also 0.326 Å above the plane defined by the pyridyl ring, N(3), C(21), C(22), C(23), C(24) and C(25).

The bond angles in the equatorial plane are: N(4)pyr-Cu-S(2) = 90.2°, N(4)pyr-Cu-N(?) = 91.7°, S(2)-Cu-N(1)pyr = 86.8°, N(1)-Cu-N(3)pyr = 81.7°. The first two values are close to the ideal value of 90° as expected between two donors in the equatorial plane of a square pyramidal structure. The last two values, however, are smaller than the expected value. This probably arises from the strain imposed by the ligand.

Model systems for type I Blue copper protein have appeared in the literature[58,104]. For example, Rorabacher and coworkers[58,104c] have prepared several copper(II)/(I) complexes with polyamino- and polypyridylthioether ligands with N_xS_{4-x} and N_xS_{5-x} as donor sets. They have studied the structural effects of these ligands on the copper(II)/(I) potentials and electron-transfer

kinetics[86,105]. Recent X-ray diffraction studies[106] on plastocyanin (which is an one electron transfer protein containing one type I copper(II) site) indicates that copper is in a pseudo-tetrahedral environment. It is coordinated to two imidazole nitrogen from histidine residues, one thioether sulphur atom from a methionine residue and one thiolate sulphur from a cysteine residue. The mean Cu-N(imidazole) bond distance is 2.07 Å, which is very close to the average Cu-N(pyr) bond distance (2.04 Å) observed in $[Cu(\mathbf{L_5})]^{2+}$. The Cu-S(cyst) bond distance is 2.13 Å and the bond length of Cu-S(methionine) is 2.90 Å. Both of these values are different from the Cu-S bond distances observed in $[Cu(\mathbf{L_5})]^{2+}$ (Cu-S(basal): 2.34 Å; Cu-S(apical): 2.51 Å). Although the coordination geometry around the Cu(II) centre in the complex $[Cu(\mathbf{L_5})]^{2+}$ is a distorted square pyramid and is quite different from the distorted tetrahedral arrangement observed in the active site of the Blue copper protein, it may still be treated as a simple structural model which mimics the primary coordination sphere of the active site of type I copper protein.

Table 43
Experimental crystallographic data for $\mathbf{L_5}$ and $[Cu(\mathbf{L_5})](ClO_4)_2$

Formula:	$C_{22}H_{32}N_4S_2$	$C_{22}H_{32}N_4S_2CuCl_2O_8$
F.W.:	416.64	679.1
Crystal colour:	clear white	emerald green
Crystal system:	monoclinic	monoclinic
Space group:	$P2_1$ (No. 4)	$P2_1/c$ (No. 14)
Cell dimensions:	a = 10.593(4) Å	a = 15.632(1)
	b = 17.195(9) Å	b = 9.753(3)
	c = 6.401(2) Å	c = 18.713(2)
	α = 90°	α = 90°
	β = 97.72(4)°	β = 96.21(1)
	γ = 90°	γ = 90°
V_{cell}:	1155.29 Å^3	2836.2 Å^3
Z:	2 molecules/cell	4 molecules/cell
Temperature:	20 °C	20 °C
Crystal dimensions:	1.051 x .098 x .427 mm^3	.105 x .136 x .546 mm^3
$D_{calc.}$:	1.198	1.590
$D_{meas.}$:	1.208	1.5815
Radiation:	Mo, 0.71069 Å	Cu, 1.542 Å
μ:	2.44 cm^{-1}	44.5 cm^{-1}
Transmission range:	0.893 - 0.927	N/A
Measurement:	2θ(0 - 50°)	2θ(0 - 120)
No. of reflections collected:	2134	3774
No. of reflections $I \geq n\sigma(I)$:	1464 (n = 6)	2197 (n = 6)
No. of parameters:	252	352
No. of standards:	0080, 003, 300	706, 820, 065
Residual electron density:	0.16 e/Å^3	0.3 e/Å^3
Maximum final shift/error:	0.1	0.01
Refinement method:	least squares	least squares
R:	0.0851	0.0938
R_w:	0.0847	0.0936

Table 44
Fractional atomic coordinate and temperature parameters for L_5

Atom	x/a	y/b	z/c	U_{eq}
S(1)	-39522(32)	15710(1)	34057(53)	669(12)
S(2)	-40124(31)	42674(28)	-8931(53)	630(11)
N(1)	-5494(8)	2072(6)	-669(14)	49(3)
N(2)	-991(8)	3065(7)	4732(14)	51(3)
N(3)	-8648(9)	1302(7)	-1969(14)	59(4)
N(4)	2290(9)	4149(7)	5987(14)	56(4)
C(1)	-4899(11)	1319(8)	-732(18)	57(4)
C(2)	-3626(12)	1243(7)	822(18)	56(4)
C(3)	-2371(8)	1389(7)	4906(15)	42(3)
C(4)	-1458(11)	2077(8)	4453(21)	64(5)
C(5)	-1808(10)	2862(7)	5447(20)	54(4)
C(6)	-1584(11)	4257(9)	4806(18)	57(4)
C(7)	-2782(10)	4372(8)	3283(17)	49(4)
C(8)	-2553(8)	4085(7)	906(15)	46(4)
C(9)	-5023(11)	3472(7)	-301(19)	53(4)
C(10)	-4696(11)	2713(7)	-1384(18)	53(4)
C(11)	-6785(10)	2080(9)	-1914(18)	58(4)
C(12)	294(10)	3457(8)	5914(17)	60(4)
C(21)	-7720(9)	1635(8)	-742(16)	50(4)
C(22)	-8677(11)	935(9)	-1107(19)	63(5)
C(23)	-9556(12)	892(10)	1085(23)	73(5)
C(24)	-8544(11)	1236(9)	2374(19)	65(5)
C(25)	-7637(12)	1607(10)	1429(18)	70(5)
C(31)	1295(10)	3850(7)	4803(17)	47(4)
C(32)	1153(12)	3859(10)	2603(19)	66(5)
C(33)	2143(11)	4189(10)	1644(17)	64(5)
C(34)	3189(11)	4508(7)	2857(19)	56(4)
C(35)	3169(11)	4461(7)	5012(20)	56(4)

Estimated standard deviations are given in parentheses. Coordinates x 10^n where n = 5,4,4 for S,N,C
Temperature parameters x 10^n where n = 3,2,2 for S,N,C.
U_{eq} = the equivalent isotropic temperature parameter. $U_{eq} = \frac{1}{3}\Sigma_i\Sigma_j U_{ij} a_i^* a_j^* (a_i.a_j)$.
Primed values indicate that U_{iso} is given. $T = \exp-(8\pi^2 U_{iso} \sin^2\theta/\lambda^2)$

Table 45
Interatomic Distances (Å) for L_5

Atoms	Distance	Atoms	Distance
C(2)-S(1)	1.824(12)	C(4)-C(3)	1.580(16)
C(3)-S(1)	1.842(9)	C(5)-C(4)	1.558(18)
C(8)-S(2)	1.827(9)	C(7)-C(6)	1.506(15)
C(9)-S(2)	1.808(12)	C(8)-C(7)	1.649(14)
C(1)-N(1)	1.444(15)	C(10)-C(9)	1.539(17)
C(10)-N(1)	1.497(14)	C(21)-C(11)	1.526(16)
C(11)-N(1)	1.487(13)	C(31)-C(12)	1.513(15)
C(5)-N(2)	1.463(15)	C(25)-C(21)	1.381(15)
C(6)-N(2)	1.503(16)	C(23)-C(22)	1.403(17)
C(12)-N(2)	1.466(13)	C(24)-C(23)	1.394(18)
C(21)-N(3)	1.306(13)	C(25)-C(24)	1.361(17)
C(22)-N(3)	1.348(14)	C(32)-C(31)	1.396(15)
C(31)-N(4)	1.317(13)	C(33)-C(32)	1.404(17)
C(35)-N(4)	1.304(14)	C(34)-C(33)	1.379(16)
C(2)-C(1)	1.570(16)	C(35)-C(34)	1.385(17)

Estimated standard deviations are given in parentheses.

Table 46
Bond Angles (deg) for L_5

Atoms	Angle	Atoms	Angle
C(3)-S(1)-C(2)	98.6(5)	C(9)-C(10)-N(1)	108.4(9)
C(9)-S(2)-C(8)	102.3(5)	C(21)-C(11)-N(1)	110.0(9)
C(10)-N(1)-C(1)	112.7(8)	C(31)-C(12)-N(2)	114.4(9)
C(11)-N(1)-C(1)	111.5(9)	C(11)-C(21)-N(3)	114.2(9)
C(11)-N(1)-C(10)	110.2(9)	C(25)-C(21)-N(3)	122.0(23)
C(6)-N(2)-C(5)	111.4(8)	C(25)-C(21)-C(11)	123.7(10)
C(12)-N(2)-C(5)	112.3(9)	C(23)-C(22)-N(3)	121.3(11)
C(12)-N(2)-C(6)	110.8(9)	C(24)-C(23)-C(22)	118.5(12)
C(22)-N(3)-C(21)	119.4(10)	C(25)-C(24)-C(23)	117.9(11)
C(35)-N(4)-C(31)	116.9(10)	C(24)-C(25)-C(21)	120.7(12)
C(2)-C(1)-N(1)	113.4(9)	C(12)-C(31)-N(4)	117.4(9)
C(1)-C(2)-S(1)	107.3(8)	C(32)-C(31)-N(4)	123.0(11)
C(4)-C(3)-S(1)	108.2(7)	C(32)-C(31)-C(12)	119.5(10)
C(5)-C(4)-C(3)	112.9(9)	C(33)-C(32)-C(31)	117.4(11)
C(4)-C(5)-N(2)	107.6(9)	C(34)-C(33)-C(32)	120.4(10)
C(7)-C(6)-N(2)	114.7(10)	C(35)-C(34)-C(33)	114.8(10)
C(8)-C(7)-C(6)	110.0(8)	C(34)-C(35)-N(4)	127.5(10)
C(7)-C(8)-S(2)	108.3(7)		
C(10)-C(9)-S(2)	111.9(8)		

Estimated standard deviations are given in parentheses.

Table 47
Fractional atomic coordinate and temperature parameters for $[Cu(L_5)](ClO_4)_2$

Atom	x/a	y/b	z/c	U_{eq}
Cu(1)	26768(12)	2105(19)	3926(10)	372(7)
Cl(1)	43081(31)	42395(41)	17260(22)	610(16)
Cl(2)	7342(37)	12052(54)	35282(27)	778(21)
S(1)	11308(25)	-3786(44)	125(22)	560(15)
S(2)	39153(27)	-11469(45)	4470(22)	594(16)
O(1)	4433(8)	4663(12)	1029(6)	78(5)
O(2)	4118(10)	2838(12)	1755(7)	100(6)
O(3)	5024(15)	4508(23)	2178(9)	222(13)
O(4)	3615(14)	4920(18)	1919(13)	203(13)
O(5)	364(13)	741(21)	4092(9)	192(11)
O(6)	579(16)	501(22)	2918(8)	202(12)
O(7)	1615(19)	906(31)	3624(15)	240(18)
O(8)	875(16)	2551(19)	3527(10)	189(13)
N(1)	2459(8)	-669(12)	1402(6)	54(5)
N(2)	2537(8)	-1300(11)	-1059(7)	50(5)
N(3)	2169(7)	1919(12)	845(6)	41(4)
N(4)	3103(7)	1336(11)	-389(6)	38(4)
C(1)	1595(11)	-1325(20)	1393(11)	80(8)
C(2)	870(11)	-613(21)	940(9)	80(8)
C(3)	881(13)	-2117(19)	-370(12)	91(9)
C(4)	941(11)	-2049(19)	-1173(11)	74(8)
C(5)	1874(11)	-2332(16)	-1366(11)	75(8)
C(6)	3407(10)	-1757(17)	-1156(9)	61(7)
C(7)	3719(13)	-2987(17)	-661(10)	81(8)
C(8)	3480(13)	-2818(16)	110(11)	85(9)
C(9)	4055(10)	-1392(22)	1413(9)	78(8)
C(10)	3140(11)	-1732(17)	1657(10)	71(7)
C(11)	2572(11)	569(16)	1899(7)	58(6)
C(12)	2344(9)	41(14)	-1414(7)	45(5)
C(21)	2135(9)	1801(15)	1547(8)	46(6)
C(22)	1787(9)	2972(16)	480(8)	49(6)
C(23)	1326(11)	3972(16)	830(10)	62(7)
C(24)	1293(10)	3839(18)	1567(10)	62(7)
C(25)	1684(10)	2777(17)	1929(8)	52(6)
C(31)	2952(8)	1155(13)	-1114(7)	35(5)
C(32)	3355(9)	1994(15)	-1583(8)	50(6)
C(33)	3888(10)	3046(17)	-1314(10)	57(7)
C(34)	4050(9)	3240(15)	-583(10)	52(6)
C(35)	3622(9)	2366(13)	-127(8)	41(5)

Estimated standard deviations are given in parentheses. Coordinates x 10^n where n = 5,5,5,4,4,4 for Cu,Cl,S,O,N,C. Temperature parameters x 10^n where n = 3,3,3,3,2,2 for Cu,Cl,S,O,N,C.
U_{eq} = the equivalent isotropic temperature parameter. $U_{eq} = \frac{1}{3}\Sigma_i\Sigma_j U_{ij} a_i^* a_j^* (a_i.a_j)$. Primed values indicate that U_{iso} is given. $T = \exp(-8\pi^2 U_{iso} \sin^2\theta/\lambda^2)$

Table 48
Interatomic Distances (Å) for $[Cu(L_6)](ClO_4)_2$

Atoms	Distance	Atoms	Distance
S(1)-Cu(1)	2.511(4)	C(12)-N(2)	1.483(17)
S(2)-Cu(1)	2.330(4)	C(21)-N(3)	1.326(17)
N(1)-Cu(1)	2.135(11)	C(22)-N(3)	1.337(17)
N(3)-Cu(1)	2.066(11)	C(31)-N(4)	1.364(16)
N(4)-Cu(1)	2.000(11)	C(35)-N(4)	1.349(16)
O(1)-Cl(1)	1.402(11)	C(2)-C(1)	1.509(23)
O(2)-Cl(1)	1.401(12)	C(4)-C(3)	1.518(26)
O(3)-Cl(1)	1.354(15)	C(5)-C(4)	1.564(23)
O(4)-Cl(1)	1.352(14)	C(7)-C(6)	1.562(22)
O(5)-Cl(2)	1.337(14)	C(8)-C(7)	1.538(26)
O(6)-Cl(2)	1.332(16)	C(10)-C(9)	1.582(23)
O(7)-Cl(2)	1.400(27)	C(21)-C(11)	1.499(20)
O(8)-Cl(2)	1.330(17)	C(31)-C(12)	1.511(18)
C(2)-S(1)	1.839(17)	C(25)-C(21)	1.422(19)
C(3)-S(1)	1.865(18)	C(23)-C(22)	1.415(20)
C(8)-S(2)	1.850(18)	C(24)-C(23)	1.393(22)
C(9)-S(2)	1.814(17)	C(25)-C(24)	1.347(21)
C(1)-N(1)	1.493(20)	C(32)-C(31)	1.397(18)
C(10)-N(1)	1.526(18)	C(33)-C(32)	1.382(21)
C(11)-N(1)	1.522(19)	C(34)-C(33)	1.377(22)
C(5)-N(2)	1.512(19)	C(35)-C(34)	1.423(20)
C(6)-N(2)	1.460(18)		

Estimated standard deviations are given in parentheses.

Table 49
Bond Angles (deg) for $[Cu(L_5)](ClO_4)_2$

Atoms	Angle	Atoms	Angle
S(2)-Cu(1)-S(1)	130.5(2)	C(12)-N(2)-C(5)	108.6(12)
N(1)-Cu(1)-S(1)	85.3(4)	C(12)-N(2)-C(6)	111.1(12)
N(1)-Cu(1)-S(2)	86.8(4)	C(21)-N(3)-Cu(1)	113.2(9)
N(3)-Cu(1)-S(1)	84.3(3)	C(22)-N(3)-Cu(1)	125.5(10)
N(3)-Cu(1)-S(2)	142.3(3)	C(22)-N(3)-C(21)	120.6(13)
N(3)-Cu(1)-N(1)	81.7(5)	C(31)-N(4)-Cu(1)	128.4(9)
N(4)-Cu(1)-S(1)	107.8(3)	C(35)-N(4)-Cu(1)	112.2(9)
N(4)-Cu(1)-S(2)	90.2(3)	C(35)-N(4)-C(31)	119.3(12)
N(4)-Cu(1)-N(1)	164.8(5)	C(2)-C(1)-N(1)	115.6(14)
N(4)-Cu(1)-N(3)	91.7(4)	C(1)-C(2)-S(1)	111.0(13)
O(2)-Cl(1)-O(1)	112.0(8)	C(4)-C(3)-S(1)	107.9(13)
O(3)-Cl(1)-O(1)	109.6(10)	C(5)-C(4)-C(3)	112.3(17)
O(3)-Cl(1)-O(2)	109.2(11)	C(4)-C(5)-N(2)	114.4(13)
O(4)-Cl(1)-O(1)	107.4(10)	C(7)-C(6)-N(2)	113.3(14)
O(4)-Cl(1)-O(2)	106.8(11)	C(8)-C(7)-C(6)	112.5(13)
O(4)-Cl(1)-O(3)	111.8(17)	C(7)-C(8)-S(2)	107.2(13)
O(6)-Cl(1)-O(5)	116.6(10)	C(10)-C(9)-S(2)	107.4(11)
O(7)-Cl(2)-O(5)	109.4(16)	C(9)-C(10)-N(1)	112.9(13)
O(7)-Cl(2)-O(6)	95.1(17)	C(21)-C(11)-N(1)	110.5(11)
O(8)-Cl(2)-O(5)	114.9(11)	C(31)-C(12)-N(2)	112.3(11)
O(8)-Cl(2)-O(6)	121.5(12)	C(11)-C(21)-N(3)	116.1(13)
O(8)-Cl(2)-O(7)	92.6(15)	C(25)-C(21)-N(3)	121.0(14)
C(2)-S(1)-Cu(1)	93.8(6)	C(25)-C(21)-C(11)	122.9(14)
C(3)-S(1)-Cu(1)	118.2(7)	C(23)-C(22)-N(3)	121.0(14)
C(3)-S(1)-C(2)	101.0(10)	C(24)-C(23)-C(22)	118.0(15)
C(8)-S(2)-Cu(1)	102.2(6)	C(25)-C(24)-C(23)	120.4(16)
C(9)-S(2)-Cu(1)	97.3(5)	C(24)-C(25)-C(21)	119.0(15)
C(9)-S(2)-C(8)	102.9(10)	C(12)-C(31)-N(4)	119.7(12)
C(1)-N(1)-Cu(1)	113.2(10)	C(32)-C(31)-N(4)	120.5(13)
C(10)-N(1)-Cu(1)	112.1(10)	C(32)-C(31)-C(12)	119.8(13)
C(10)-N(1)-C(1)	108.2(12)	C(33)-C(32)-C(31)	120.1(15)
C(11)-N(1)-Cu(1)	101.7(8)	C(34)-C(33)-C(32)	120.1(15)
C(11)-N(1)-C(1)	113.1(13)	C(35)-C(34)-C(33)	117.7(15)
C(11)-N(1)-C(10)	108.5(12)	C(34)-C(35)-N(4)	122.1(14)
C(6)-N(2)-C(5)	111.0(12)		

Estimated standard deviations are given in parentheses.

Table 50
Mean plane for $[Cu(L_5)](ClO_4)_2$

(a) The equation of the plane containing the atoms in the first pyridine moiety is:
-0.8219X - 0.5421Y - 0.1749Z + 3.9389 = 0

Atoms	X	Y	Z	P
N(3)	3.2203	1.8720	1.5720	0.0024
C(21)	3.0241	1.7561	2.8781	-0.0020
C(22)	2.6962	2.8983	0.8933	-0.0045
C(23)	1.9045	3.8740	1.5435	0.0036
C(24)	1.7038	3.7443	2.9159	-0.0011
C(25)	2.2422	2.7083	3.5880	0.0004
Cu(1)	4.1049	0.2053	0.7304	0.3259

(b) The equation of the plane containig atoms N(1), N(3) and N(4) is:
-0.7965X - 0.3180Y - 0.5143Z + 3.9687 = 0

Atoms	X	Y	Z	P
N(1)	3.5594	-0.6521	2.6076	0.0000
N(3)	3.2203	1.8720	1.5720	0.0000
N(4)	4.9295	1.3033	-0.7233	0.0000
Cu(1)	4.1049	0.2053	0.7304	0.2583
S(2)	6.0299	-1.1186	0.8316	-0.9059

where P is the perpendicular distance between the atom and the mean plane, given in Å.

4.4 ESR Spectroscopy

The ESR spectral data for various Cu(II) and Co(II) complexes studied in this work are listed in Table 51. For the complexes $[Cu(\mathbf{L_2})]^{2+}$ and $[Cu(\mathbf{L_3})]^{2+}$, the ESR spectra (Figures 57 and 58) show characteristics of a d^9 ion in a tetragonal elongated environment[59], with $g_{\parallel} \geq g_{\perp}$. Four hyperfine lines are also observed in the $g_{\parallel}$ region, with the coupling constants ranging from 115 - 125 G. The coupling observed is due to the interaction of the unpaired electron with the nuclear spin of the copper nucleus ($^{63,65}Cu$, I = 3/2).

Table 51
ESR data for the Cu(II) complexes of $\mathbf{L_2}$ - $\mathbf{L_5}$ and the Co(II) complex of $\mathbf{L_4}$ at 77 K

Complex	$g_{\parallel}$ ($A_{\parallel}$ in Gauss)	$g_{\perp}$
$[Cu(\mathbf{L_2})]^{2+}$	2.467 (115)	2.121
$[Cu(\mathbf{L_3})]^{2+}$	2.167 (125)	1.983
$[Cu(\mathbf{L_4})]^{2+}$	2.070[a]	---
$[Cu(\mathbf{L_5})]^{2+}$	2.100[a]	---
$[Co(\mathbf{L_4})(NO_3)_2(CH_3CN)]$	ESR silent	---
$[Co(\mathbf{L_4})(ClO_4)]^+$	2.020 (75)	2.290

[a] g_{iso} value is given.

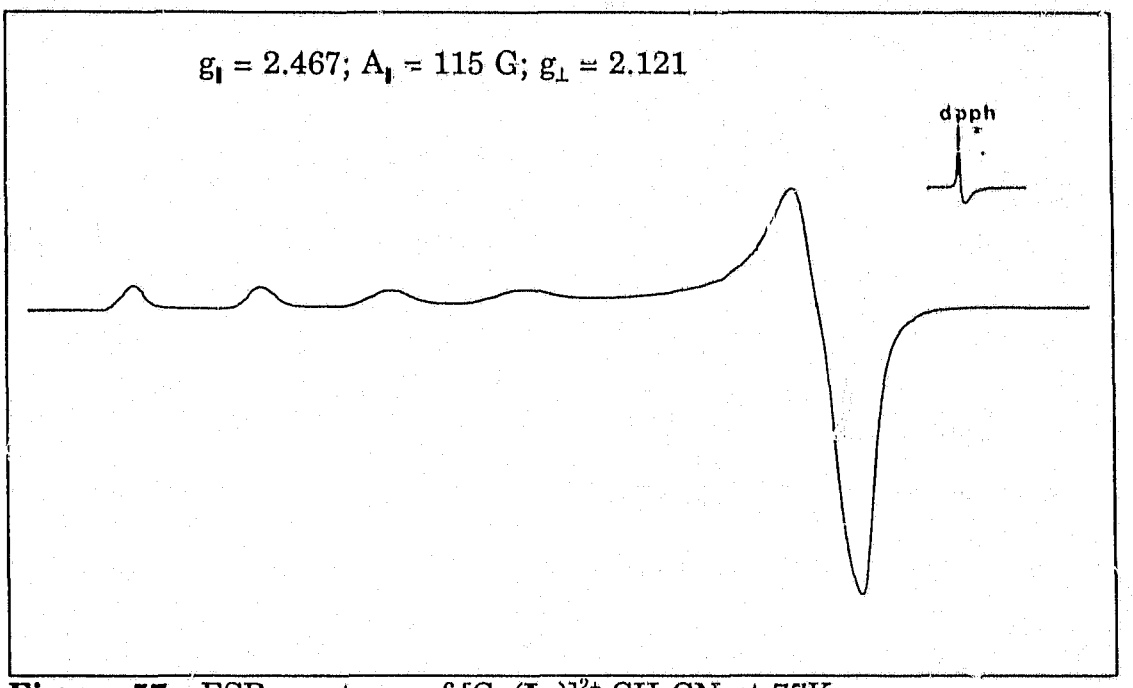

Figure 57 ESR spectrum of $[Cu(\mathbf{L}_2)]^{2+}$ CH_3CN at 77K.

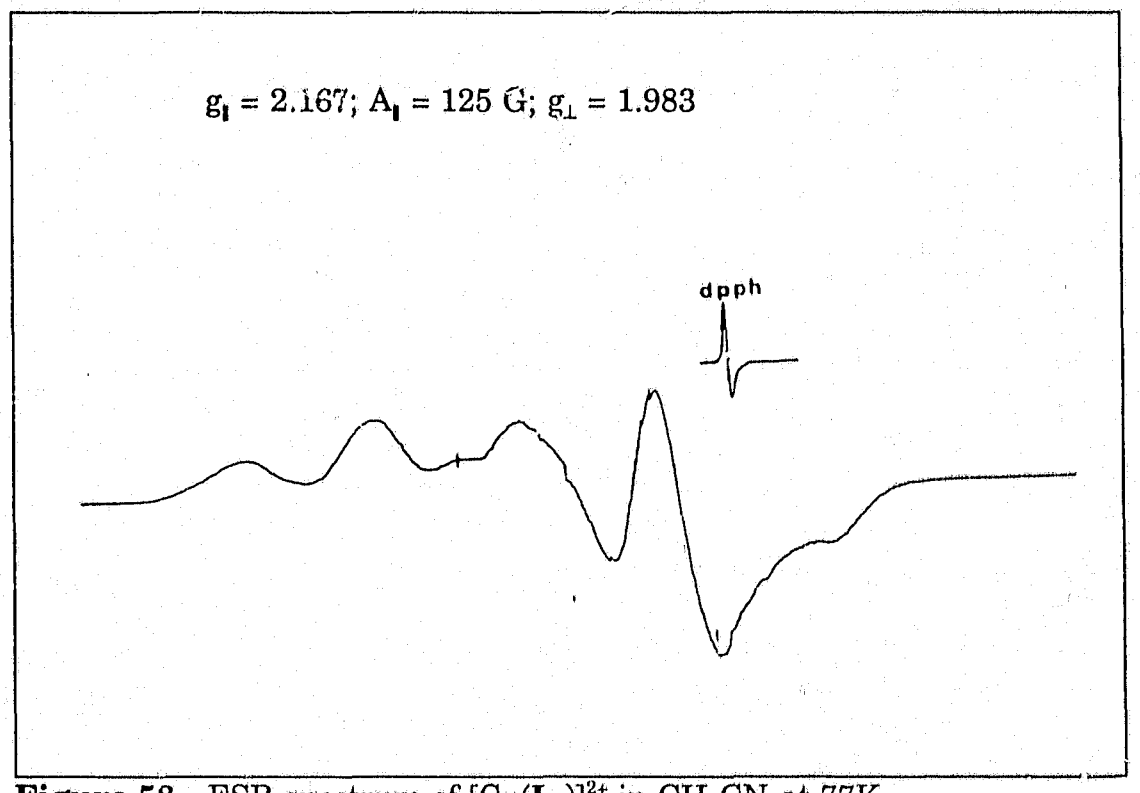

Figure 58 ESR spectrum of $[Cu(\mathbf{L}_3)]^{2+}$ in CH_3CN at 77K.

The $g_{\parallel}$ value of $[Cu(\mathbf{L}_2)]^{2+}$ is greater than $[Cu(cyclam)]^{2+}$ ($g_{\parallel}$ = 2.194, $A_{\parallel}$ = 206 G)[107], $[Cu([14]aneS_4)]^{2+}$ ($g_{\parallel}$ = 2.10; $A_{\parallel}$ = 165 G) and also other Cu(II) N_2S_2 complexes prepared by Kaden et al[57e]. The $g_{\parallel}$ value for $[Cu(\mathbf{L}_3)]^{2+}$, on the other hand, is very similar to a structurally related Cu(II) complex, $[Cu(\mathbf{34})]^{2+}$ ($g_{\parallel}$ = 2.162, $A_{\parallel}$ = 161 G)[57e]. However, the coupling constants $A_{\parallel}$ in these Cu(II) complexes are greater than those observed in type I Blue Copper protein (35 - 90 G)[58].

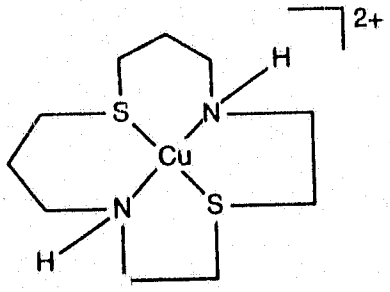

$g_{\parallel}$ = 2.162

$A_{\parallel}$ = 161 G

$[Cu(\mathbf{34})]^{2+}$

Isotropic ESR spectra were obtained for the copper(II) complexes with pyridine pendant arms, $[Cu(\mathbf{L}_4)]^{2+}$ and $[Cu(\mathbf{L}_5)]^{2+}$ (Figures 59 and 60) even at 77K. Such ESR spectra are very different from that of a typical Cu(II) complex. The isotropic ESR signal spans a range of 500 G and no hyperfine coupling with the copper nucleus was observed. It is unlikely that the unpaired electron is organic-based, due to the broadness of the observed ESR

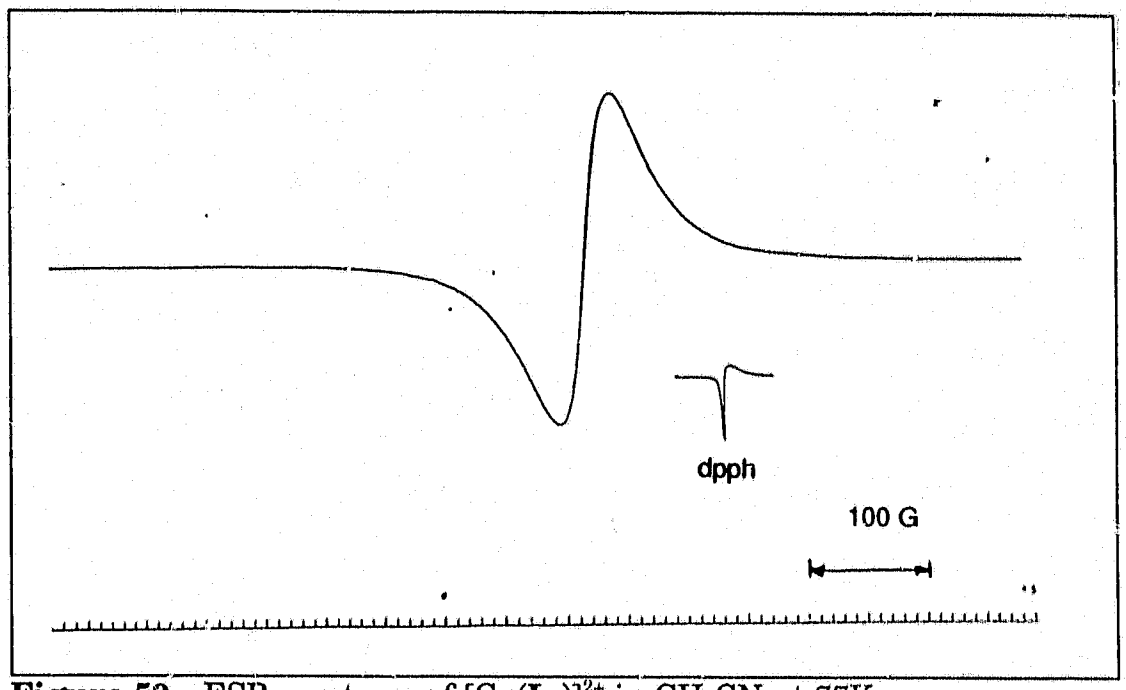

Figure 59 ESR spectrum of $[Cu(L_4)]^{2+}$ in CH_3CN at 77K.

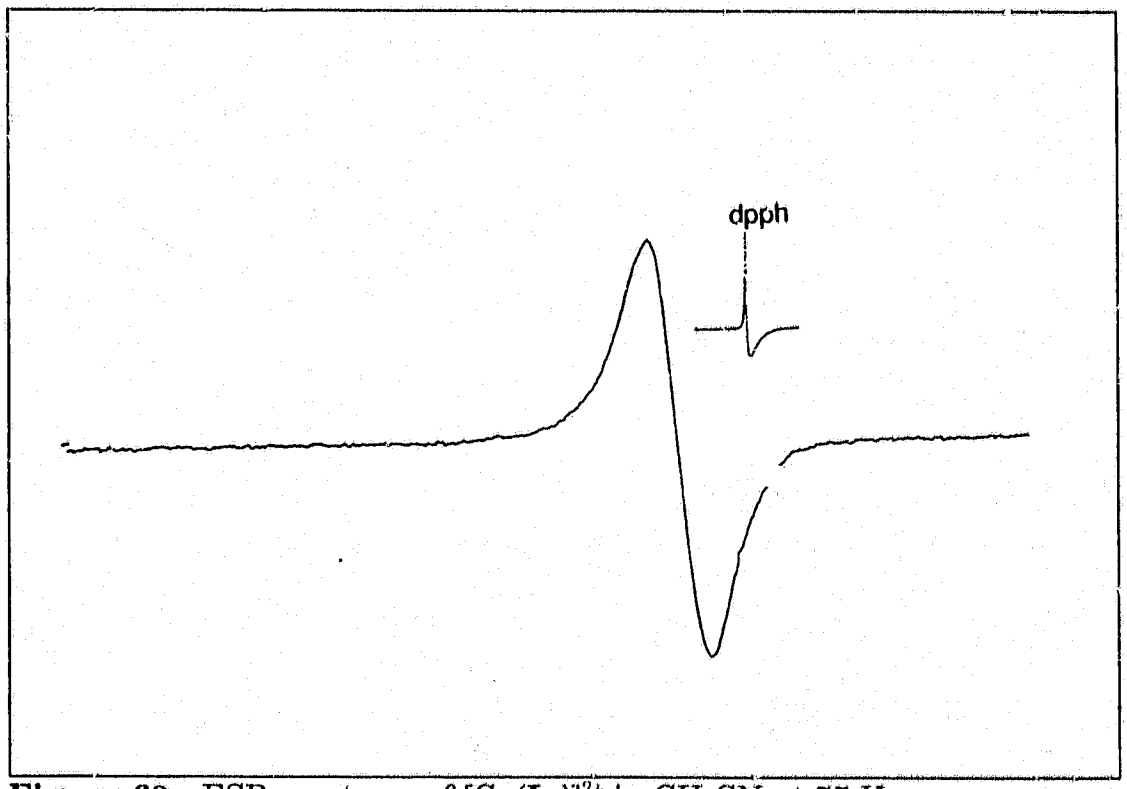

Figure 60 ESR spectrum of $[Cu(L_5)]^{2+}$ in CH_3CN at 77 K.

signal and the lack of hyperfine couplings to the nitrogen atoms in the pyridine moiety and also the tertiary amine. A possible explanation for the abnormal ESR spectra observed is that the five coordinate geometry in $[Cu(\mathbf{L_5})]^{2+}$ is flexible. In view of the crystal structure of $[Cu(\mathbf{L_5})]^{2+}$ shown in Figure 56, the possibility exists that there is an exchange between the Cu-coordinated nitrogen atom from the pyridine and the uncoordinated nitrogen atom from the tertiary amine even at 77 K. Although the crystal structure of $[Cu(\mathbf{L_4})]^{2+}$ is not available currently, a five coordinate geometry is anticipated and certain fluxional processes may be present.

For the Co(II) complexes of $\mathbf{L_4}$, only Compound B, $[Co(\mathbf{L_4})(ClO_4)]^+$, is ESR active. The ESR spectrum at 77K (Figure 61) exhibits characteristics of a low spin d^7 ion in a distorted octahedral environment[14], with $g_{\parallel} = 2.020$ and $g_{\perp} = 2.290$. This is consistent with a Co(II) ion being coordinated to the nitrogen and sulphur donor atoms from the ligand $\mathbf{L_4}$ and perchlorate ion in a tetragonal elongated geometry. Since no hyperfine coupling from the nitrogen atoms was observed in the ESR spectrum of $[Co(\mathbf{L_4})ClO_4)]^+$, the tertiary amine and pyridine moiety from the ligand are most likely to be coordinated in the equatorial plane of the distorted octahedron. The eight hyperfine lines observed in the $g_{\parallel}$ region arises from the interaction of the unpaired electron with the Co nucleus (^{59}Co, I = 7/2).

For Compound A, $[Co(L_4)(NO_3)_2(CH_3CN)]$, no ESR signal was detected. Instead, a paramagnetic ^1H NMR spectrum spanning from -30 to + 50 ppm was obtained, which arises from the presence of an unpaired electron in the d^7 Co(II) ion. This is consistent with the persistence of the crystalline structure (Figure 54) in solution although the paramagnetic spectrum shown in Figure 62 is not amenable to further analysis.

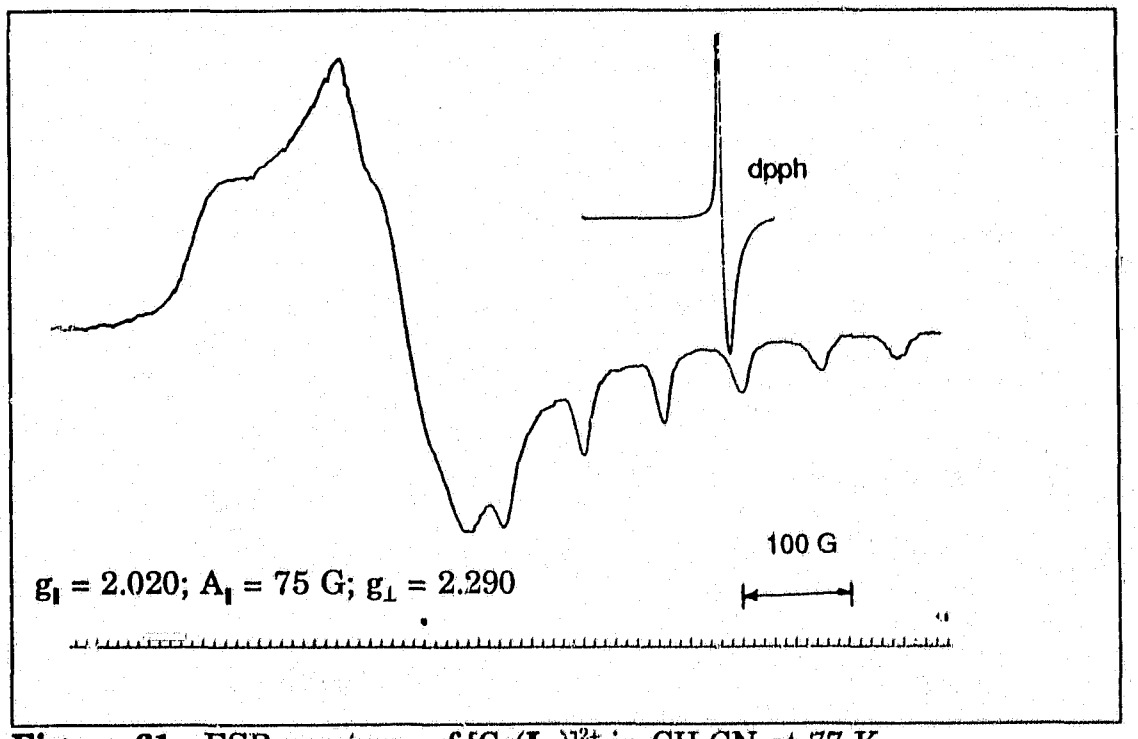

Figure 61 ESR spectrum of $[Co(L_4)]^{2+}$ in CH_3CN at 77 K.

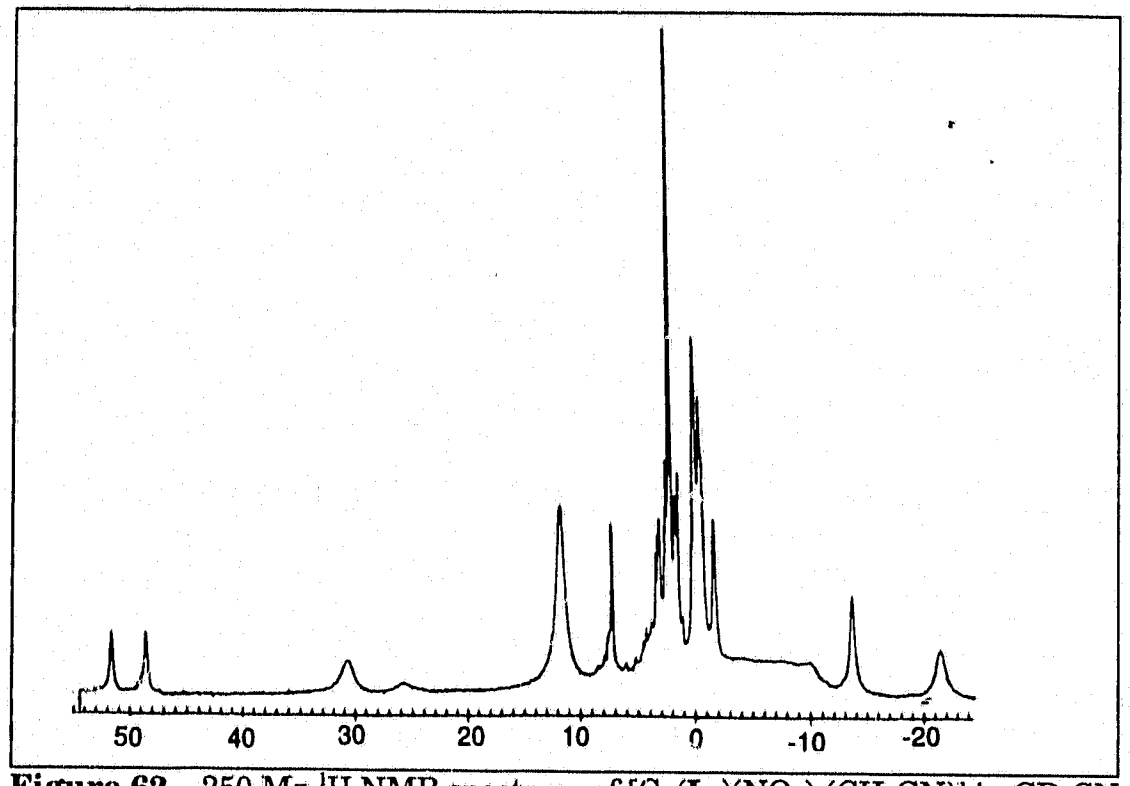

Figure 62 250 Mz ^{1}H NMR spectrum of $[Co(L_4)(NO_3)_2(CH_3CN)]$ in CD_3CN at room temperature.

4.5 UV/Vis Spectroscopy

The UV/Vis spectal data for various Ni(II), Cu(II) and Co(II) complexes studied in this work are presented in Table 52. The absorption spectra of all the Ni(II) complexes are typical of octahedral geometry[1], indicating that solvent molecules are coordinated in the axial positions. The three absorption bands observed in the visible region are assigned[1,101] to the following d-d transitions: $^3A_{2g} \rightarrow {}^3T_{2g}$ (820 - 900 nm); $^3A_{2g} \rightarrow {}^3T_{1g}(F)$ (556 - 578 nm); $^3A_{2g} \rightarrow {}^3T_{1g}(P)$ (373 nm). The molar extinction coefficients ε for these complexes are very similar to the analogous Ni(II) complex **34** reported in the literature[57f]. Their values ranges from 20 - 40 $M^{-1}cm^{-1}$, which are in the low end for octahedral complexes (1 -100) of the first transition series[101].

The Cu(II) complexes are green in acetonitrile and their UV/Vis spectra show absorptions bands around 324 - 380 nm and 704 - 760 nm. These are assigned as the S $\rightarrow$ Cu^{2+} ligand to metal charge transfer (LMCT) and d-d transitions, respectively, after comparing with similar Cu(II)N_2S_2 complexes reported by Kaden and coworkers[57f].

The absorption spectra of Type I copper proteins[58] are characterized by an intensive absorption band around 600 nm with molar extinction coefficient in the range of 3000 - 5000 $M^{-1}cm^{-1}$. In the active site, the copper(II) ion is in a pseudo-tetrahedral environment, with two imidazole nitrogen from histidine residues and one thioether sulphur from a methionine residue and one thiolate sulphur from a cysteine as ligands[106]. Although the Cu(II) complexes found for

Table 52
UV/Vis Spectra Data for Transition Metal Complexes Derived from L_2 -L_5 in acetonitrile.

Complex	Anion	λ_{max} [nm](ε_{max} in $M^{-1}cm^{-1}$)
$[Ni(L_2)]^{2+}$	PF_6^-	282 (1700) 373 (38) 578 (23) 900 (31)
$[Ni(L_4)]^{2+}$	PF_6^-	282 (4870) 556 (28) 820 (24)
$[Cu(L_2)]^{2+}$	PF_6^-	278 (2100) 368 (4500) 750 (430)
$[Cu(L_4)]^{2+}$	ClO_4^-	380 (5610) 704 (540) 871 (570)
$[Cu(L_5)]^{2+}$	ClO_4^-	356 (3020) 737 (390)
$[Co(L_4)(NO_3)_2(CH_3CN)]$ (Compound A)	---	261 (4410) 531 (32)
$[Co(L_4)(ClO_4)]^+$ (Compound B)	ClO_4^-	500 (396)[a] 800 (153)

[a] the spectrum was recorded in nitromethane.

this study have a similar coordination environment as the type I copper protein, no intense absorption band around 600 nm was observed. Therefore they can be treated as static or structural models only.

The absorption spectra of the two isomers of the Co(II) complexes of L_4 show slightly different characteristics. Although both isomers have an absorption band around 500 nm, Compound B has a slightly larger extinction coefficient. In addition, it has an additional absorption band at 800 nm. These observations can be rationalized by the different coordination environment at the cobalt centre in the two species. The ESR spectrum of Compound B at 77K (Figure 61) is typical of a low spin d^7 ion in a tetragonal elongated environment. This is consistent with a Co(II) ion being coordinated to all of the donor atoms in L_4 with weak interaction with a perchlorate ion in the axial position. For Compound A, the macrocyclic ligand L_4 does not encircle the cobalt ion as shown by the crystal structure (Figure 54), instead the metal centre is coordinated to three oxygen atoms from two nitrate groups and three nitrogen atoms (one from acetonitrile and two from L_4).

4.6 Electrochemistry

The redox chemistry of the Cu(II), Ni(II) and Co(II) complexes of $\mathbf{L_2}$ - $\mathbf{L_5}$ was studied by cyclic voltammetry. The results are summarized in Table 53. For the Cu(II) complexes, the reduction to Cu(I) is reversible and the CV of $[Cu(\mathbf{L_5})]^{2+}$ in CH_3CN was shown in Figure 63 as an example. Since Cu(II) complexes prefer a tetragonal distorted geometry whereas Cu(I) complexes prefer tetrahedral coordination, rearrangement of the structure of the complexes is required when Cu(II) is reduced to Cu(I). This may account for the value of ΔE being greater than the theoretical value of 59 mV for a reversible one-electron reduction[108].

Both the cyclic voltammograms of $[Ni(\mathbf{L_2})]^{2+}$ and $[Ni(\mathbf{L_4})]^{2+}$ show irreversible reduction waves to Ni(I) at -1.18 and -1.29 V vs Fc/Fc^+, respectively. However, for the complex $[Ni(\mathbf{L_5})]^{2+}$, a reversible reduction from Ni(II) to Ni(I) is observed (Figure 64). The peak potentials were separated by 0.14 V. This may be accounted for by the occurrence of some reorganization since Ni(I) which is a d^9 ion, is subjected to Jahn-Teller distortion and a tetragonal geometry is preferred.

For the complex $[Co(\mathbf{L_4})(ClO_4)]^+$ (Compound B), a quasi-reversible oxidation to Co(III) was observed at $E_{1/2}$ = 0.18 V vs Fc/Fc^+. The peak to peak separation is 0.23 V. This redox couple for Co(II) to Co(III) occurs at a more positive value relative to other thioether complexes such as $[Co([9]aneS_3)]^{2+}$ (0.02 V vs Fc/Fc^+)[109] and $[Co([10]aneS_3)_2]^{2+}$ (0.01 V vs Fc/Fc^+)[110].

Table 53
Electrochemical data for the Ni(II), Cu(II) and Co(II) complexes studied in this work.

Complex	E vs Fc/Fc^+ (V)	ΔE (V)
Cu(II) to Cu(I):		
$[Cu(L_2)]^{2+}$	$E_{½} = -0.045$	0.150
$[Cu(L_4)]^{2+}$	$E_{½} = -0.024$	0.077
$[Cu(L_5)]^{2+}$	$E_{½} = -0.137$	0.086
Ni(II) to Ni(I):		
$[Ni(L_2)]^{2+}$	$E_{red} = -1.18$	a
$[Ni(L_4)]^{2+}$	$E_{red} = -1.29$	a
$[Ni(L_5)]^{2+}$	$E_{½} = -1.16$	0.14
Co(II) to Co(III):		
$[Co(L_4)]^{2+}$ (Compound B)	$E_{½} = 0.18$	0.23
$[Co(L_4)(NO_3)_2(CH_3CN)]$ (Compound A)	$E_{red} = -1.83$	a
	$E_{ox} = 1.71$	b

[a] irreversible reduction
[b] irreversible oxidation

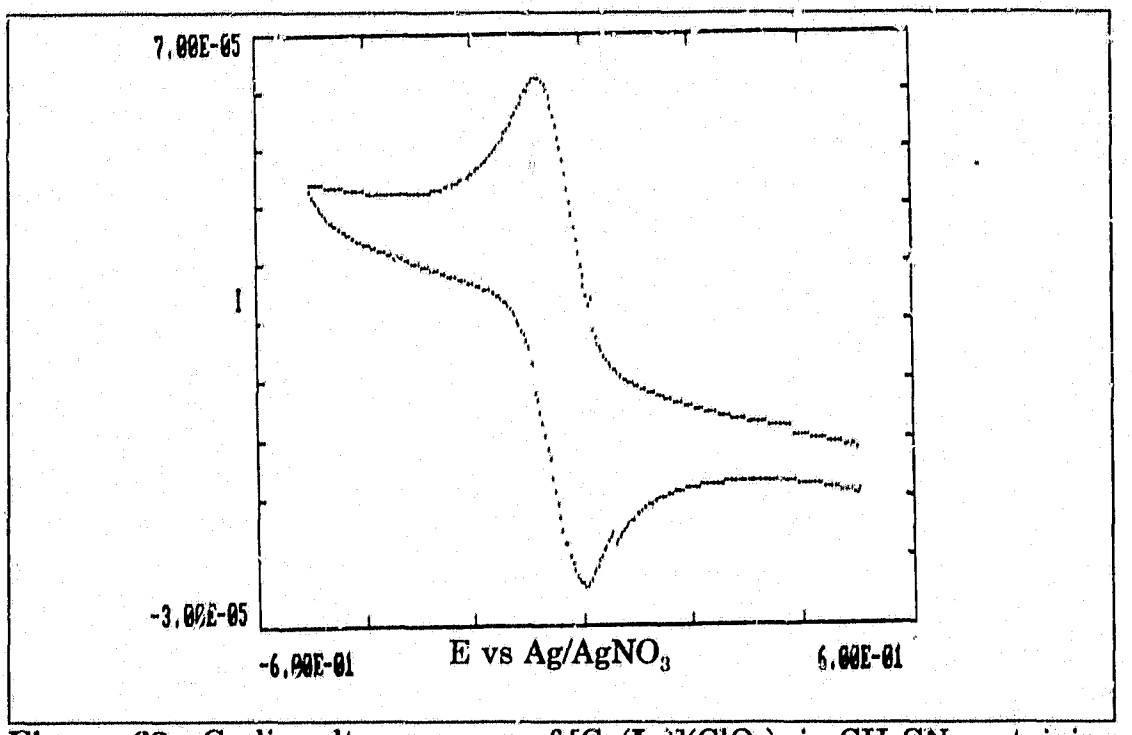

Figure 63 Cyclic voltammagram of $[Cu(L_6)](ClO_4)_2$ in CH_3CN containing 0.1 M Bu_4NPF_6. Fc/Fc^+ occurs at 0.09 V.

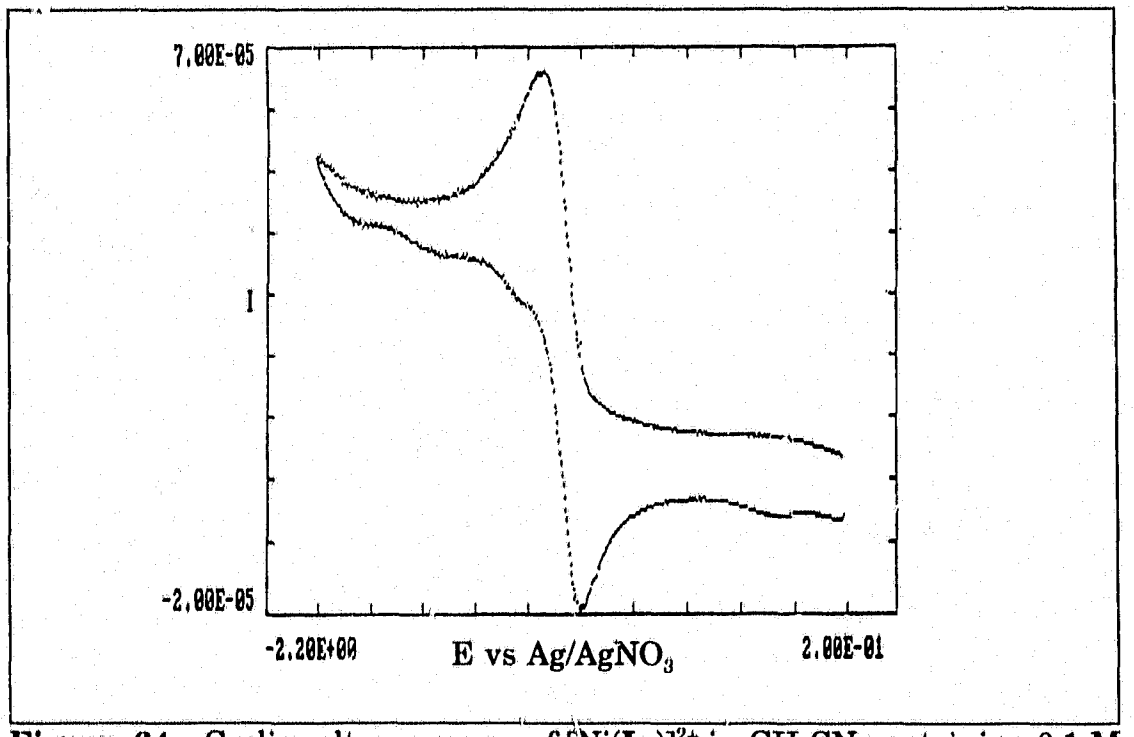

Figure 64 Cyclic voltammogram of $[Ni(L_6)]^{2+}$ in CH_3CN containing 0.1 M Bu_4NPF_6. Fc/Fc^+ occurs at 0.09 V.

For the complex $[Co(L_4)(NO_3)_2(CH_3CN)]$ (Compound A), an irreversible reduction wave was observed at -1.83 V vs Fc/Fc^+ and an irreversible oxidation wave was observed at 1.71 V vs Fc/Fc^+. These redox potentials are higher than the Co(II) to Co(I) and Co(II) to Co(III) couples observed in Co(II) thioether complexes[109,110] and may suggest the reaction is ligand based.

An attempt to synthesize a trinuclear Co(II) complex was made by the reaction of two equivalents of Compound A with an equivalent of $[Co(H_2O)_6](NO_3)_2$ (eq. 9). A preliminary study of the pink crystals obtained from this reaction by CV shows two quasi-reversible waves at 0.26 V vs Fc/Fc^+ (ΔE = 0.22 V) and 0.80 V vs Fc/Fc^+ (ΔE = 0.15 V) in addition to an irreversible oxidation at 1.67 V vs Fc/Fc^+ and an irreversible reduction at -1.98 V vs Fc/Fc^+ (Figure 65). The quasi-reversible waves observed may be due to the Co(II)/Co(I) and Co(II)/Co(III) redox couple in the central $[Co^{II}S_6]$ of the trinuclear Co(II) complex. However, more extensive characterization of the pink crystals is required before any definite conclusion can be made.

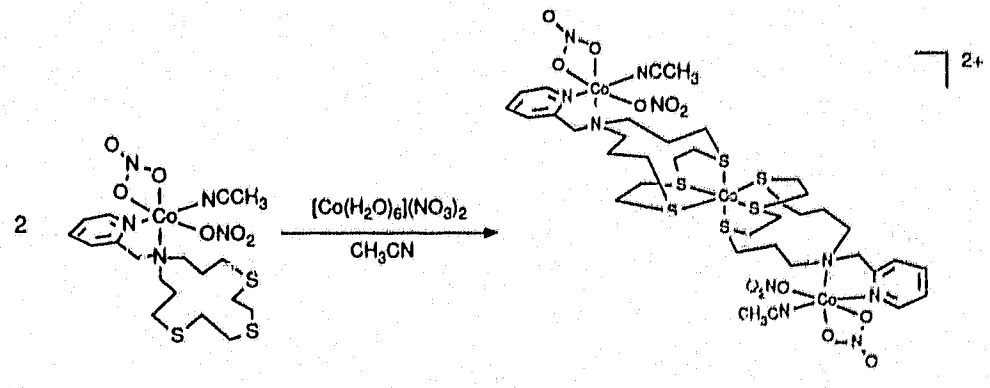

(9)

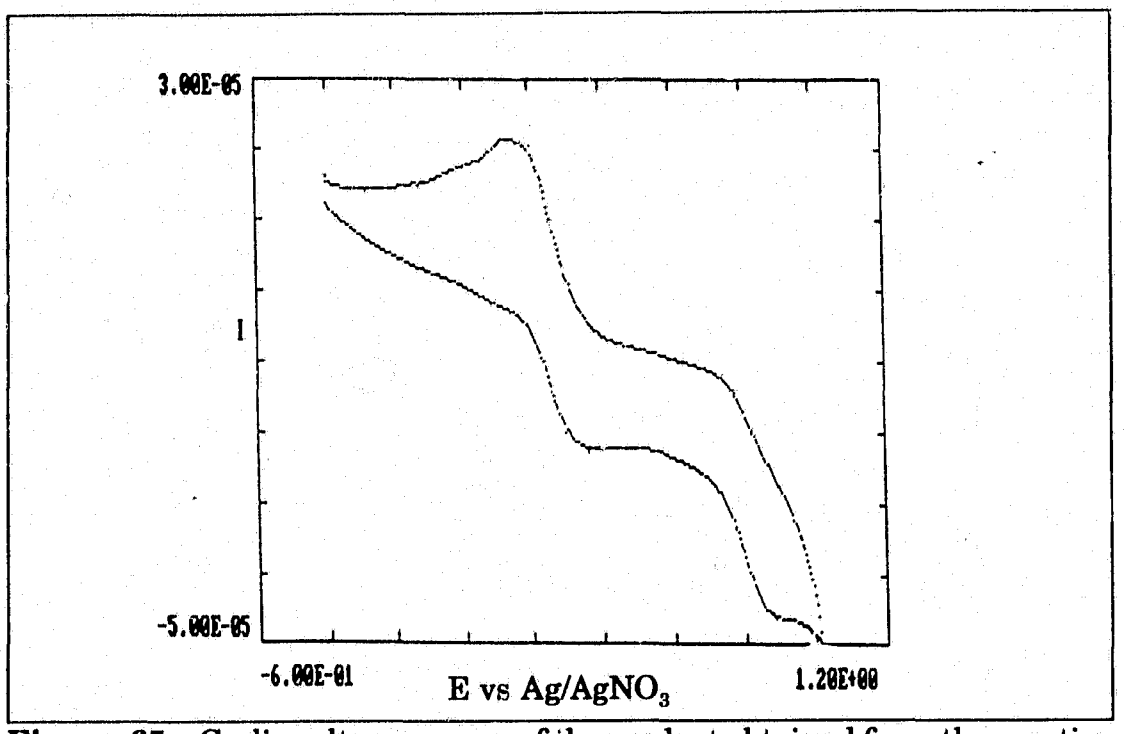

Figure 65 Cyclic voltammogram of the product obtained from the reaction of two equivalents of Compound A with an equivalent of $[Co(H_20)_6](NO_3)_2$ in CH_3CN.

4.7 Conclusion

The Ni(II) complex of $\mathbf{L_4}$ had been synthesized and its solid state structure characterized by X-ray crystallography. In this complex, the nickel centre is in an pseudo-octahedral environment, coordinated to three nitrogen atoms (two from the ligand and one from acetonitrile) and three thioether sulphur atoms. The CV study of this cation in acetonitrile under an argon atmosphere indicates that it did not form a stable $[Ni(\mathbf{L_4})]^+$ ion.

The Co(II) complex prepared from the reaction of $[Co(H_2O)_6](NO_3)_2$ with $\mathbf{L_4}$ in acetonitrile, Compound A, has a formula of $[Co(\mathbf{L_4})(CH_3CN)(NO_3)_2]$. This species has an octahedral geometry as confirmed by X-ray crystallography. The cobalt centre is coordinated to three oxygen atoms from a monodentate and a bidentate nitrates and three nitrogen atoms (two from the ligand and one from acetonitrile). None of the thioether sulphur atoms is coordinated to the metal centre. This complex, $[Co(\mathbf{L_4})(NO_3)_2(CH_3CN)]$, is air stable and ESR silent. The CV in acetonitrile shows irreversible oxidation and reduction waves at 1.71 V and -1.83 V vs Fc/Fc^+, respectively.

The Co(II) complex prepared from the reaction of $[Co(H_2O)_6](ClO_4)_2$ and $\mathbf{L_4}$ in nitromethane, Compound B, has a formula of $[Co(\mathbf{L_4})(ClO_4)](ClO_4)$. This compound is air stable and ESR active. The ESR spectrum at 77 K is typical of a low spin d^7 ion in a tetragonal elongated environment, consistent with a Co(II) ion being coordinated to two nitrogen and three sulphur atoms from the ligand $\mathbf{L_4}$. The CV of this isomer in acetonitrile shows a quasi-reversible

oxidation wave at $E_{1/2}$ = 0.18 V vs Fc/Fc^+, (ΔE = 0.23 V). This is assigned as the Co(II)/Co(III) couple.

The crystal structure of $[Cu(\mathbf{L_5})](ClO_4)_2$ shows the copper ion is in a distorted square pyramidal environment. It is coordinated to three nitrogen and three thioether sulphur atoms from the ligand. There is one nitrogen atom in the ligand which remained uncoordinated. The Cu(II) complexes of $\mathbf{L_4}$ and $\mathbf{L_5}$ had been characterized by UV/Vis and ESR spectroscopy. The ESR spectra of these complexes are isotropic at 77 K and exhibit spectroscopic features different from a typical d^9 ion in a tetragonal elongated environment. The cyclic voltammograms of these complexes in acetonitrile show reversible reduction to Cu(I), with the value of $E_{1/2}$ ranges from -0.024 to -0.137 V vs Fc/Fc^+.

CHAPTER 5

SYNTHESIS AND CHARACTERIZATION OF A PD(II) COMPLEX WITH THIOPHENE PENDANT ARMS

5.1 Introduction

The structure of thiophene as determined by microwave spectroscopy[111] shows that there is some delocalization of the π-electrons. The C-C bond lengths, as shown in Figure 66, are intermediate between a normal $C(sp^2)=C(sp^2)$ double bond (1.34 Å) and $C(sp^3)$-$C(sp^3)$ single bond distance (1.54 Å). That is, the C=C double bonds are slightly longer and the C-C single bonds are slightly shorter than "normal" double and single bond lengths.

The most probable coordination sites in thiophene are the C(2)=C(3) and C(4)=C(5) bonds (where the π-electron density is high) and also at the sulphur atom. Several types of thiophene binding in transition metal complexes[112] are known and they are summarized in Figure 67. Traditionally[112], thiophene is considered a weak sulphur donor ligand for transition metal ions compared to dialkyl sulphides (R_2S). However, there is an increased interest in the study of transition metal complexes of thiophene recently because hydrodesulfurization of thiophene, which is a major industrial process, may involve M-S(thiophene) coordination[113].

Several examples of transition metal thiophene complexes in which the M-S(thiophene) distances are within the range of the sum of the covalent radii of divalent sulphur and the metal involved have been reported[114]. Macrocyclic thioether complexes incorporating a thiophene moiety as a part of the ligand framework have also been documented[115]. For these transition

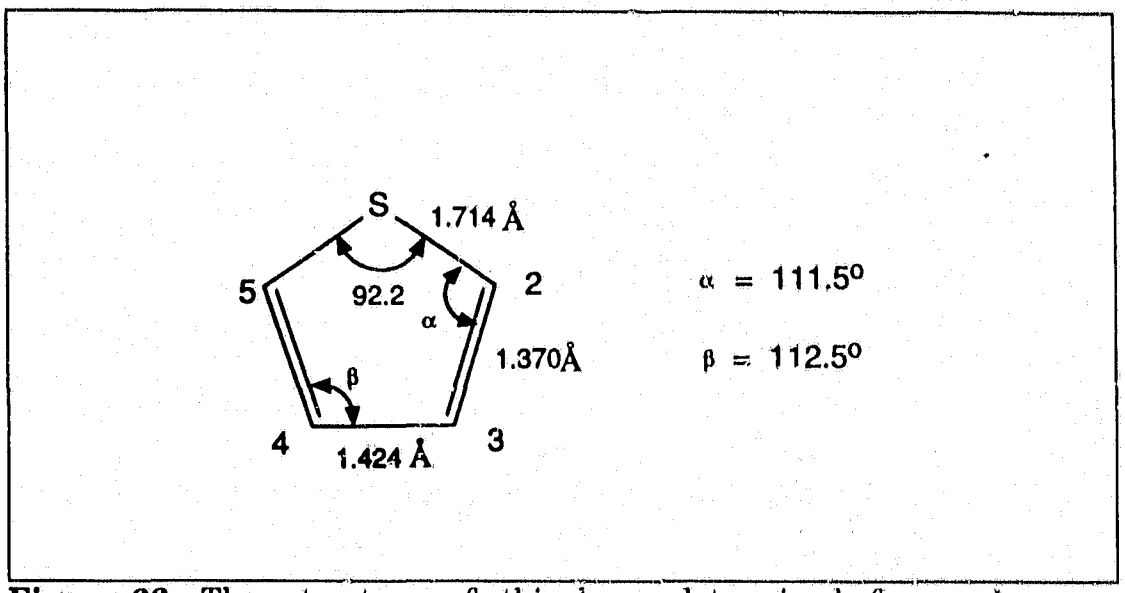

Figure 66 The structure of thiophene determined from microwave spectroscopy (from ref. 111)

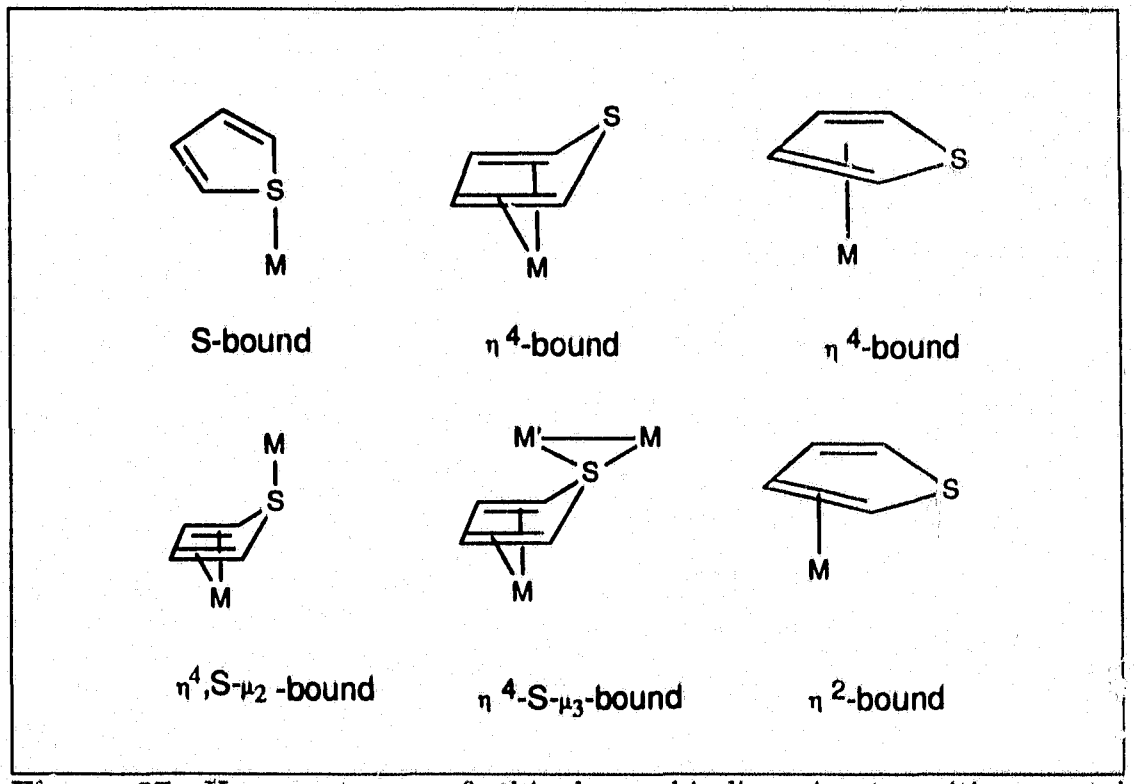

Figure 67 Known types of thiophene binding in transition metal complexes.

metal complexes in which there is a M-S(thiophene) interaction, the thiophene moiety is no longer planar, puckering into an envelope conformer in order to achieve the M-S(thiophene) coordination. This can be demonstrated by the structure[117b] of $[(PPh_3)_2Ru(C_5H_4CH_2C_4H_3S)]^+$, **35**. This arrangement is different from the M-N(pyridine) coordination in transition metal pyridine complexes in which the metal is in the plane of the pyridine ring.

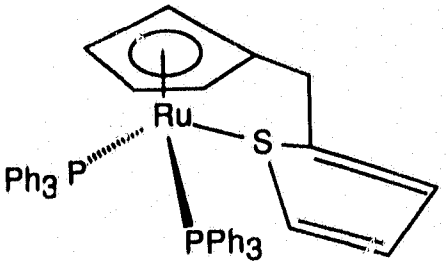

35

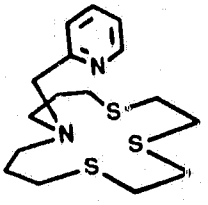

L_4

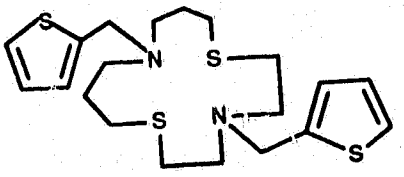

L_6

The study of the transition metal complexes of macrocyclic ligand L_4, which has a pyridine moiety as the pendant arm, as discussed previously in Chapters 3 and 4 of this thesis, indicates that in most cases the transition metal ion prefers to coordinate to the nitrogen atoms from the macrocycle and the pyridine pendant arm to form a five-membered chelate ring (see for example, Figures 26, 28 and 53). As a result, the rest of the ligand framework adopts a "folded" conformation. In using thiophene moieties as pendant arms in the ligand L_6, the coordination of thiophene as a weak sulphur donor ligand may be achieved. However, it may not compete effectively with the N and S donors in the macrocyclic framework in coordination to a Pd(II) ion. Hence, it

may also lead to the stabilization of the less accessible oxidation states of palladium by blocking the two axial sites available for the formation of polymeric species upon reduction to Pd(I) or oxidation to Pd(III). The synthesis and characterization of the Pd(II) complex of $\mathbf{L_6}$ will be presented in this chapter.

5.2 Synthesis

The synthetic route leading to ligand $\mathbf{L_6}$ and its Pd(II) complex is outlined in Scheme 13. The ligand $\mathbf{L_3}$ was prepared according to the steps shown in Scheme 6 of chapter 3. The thiophene moiety was introduced into the side arms of $\mathbf{L_3}$ by the reaction of thiophene carbonyl chloride followed by a reduction by $LiAlH_4$. The free ligand $\mathbf{L_6}$ was isolated as a white solid in 30% yield. It was characterized by ^1H and ^{13}C NMR, as well as mass spectroscopy (MS).

The ^{13}C NMR of $\mathbf{L_6}$ exhibits fifteen lines which corresponds to the fifteen inequivalent carbon atoms in the molecule (Figure 68). The peaks at δ 142.1 and 143.2 correspond to the carbons at the α-position of the two thiophene moieties. The six lines observed at δ 124 - 127 arise from the inequivalent aromatic carbons in thiophenes. The two singlets at δ 53.4 and 53.5 correspond to "benzylic-like" carbons adjacent of the pendant arms. The carbon resonances for the CH_2-S and CH_2N portions of the molecule are observed at δ 29.4, 29.5 and 51.8, 52.3, respectively. The resonance at δ 27.5 corresponds to the apical carbon from the $NCH_2\underline{C}H_2CH_2S$ fragment.

Scheme 13

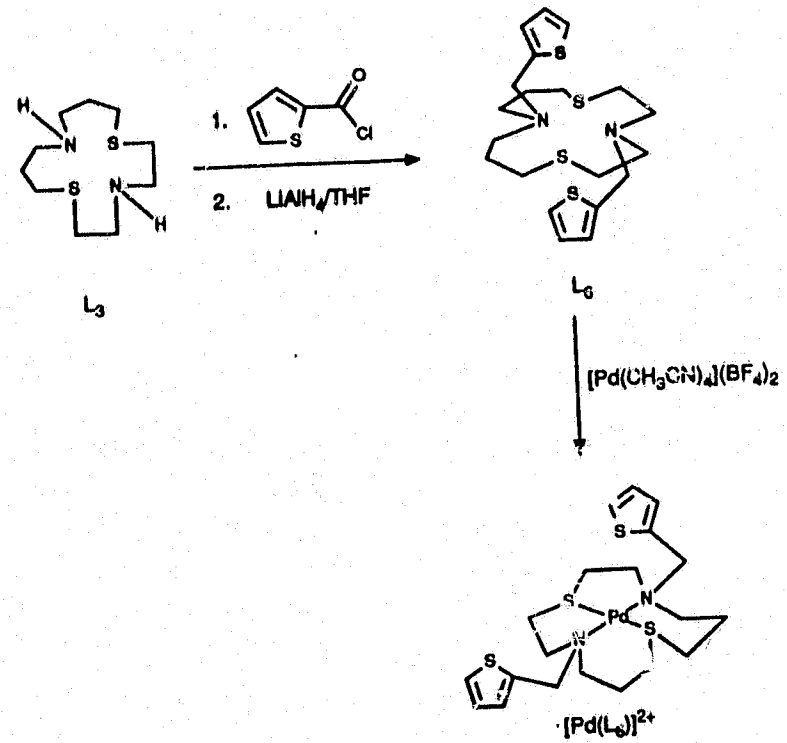

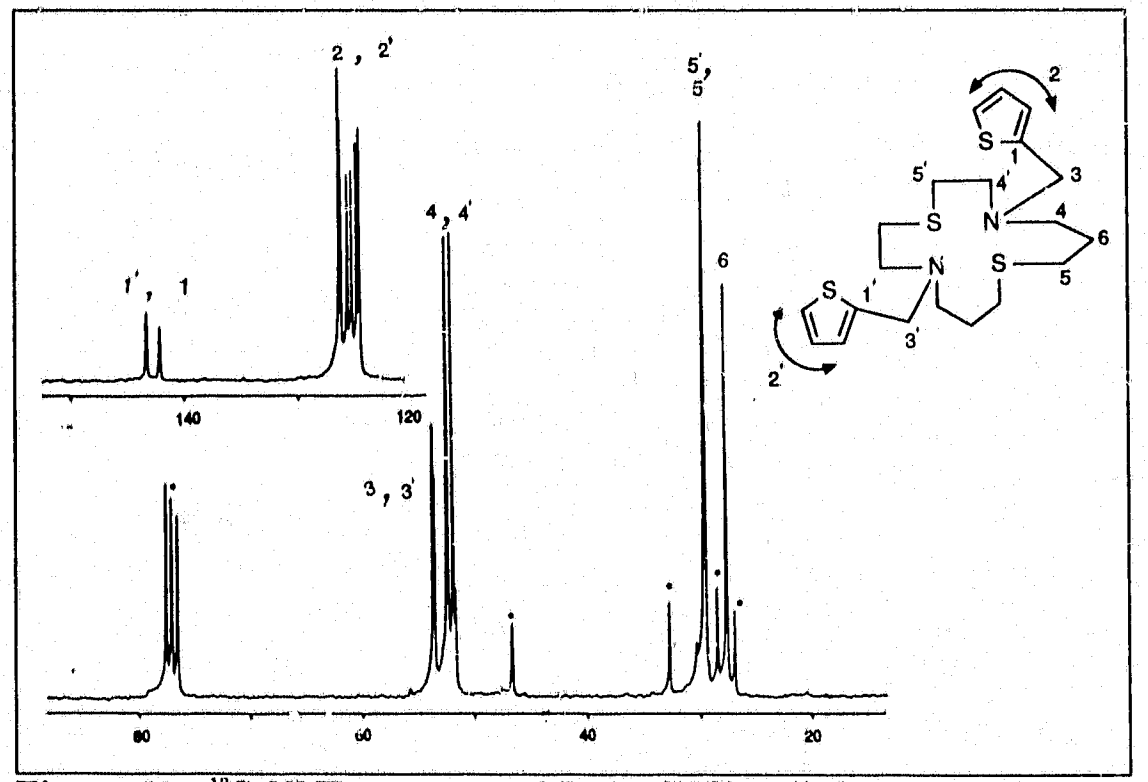

Figure 68 ^{13}C NMR spectrum of $\mathbf{L_6}$ in $CDCl_3$. (* denotes peaks from solvent or impurities).

^{1}H NMR of $\mathbf{L_6}$ shows two singlets at δ 3.90 and 3.70 corresponding to methylene protons adjacent to the thiophene moiety. The multiplets at δ 2.80 and 2.50 -- 2.70 correspond to the protons in the NCH_2 and SCH_2 fragments. Proton resonances from the thiophene moiety are observed in the region of δ 6.90 -- 7.30.

The palladium(II) complex was prepared by the reaction of equimolar quantities of the ligand with $[Pd(CH_3CN)_4](BF_4)_2$ in dry CH_3CN under an atmosphere of nitrogen. X-ray quality crystals were obtained by evaporation of a concentrated solution of the $[Pd(\mathbf{L_6})]^{2+}$ in $CH_3NO_2/CH_2Cl_2/CH_3OH$.

$[Pd(\mathbf{L_6})](BF_4)_2$ has been characterized by elemental analyses, NMR, UV/Vis spectroscopy and X-ray crystallography. The ^{13}C NMR of $[Pd(\mathbf{L_6})]^{2+}$ in CD_3CN at room temperature (Figure 69) shows eight peaks in the aromatic region (δ 128 - 135) which arise from the aromatic carbons of the two thiophenes. The two smaller peaks in this region (δ 129.8 and 134.7) are due to carbons at the α-position of the thiophenes. The signal at δ 23.7 is from the apical carbon in the $NCH_2\underline{C}H_2CH_2S$ fragment of the complex and the peak at δ 62.2 is from carbons adjacent to the two thiophenes. The remaining resonances observed in the aliphatic region arise from carbons in the CH_2N and CH_2S fragments of the complex.

An acetonitrile solution of $[Pd(\mathbf{L_6})]^{2+}$ is yellow in color and shows an absorption at 320 nm ($\varepsilon = 5060$ L mol^{-1} cm^{-1}). No distinctive absorption bands

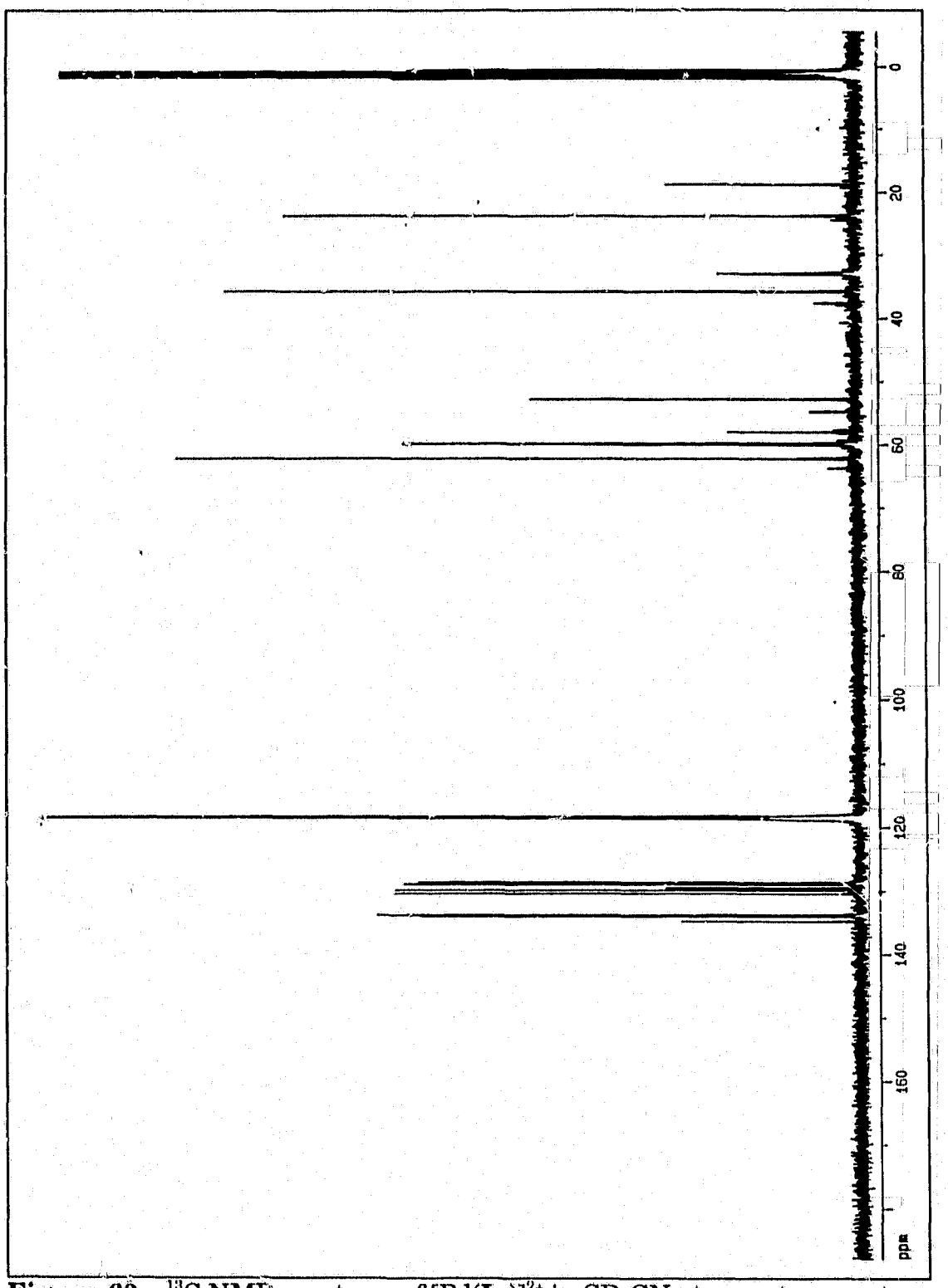

Figure 69 ^{13}C NMR spectrum of $[Pd(L_6)]^{2+}$ in CD_3CN at room temperature (* denotes peaks from solvent and impurities).

Table 54
Electronic spectral data for $[Pd(\mathbf{L_6})](BF_4)_2$ and analogous species

Complex	Solvent	Color	λ_{max}/nm (ε_{max}, $M^{-1}cm^{-1}$)	Ref.
$Pd(\mathbf{L_6})](BF_4)_2$	CH_3CN	yellow	320 (5060)	present work
$Pd(\mathbf{L_2})](BF_4)_2$	CH_3CN	yellow	314 (4300) 257 (shoulder)	present work
[Pd(**29**)Cl_2]	CH_2Cl_2	orange	395 (1000) 310 (shoulder) 250 (14000)	115
[Pd(**29**)Br_2]	CH_2Cl_2	red	415 (800) 355 (shoulder) 260 (13000)	115
[Pd(**10**)]$(PF_6)_2$	CH_3CN	yellow-orange	298(14460) 373(2175)	41
[Pd(**31**)]$(PF_6)_2$	CH_3CN	green	266(10000) 332(4250) 514(124)	41

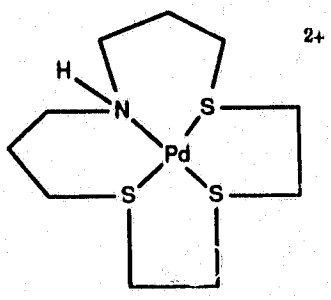

$[Pd(\mathbf{L_2})]^{2+}$

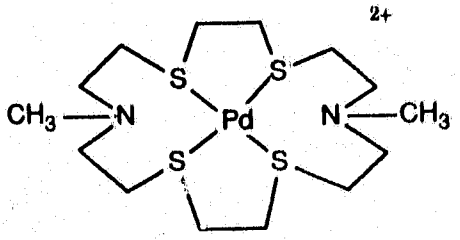

$[Pd(\mathbf{10})]^{2+}$

were observed above 350 nm even when a more concentrated solution (ca. 0.01 M) in acetonitrile was prepared. The electronic spectral data for[Pd($\mathbf{L_6}$)]$(BF_4)_2$ and other analogues Pd(II) complexes[41,115] are summarized in Table 54.

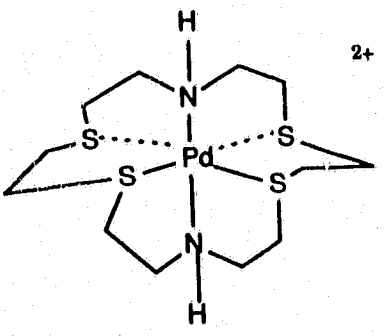

[Pd(**31**)]$^{2+}$

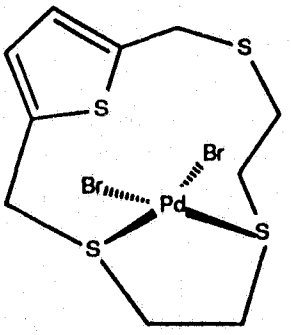

[$PdBr_2$(**29**)]

5.3 Crystal Structure

The Pd(II) complex of $\mathbf{L_6}$ has been characterized by crystallography and the molecular structure is shown in Figure 70, along with the atomic labelling scheme. The crystallographic parameters are listed in Table 55. The fractional atomic coordinates, interatomic distances and bond angles are shown in Tables 56 - 58.

As illustrated in Figure 70, the Pd(II) center is in a distorted square-planar environment. It is coordinated to two nitrogen atoms and two sulphur atoms from the ligand. The sulphur atom S(4) from one of the thiophene moieties is pointed towards the Pd ion with the interatomic distance Pd...S(4)

(a) perspective view:

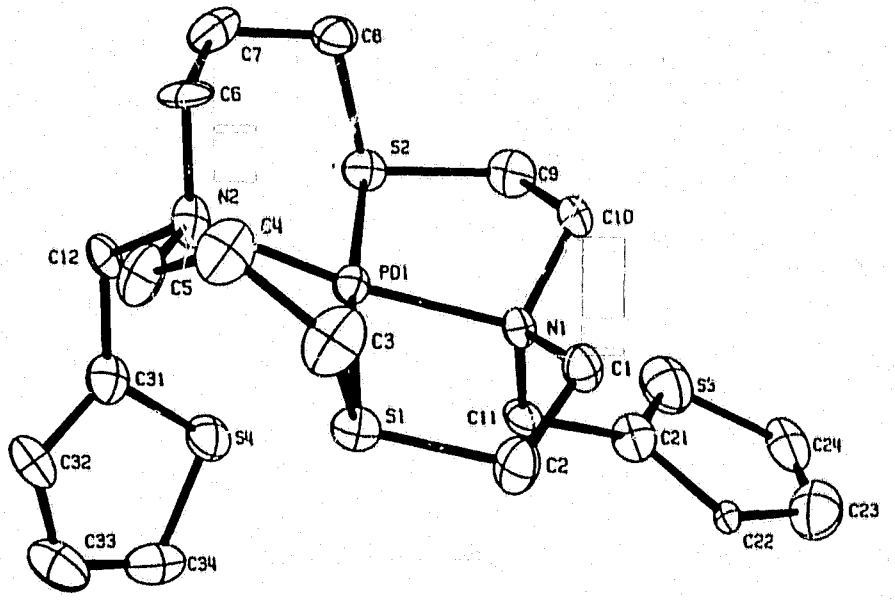

(b) side view:

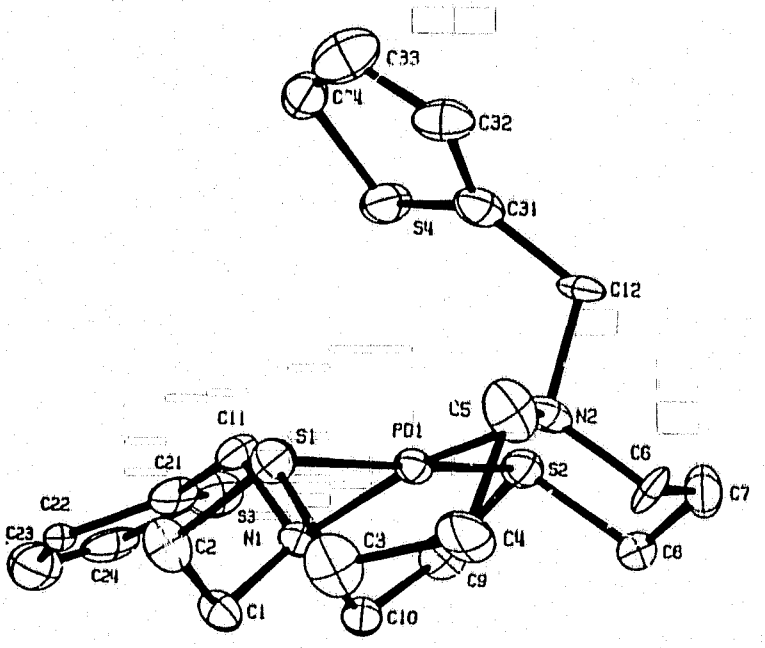

Figure 70 ORTEP diagram of $[Pd(L_6)]^{2+}$. Selected bond distances (Å): Pd-S(1) = 2.295(5); Pd-S(2) = 2.300(5); Pd-N(1) = 2.068(12); Pd-N(2) = 2.075(14); Pd...S(4) = 3.210.

Table 56
Experimental crystallographic data for $[Pd(\mathbf{L}_6)](BF_4)_2.CH_3OH.H_2O$

Formula:	$PdC_{21}H_{36}N_2S_4O_2B_2F_8$
F.W.:	756.8
Crystal colour:	yellow
Crystal system:	monoclinic
Space group:	$P2_1/c$ (No. 14)
Cell dimensions:	
	a = 10.523(2) Å α = 90°
	b = 36.080(7) Å β = 107.90(2)°
	c = 8.332(3) Å γ = 90°
V_{cell} :	3010 Å^3
Z:	4 molecules/cell
Temperature:	20 °C
Crystal dimensions:	0.70 x 0.20 x 0.20 mm^3
$D_{calcd.}$:	1.670 g/cm^3
$D_{meas.}$:	1.676 g/cm^3
Radiation:	Mo, 0.71069 Å
μ:	8.69 cm^{-1}
transmission range:	N/A
Measurement:	2θ(0-45°)
No. of reflections collected:	3659
No. of reflections $I \geq n\sigma(I)$:	2522 (n = 6)
No. of parameters:	346
Residual electron density:	0.5 e/Å^3
Maximum final shift/error:	0.04
Refinement method:	SHELX least squares
R:	0.087
R_w:	0.090

Table 56
Fractional atomic coordinates and temperature parameters for $[Pd(\mathbf{L}_6)](BF_4)_2.CH_3OH.H_2O$

Atom	x/a	y/b	z/c	U_{eq}
Pd(1)	30184(12)	11512(4)	18906(15)	394(5)
S(1)	42281(47)	14302(14)	3572(59)	546(20)
S(2)	20920(48)	8632(14)	37281(59)	541(20)
S(3)	66411(74)	5446(21)	72987(89)	1008(33)
S(4)	33242(54)	18847(15)	41574(67)	662(22)
N(1)	4683(12)	825(4)	2935(15)	39(5)
N(2)	1248(14)	1413(4)	[illegible]9(16)	52(6)
C(1)	5408(18)	766(5)	1635(22)	51(8)
C(2)	5685(19)	1126(6)	946(24)	65(9)
C(3)	3297(22)	1289(7)	-1789(23)	82(10)
C(4)	1810(21)	1367(7)	-2[illegible]41(23)	78(10)
C(5)	1379(19)	1624(6)	-1003(23)	70(9)
C(6)	107(10)	1153(6)	-32(28)	73(9)
C(7)	-332(19)	945(7)	1372(27)	74(10)
C(8)	641(18)	641(5)	2305(24)	59(8)
C(9)	3299(20)	485(6)	4377(23)	65(9)
C(10)	4146(17)	440(5)	3264(23)	50(7)
C(11)	5597(17)	1010(5)	4548(23)	53(7)
C(12)	867(18)	1719(5)	1698(22)	50(7)
C(21)	6699(18)	770(5)	5532(21)	60(8)
C(22)	8060(13)	710(4)	5260(16)	23(5)
C(23)	8842(29)	466(10)	6497(42)	122(17)
C(24)	8212(27)	363(7)	7638(36)	107(13)
C(31)	1981(18)	1986(5)	2392(22)	57(8)
C(32)	2150(23)	2343(5)	1859(26)	66(9)
C(33)	3288(28)	2520(7)	2867(32)	91(13)
C(34)	4069(21)	2300(7)	4182(29)	75(10)
B(1)	2405(24)	4829(9)	3208(37)	68(12)
B(2)	6855(26)	3199(8)	3131(42)	69(12)
F(1)	3673(15)	4789(5)	3261(21)	138(9)
F(2)	2063(15)	4604(5)	4360(18)	126(8)
F(3)	2222(26)	5175(6)	3544(40)	222(20)
F(4)	1642(15)	4758(7)	1604(19)	168(12)
F(5)	7827(23)	3128(7)	2619(29)	214(16)
F(6)	7463(21)	3203(8)	4837(29)	202(14)
F(7)	6248(30)	3477(7)	2719(27)	238(18)
F(8)	6051(21)	2935(7)	2964(44)	267(20)
O(1)	8468(18)	1648(6)	4018(23)	117(6)'
O(2)	7680(32)	2130(9)	3762(41)	229(13)'
C(41)	9481(26)	1961(8)	4674(33)	103(8)'

Estimated standard deviations are given in parentheses. Coordinates x 10^n where n = 5,5,4,4,4,4,4 for Pd,S,N,C,B,F,O. Temperature parameters x 10^n where n = 4,4,3,3,3,3,3 for Pd,S,N,C,B,F,O. $U_{eq} = \frac{1}{3}\Sigma_i\Sigma_j U_{ij} a_i^* a_j^* (a_i.a_j)$. Primed values indicate that U_{iso} is given. $T = \exp-(8\pi^2 U_{iso} \sin^2\theta/\lambda^2)$

Table 57
Interatomic Distances (Å) for $[Pd(L_6)](BF_4)_2.CH_3OH.H_2O$

Atoms	Distance	Atoms	Distance
S(1)-Pd(1)	2.295(5)	C(7)-C(6)	1.574(29)
S(2)-Pd(1)	2.300(5)	C(8)-C(7)	1.536(28)
N(1)-Pd(1)	2.068(12)	C(10)-C(9)	1.479(26)
N(2)-Pd(1)	2.075(14)	C(21)-C(11)	1.478(23)
C(2)-S(1)	1.827(19)	C(31)-C(12)	1.490(25)
C(3)-S(1)	1.827(19)	C(22)-C(21)	1.532(24)
C(8)-S(2)	1.807(18)	C(23)-C(22)	1.413(37)
C(9)-S(2)	1.830(21)	C(24)-C(23)	1.367(39)
C(21)-S(3)	1.699(21)	C(32)-C(31)	1.393(26)
C(24)-S(3)	1.719(27)	C(33)-C(32)	1.389(30)
C(31)-S(4)	1.737(19)	C(34)-C(33)	1.397(31)
C(34)-S(4)	1.689(22)	F(1)-B(1)	1.329(25)
C(1)-N(1)	1.519(20)	F(2)-B(1)	1.388(27)
C(10)-N(1)	1.555(21)	F(3)-B(1)	1.304(31)
C(11)-N(1)	1.543(21)	F(4)-B(1)	1.356(30)
C(5)-N(2)	1.565(23)	F(5)-B(2)	1.249(26)
C(6)-N(2)	1.485(22)	F(6)-B(2)	1.368(32)
C(12)-N(2)	1.574(19)	F(7)-B(2)	1.184(28)
C(2)-C(1)	1.485(26)	F(8)-B(2)	1.252(30)
C(4)-C(3)	1.519(27)	C(41)-O(1)	1.535(29)
C(5)-C(4)	1.533(26)		

Estimated standard deviations are given in parentheses.

Table 58
Bond Angles (deg) for $[Pd(L_6)](BF_4)_2.C_3H_3OH.H_2O$

Atoms	Angle	Atoms	Angle
S(2)-Pd(1)-S(1)	171.8(2)	C(7)-C(6)-N(2)	115.9(16)
N(1)-Pd(1)-S(1)	86.6(4)	C(8)-C(7)-C(6)	114.4(16)
N(1)-Pd(1)-S(2)	86.6(4)	C(7)-C(8)-S(2)	108.3(14)
N(2)-Pd(1)-S(1)	94.0(4)	C(10)-C(9)-S(2)	113.1(13)
N(2)-Pd(1)-S(2)	93.4(4)	C(9)-C(10)-N(1)	109.6(15)
N(2)-Pd(1)-N(1)	171.2(5)	C(21)-C(11)-N(1)	113.7(14)
C(2)-S(1)-Pd(1)	98.6(6)	C(31)-C(12)-N(2)	111.7(14)
C(3)-S(1)-Pd(1)	101.6(8)	C(11)-C(21)-S(3)	122.0(16)
C(3)-S(1)-C(2)	104.4(10)	C(22)-C(21)-S(3)	110.2(11)
C(8)-S(2)-Pd(1)	102.0(7)	C(22)-C(21)-C(11)	127.6(17)
C(9)-S(2)-Pd(1)	97.8(6)	C(23)-C(22)-C(21)	110.0(17)
C(9)-S(2)-C(8)	103.5(10)	C(24)-C(23)-C(22)	112.2(24)
C(24)-S(3)-C(21)	92.1(14)	C(23)-C(24)-S(3)	115.5(22)
C(34)-S(4)-C(31)	94.4(11)	C(12)-C(31)-S(4)	122.1(14)
C(1)-N(1)-Pd(1)	109.0(9)	C(32)-C(31)-S(4)	108.3(15)
C(10)-N(1)-Pd(1)	106.0(9)	C(32)-C(31)-C(12)	129.6(18)
C(10)-N(1)-C(1)	106.8(12)	C(33)-C(32)-C(31)	113.8(20)
C(11)-N(1)-Pd(1)	109.9(10)	C(34)-C(33)-C(32)	113.8(20)
C(11)-N(1)-C(1)	111.5(13)	C(33)-C(34)-S(4)	109.6(17)
C(11)-N(1)-C(10)	113.3(12)	F(2)-B(1)-F(1)	112.6(23)
C(5)-N(2)-Pd(1)	111.5(10)	F(3)-B(1)-F(1)	108.1(24)
C(6)-N(2)-Pd(1)	113.2(12)	F(3)-B(1)-F(2)	108.9(24)
C(6)-N(2)-C(5)	106.8(14)	F(4)-B(1)-F(1)	107.2(22)
C(12)-N(2)-Pd(1)	111.0(9)	F(4)-B(1)-F(2)	111.6(22)
C(12)-N(2)-C(5)	105.2(14)	F(4)-B(1)-F(3)	108.2(27)
C(12)-N(2)-C(6)	108.7(14)	F(6)-B(2)-F(5)	100.7(25)
C(2)-C(1)-N(1)	110.7(14)	F(7)-B(2)-F(5)	119.9(31)
C(1)-C(2)-S(1)	112.5(13)	F(7)-B(2)-F(6)	109.2(27)
C(4)-C(3)-S(1)	113.1(14)	F(8)-B(2)-F(5)	113.8(28)
C(5)-C(4)-C(3)	115.7(16)	F(8)-B(2)-F(6)	102.1(29)
C(4)-C(5)-N(2)	112.9(17)	F(8)-B(2)-F(7)	109.2(28)

Estimated standard deviations are given in parentheses.

Table 59
Mean plane for $[Pd(L_6)](BF_4)_2$

(a) The equation of the plane containing atoms S(1), S(2), N(1) and N(2) is:
-0.1009X - 0.7298Y - 0.6762Z + 4.3691 = 0

Atoms	X	Y	Z	P
S(1)	4.3578	5.1602	0.2832	-0.0278
S(2)	1.2467	3.1144	2.9559	-0.0283
N(1)	4.1767	2.9759	2.3270	0.2025
N(2)	1.1645	5.0974	0.4599	0.2207
Pd(1)	2.6921	4.1535	1.4990	0.0527
S(3)	5.1193	1.9649	5.7869	-1.4944
S(4)	2.4334	6.8000	3.2963	-3.0678

(b) The equation of the plane containing atoms S(1), S(2) and N(2) is:
-0.0190X - 0.7831Y - 0.6215Z + 4.2999 = 0

Atoms	X	Y	Z	P
S(1)	4.3578	5.1602	0.2832	0.000
S(2)	1.2467	3.1144	2.9559	0.000
N(2)	1.1645	5.0974	0.4599	0.000
Pd(1)	2.6921	4.1535	1.4990	0.0643
N(1)	4.1767	2.9759	2.3270	0.4438
S(3)	5.1193	1.9649	5.7869	-0.9329
S(4)	2.4332	6.8000	3.2963	-3.1204

where P is the perpendicular distance between the atom and the mean plane, given in Å.

Table 60
Mean plane for $[Pd(L_6)](BF_4)_2$ (Continued)

(c) The equation of the plane of the first thiophene moiety is:
-0.2016X - 0.7918Y - 0.5766Z + 5.8675 = 0

Atoms	X	Y	Z	P
C(21)	5.6324	2.7771	4.3859	0.0041
C(22)	7.1343	2.5617	4.1705	-0.0040
C(23)	7.6410	1.6802	5.1515	0.0261
C(24)	6.6855	1.3104	6.0561	-0.0100
S(3)	5.1993	1.9649	5.7869	-0.0572

(d) The equation of the plane of the second thiophene moiety is:
0.7223X - 0.3595Y - 0.5908Z + 2.6293 = 0

Atoms	X	Y	Z	P
C(31)	1.4724	7.1651	1.8966	-0.0038
C(32)	1.7863	8.4546	1.4742	0.0089
C(33)	2.7260	9.0925	2.2730	-0.0136
C(34)	3.2109	8.2998	3.3156	0.0056
S(4)	2.4334	6.800	3.2962	-0.0053

where P is the perpendicular distance between the atom and the mean plane, given in Å.

Table 61
Pd-S bond distances in various macrocyclic thioether complexes

Complex	Mean equatorial Pd-S bond (Å)	Mean apical Pd-S bond (Å)	Ref
$\{Pd([9]aneS_3)_2\}^{2+}$	2.276	3.125	68
$\{Pd([10]aneS_3)_2\}^{2+}$	2.329	3.034	119
$\{Pd([18]aneS_6)\}^{2+}$	2.309	3.273	120
$[PdBr_2(\mathbf{29})]$	2.280	3.182	118a
$[Pd(\eta^3\text{-ally})(\mathbf{29})]^+$	2.320	2.786	118b
$[Pd(\mathbf{31})]^{2+}$	2.334	2.977	41
$[Pd(\mathbf{L_4})]^{2+}$	2.284	3.120	present work
$[Pd(\mathbf{L_6})]^{2+}$	2.297	3.210	present work
$[Pd(\mathbf{L_2})]^{2+}$	2.036[a] 2.041[b]	2.915	present work
$[Pd(bicycloSN_4)]^{2+}$	2.071[a]	2.875	78

[a] Mean equatorial Pd-N distance is given
[b] Mean equatorial Pd-N(pyr) distance is given

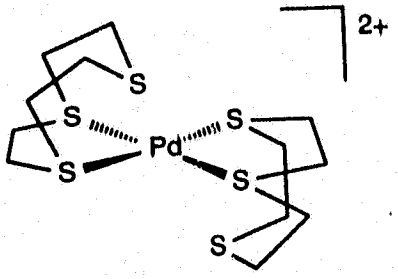

$\{Pd([9]aneS_3)_2\}^{2+}$

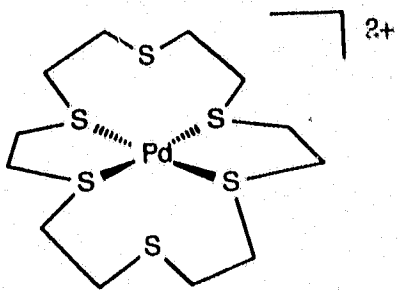

$\{Pd([18]aneS_6)\}^{2+}$

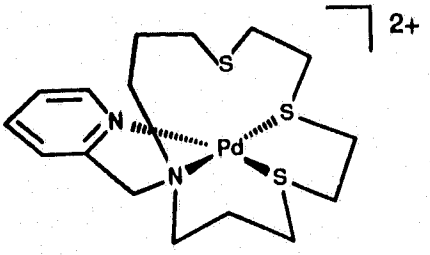

$[Pd(\mathbf{L_4})]^{2+}$

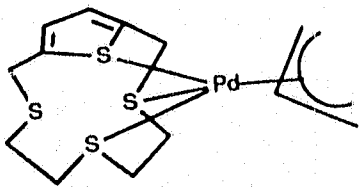

$[Pd(\eta^3\text{-allyl})(\mathbf{29})]^{+}$

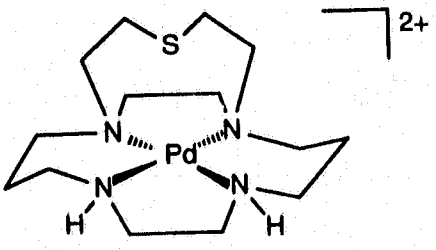

$[Pd(bicycloSN_4)]^{2+}$

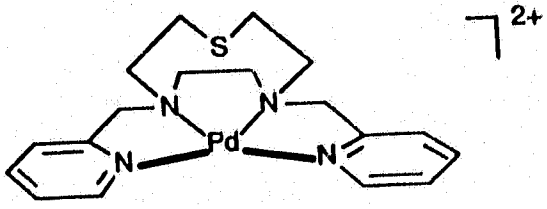

$[Pd(\mathbf{L_1})]^{2+}$

being 3.210 Å. This is slightly less than the sum of the van der Waals' radii of palladium and sulphur (3.40 Å)[67] and may suggest a weak apical thiophene sulphur to metal interaction. The average Pd-S bond distance is 2.297 Å and that of Pd-N is 2.071 Å. These values are comparable to those observed in $[Pd(\mathbf{L_2})]^{2+}$ (mean Pd-S = 2.29 Å, Pd-N = 2.09 Å), $[Pd(\mathbf{10})]^{2+}$ (avg. Pd-S = 2.33 Å)[41], $[Pd(\mathbf{31})]^{2+}$ (mean Pd-S = 2.33 Å, Pd-N = 2.10 Å)[6] and $[PdBr_2(\mathbf{29})]^{2+}$ (mean Pd-S = 2.28 Å)[115].

Macrocyclic thioether complexes of Pd(II) which are square-planar but show significant interaction with apical donors are well-documented. The mean Pd-S equatorial bond distance in $[Pd(\mathbf{L_6})]^{2+}$ is 2.297 Å and that of the apical Pd-S(thiophene) is 3.210 Å. These values are comparable to the $[Pd([9]aneS_3)_2]^{2+}$,[66] $[Pd[10]aneS_3)_2]^{2+}$,[116] and $[Pd[18]aneS_6]^{2+}$,[117] (Table 61).

Both of the five-membered chelate rings in $[Pd(\mathbf{L_6})]^{2+}$ adopt an envelope conformation and the chelate bite angles of N(1)-Pd-S(1) and N(1)-Pd-S(2) are equal to 86.6°. The six-membered chelate ring defined by atoms Pd, N(2), C(6), C(7), C(8) and S(2) adopts a chair conformation and the chelate bite angle N(2)-Pd-S(2) = 93.4°. The other six-membered chelate ring defined by atoms Pd, S(1), C(3), C(4), C(5) and N(2) adopts a twist-boat conformation. This observed conformation may arise from the weak apical interaction between the thiophene sulphur atom S(4) and the palladium ion, which constraints the carbon bridges C(3) and C(4) from adopting a chair conformation. However, in the crystal structure of the $[Pd(\mathbf{L_2})]^{2+}$ cation complex (Figure 24), a similar

twist-boat conformation is also observed. Therefore, such a geometry in the six-membered chelate ring is more likely to be caused by the spatial arrangement of the donor atoms in the carbon bridges of these "isocyclam-type" ligands. The chelate bite angle for N(2)-Pd-S(1) is equal to 94.0°. These bond angles are comparable to those observed in $[Pd(\mathbf{L}_2)]^{2+}$, which has six-membered chelate bite angles of 90.4° for the chair conformation and 93.4° for the twist-boat conformation.

It is interesting to note that the interatomic distances in the two thiophene moieties of $[Pd(\mathbf{L}_6)]^{2+}$ are not identical. The thiophene moiety which has a sulphur atom showing a weak apical interaction with the palladium(II) ion (Figure 70), shows a greater extent of delocalization of its π-electrons. This is illustrated by the bond distances among C(34)-C(33); C(33)-C(32) and (32)-C(31), which are crystallographically identical and have a value of ≈ 1.390 Å. The bond distances among C(21)-C(22), C(22)-C(23) and C(23)-C(24) show a greater degree of bond alternation and have bond distances range from 1.367 to 1.532 Å.

The mean plane calculation in Table 59 indicates that in $[Pd(\mathbf{L}_6)]^{2+}$, the four donor atoms S(1), S(2), N(1) and N(2) do not lie in the same plane. The palladium ion is 0.0643 Å below the plane defined by the donor atoms S(1), S(2) and N(2). In addition, N(1) is also 0.4438 Å below this plane (Table 59). Thus the geometry of the complex ion $[Pd(\mathbf{L}_6)]^{2+}$ is best described as square-planar showing distortion towards a tetrahedron.

Several hydrodesulfurization studies[112,113,118] have proposed that in S-bound thiophene transition metal complexes, there is a loss of aromaticity of the thiophene, which causes folding of the ring and the thiophene moiety adopts an envelope conformation. The mean plane calculation in Table 60 shows that both of the thiophene moieties in $[Pd(\mathbf{L_6})]^{2+}$ are essentially planar suggesting that the apical Pd-S(4)thiophene interaction is very weak.

In the complex cation $[Pd(\mathbf{L_6})]^{2+}$, the ligand $\mathbf{L_6}$ adopts a "puckered crown" conformation (Figure 70), as previously observed in $[Pd(\mathbf{L_2})]^{2+}$. The lone pairs in the sulphur atoms are oriented above the ligand-metal plane and the rest of the carbon backbones in the ligand framework are situated below the plane defined by the ligating atoms N(2), S(2) and S(1). This configuration indirectly puts one of the pendant arm ligating groups above the palladium(II) ion. It is interesting to note that the proximity of such an axial donor in an "entatic state" has a profound influence on the redox behavior of $[Pd(\mathbf{L_6})]^{2+}$, which will be discussed in the following section.

5.4 CV Study

The cyclic voltammogram of $[Pd(\mathbf{L_6})]^{2+}$ in acetonitrile under an argon atmosphere showed no oxidative activity up to 2.0 V vs $Ag/AgNO_3$ but a reversible reduction wave at -1.03 V vs Fc/Fc^+ was observed (Figure 71). The peak to peak separation for the reduction was 80 mV and may suggest there is a rearrangement in the structure of the complex upon reduction. The reduction wave observed is assigned as the $[Pd(\mathbf{L_6})]^{2+/+}$ couple. An attempt to

generate electrochemically the Pd(I) species and to carry out characterization by ESR spectroscopy was unsuccessful due to the its sensitivity to air and moisture.

Of all the palladium pendant arm macrocyclic complexes studied within the scope of this project, $[Pd(\mathbf{L_6})]^{2+}$ is the only one that shows a reversible Pd(II)/(I) couple. This behavior may arise from the proximity of a thiophene moiety in the apical position of the complex, which inhibits dimerisation of Pd(I) generated, due to steric reasons.

Very few macrocyclic complexes showing a reversible Pd(II)/Pd(I) couple at room temperature have been reported[40,41]. These are summarized in Table 62. The Pd(II)/Pd(I) couple occurred at a "more positive" potential in the tetrathia complex $[Pd(\mathbf{10})]^{2+}$ than the tetraaza complexes $[Pd(\mathbf{9})]^{2+}$ and $[Pd(\mathbf{36})]^{2+}$. This is attributed to the greater π-acidity of thioether donors which can better stabilize Pd(I) than the nitrogen donors[41]. It is interesting to note that for the complex $[Pd(\mathbf{L_6})]^{2+}$, which consist of both sulphur and two nitrogen donors, the Pd(II)/Pd(I) couple occurred at a potential intermediate between the tetraaza and tetrathia systems.

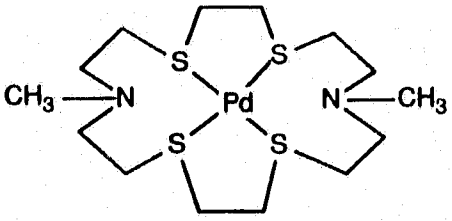

$[Pd(\mathbf{10})]^{2+}$

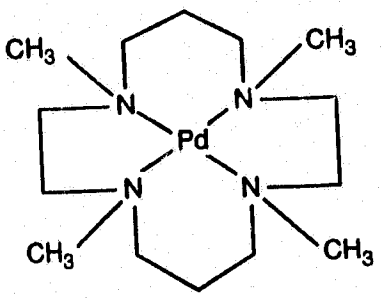

$[Pd(\mathbf{9})]^{2+}$

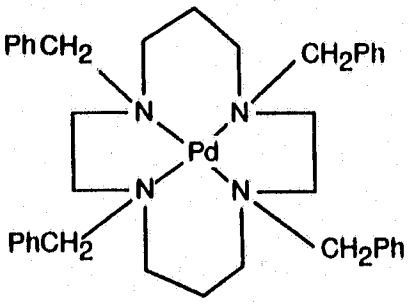

$[Pd(\mathbf{36})]^{2+}$

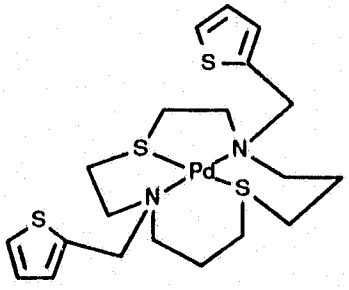

$[Pd(\mathbf{L}_6)]^{2+}$

Table 62
Reduction potentials of Pd(II) complexes in acetonitrile.

Complex	Scan Rate (mV/s)	E_{red} vs Fc/Fc^+ (V)	Ref.
$[Pd(\mathbf{L_6})]^{2+}$	50	$E_{½} = -1.03$	present work
$[Pd(\mathbf{10})]^{2+}$	100	$E_{½} = -0.74$	40
$[Pd(\mathbf{9})]^{2+}$	100	$E_{½} = -1.53$	40, 41
$[Pd(\mathbf{36})]^{2+}$	100	$E_{½} = -1.27$	40

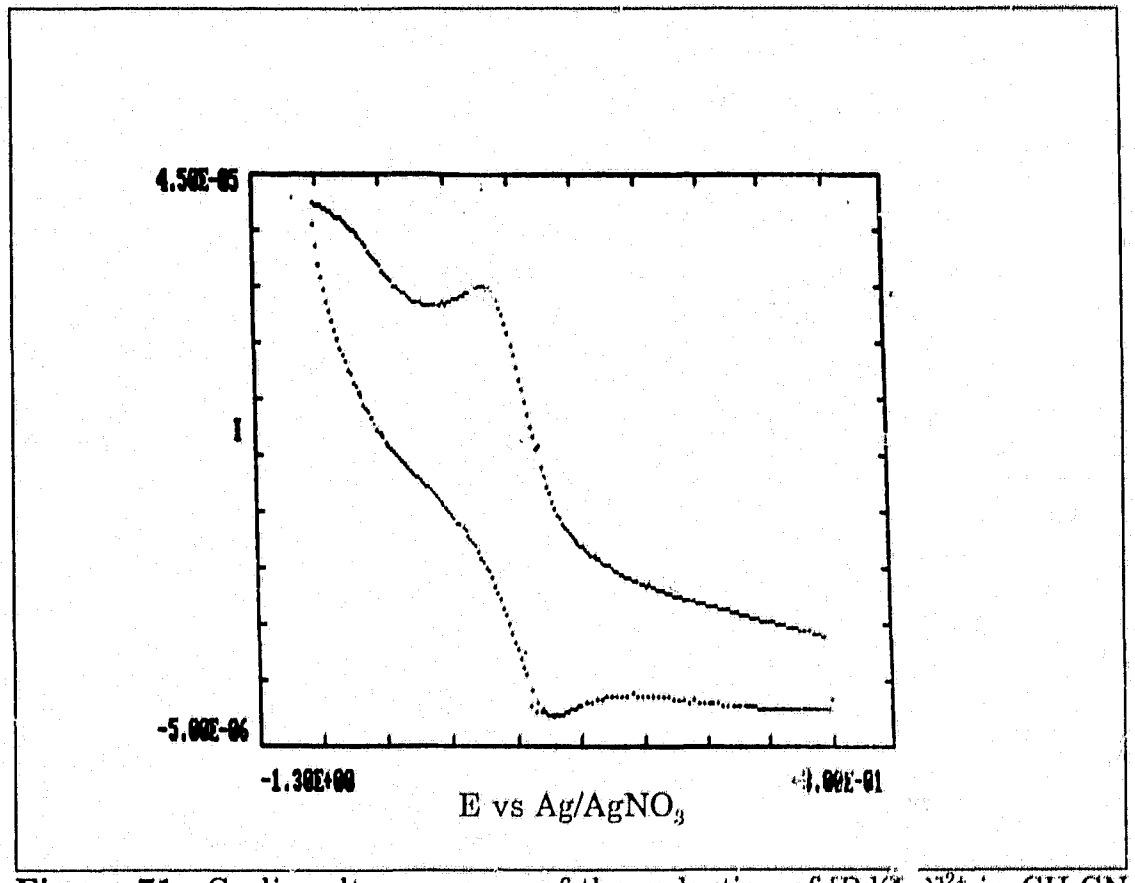

Figure 71 Cyclic voltammogram of the reduction of $[Pd(\mathbf{L_6})]^{2+}$ in CH_3CN at a scan rate of 50 mV/s. Fc/Fc^+ occurs at 0.097 V.

5.5 Conclusions

The structure of $[Pd(\mathbf{L_6})]^{2+}$ in the solid state as determined by X-ray crystallography consists of a Pd(II) ion in a distorted square planar environment. The palladium centre is coordinated to two nitrogen and two sulphur atoms from the ligand. There is also a weak apical interaction between a thiophene sulphur atom and the palladium ion. The CV of $[Pd(\mathbf{L_6})]^{2+}$ in acetonitrile under an argon atmosphere shows a reversible Pd(II)/Pd(I) reduction at -1.03 V vs Fc/Fc^+, with a peak to peak separation of 80 mV. This is the only case when reversible Pd(II)/Pd(I) couple was observed among the Pd(II) macrocyclic complexes studied. Such an unique behavior of $[Pd(\mathbf{L_6})]^{2+}$ was rationalized as due to the proximity of a thiophene moiety in the apical position, which inhibits dimerization of Pd(I) generated, due to steric reasons. Future work in this project will involve the electrochemical generation of $[Pd(\mathbf{L_6})]^{+}$ and its characterization by ESR and UV/Vis spectroscopy. In addition, the study of variable temperature NMR spectra of $[Pd(\mathbf{L_6})]^{2+}$ is also require to detect the presence of any fluxional behavior in solution.

CHAPTER 6

CONCLUSIONS

Several macrocyclic ligands containing nitrogen and sulphur donor atoms as well as with pyridine or thiophene pendant arms were synthesized. The intention is that these ligands may combine the complex properties of aza and thia macrocycles and will therefore stabilize high and low oxidation states of a metal centre.

In this work, Pd(II) complexes had been studied extensively, in particular, the Pd(II) complex of the ligand py[14]aneNS$_3$, (N-(2'-pyridylmethyl)-1,4,7-trithia-11-azacyclotetradecane). In the crystalline state of this complex, the metal centre is pseudo five-coordinate. There is considerable interaction between the bonding orbital of the sulphur atom in the apical position and the palladium metal centre. However, variable temperature NMR studies suggest the presence of two linkage isomers and also several exchange processes are taking place in solution. In one isomer (Isomer A), the complex has a structure similar to that of the crystalline state, with the Pd(II) ion coordinated to nitrogen atoms from the pyridine moiety and the tertiary amine and two thioether atoms from the macrocycle. There is one thioether sulphur atom in the apical position that is not directly bonded to the metal ion. In the other isomer (Isomer B) the Pd(II) ion is coordinated to one nitrogen and three thioether sulphur atoms from the macrocycle, with the pyridine moiety uncoordinated but in close proximity. At temperatures above 0°C, one of the exchange processes involves the commutation of metal-coordinated and -uncoordinated thioether sulphur atoms in Isomer A. At

higher temperatures (ca. >60 °C), the exchange of Isomers A and B can also be detected in the ^{1}H and ^{13}C NMR spectra recorded.

The redox behavior of the Pd(II) complexes in acetonitrile was investigated by cyclic voltammetry. The present study shows that these ligands do not stabilize Pd(I) nor Pd(III) ions. The only exception being the Pd(II) complex with thiophene pendant arms, a quasi-reversible reduction to Pd(I) was observed. The difference in redox behavior between Pd(II) complexes of the pyridine and thiophene pendant arm ligands was interpreted as a consequence of the different mode of coordination of the metal centres in the two ligands. In the case of the pyridine pendant arm complex, the ligand adopts a folded conformation, only the nitrogen atoms from the pyrdine moiety and the tertiary amines from the macrocycle are coordinated to the metal centre. This reduces the in-plane ligand field imposed on the metal ion and upon reduction to Pd(I), which is substitution-labile, rapidly decomposes in solution. On the other hand, the Pd(II) ion is coordinated to two nitrogen and two sulphur donor atoms in a square plane in the thiophene pendant arm complex. This increases the strength of the in-plane ligand field. In addition, there is also one thiophene moiety in close proximity which inhibits the dimerization or polymerization of the Pd(I) ion upon reduction. Hence a quasi-reversible wave is observed.

In summary, studies from this work suggest that the stabilization of a Pd(I) ion in a tetradentate ligand may be best achieved by incorporating soft

donor atoms, e.g. sulphur, in both the ligand framework and the pendant arms. This is because the thioether sulphur atoms can act as π-acceptors which will remove some electron density from the Pd(I) metal centre. In addition, the presence of pendant groups in close promixity to the metal centre may serve as blocking groups which hinder the rapid decomposition of monomeric Pd(I) complexes in solution by processes such as dimerization, polymerization or demetallation.

CHAPTER 7

EXPERIMENTAL METHODS

7.1 Ligand Syntheses

(a) Preparation of 1-thia-4,7-bis(2-pyridylmethyl)-diazacyclononane $\mathbf{L_1}$ (Scheme 4, p.36)

To a round bottomed flask equipped with a magnetic stirrer, reflux condenser and nitrogen inlet was added an ethanolic solution of the dihydrobromide salt of [9]aneSN$_2$ (0.465 g, 1.51 mmol), triethylamine (14.3 mmol, 9.5 eqv.) and 2-(chloromethyl)pyridine hydrochloride (0.50 g, 3.05 mmol). The reaction mixture was refluxed for 12 hours under a nitrogen atmosphere and extracted with chloroform (3 x 100 mL). After the organic phase was washed with water (5 x 100 mL) and dried over anhydrous Na_2SO_4, the solvent was removed by rotatory evaporation. The pale yellow oil obtained contained mainly the desired product with trace amount of unreacted 2-(chloromethyl)pyridine hydrochloride. It was used for metal complexation studies without further purification. Yield: 0.3 g (ca. 60 %). ^{1}H NMR ($CDCl_3$): δ2.65 (s, 4H, NCH_2CH_2N), 2.95 (m, 4H, CH_2N), 3.05 (m, 4H, CH_2S), 3.82 (s, 4H, CH_2-pyridine), 7.12, 7.51, 7.63, 8.48 (m, 8H, pyridine-H). ^{13}C NMR ($CDCl_3$): δ32.01 (CH_2S), 56.03 (NCH_2CH_2N), 58.96 (CH_2N), 64.24 (CH_2-pyridine), 121.82, 123.17, 136.21, 148.87, 160.0 (pyridine-C). MS (CI): 329 (M+1), 357 (M+29).

(b) Preparation of 1,4,7-trithia-11-aza-cyclotetradecane $\mathbf{L_2}$ (Scheme 5)

***Bis(3-hydroxypropyl)amine* (20).** To 500 mL of ethanol contained in a 5 L three-necked round bottom flask provided with a reflux condenser, a mechanical stirrer and a dropping funnel, 117.8 g (1.57 mol) of 3-amino-1-

propanol and 105g (0.99 mol) of Na_2CO_3 were added. The resulting suspension was refluxed. 94.5g (1 mol) of 3-chloro-1-propanol, dissolved in 150 mL of ethanol was added dropwise during the course of 12 hours. Heating was continued overnight. After cooling to room temperature, the solid material was removed by suction filtration. The solvent was removed by rotatory evaporation and the oily residue was distilled under reduced pressure. The fraction passing at 110-120 ° C (ca. 0.1 torr) was collected. The yield was 30%. ^1H NMR (90 MHz, $CDCl_3$): δ3.9 (s, OH, NH, 3H), 3.7 (t, 6 Hz, 4H, CH_2O), 2.75 (t, 6 Hz, 4H, CH_2N), 1.7 (tt, 6 Hz, 4H, $CH_2\underline{CH_2}CH_2$). MS (CI): 134 (M+1), 162 (M+29), 174 (M+41), 116 (M+1-18).

***N-tosylbis(3-(tosyloxy)propyl)amine* (21).** Bis(3-hydroxypropyl)amine (65g, 0.488 mol) was dissolved in 800 mL of distilled CH_2Cl_2 in a 2 L three-necked round bottom flask. The solution was cooled to -5 °C in a stream of dry nitrogen and 218 mL of triethylamine (1.56 mol) was added. With the temperature kept below 0 °C, solid p-toluenesulphonyl chloride (285 g, 1.49 mol) was added in portions to the above solution in the course of 2½ hours. The reaction mixture was stirred in an ice bath for 3 hours and then at ambient temperature overnight. The white triethylamine hydrochloride formed was filtered off and washed with CH_2Cl_2. The pale yellow filtrate was washed with water (5 x 250 mL), 1 M HCl (5 x 250 mL), water (5 x 250 mL) and saturated $NaHCO_3$ solution. The CH_2Cl_2 layer was dried over anhydrous $MgSO_4$. Removal of the solvent by rotatory evaporation resulted a pale yellow

viscous oil which was triturated to a white solid by the addition of diethyl ether. Yield: 232 g (80 %), m.p. 68-69 °C. ^{1}H NMR (250 MHz, $CDCl_3$): δ7.74 (d, 8 Hz, 4H, ArH), 7.58 (d, 8 Hz, 4H, ArH), 7.25 - 7.39 (m, 6H, ArH), 4.00 (t, 7 Hz, 4H, CH_2OTs), 3.05 (t, 7 Hz, 4H, CH_2NTs), 2.42 (s, $ArCH_3$, 6H), 2.40 (s, $ArCH_3$, 3H), 1.84 (tt, 7 Hz, 4H, $CH_2C\underline{H}_2CH_2$). $^{13}C\{^1H\}$ NMR ($CDCl_3$): δ144.9, 143.6, 135.4, 132.7 (quat. ArC), 129.9, 129.8, 127.8, 127.1 (ArC), 67.62 (CH_2OTs), 45.76 (CH_2NTs), 28.62 ($CH_2\underline{C}H_2CH_2$), 21.54, 21.41 ($ArCH_3$). MS (CI) 596 (M+1), 424 (M+1-172). An analytical sample was obtained by recrystallizing the white solid twice with hot ethanol. Calc. for $C_{27}H_{33}NS_3O_8$: C, 54.44; H, 5.58; N, 2.35; S, 16.14. Found: C, 54.33; H, 5.43; N, 2.38; S, 16.53.

***N-tosyl-1,4,7-trithia-11-azacyclotetradecane* (22).** A 5 L three-necked round bottom flask was equipped with reflux condenser, mechanical stirrer and an additional funnel. The entire system was kept under positive nitrogen pressure. The flask was charged with 13 g (40 mmol) of Cs_2CO_3 and 2.2 L of N,N-dimethylformamide (DMF). The suspension was stirred vigorously and heated to 55-60 °C. A solution containing 23.82 (40 mmol) of the tritosylate **(21)** and 5.22 mL of 2-mercaptoethyl sulfide in 300 mL DMF was prepared. Half of this solution was placed in the additional funnel and added to the vigorously stirred suspension of Cs_2CO_3 in DMF over a period of 24 hours. The reaction mixture was charged with another 13.04 g (40 mmol) of Cs_2CO_3 and the second half of the solution containing **(21)** and 2-mercaptoethyl sulfide was added dropwise in the course of a further 24 hours.

After the addition was completed, the reaction mixture was stirred overnight at 55-60 °C. Upon cooling to room temperature, DMF was distilled off by rotatory evaporation. The pale yellow solid obtained was pumped overnight to remove trace amounts of DMF. It was then taken in 500 mL $CHCl_3$ and washed once with 200 mL of distilled water. The $CHCl_3$ layer was dried with anhydrous $MgSO_4$, filtered and roto-evaporated to dryness. The yellow sticky solid was recrystallized in hot $CHCl_3$/EtOH and stored in the refrigerator at 0 °C overnight. The white solid obtained was filtered, washed with diethyl ether and air-dried. Yield: 10 g (62.5%), m.p. 112-118 °C. ^1H NMR (250 MHz, $CDCl_3$): δ7.64, (d, 8 Hz, 2H, ArH), 7.29 (d, 8 Hz, 2H, ArH), 3.11 (t, 7 Hz, 4H, CH_2NTs), 2.73 (s, 8H, SCH_2CH_2S), 2.60 (t, 7 Hz, 4H, CH_2S), 2.40 (s, 3H, $ArCH_3$), 1.92 (tt, 7 Hz, 4H, $CH_2\underline{C}H_2CH_2$). $^{13}C\{^1H\}$ NMR ($CDCl_3$): δ143.5, 136.4 (quat. ArC), 129.8, 127.2 (ArC), 49.5 (CH_2NTs), 31.7, 31.6 (SCH_2CH_2S), 30.1 (CH_2S), 28.8 ($CH_2\underline{C}H_2CH_2$), 21.5 ($ArCH_3$). MS (CI): 406 (M+1), 434 (M+29). An analytical sample was obtained by recrystallizing the white solid twice in hot $CHCl_3$/EtOH. Calc. for $C_{17}H_{27}NS_4O_2$: C, 50.34; H, 6.71; N, 3.45. Found: C, 50.59; H, 6.70, N, 3.71.

1,4,7-trithia-11-azacyclotetradecane **(L_2).** A sample of 3.5 g (8.63 mmol) of **22** in dry THF (20 mL) was added dropwise to a stirred suspension of 4.6 g (0.121 mmol, 14 eqv.) of $LiAlH_4$ in 75 mL dry THF in a three-necked round-bottomed flask equipped with reflux condenser, magnetic stirrer, additional funnel and nitrogen inlet. The reaction mixture was stirred and

refluxed under nitrogen atmosphere for 72 hours. After cooling to room temperature overnight, the excess $LiAlH_4$ was destroyed by dropwise addition of 45 mL THF/H_2O (2:1, v/v). The white solid formed was filtered and carefully washed several times with CH_2Cl_2. The CH_2Cl_2 extracts were combined. Evaporation of the solvent afforded 1.56 g of colorless oil which was used for metal complexation without further purification. ^1H NMR (90 MHz, $CDCl_3$): δ2.60-2.75 (m, 17H, CH_2N, CH_2S, N<u>H</u>), 1.70 (tt, 4H, $CH_2C\underline{H_2}CH_2$). $^{13}C\{^1H\}$ NMR ($CDCl_3$): δ46.7 (CH_2N), 32.3, 31.8 (SCH_2CH_2S), 30.2 (CH_2S), 28.8 ($CH_2\underline{C}H_2CH_2$). MS (EI): 251 (M^+).

(c) Preparation of 1,7-dithia-4,11-diazacyclotetradecane L_3 (Scheme 6)

***N-tosylbis(2-(tosyloxy)ethyl)amine* (23).** Diethanolamine (27.5 g, 0.262 mol) was dissolved in 500 mL of distilled CH_2Cl_2 in a three-necked flask. The solution was cooled to 0 °C in a stream of dry nitrogen and 122 mL of triethylamine (88.6 g, 0.88 mol) was added. With the temperature maintained at 0 °C, solid p-toluenesulfonyl chloride (157 g, 0.823 mol) was added in portions with vigorous stirring in the course of 5 hours. The reaction mixture was stirred at ambient temperature overnight. The Et_3NHCl formed was filtered off and the resulting pale yellow filtrate was washed three times with 1 M HCl, followed by 5 x 200 mL portions of water and 5 x 200 mL portions of saturated $NaHCO_3$ solution. The organic layer was dried over anhydrous $MgSO_4$. Removal of the solvent by rotatory evaporation gave the white product. Yield: 120 g (ca. 80%), m.p. 98 °C. ^1H NMR (90 MHz, $CDCl_3$): δ7.2 -

7.9 (m, 12H, ArH), 4.14 (t, 6 Hz, 4H, CH_2OTs), 3.4 (t, 6 Hz, 4H, CH_2NTs), 2.47 (two singlets, 9H, $ArCH_3$). MS (CI): 568 (M+1), 396 (M-OTs).

***N-Tosylbis(2-bromoethyl)amine* (24).** To a solution of 43 g (0.076 mol) of the tritosylate **23** in 250 mL of DMF was added 40 g (0.39 mol) of NaBr. The resulting suspension was stirred in an oil bath of 120 °C for 4 hours, After cooling to room temperature, the reaction mixture was concentrated by rotatory evaporation to about 50 mL. The viscous milky product mixture was poured into a rapidly stirred 1 L of ice/water mixture where a white solid separated out. This material was filtered, washed with water and air-dried. Yield: 24 g (ca. 80 %), m.p. 56 - 58 °C. ^1H NMR (90 MHz, $CDCl_3$): δ7.36 -7.75 (m, 4H, ArH), 3.5 (s, 8H, CH_2NTs, CH_2Br), 2.45 (s, 3H, CH_3Ar). MS (EI):383, 385, 387 (M^+ in a ratio of 1:2:1).

***N-Tosylbis(3-mercaptopropyl)amine* (25).** To a solution of 20 g of dibromide **24** (0.034 mol) dissolved in 200 mL 95 % ethanol in a 500 mL round-bottomed flask was added 5.6 g of thiourea (0.074 mol). The suspension was refluxed for 12 hours. After cooling to room temperature, the reaction mixture was concentrated by rotatory evaporation and pump-dried. A crystalline white solid of isothiouronium salt was obtained. A solution of 13 g NaOH in 215 mL water (6% NaOH) was prepared and bubbled with nitrogen for 15 minutes. To the white isothiouronium salt was added a 6% de-aerated NaOH solution and the reaction mixture was well stirred and refluxed in nitrogen atmosphere for 2 hours. After the mixture was cooled to room temperature and then further

in an ice bath, 6M HCl was added dropwise until pH of the solution decreased to 1. The milky solution obtained was saturated with NaCl and extracted with 3 x 100 mL CH_2Cl_2. The CH_2Cl_2 layers were combined and dried with anhydrous $MgSO_4$, concentrated by rotavap and pumped. The desired product was isolated as a colorless viscous oil. Yield: 90 %. ^{1}H NMR (90 MHz, $CDCl_3$): δ7.35-7.75 (m, 4H, ArH), 3.20 (t, 4H, 6 Hz, CH_2NTs), 2.6 (q, 4H, 6 Hz, CH_2S), 2.40 (s, 3H, CH_2Ar), 1.90 (m, 4H, $CH_2C\underline{H}_2CH_2$), 1.45 (t, 2H, 6 Hz, SH). MS (CI): 318 (M+1), 348 (M+29), 360 (M+41).

***N,N'-bistosyl-1,7-dithia-4,11-diazacyclotetradecane* (26).** To a 5 L three-necked round flask equipped with a mechanical stirrer, condenser and a high dilution dropping funnel was added oven-dried Cs_2CO_3 (14.8 g, 0.0454 mol) and 1 L of freshly-opened DMF. The resulting suspension was stirred vigorously in an nitrogen atmosphere and warmed to 50 °C. A solution containing the dibromide **(24)** (4.82 g, 0.0125 mol) and dithiol **25** (4 g, 0.0125 mol) in 500 mL of DMF was prepared and bubbled in nitrogen for 20 minutes. It was then transferred to a high dilution funnel and added to the Cs_2CO_3/DMF suspension at a rate of 4 - 5 mL /hr. After the addition of all reactants, the reaction mixture was stirred overnight. Upon cooling to room temperature, DMF was removed by rotatory evaporation. The residual pale yellow solid in the reaction flask was extracted with $CHCl_3$ several times. The yellow solution obtained was rotavap to dryness and pump dried, yielding a pale brown oil which was purified by column chromatography (silica gel, 95% CH_2Cl_2/5%

EtOAc). Fractions with R_f = 0.7 were collected. The desirable product was isolated as a white crystalline solid. Yield: 30 %. ^{1}H NMR (90 MHz, $CDCl_3$): δ7.8 (m, ArH), 7.35 (m, ArH), 3.00 - 3.5 (m, CH_2NTs), 2.5 - 2.9 (m, CH_2S), 2.45 (s, CH_3Ar), 2.00 (m, $CH_2C\underline{H_2}CH_2$). MS (CI): 543 (M+1), 571 (M+29).

1,7-dithia-4,11-diazacyclotetradecane **(L_3).** A sample of 0.5 g (0.92 mmol) of **26** was added slowly to a stirred suspension of 0.41 g (10.8 mmol) of $LiAlH_4$ in 40 mL of dry THF under a nitrogen atmosphere. The reaction mixture was stirred under reflux for 72 hours. After cooling to room temperature, the excess $LiAlH_4$ was destroyed by dropwise addition of 30 mL of THF/H_2O (2:1 v/v). The mixture was filtered and the precipitate was carefully washed with CH_2Cl_2. Evaporation of the solvent afforded 150 mg of L_3 as a white crystalline waxy solid which was used for subsequent reactions without further purification. ^{1}H NMR (90 MHz, $CDCl_3$): δ2.6 - 2.8 (m, 16H, CH_2S, CH_2N), 1.8 (m, 4H, $CH_2C\underline{H_2}CH_2$), 1.45 (s, 2H, NH). MS (CI): 235 (M+1), 263 (M+29), 275 (M+41).

(d) Preparation of N-(2'-pyridylmethyl)-1,4,7-trithia-11-azacyclotetradecane L_4 (Scheme 5)

To a two-necked round bottomed flask equipped with a magnetic stirrer, reflux condenser and nitrogen inlet was added a solution of L_3 (1.12g, 4.5 mmol), triethylamine (1.2g, 11.8 mmol) and 2-(chloroethyl)pyridine hydrochloride (0.73 g, 4.4 mmol) in 50 mL of absolute ethanol. The solution was heated to a gentle reflux under a nitrogen atmosphere for 12 hours. After

cooling to room temperature, $CHCl_3$ (3 x 100 mL) was added to the orange-red reaction mixture. The organic phase was washed with water (5 x 100 mL) and dried over anhydrous Na_2SO_4. The solvent was removed by rotovap and the resultant brown residue was purified by column chromatography (silica gel, 30% EtOAc/70% CH_2Cl_2). Fractions with a R_f value of 0.2 were collected. The title product was obtained as a pale yellow solid. Yield: 500 mg, 33.3 %. ^1H NMR (360 MHz, $CDCl_3$): δ8.49, 7.62, 7.38, 7.14 (m, 4H, pyridine H's), 3.64 (s, 2H, $C\underline{H}_2$-pyridine), 2.70 (s, 8H, $SC\underline{H}_2C\underline{H}_2S$), 2.50 (t, 7 Hz, 8H, $C\underline{H}_2N$, $C\underline{H}_2S$), 1.71 (tt, 7 Hz, 4H, $CH_2C\underline{H}_2CH_2$). $^{13}C\{^1H\}$ NMR ($CDCl_3$): δ159.75 (quat. ArC), 148.8, 136.2, 122.8, 121.8 (ArC), 61.7 ($\underline{C}H_2$-pyridine), 52.8 ($\underline{C}H_2N$), 31.2, 30.8 ($S\underline{C}H_2\underline{C}H_2S$), 29.3 ($CH_2S$), 27.8 ($CH_2\underline{C}H_2CH_2$). MS (CI): 406 (M+1), 434 (M+29).

(e) Preparation of N,N'-bis(2'-pyridylmethyl)-1,7-dithia-4,11-diazacyclotetradecane L_5 (Eq. 7)

To a two-necked round bottomed flask equipped with a magnetic stirrer, reflux condenser and nitrogen inlet was added a solution of L_3 (6.1 mmol), triethylamine (4.5 mL, 32.3 mmol, 5 eqv.) and 2-(chloroethyl)pyridine hydrochloride (2 g, 12.2 mmol) in 50 mL of abs. ethanol. The solution was heated to a gentle reflux under nitrogen atmosphere for 12 hours. After cooling to room temperature, $CHCl_3$ (3 x 100 mL) was added to the orange-red reaction mixture. The organic phase was washed with water (5 x 100 mL) and dried over anhydrous Na_2SO_4. $CHCl_3$ was removed by rotovap and the brown oil obtained was purified by column (silica gel, 60% EtOAc/40% CH_2Cl_2).

Fractions with a R_f value of 0.2 were collected. The title product was obtained as a pale yellow oil. Yield: 500 mg, 20 %. ^1H NMR (250 MHz, $CDCl_3$): δ8.42, 7.61, 7.56, 7.38, 7.07 (m, 8H, pyridine H's), 3.74 (s, 2H, $C\underline{H}_2$-pyridine), 3.62 (s, 2H, $C\underline{H}_2$-pyridine), 2.60 - 2.73 (m, 8H, $C\underline{H}_2S$), 2.51 (t, 7 Hz, 8H, $C\underline{H}_2N$), 1.75 (tt, 7 Hz, 4H, $CH_2C\underline{H}_2CH_2$). $^{13}C\{^1H\}$ NMR ($CDCl_3$): δ159.9, 159.6 (quat. ArC), 148.8, 136.3, 136.1, 122.7, 122.6, 121.8, 121.7 (ArC), 61.3, 61.0 ($\underline{C}H_2$-pyridine), 52.6, 52.1 ($\underline{C}H_2N$), 29.3, 29.2 ($S\underline{C}H_2$), 27.1 ($CH_2\underline{C}H_2CH_2$). MS (CI): 417 (M+1), 445 (M+29).

(f) Preparation of N,N'-bis(2'-thiophenemethyl)-1,7-dithia-4,11-diazacyclotetradecane L_6 (Scheme 13)

(i) Formation of an amide: To a two-necked round bottomed flask equipped with a magnetic stirrer and nitrogen inlet was added a solution of L_3 (1.5g, 6.41 mmol) and triethylamine (2 mL, 14.3 mmol) in toluene. The mixture was stirred and cooled in an ice bath. 1.878 g (12.8 mmol) of 2-thiophenecarbonyl chloride was added. After stirring in an ice bath for 2 hours, the reaction mixture was stirred overnight at ambient temperature and the NEt_3HCl which formed was filtered. The reaction flask was rinsed with toluene several times. The toluene extracts were combined and washed with 100 mL H_2O, saturated $NaHCO_3$ solution and again with 100 mL H_2O. The organic layer was dried by anhydrous $MgSO_4$, rota-evaporated and pumped. The yellow oil obtained was purified by column (silica gel, 10 % EtOAc/90 % CH_2Cl_2). Fractions with an R_f value of 0.2 were collected. The amide was

isolated as a white solid. Yield: 1 g (34 %). ^{1}H NMR (360 MHz, $CDCl_3$): δ7.02 - 7.64 (m, 6H, thiophene H's), 3.65 (m, 8H, C$\underline{H_2}$-N-C=O), 2.89 (m, 4H, C$\underline{H_2}$S), 2.62 (m, 4H, C$\underline{H_2}$S), 2.03 (m, 4H, $CH_2C\underline{H_2}CH_2$). ^{13}C{^{1}H} NMR ($CDCl_3$): δ164.8, 164.5 (C=O), 137.1, 136.7 (quat. ArC), 128.8, 128.7, 128.3, 126.7, 126.6 (ArC), 48.9, 47.5 (C$\underline{H_2}$-N-C=O), 29.2 (S$\underline{C}H_2$), 27.9 ($CH_2\underline{C}H_2CH_2$). MS (CI): 455 (M+1), 483 (M+29).

(ii) Reduction of the amide: A sample of 0.5 g (10.0 mmol) of the diamide was slowly added to a stirring suspension of 0.93 g (24.5 mmol) of $LiAlH_4$ in 40 mL of dry THF in a two-necked round bottomed flask under nitrogen atmosphere. The reaction mixture was stirred and refluxed for 24 hours. After cooling to room temperature, the reaction flask was cooled in an ice bath. The excess of $LiAlH_4$ was destroyed by dropwise addition of THF/H_2O (100 mL THF/25 mL H_2O). The product mixture was acidified to pH 1 by dropwise addition of conc. HCl. An additional 50 mL of water was then added and the solution was stirred at room temperature for 2 hours. NaOH pellets were added until pH of the solution was 13 and the product mixture was extracted with CH_2Cl_2. The organic extract was dried by anhydrous $MgSO_4$. Evaporation of the solvent afforded 460 mg of $\mathbf{L_6}$ as a white solid which was used for subsequent complexation studies without further purification. ^{1}H NMR (250 MHz, $CDCl_3$): δ6.9 - 7.3 (m, 6H, thiophene H's) 3.9 (s, 2H, CH_2-thiophene), 3.7 (s, 2H, CH_2-thiophene), 2.8 (m, 4H, CH_2S), 2.5 - 2.7 (m, 4H, CH_2N), 1.8 (m, 4H, $CH_2C\underline{H_2}CH_2$). ^{13}C{^{1}H} NMR ($CDCl_3$): δ143.2, 142.1 (quat.

ArC), 126.3, 126.2, 125.6, 125.2, 124.8, 124.5 (ArC), 53.5, 53.4 ($\underline{C}H_2$-thiophene), 52.3, 51.8 (CH_2N), 29.5, 29.4 ($S\underline{C}H_2$) , 27.5 ($CH_2\underline{C}H_2CH_2$).

7.2 Syntheses of Pd(II) complexes

[Pd(L$_1$)](BF$_4$)$_2$. To an acetonitrile solution of L_1 (0.11 g, 0.335 mmol) was added $[Pd(CH_3CN)_4](BF_4)_2$ (0.13 g, 0.293 mmol) and the orange brown solution obtained was heated to a gentle reflux for an hour under a nitrogen atmosphere to ensure complete complexation. After cooling to room temperature, the solution was taken to dryness to give an orange brown solid. Slow diffusion of diethyl ether into an acetonitrile solution of the Pd(II) complex yielded orange brown crystals of X-ray quality. Yield: 120 mg. Anal. Calcd for $C_{18}H_{24}N_4SPdB_2F_8$: C, 35.53; H, 3.98; N, 9.21. Found: C, 35.74; H, 3.91; N, 9.29.

[Pd(L$_2$)]$^{2+}$. $PdCl_2$ (0.25g, 1.41 mmol) was added to 40 mL of dry CH_3CN in a round bottomed flask equipped with a nitrogen inlet and reflux condenser. The yellow solution was stirred and warmed to 55 °C until most of the $PdCl_2$ dissolved. The trace amount of insoluble $PdCl_2$ was filtered. The yellow $Pd(CH_3CN)_2Cl_2/CH_3CN$ solution was added dropwise to an acetonitrile solution containing $\mathbf{L_2}$ (0.354 g). A yellow precipitate formed instantly and the reaction mixture was stirred at room temperature overnight. The yellow precipitate was filtered, washed with anhydrous diethyl ether and air-dried. Yield: 0.34 g. The yellow $Pd(\mathbf{L_2})Cl_2$ (100 mg) was then dissolved in absolute EtOH and added to a saturated ethanolic solution of NH_4PF_6. The creamy yellow

precipitate formed was filtered and redissolved in the minimum amount of CH_3CN. Slow diffusion of diethyl ether into the supernatant yielded yellow crystals suitable for X ray crystallography. Yield: 150 mg. Anal. Calcd for $C_{10}H_{21}NS_3PF_6ClPd.(H_2O)$: C, 21.59; H, 4.17; N, 2.52. Found: C, 21.65; H, 3.91; N, 2.85.

[Pd(L$_4$)Cl](PF$_6$). To a two necked round bottom flask containing 10 mL solution of 0.0467 M L_4 in dichloromethane (0.467 mmol) was added an acetonitrile solution of 0.142 g $Pd(PhCN)_2Cl_2$ (0.37 mmol) and the reaction mixture was stirred at room temperature under nitrogen atmosphere overnight. A creamy yellow precipitate was formed, leaving a very pale yellow supernatant. The yellow precipitate was filtered under suction, washed with diethyl ether and dried. The PF_6^- salt was obtained by dissolving the yellow solid in hot methanol and added to a saturated methanolic solution of NH_4PF_6. After stirring on a hot plate for 30 minutes, methanol was removed by rotavap. The solid which remained was dissolved in acetonitrile and yellow crystals were obtained by slow evaporation. Yield : 180 mg (77 %). Anal. Calc. for $[Pd(C_{16}H_{26}N_2S_3)Cl](PF_6)$: C, 30.53; H, 4.16; N, 4.45. Found: C, 30.82; H, 4.11; N, 4.68. IR: Pd-Cl, 340 cm^{-1}; PF_6^-, 530, 560, 770, 830, 880 cm^{-1}.

[Pd(L$_4$)](BF$_4$)$_2$. An acetonitrile solution of L_4 (0.174 g, 0.51 mmol) in a round bottomed flask was purged with nitrogen for 10 minutes. An acetonitrile solution of $[Pd(CH_3CN)_4](BF_4)_2$ (0.20 g, 0.45 mmol) was added dropwise to the ligand solution. The reaction mixture changed to orange-

brown and was heated to a gentle reflux under a nitrogen atmosphere for 1½ hour to ensure complete complexation. After cooling to room temperature, the orange brown solution was concentrated to ~ 1 mL. Slow diffusion of diethyl ether into the acetonitrile solution of the Pd(II) complex yielded orange-brown crystals of X- ray quality. Yield: 200 mg. (71 %). Anal. Calcd for $C_{16}H_{26}N_2S_3PdB_2F_8.(½\ CH_3CN)$: C, 31.75; H, 4.31; N, 5.44. Found: C, 31.71; H, 4.29; N, 5.42.

$Pd(L_6)(BF_4)_2$. To an acetonitrile solution of L_6 (0.215 mmol) was added $[Pd(CH_3CN)_4](BF_4)_2$ (0.0795 g, 0.179 mmol) and the lemon-yellow solution obtained was heated to a gentle reflux for an hour under nitrogen atmosphere to ensure complete complexation. After cooling to room temperature, the solution was taken to dryness to give a yellow powder. The yellow solid was recrystallized by dissolving in minimum amount of $CH_3NO_2/CH_2Cl_2/EtOH$. Slow evaporation of the solvent yielded yellow crystals of X-ray quality. Yield: 80 mg (66.6 %). Anal. Calcd for $C_{20}H_{30}N_2S_4PdB_2F_8.(CH_3OH)(H_2O)(CH_3NO_2)$: C, 32.30; H, 4.80; N, 5.14. Found: C, 32.67; H, 4.37; N, 5.19.

7.3 Syntheses of Co(II), Ni(II) and Cu(II) complexes

$[Co(L_4)(CH_3CN)(NO_3)_2].xCH_3CN$. An acetonitrile solution of L_4 (0.06 g, 0.175 mmol) in a round bottomed flask was purged with nitrogen for 20 minutes. An acetonitrile solution of $[Co(H_2O)_6](NO_3)_2$ (0.0496 g, 0.17 mmol) was added dropwise to the ligand solution. The reaction mixture changed to pink and was stirred at room temperature under a nitrogen atmosphere

overnight to ensure complete complexation. The pink soluion was concentrated to ~ 1 mL on rotavap. Slow evaporation of the solvent at room temperature yielded pink crystals of X-ray quality. Yield: 40 mg. Anal. Calcd for $C_{18}H_{29}N_5S_3O_6Co.(½CH_3CN)$: C, 37.39; H, 5.07; N, 11.54. Found: C, 37.54; H, 4.93; N: 11.99.

[Ni(L$_4$)(CH$_3$CN)](ClO$_4$)$_2$. An acetonitrile solution of L_4 (0.170 g, 0.496 mmol) in a round bottomed flask was purged with nitrogen for 20 minutes. An acetonitrile solution of $[Ni(H_2O)_6](ClO_4)_2$ (0.145 g, 0.396 mmol) was added dropwise to the ligand solution. The reaction mixture changed to purple and was stirred at room temperature under nitrogen overnight to ensure complete complexation. The purple solution was concentrated by rotoevaporation to ~ 1 mL. Slow evaporation of the solvent at room temperature yielded purple crystals of X-ray quality. Yield: 200 mg (83 %). Anal. Calcd for $C_{16}H_{26}N_2S_3Cl_2O_8Ni.(2CH_3CN)$: C, 35.20; H, 4.73; N, 8.21. Found: C, 35.05; H, 4.60; N: 7.79.

[Cu(L$_4$)](ClO$_4$)$_2$. A CH_2Cl_2 solution of L_4 (0.059 g, 0.172 mmol) in a round bottomed flask was purged with nitrogen for 20 minutes. An ethanolic solution of $[Cu(H_2O)_6](ClO_4)_2$ (0.060 g, 0.16 mmol) was added dropwise to the ligand solution. The reaction mixture changed to bluish green and was stirred at room temperature under nitrogen overnight to ensure complete complexation. The green precipitate formed was filtered, washed with diethyl ether and air-dried. Yield: 55 mg (57 %). The green powder was recrystallized

by dissolving in EtOH/CH_3CN. Some microcrystalline green solid was obtained. Anal. Calcd for $C_{16}H_{26}N_2S_3O_8Cl_2Cu$: C, 31.76; H, 4.33; N, 4.63. Found: C, 31.86; H, 4.18; N: 4.69.

[Cu(L_5)](ClO$_4$)$_2$. A CH_2Cl_2 solution of L_5 (0.164 mmol) in a round bottomed flask was purged with nitrogen for 20 minutes. An ethanolic solution of $[Cu(H_2O)_6](ClO_4)_2$ (0.058 g, 0.156 mmol) was added dropwise to the ligand solution. The reaction mixture changed to green and was stirred at room temperature under nitrogen overnight to ensure complete complexation. The green precipitate formed was filtered, washed with diethyl ether and air-dried. Yield: 66 mg (66 %). The green powder was recrystallized by dissolving in EtOH/CH_3CN. Slow evaporation of the solvent at room temperature yielded green crystals of X-ray quality. Anal. Calcd for $C_{22}H_{32}N_4S_2O_8Cl_2Cu$: C, 38.91; H, 4.75; N, 8.25. Found: C, 38.83; H, 4.69; N: 8.19.

7.4 Instrumentation

(a) Electrochemistry

Cyclic voltammograms presented in this study were recorded with a Princeton Applied Research Model 273 Potentiostat/Galvanostat interfaced to an IBM PC computer and an EPSON FX-80 dot matrix printer. All measurements were carried out in acetonitrile, which was dried before use by distilling over calcium hydride overnight under nitrogen atmosphere. A solution of 0.1 M n-Bu_4NPF_6 in acetonitrile was used as the supporting electrolyte. Platinum beads were used as the working electrode and counter

electrode. The reference electrode was $Ag/AgNO_3$ (0.01 M in CH_3CN) linked to the cell via a salt bridge containing an acetonitrile solution of n-Bu_4NPF_6 (0.1 M).

(b) Crystallography

The crystal structures presented in this thesis were solved by Ms. K Beveridge. In general, the crystallographic data were obtained as follows. Crystals were mounted in glass Lindemann tubes. The unit cells and space groups were determined by using Weissenberg and precession photography, after which the crystals were transferred to a Picker four-circle diffractometer automated with a PDP 11/10 computer or an Enraf Nonius CAD4 diffractometer to collect the data. Intensity measurements were obtained with Zr-filtered Mo radiation, $\lambda = 0.71069$ Å. Background counting was introduced at the end of each scan. A set of three internal standard reflections preceded each batch of 50 measurement, with no noticeable change in intensity observed during the collection.

The solution of the phase problem was achieved with MULTAN[119] and refined by direct methods with SHELX-76[120]. The atomic scattering factors used were those included in the SHELX-76 program together with the metal *f*-curve from the International Tables[121]. Completion and refinement of the structure was carried out by using difference electron density maps and least-squares techniques. All atoms were refined anisotropically except for hydrogen atoms, which were observed and refined isotropically when possible, otherwise,

the H-atoms positions were calculated. In general, the refinement converged with a maximum shift/e.s.d. of less than 0.2 on the final cycle.

(c) Electron Spin Resonance

ESR spectra were obtained by use of a Varian E6 ESR spectrometer using DPPH (2,2-diphenyl-1-picrylhydrazyl hydrate, a stable free radical) as the external standard. The stimulated transition between two spin states is achieved by keeping the energy of stimulation constant and scanning the magnetic field. The energy source is a microwave generator which emits a radiation of wavelength 3.2 cm. This corresponds to a frequency of 9.2 GHz which is sent to the sample by a waveguide apparatus. The low temperature spectra were obtained using a quartz insert dewar filled with liquid nitrogen.

(d) Nuclear Magnetic Resonance

^{1}H NMR spectra were recorded on a 90 MHz Perkin-Elmer R-32 instrument, high-field ^{1}H and ^{13}C NMR spectra were obtained on either Brüker WM 250 or AMX 360 instrument. Two-dimensional NMR spectra (e.g., ^{1}H COSY and ^{1}H-^{13}C correlated spectra) were recorded on the Brüker AMX 360 instrument by Ms. C. Greenwood. All chemical shifts are reported relative to tetramethylsilane (TMS). Simulated ^{1}H and ^{13}C NMR spectra were calculated using NMRPLOT[122] on an IBM PS/2 computer. The program enables the iterations of the coupling constants once an approximate set of values was obtained from visual line shape analysis.

(e) Other Instrumentation

Infrared spectra were obtained as neat samples on NaCl plates or KBr discs by using either Perkin-Elmer 283 grating spectrometer or Brüker FT IR spectrometer. Mass spectra of all organic intermediates and the ligands were obtained from a Finnegan GC 360 mass spectrograph by electron impact or chemical ionization methods.

UV-visible spectra were run on a Cary 5 UV-Vis-NIR dual beam spectrophotometer.

Elemental analyses were performed by Canadian Microanalytical Services, Vancouver, BC, Canada.

REFERENCES

1. F.A. Cotton and G. Wilkinson, "Advanced Inorganic Chemistry", 5th Ed., John Wiley and Sons, New York, 1988.

2. J.C. Bailar in "Coordination Chemistry. Vol. I", A.C.S. Monograph 168, A.E. Martell Ed., Van Nostran Reinhold Co., 1971, ix.

3. W.W. Porterfield, "Inorganic Chemistry - A Unified Approach", Addison-Wesley Publishing Company Inc., 1984, pp. 465-505.

4. G.B. Kauffman, *J. Chem. Educ.*, **36**, 521 (1959).

5. (a) J.D. Lee, "A New Concise Inorganic Chemistry", 3rd Ed., Van Nostrand Reinhold Co. Ltd., London, 1977, Ch. 8; (b) I.B. Butler and J.F. Harrod, "Inorganic Chemistry - Principles and Applications", Benjamin and Cummings Publishing Co. Inc., Redwood City, 1989, Ch. 12.

6. N.V. Sidgwick, "The Electronic Theory of Valency", Clarendon Press, Oxford, 1927.

7. L. Pauling, "The Nature of the Chemical Bond", 3rd Ed., Cornell University Press, Ithaca, New York, 1960.

8. M. Bethe, *Ann. Physik.*, **3**, 133 (1929).

9. J.H. Van Vleck, "Theory of Electric and Magnetic Susceptibilities", Oxford University Press, London, 1932.

10. (a) A. Yamamoto, "Organotransition Metal Chemistry: Fundamental Concepts and Applications", John Wiley and Sons, New York, 1986, Ch.2; (b) L.E. Orgel, "An Introduction to Transition Metal Chemistry, Ligand Field Theory", 2nd Ed., Methuen, London, 1966; (c) C.J. Ballhausen, "Introduction to Ligand Field Theory", McGraw-Hill, New York, 1962.

11. R.S. Mulliken, *Phys. Rev.*, **40**, 55 (1932).

12. (a) F.A. Cotton, "Chemical Application of Group Theory", 2nd Ed., New York, 1971; (b) S.F.A. Kettle, "Coordination Compounds", Appleton, Century, 1969.

13. A.E. Derome, "Modern NMR Techniques for Chemical Research", Pergamon Press, Oxford, 1987.

14. B.A. Goodman and J.B. Raynor, *Adv. Inorg. Chem. and Radiochem.*, **13**, 135 (1970).

15. E.A.V. Ebsworth, D.W.H. Rankin and S. Cradock, "Structural Methods in Inorganic Chemistry", Blackwell, Oxford, 1987.

16. J. Burgess, "Ions in Solution: Basic Principles of Chemical Interactions", Ellis Horwood Ltd., Chichester, 1988, Ch. 6.

17. (a) S. Ahrland, J. Chatt and N.R. Davies, *Quart. Rev.*, **12**, 265 (1958); (b) R.G. Pearson, *J. Chem. Educ.*, **45**, 581, 643 (1968).

18. (a) R.D. Hancock and A.E. Martell *Comments Inorg. Chem.*, **6**, 237 (1988); (b) R.D. Hancock and F. Marsicano, *J. Chem. Soc. Dalton Trans.*, 1066 (1976); (c) J.R. Frausto da Silva, *J. Chem. Educ.*, **60**, 390 (1983).

19. D.F. Shriver, P.W. Atkins and C.H. Langford, "Inorganic Chemistry", Oxford University Press, 1990, p. 220.

20. (a) L.F. Lindoy, "The Chemistry of Macrocyclic Ligand Complexes", Cambridge University Press, Cambridge, 1989; (b) G.A. Melson, "Coordination Chemistry of Macrocyclic Compounds", Plenum Press, New York, 1979.

21. C.J. Pedersen, *J. Am. Chem. Soc.* **89**, 2495, 7017 (1967).

22. B. Dietrich, J.M. Lehn and J.P. Sauvage, *Tetrahedron Lett.*, 2885, 2889 (1969).

23. D.K. Cabbiness and D.W. Margerum, *J. Am. Chem. Soc.*, **91**, 6540 (1969).

24. B.L. Haymore, J.D. Lamb, R.M. Izatt and J.J. Christensen, *Inorg. Chem.*, **21**, 1598 (1982).

25. D. Hinz and D.W. Margerum, *Inorg. Chem.*, **13**, 2941 (1974).

26. (a) G.J. McDougall, R.D. Hancock and J.C.A. Boeyens, *J. Chem. Soc. Dalton Trans.*, 1438 (1978); (b) A. Anicini, L. Fabbrizzi, P. Paoletti and R.M. Clay, *J. Chem. Soc. Dalton Trans.*, 577 (1978); (c) D.J. Cram, T. Kaneda, R.C. Helgeson, S.B. Brown, C.B. Knobler, E. Maverick and K.N. Trueblood, *J. Am. Chem. Soc.*, **107**, 3645 (1985).

27. R.D. Hancock and G.J. McDougall, *J. Am. Chem. Soc.*, **102**, 6551 (1980).

28. (a) L.L. Diaddario, L.L. Zimmer, T.E. Jones, L.S.W.L. Sokol, R.B. Cruz, E.L. Yee, L.A. Ochrymowycz and D.B. Rorabacher, *J. Am. Chem. Soc.*, **101**, 3511 (1979); (b) L.S.W.L. Sokol, L.A. Ochrymowycz and D.B. Rorabacher, *Inorg. Chem.*, **20**, 3189 (1981).

29. (a) J.R. Hartman, R.E. Wolf, B.M. Foxman and S.R. Cooper, *J. Am. Chem. Soc.*, **105**, 131 (1983); (b) R.E. Wolf, J.R. Hartman, J.M.E. Storey, B.M. Foxman and S.R. Cooper, *J. Am. Chem. Soc.*, **109** , 4328 (1987).

30. D.H. Busch, *Acc. Chem. Res.*, **11**, 392 (1978).

31. J.D. Vitiello and E.J. Billo, *Inorg. Chem.*, **19** 3477 (1980)

32. E.J. Billo, *Inorg. Chem.*, **23**, 236 (1984).

33. C.F. Cook and N.F. Curtis, *J. Chem. Soc., Chem. Commun.*, 962 (1967).

34. (a) D.C. Olson and J. Vasilevskis, *Inorg. Chem.*, **8**, 1611 (1969); (b) D.C. Olson and J.Vasilevskis, *Inorg. Chem.*, **10**, 463 (1971).

35. F.V. Lovecchio, E.S. Gore and D.H. Busch, *J. Am. Chem. Soc.*, **96**, 3109 (1974).

36. L. Fabbrizzi, *Comments in Inorg. Chem.*, **4**, 33 (1985).

37. (a) M.O. Kestner and A.L. Allred, *J. Am. Chem. Soc.*, **94**, 7189 (1972); (b) E.K. Barefield and M.T. Mocella, *Inorg. Chem.*, **12**, 2829 (1973).

38. A. McAuley and T.W. Whitcombe, *Inorg. Chem.*, **27**, 3090 (1988).

39. A.J. Blake, A.J. Holder, T.I. Hyde and M. Schröder, *J. Chem. Soc., Chem. Commun.*, 987 (1987).

40. A.J. Blake, R.O.Gould, T.I. Hyde and M. Schröder, *J. Chem. Soc., Chem. Commun.*, 431 (1987).

41. G. Reid, A.J. Blake, T.I. Hyde and M. Schröder, *J. Chem. Soc., Chem. Commun.*, 1397 (1988).

42. R.M. Izatt and J.J. Christensen (ed.), *Prog. in Macrocyclic Chemistry*, **3**, 1 (1987)

43. A.B.P. Lever, *Advances in Inorganic Chemistry and Radiochemistry*, **7**, 27 (1965).

44. N.F. Curtis, *J. Chem. Soc.*, 4409 (1960).

45. M.C. Thompson and D.H. Busch, *J. Am. Chem. Soc.* **86**, 3651 (1964).

46. E.L. Blinn and D.H. Busch, *Inorg. Chem.*, **7**, 820 (1968).

47. (a) E.K. Barefield, F. Wagner, A.W. Herlinger and A.R. Dahl, *Inorg. Synth.*, **16**, 220 (1976); (b) B. Bosnich, C.K. Poon, M.L. Tobe, *Inorg. Chem.*, **4**, 1102 (1965).

48. (a) G.A. Melson and D.H. Busch, *J. Am. Chem. Soc.*,**87**, 1706 (1965); (b) S.C. Cummings and D.H. Busch, *J. Am. Chem. Soc.*, **92**, 1924 (1970).

49. A.M. Sargeson, *Pure and Applied Chemistry*, **56**, 2603 (1984), and references therein.

50. (a) C.C. Deitrich-Buchecker, J.-P. Sauvage and J.-M. Kern, *J. Am. Chem. Soc.*, **106**, 3043 (1984); (b) J.-P. Sauvage, *Acc. Chem. Res.*, **23**, 345 (1990) and references therein.

51. S.M. Nelson, *Pure and Applied Chemistry*, **52**, 461 (1980).

52. L. Rossa and F. Vögtle, in *Topics in Current Chemistry*, **113**, 1 (1983).

53. (a) W. Rosen and D.H. Busch, *J. Am. Chem. Soc.*, **91**, 4694 (1969); (b) K. Travis and D.H. Busch, *Inorg. Chem.*, **13**, 2951 (1974).

54. (a) J.E. Richman and T.J. Atkins, *J. Am. Chem. Soc.*, **96**, 2268 (1974); (b) T.J. Atkins, J.E. Richman and W.F. Oettle, *Org. Synthesis*, **58**, 87 (1978).

55. (a) J.Buter, R.M. Kellogg, *J. Chem. Soc., Chem. Commun.*, 466 (1980); (b) J. Buter, R.M. Kellogg, *J. Org. Chem.*, **46**, 4481 (1981); (c) J. Buter, R.M. Kellogg and F. van Bolhuis, *J. Chem. Soc., Chem. Commun.*, 282 (1990).

56. J. Buter and R.M. Kellogg, *Org. Synthesis*, **65**, 150 (1987).

57. (a) B. Dietrich, J.M. Lehn and J.P. Sauvage, *J. Chem. Soc. Chem. Commun.*, 1055 (1970); (b) A.A. Alberts, R. Annunziata and J.M. Lehn, *J. Am. Chem. Soc.*, **99**, 8502 (1977); (c) R. Louis, Y. Agnus and R. Weiss, *J. Am. Chem. Soc.*, **78**, 3604 (1978); (d) R. McCrindle, G. Ferguson, A.J. McAless, M. Parvez and D.K. Stephenson, *J. Chem. Soc. Dalton Trans.*, 1291 (1982), *ibid.*, 1865 (1983); (e) L. Siegfried and Th.A. Kaden, *Helv. Chimica Acta*, **67**, 29 (1984); (f) M. Micheloni, P. Paoletti, L. Siefgried-Hertli and Th.A. Kaden, *J. Chem. Soc. Dalton Trans.*, 1169 (1985); (g) M. Kodama, T. Koike, N. Hoshiga, R. Machida and E. Kimura, *J. Chem. Soc. Dalton Trans.*, 673 (1984); (h) H.-J. Krüger and R.H. Holm, *Inorg.*

Chem., **26**, 3647 (1987); (i) U. Kallert and R. Mattes, *Inorg. Chimica Acta*, **180**, 263 (1991).

58. K.D. Karlin, J.A. Zubieta, Ed., "Copper Coordination Chemistry: Biochemical and Inorganic Perspectives", Adenine Press, New York, 1983.

59. F.R. Hartley, "The Chemistry of Platinum and Palladium", Applied Science Publishers, London, 1973.

60. P. Chaudhuri and K. Wieghardt, *Prog. Inorg. Chem.*, **35**, 329 (1987).

61. A.J. Blake and M. Schröder, *Adv. Inorg. Chem.*, **35**, 1 (1990).

62. (a) J.C.A. Boeyens, S.M. Dobson and R.D. Hancock, *Inorg. Chem.*, **24**, 3073 (1985); (b) S.M. Hart, J.C.A. Boeyens, J.P. Michael and R.D. Hancock, *J. Chem. Soc. Dalton Trans.*, 1601 (1983).

63. A. McAuley and S. Subramanian, *Inorg. Chem.*, **29**, 2830 (1990).

64. (a) A. McAuley, P.R. Norman and O. Olubuyide, *Inorg. Chem.*, **23**, 1938 (1985); (b) R.I. Haines and A. McAuley, *Coord. Chem. Rev.*, **39**, 77 (1981); (c) L. Fabbrizzi and D.M. Proserpio, *J. Chem. Soc. Dalton Trans.*, 229 (1989).

65. F. Hori, M. Matsumoto, S. Ooi and H. Kuroya, *Bull. Chem. Soc. Jpn.*, **50**, 138 (1977).

66. (a) A.J. Blake, A.J. Holder, T.I. Hyde, Y.V. Roberts, A.J. Lavery and M. Schröder, *J. Organomet. Chem.*, **323**, 261 (1987); (b) K. Weighardt, H.J. Küppers, E. Raabe and C. Krüger, *Angew. Chem. Int. Ed. Eng.*, **25**, 1101 (1986).

67. A. Bondi, *J. Phys. Chem.*, **68**, 441 (1964).

68. (a) G. Hunter, A. McAuley and T.W. Whitcombe, *Inorg. Chem.*, **27**, 2634 (1988); (b) T.W. Whitcombe, Ph.D. Thesis, University of Victoria, 1988.

69. D.G. Fortier, Ph.D. Thesis, University of Victoria, B.C., 1988.

70. A.R. Rossi and R. Hoffmann, *Inorg. Chem.*, **14**, 365 (1975).

71. E.L. Muetterties and R.A. Schunn, *Q. Rev.*, **20**, 245 (1966).

72. (a) J.W. Collier, F.G. Mann, D.G. Watson, H.R. Watson, *J. Chem. Soc.*, 1803 (1964); (b) C.M. Harris, R.S. Nyholm, *J. Chem. Soc.*, 4375 (1956);

(c) O.S.C. Headley, R.S. Nyholm, C.A. McAuliffe, L. Sindellari, M.L. Tobe, L.M. Venanzi, *Inorg. Chim. Acta*, **4**, 93 (1970); (d) T. Tarantelli, C.J. Furlani, *J. Chem. Soc. A*, 1717 (1970); (e) G. Dyer, M.O. Workman, D.W. Meek, *Inorg. Chem.*, **6**, 1405 (1967).

73. (a) S. Yamazaki, *Inorg. Chem.*, **21**, 1638 (1982); (b) S. Yamazaki, *Polyhedron*, **4**, 1915 (1985); (c) Z. Taira and S. Yamazaki, *Bull. Chem. Soc. Jpn.*, **59**, 649 (1986).

74. K. Wieghardt, E. Schöffmann, B. Nuber, J. Weiss, *Inorg. Chem.*, **25**, 4877 (1986).

75. D.G. Fortier and A. McAuley, *Inorg. Chem.*, **28**, 655 (1989).

76. K. Coulter and A. McAuley, unpublished results.

77. M.J. Karplus, *J. Am. Chem. Soc.*, **85**, 2870 (1963).

78. H. Günther, "NMR Spectroscopy: An Introduction", John Wiley and Sons, New York, 1980.

79. A.G. Lappin and A. McAuley, *Adv. in Inorg. Chem.*, **32**, 241 (1988).

80. (a) E.K. Barefield, A. Bianchi, E.J. Billo, P.J. Connolly, P. Paoletti, J.S. Summers and D.G. Van Derveer, *Inorg. Chem.*, **25**, 4197 (1986); (b) V.J. Thöm, C.C. Fox, J.C.A. Boeyens and R.D. Hancock, *J. Am. Chem. Soc.*, **106**, 5947 (1984); (c) L.S. Sabatini and L. Fabbrizzi, *Inorg. Chem.*, **18**, 438 (1979).

81. (a) S.R. Cooper and S.C. Rawle, *Structure and Bonding*, **72**, 1 (1990); (b) S.R. Cooper, *Acc. Chem. Res.*, **21**, 141 (1988).

82. R.E. DeSimone and M.D. Glick, *J. Am. Chem. Soc.*, **98**, 762 (1976).

83. R.E. DeSimone, M.D. Glick, *J. Am. Chem. Soc.*, **97**, 942 (1975).

84. T. Yoshida, T. Ueda, T. Adachi, K. Yamamoto, T. Higuchi, *J. Chem. Soc. Chem. Commun.*, 1137 (1985).

85. D.St.C. Black and I.A. McLean, *J. Chem. Soc., Chem. Commun.*, 1004 (1968); *Tetrahedron Lett.*, 3961 (1969); *Aust. J. Chem.*, **24**, 1401 (1971).

86. B.C. Westerby, K.L. Juntunen, G.H. Leggett, V.B. Pett, M.J. Koenigbauer, M.D. Purgett, M.J. Taschner, L.A. Ochrymowycz and D.B. Rorabacher, *Inorg. Chem.*, **30**, 2109 (1991).

87. H. Koyama and T. Yoshino, *Bull. Chem. Soc. Jpn.*, **45**, 481 (1972).

88. P.L. Anelli, F. Montanari and S. Quici, *J. Org. Chem.*, **53**, 5291 (1988).

89. D. Waknine, M.J. Heeg, J.F. Endicott and L.A. Ochrymowycz, *Inorg. Chem.*, **30**, 3691 (1991).

90. K. Toriumi, M. Yamashita, H. Ito, T. Ito, *Acta Crystallogr.* **C42**, 963 (1986).

91. (a) F.D. Rochen, R. Melanson, *Acta Crystallogr.*, **B36**, 691 (1980); (b) P.Khodadad, N. Rodier, *Acta Crystallogr.*, **C43**, 1690 (1987).

92. (a) W.A. Freeman, *Inorg. Chem*, **15**, 2235 (1976); (b) P.R. Robinson, E.O. Schlemper, R.K. Murmann, *Inorg. Chem.*, **14**, 2035 (1975).

93. (a) E.W. Abel, S.K. Bhargava and K.G. Orrell, *Prog. Inorg. Chem.*, **32**, 1 (1984); (b) K.G. Orrell, *Coord. Chem. Rev.*, **96**, 1 (1989).

94. E.W. Abel, R.P. Bush, F.J. Hopton and C.R. Jenkins, *J. Chem. Soc. Chem. Commun.*, 58 (1966).

95. S. Liu, C.R. Lucas, M.J. Newlands and J.-P.Charland, *Inorg, Chem.*, **29**, 4380 (1990).

96. (a) E.W. Abel, P.D. Beer, I. Moss, K.G. Orrell, V. Sik, P.A. Bates and M.B. Hursthouse, *J. Chem. Soc. Chem. Commun.*, 978 (1987); (b) E.W. Abel, P.D. Beer, I. Moss, K.G. Orrell and V. Sik, *J. Organomet. Chem.*, **341**, 559 (1988).

97. A.B.P. Lever, "Inorganic Electronic Spectroscopy", Elsevier, New York, 1968.

98. (a) R. Cammack, *Adv. Inorg. Chem.*, **32**, 297 (19880: (b) N. Baidya, M.M. Olmstead, J.P. Whitehead, A. Bagyinka, M.J. Maroney and P.K. Mascharak, *Inorg. Chem.*, **31**, 3612 (1992); (c) M.J. Karoney, G.J. Colpas, C. Bagyinka, N. Baidya, P.K. Mascharak, *J. Am. Chem. Soc.*, **113**, 3962 (1991); (d) M.J. Maroney, G.J. Colpas, C. Bagyinka, *J. Am. Chem. Soc.*, **112**, 7067 (1990).

99. A.G. Sykes, *Adv. Inorg. Chem.*, **36**, 377 (1991).

100. E. Kimura, T. Koike, H. Nada and Y. Iitaka, *J. Chem. Soc., Chem. Commun.*, 1322 (1986).

101. K. Nakamoto and P.J. McCarthy, " Spectroscopy and Structure of Metal Chelate Compounds", John Wiley and Sons, New York, 1968.

102. G.H. Robinson and S.A. Sangokoya, *J. Am. Chem. Soc.*, **110**, 1494 (1988).

103. M.D. Glick, D.P. Gavel, L.L. Diaddario and R.B. Rorabacher, *Inorg. Chem.*, **15**, 1190 (1976).

104. (a) A.R. Amundsen, J. Whelan and B.Bosnich, *J. Am. Chem. Soc.*, **99**, 6730 (1977); (b) R. Österberg, *Coord. Chem. Rev.*, **12**, 309 (1974); (c) E.R. Dockal, T.E. Jones, W.F. Sokol, R.J. Engerer and D.B. Rorabacher, *J. Am. Chem. Soc.*, **98**, 4322 (1976).

105. (a) M.J. Martin, J.F. Endicott, L.A. Ochrymowyca and D.B. Rorabacher, *Inorg. Chem.*, **26**, 3012 (1987).

106. P.M. Coleman, H.C. Freeman, J.M. Guss, M. Murata, V.A. Norris, J.A.M. Ramshaw and M.P. Venkatapa, *Nature*, 272, 319 (1978).

107. V.L. Goedken and D.H. Busch, *Inorg. Chem.*, **10**, 2679 (1971).

108. (a) D.H. Evans, K.M. O'Connell, R.A. Petersen and M.J. Kelley, *J. Chem. Educ.*, **66**, 290 (1983); (b) P.T. Kissinger and W.R. Heineman, *ibid.*, 702; (c) P.T. Kissinger and W.R. Heineman, Ed., "Laboratory Techniquew in Electroanalytical Chemistry", Dekker, New York, 1984.

109. J.R. Hartman, E.J. Hintsa, S.R. Cooper, *J. Chem. Soc., Chem. Commun.*, 386 (1984).

110. S. Chandrasekhar and A. McAuley, *Inorg. Chem.*, **31**, 480 (1992).

111. B. Bak, D. Christensen, L. Hansen-Nygarrd and J.R. Rastrup-Andersen, *J. Mol. Spectrosc.*, **7**, 58 (1968).

112. R.J. Angelici, *Coord. Chem. Rev.*, **105**, 61 (1990).

113. R.J. Angelici, *Acc. Chem. Res.*, **21**, 387 (1988).

114. (a) G.C. Van Stein, G. Van Koten, K. Vrieze, A.L. Spek, E.A. Klop and C. Brevard, *Inorg. Chem.*, **24**, 1367 (1985); (b) M. Draganjac, C.J. Ruffing and T.B. Rauchfuss, *Organometallics*, **4**, 1909 (1985); (c) J.D. Goodrich, P.N. Nickias and J.P. Selegue, *Inorg. Chem.*, **26**, 3426 (1987); (d) J.R. Ledkemeyer, T.B. Rauchfuss, A.L. Rheingold and S.R. Wilson, *J. Am. Chem. Soc.*, **111**, 8753 (1989); (e) J. Chen, L.M. Daniels and R.J. Anglici, *J. Am. Chem. Soc.*, **112**, 199 (1990).

115. (a) C.R. Lucas, S. Liu, M.J. Newlands, J.-P. Charland and E.J. Gabe, *Can. J. Chem.*, **66**, 1506 (1988); (b) C.R. Lucas, S. Liu, M.J. Newlands and E.R. Gabe, *Can. J. Chem.*, **68**, 1357 (1990).

116. (a) S. Chandrasekhar and A. McAuley, *Inorg. Chem.*, **31**, 2663 (1992); (b) G.J. Grant, K.A. Sanders, W.N. Setzer and D.G. VanDerveer, *Inorg. Chem.*, **30**, 4053 (1991).

117. A.J. Blake, R.O. Gould, A.J. Lavery, M. Schröder, *Angew. Chem. Int. Ed. Engl.*, **25**, 274 (1986).

118. M.-G. Choi and R.J. Angelici, *J. Am. Chem. Soc.*, **111**, 8753 (1989).

119. MULTAN77, a system of computer programs for the automatic solution of crystal structures from X-ray diffraction data, P. Main, L. Lessinger, M.M. Woolfson, G. Germain and J.P. Declarecq, Univeristy of York (U.K.) and Louvain (Belg.), 1977.

120. G.M. Sheldrick, SHELX-76, Program for Crystal Structure Refinement. University of Cambridge, Cambridge, U.K., 1976.

121. "Internation Tables for X-ray Crystallography", Vol IV; Kynoch Press, Birminghan, U.K, 1974.

122. J.D. Swalen, "Computer Programs for Chemistry", D.F. Detar, Ed., W.A. Benjamin, New York, 1968, Vol. 1.